UNIVERSITÉ DU QUÉBEC À CHICOUTIMI

THÈSE PRÉSENTÉE À

L'UNIVERSITÉ DU QUÉBEC À CHICOUTIMI

COMME EXIGENCE PARTIELLE

DU DOCTORAT EN INGÉNIERIE

PAR

MAHMOUD M. TASH

EFFECT DES PARAMÈTRES MÉTALLURGIQUES SUR LE COMPORTEMENT D'USINAGE DES ALLIAGES 356 ET 319 (ÉTUDE DE FORAGE ET DE TARAUDAGE)

July 2005

Bibliothèque
Paul-Émile-Boulet

UQAC
Université du Québec
à Chicoutimi

Mise en garde/Advice

Afin de rendre accessible au plus grand nombre le résultat des travaux de recherche menés par ses étudiants gradués et dans l'esprit des règles qui régissent le dépôt et la diffusion des mémoires et thèses produits dans cette Institution, **l'Université du Québec à Chicoutimi (UQAC)** est fière de rendre accessible une version complète et gratuite de cette œuvre.

Motivated by a desire to make the results of its graduate students' research accessible to all, and in accordance with the rules governing the acceptation and diffusion of dissertations and theses in this Institution, the **Université du Québec à Chicoutimi (UQAC)** is proud to make a complete version of this work available at no cost to the reader.

L'auteur conserve néanmoins la propriété du droit d'auteur qui protège ce mémoire ou cette thèse. Ni le mémoire ou la thèse ni des extraits substantiels de ceux-ci ne peuvent être imprimés ou autrement reproduits sans son autorisation.

The author retains ownership of the copyright of this dissertation or thesis. Neither the dissertation or thesis, nor substantial extracts from it, may be printed or otherwise reproduced without the author's permission.

UNIVERSITÉ DU QUÉBEC À CHICOUTIMI

THÈSE PRÉSENTÉ À

L'UNIVERSITÉ DU QUÉBEC À CHICOUTIMI

COMME EXIGENCE PARTIELLE

DU DOCTORAT EN INGÉNIERIE

PAR

MAHMOUD M. TASH

EFFECT OF METALLURGICAL PARAMETERS ON THE MACHINING BEHAVIOR OF 356 AND 319 ALLOYS (DRILLING AND TAPPING STUDY)

July 2005

Dedicated To my Parents, Brothers and my Fiancée Noura

إهداء لأسرتي وحبيبتي نورا

RÉSUMÉ

La présente étude a été entreprise pour étudier l'effet des paramètres métallurgiques sur la dureté et des caractérisations microstructurales dans les alliages 356 et 319 tels que coulés et soumis à un traitement thermique. Ceci est dans le but d'ajuster ces paramètres pour avoir une dureté appropriée et une fraction volumique des intermétalliques de fer pour l'usage dans les études concernant l'usinabilité de ces alliages. La gamme de la dureté et les fractions volumiques des intermétalliques de fer utilisées dans cette étude est la plus connue des applications commerciales de ces alliages. Des mesures de dureté ont été effectuées sur des spécimens préparés à partir de des alliages 356 et 319 tels coulés soumis à un traitement thermique, en utilisant différentes combinaisons du raffinage de grain, modification au strontium Sr et en ajoutant des éléments alliés. Des traitements de vieillissement ont été effectués à 155°C, 180°C, 200°C et 220°C pour 4 h, suivis du refroidissement à l'air, aussi bien qu'à 180°C et à 220°C pour 2, 4, 6, et 8 h pour déterminer des conditions dans lesquelles la dureté spécifique atteigne 85 et 115. L'addition du magnésium aux alliages 319 contenant le β- et/ou le α-intermétalliques de fer produit une augmentation remarquable de dureté à toutes les températures de vieillissement en conditions non modifiées et modifiées par le strontium.

Des additions du magnésium aux alliages 319 avec différentes conditions de traitement thermique pour des alliages 356 et 319 ont été effectuées pour obtenir des niveaux semblables de la dureté pour les deux alliages. Des conditions de 356 et de 319 modifiés au strontium (200-250 ppm) contenant principalement des intermétalliques α-Fe liées à différents niveaux de la dureté (90, 100 et 110 HB) ont été choisies pour l'étude de forage et de taraudage. L'effet du magnésium et de la fraction volumique des intermétalliques α-Fe sur l'usinabilité des alliages 319 soumis à un traitement thermique a été étudié pour deux niveaux de magnésium (0.1 et 0.28%), et deux niveaux de fraction volumique des intermétalliques α-Fe (2 et 5%), respectivement.

Les facteurs les plus importants entrepris dans la présente étude qui déterminent l'état du matériel de travail qui peuvent influencer les résultats de l'usinabilité des alliages 356 et 319 sont :

- Chimie et additions (Cu, Mg et Fraction volumique des intermétalliques de α-Fe)
    1. Le rôle des intermétalliques du cuivre en usinant les alliages 356 (sans du cuivre vieilli à 180°C/2h) et 319 (avec du cuivre vieilli à 220°C/2h), tous les deux ont le même niveau de la dureté (100 HB).
    2. Rôle de l'addition du magnésium à l'alliage 319 à deux niveaux de contenu de magnésium (0.1 et 0.28%) donne le même traitement de vieillissement (220°C/2h) et deux niveaux différents de dureté (90 et 100 HB), les mêmes alliages subis un traitement différent de vieillissement (180°C/2h et 220°C/2h) donnent le même niveau de la dureté (100 HB).

3. L'effet d'augmenter la fraction volumique des intermétalliques α-Fe aux alliages 319 (2 et 5%) et quand le vieillissement est effectué à 220°C/2h et à 180°C/2h rapportent des duretés de l'ordre (90 HB) et (100 HB) respectivement.

- Taux de refroidissement et vitesse de trempe
- Dureté

Les différences dans le comportement d'usinage entre les alliages 356 et 319 sont principalement attribuées à la différence dans la dureté de matrice, la chimie d'alliage, les additions d'éléments et le traitement thermique. La dureté de matrice (salutaire) et les abrasif d'alliage (nuisible) semblent être de vraies issues commandant l'usinabilité d'alliage. Le magnésium et le cuivre renforcent la matrice de l'alliage et par conséquent améliorent l'usinabilité de ce dernier. Le magnésium durcit les alliages 356 et 319, mais n'augmente pas l'abrasif puisqu'en petite quantité, il ne contribue pas à la formation des phases dures d'intermétalliques. En conséquence, les alliages contenant du Mg montrent un nombre plus haut de trous forés et tapés.

Un contenu plus élevé de magnésium résulte dans une force de découpage plus élevée au même niveau de la dureté. Ceci peut être expliqué en notant que la fraction volumique des intermétalliques de magnésium ou des précipités plus élevés qui peut être formée dans la matrice d'alliage en conditions des alliages 319 contenant du Mg élevé (0.28%) comparées au bas contenu du Mg (0.1%). Les alliages 319 contenant un niveau bas en Mg (0.1%) présentent une vie supérieure d'outil, et ce deux fois plus que des alliages 356 (0.3% Mg) et une fois et demi que des alliages 319 contenant Mg (0.28%). En comparant un système primaire d'alliage de bâti à l'autre (356 contre 319 ou 319 (0.1%Mg) contre 319 (0.28%Mg), par exemple), l'usinabilité des alliages 319 est plus haut que celle des alliages 356 et l'usinabilité des alliages 319 contenant un niveau bas en Mg (0.1%) sont plus haut que des alliages 319 contenant Mg (0.28%).

Un alliage avec un contenu bas en cuivre comme l'alliage 356 montre une force de découpage plus élevée comparée à celle des alliages 319 au même niveau de la dureté. Ceci peut être expliqué par l'amélioration de la homogénéité de la dureté de matrice d'alliage 319 sur la base de l'effet des intermétalliques du Cu et du Mg combinés, tandis que le durcissement se produit par la précipitation coopérative des particules de phase de Al_2Cu et de Mg_2Si comparées seulement à la précipitation de Mg_2Si dans le cas des alliages 356. La teneur de cuivre des alliages 319 tendrait à durcir l'alliage et par conséquent améliore leur usinabilité. En conséquence, les alliages 319 contenant Mg montrent une meilleure usinabilité comparée avec les alliages 356.

La morphologie des intermétalliques de fer peut affecter les résultats de force de découpage quand le vieillissement a été effectué pour deux heures à 180 °C et pas à 220 °C. On l'a observé que la fraction volumique des intermétalliques α-Fe peut affecter la force et le moment de découpage quand le vieillissement a été effectué à 180° C/2h plutôt qu'à 220°C/2h.

Pendant le temps de solidification dans la gamme de 25 à 45 secondes, il semble que la force et le moment de découpage sont légèrement influencés par le taux de refroidissement et la vitesse de trempe dans les états T6 et T7.

Les traitements thermiques qui augmentent la dureté réduisent (heat build-up (BUE)) sur l'outil de coupe. La dureté affecte l'usinabilité des alliages 319 du fait que l'usinabilité s'améliore avec l'augmentation de dureté. On l'observe que la force et le moment de découpage augmentent avec la dureté tandis que (heat build-up (BUE)) diminue. Dans le tapement, on l'a observé que les outils de l'acier à coupe rapide réagissent considérablement plus avec la sensibilité à la dureté. L'outil (HSS-E) est cassé quand le changement de taper seulement 230 trous dans tels que coulés états (88 HB) aux 230 autres trous dans les conditions T6 (110 HB).

On a observé la formation trompeuse des morceaux ou chip sur les conditions des alliages 356 et 319 (M1 et M3). Un critère important d'évaluation pendant le forage et le tapement est la qualité du trou. L'essai (Go-No-Go) est pris comme évaluation caractéristique pour l'exactitude de trou. Le diamètre de référence de (6.5024-6.5278 mm) et (7.02056-7.15518 mm) est employé pour forer et taper respectivement. Tous les résultats des essais (Go-No-Go) sont corrects.

On observe des morceaux discontinus pendant l'usinage des alliages 356 et 319. À l'heure actuelle de l'effort critique, les processus durcissants excédent les processus ramollissants et une ligne principale fente se développe qui résulte en cassant le morceau, et de ce fait au développement d'un morceau complètement cassé. Plein, demi de tour et morceaux hélicoïdaux sont produits au début d'une opération de découpage quand l'outil est nouveau (processus de cisaillement). Pendant que l'outil commence usage, le morceau devient graduellement bien déformé, et le cisaillement et la déformation se produisent.

Dans la contribution à la connaissance originale, les corrélations expérimentales qui relient les additions d'éléments et le traitement thermique avec la dureté ont été trouvées des résultats expérimentaux. De ces corrélations, on l'a noté que la dureté produite pour des alliages 319 augmente avec le magnésium et les fractions volumiques des intermétalliques de α-Fe et diminue comme la modification par le strontium et les paramètres de traitement de vieillissement (la température de vieillissement et temps de vieillissement). Dans des autres corrélations qui relient les additions d'éléments et le traitement thermique avec la force et le moment de découpage de forage aussi bien que (heat build-up (BUE)), on l'a observé que tous les deux la force et moment de découpage produits pendant de forage augmentent avec le magnésium et les fractions volumiques des intermétalliques de α-Fe et diminuent avec la température de vieillissement. Cependant, (heat build-up (BUE)) produite pendant le forage diminue avec l'augmentation de magnésium et les fractions volumiques des intermétalliques de α-Fe et augmente avec la température de vieillissement.

ABSTRACT

The present study was undertaken to investigate the effect of metallurgical parameters on the hardness and microstructural characterisation of as-cast and heat-treated 356 and 319 alloys, with the aim of adjusting these parameters to produce castings of suitable hardness and Fe-intermetallic volume fractions for subsequent use in studies relating to the machinability of these alloys. Hardness measurements were carried out on specimens prepared from 356 and 319 alloys in as-cast and heat-treated conditions, using different combinations of grain refining, Sr-modification, and alloying additions. Aging treatments were carried out at 155°C, 180°C, 200°C, and 220°C for 4 h, followed by air cooling, as well as at 180°C and 220°C for 2, 4, 6, and 8 h to determine conditions under which specific hardness levels *viz.*, 85 and 115 HBN could be obtained. Addition of Mg to 319 alloys containing β- and/or α-Fe intermetallics was found to produce a remarkable increase in hardness at all aging temperatures in both the unmodified and Sr-modified conditions.

Additions of Mg to 319 alloys coupled with different heat treatment conditions for both 356 and 319 alloys were carried out to get similar levels of hardness for both alloys. Conditions of Sr-modified (200-250ppm) 356 and 319 alloys-containing mainly α-Fe-intermetallics related to different levels of hardness (90, 100 and 110 HB) were selected for the drilling and tapping study. Effect of Mg and α-Fe-intermetallic volume fraction on the machinability of heat treated 319 alloys was studied for two levels of Mg (0.1 and 0.28%) and two levels of α-Fe-intermetallic volume fractions (2 and 5%), respectively. The range of the hardness and Fe-intermetallic volume fractions used in this study conforms to the most common levels of the commercial applications of these alloys.

The most important factors undertaken in the present study that determine the condition of the work material that can influence the outcome of the machinability of 356 and 319 alloys are:

- Chemistry and additions (Cu, Mg and α-Fe-intermetallic volume fractions)
    1. Role of Cu-intermetallics when machining 356 (without Cu- aged at 180°C/2h) and 319 (with Cu- aged at 220°C/2h) alloys, both have the same level of hardness (100 HB).
    2. Role of Mg addition to 319 alloys at two levels of Mg content (0.1 and 0.28%) given the same aging treatment (220°C/2h) that yields different levels of hardness (90 and 100 HB) and given different aging treatment (180°C/2h and 220°C/2h) that yield the same level of hardness (100 HB).
    3. Effect of increasing α-Fe intermetallic volume fractions to 319 alloys (2 and 5%) when aging carried out at 220°C/2h and at 180°C/2h that yields hardness of (90 HB) and (100 HB), respectively.
- Solidification time (25-45)s and quenching rate (100-145)°C/s
- Hardness (100 ±10 HB)

The differences in machining behaviour of 356 and 319 alloys are mainly attributed to the difference in matrix hardness, alloy chemistry, additions and heat treatment. Matrix hardness (beneficial) and alloy abrasiveness (detrimental) seem to be the real issues controlling alloy machinability. Magnesium and Cu strengthen the alloy matrix and improve the alloy machinability. Magnesium hardens both 356 and 319 alloys, but does not increase abrasiveness since, in small amounts; it does not contribute to the formation of hard intermetallics phases. Consequently, the Mg-containing alloys show higher numbers of holes drilled and tapped. The copper content of 319 alloys would tend to harden the alloy and hence improve the machinability.

Higher Mg content results in a higher cutting force at the same level of hardness. This can be explained by noting the high volume fraction of Mg-intermetallics or precipitates that can form within the alloy matrix in the high Mg content 319 alloys compared to the low Mg content ones. The low Mg-content 319 alloys (0.1%) yielded the longest tool life, more than two times that of 356 alloys (0.3%Mg) and one and half times that of the high Mg-content 319 alloys (0.28%). When comparing one primary casting alloy system to another (356 versus 319 or 319 (0.1%Mg) versus 319 (0.28%Mg), for instance), it is customary to rate the machinability of the 319 alloy higher than 356 alloy and the machinability of the low Mg-content 319 alloy higher than the high Mg-content one.

Lower copper content i.e. 356 alloy results in higher cutting force compared to 319 alloys at the same level of hardness. This may be explained by the improvement in the homogeneity of alloy matrix hardness in the 319 alloys on the basis of the combined effect of Cu-and Mg-intermetallics, where hardening occurs by cooperative precipitation of Al_2Cu and Mg_2Si phase particles as compared to only Mg_2Si precipitation in the case of 356 alloys. As a result, the Mg-containing 319 alloys have better machinability compared to 356 alloys.

The morphology of iron intermetallics can affect the cutting force results when aging was carried out for two hours at 180° and not at 220°C. It was observed that α-Fe intermetallic volume fractions can affect the cutting force and moment when aging was carried out at 180°C rather than at 220°C.

For solidification time in the range of 25 to 45 seconds, it seems that both cutting force and moment is slightly influenced by the cooling and quenching rates.

Heat treatments that increase the hardness will reduce the built-up-edge on the cutting tool. Hardness affects the machinability of 319 alloys in that machinability improves as the hardness increases. It is observed that both cutting force and moment increase with the hardness while the heat build-up depth on the cutting edge decreases. In a tapping test, it was observed that high speed steel tools react with considerably more sensitivity to the hardness. The tap was broken when changed from tapping only 230 holes in the as-cast condition (88 HB) to the 230 holes in the T6-condtion (110 HB).

Deceptive chip formation was observed for 356 and 319 alloys (M1 and M3). An important assessment criterion during drilling and tapping is the quality of the hole. The Go-No-Go test is taken as an assessment characteristic for hole accuracy, with a reference diameter of (6.5024-6.5278 mm) and (7.02056-7.15518 mm) for drilling and tapping, respectively. Results of Go-No-Go tests for all 356 and 319 alloys in all conditions are verified in this acceptable level of tolerance.

Discontinuous chips were observed during machining of both 356 and 319 alloys. At the point of critical stress the hardening processes prevail over the softening processes and a main line crack develops which results in breaking some elements off the chip, leading thereby to the development of a completely broken chip. Full, half turn and helical chips are generated at the start of a cutting operation when the drill is new (shearing process). As the drill begins to wear, the chip gradually becomes deformed and both shearing and deformation occurs.

Experimental correlations relating the alloying additions and heat-treatment to the hardness were obtained from the experimental results. From these correlations, it was observed that the hardness generated for 319 alloys increases with increasing Mg content and α-Fe-intermetallic volume fraction, and decreases with increasing Sr-modification (Sr-ppm) and aging treatment parameters (aging temperature and aging time). In another correlation that related the alloying additions and heat-treatment to the drilling cutting force and moment, as well as the heat build-up, it was observed that the cutting force and moment increase with the Mg content and the α-Fe-intermetallic volume fraction and decrease with the aging temperature. However, the heat build-up on the cutting edge decreases with the magnesium content and volume fraction of α-Fe-intermetallics and increases with aging temperature. In both correlations, the precipitations of Mg_2Si and MgCuAl, due to magnesium content, increase the alloy microhardness. Moreover, the volume fraction of α-Fe-intermetallics improves both microhardness and microstructure homogeneity. However, Sr-modification retards the precipitation process and increasing the aging parameters leads to precipitate coarsening and, hence, softening.

ACKNOWLEDGEMENTS

I would like to express my endless praise to God, the most merciful, the most generous for His guidance throughout my life.

My best regards and gratitude to my supervisors Professors F. H. Samuel and F. Mucciardi for their considerable support and helpful criticisms of the work contained in this thesis. I also like to express my deep gratitude to Dr. H. Doty and Dr. S. Valtierra for their guidance, kind interest, and valuable discussions. Special thanks to Professor F. Mucciardi and Dr A.M Samuel for reviewing the manuscript.

Financial support from the Natural Sciences and Engineering Research Council of Canada (NSERC), General Motors Powertrain Group and Corporativo Nemak and the Fondation de l'Université du Québec à chicoutimi (FUQAC) is gratefully acknowledged.

I would like to extend my appreciation to Mr. Régis Boucher and Mr. Alain Bérubé of the TAMLA group, UQAC for their invaluable assistance during the various stages of my work, as also to Mr. Lang Shi of the Microanalysis Laboratory, Earth and Planetary Sciences, McGill University for carrying out the WDS analysis. I also wish to thank Mr. kanVo and Mr. Demaris and all the group of the Machining workshop at the Aeronautical Technological Centre, St. Hurbert, Montreal for carrying out the drilling and tapping tests.

Finally, I would like to record my deep gratitude to all my family, especially my parents, my brothers and to my fiancée Noura. This work would not have come to light without their generous encouragement.

PUBLICATIONS

Five research articles have been prepared from this work.[1, 2, 3, 4, 5] for publication. Of these, three have been submitted for publication and are currently under review.

1. Effect of Metallurgical Parameters on the Hardness and Microstructural Characterization of As-Cast and Heat-Treated 356 and 319 Aluminum Alloys, M.M Tash, F.H. Samuel, F. Mucciardi, H.W. Doty.
   Submitted for Publication to *Materials Science and Engineering*, 2005.

2. Effect of Metallurgical Parameters on the Machinability of Heat-Treated 356 and 319 Aluminum Alloys, M.M Tash, F.H. Samuel, F. Mucciardi, H.W. Doty.
   Submitted for Publication to *Materials Science and Engineering*, 2005.

3. Methodology for Data Processing: Calculation of Cutting Force, Moment and Peak-to Valley Range During Drilling Processes of Heat-Treated 356 and 319 Aluminum Alloys , M.M Tash, F.H. Samuel, F. Mucciardi, H.W. Doty.
   Submitted for Publication to *Materials Science and Engineering*, 2005.

4. Experimental Correlation of the Effect of Metallurgical Parameters on the Hardness of Heat Treated 319 Alloys. M.M Tash, F.H. Samuel, F. Mucciardi, H.W. Doty.
   Prepared for Submission to *Materials Science and Engineering*, 2005.

5. Experimental Correlation of the Effect of Metallurgical Parameters on the Drilling Force, Moment and Heat Build-Up in Heat Treated 319 Alloys, M.M Tash, F.H. Samuel, F. Mucciardi, H.W. Doty.
   Prepared for Submission to *Materials Science and Engineering*, 2005.

TABLE OF CONTENTS

LIST OF TABLES

LIST OF FIGURES

LIST OF SYMBOLS

P_m	Energy consumption or heat generated
F_c	Cutting force
V	Cutting speed
P_s	Heat generated in primary shear zone
P_f	Heat generated in secondary shear zone (friction zone)
F_f	Friction force
V_0	Chip velocity
R_c	Cutting ratio
a_c	Undeformed chip thickness
a_w or a_0	Depth of cut
Γ	Portion of Ps conducted to workpiece
θ_s	Average temperature rise in shear zone
c	Specific heat
P	Density
θ_f	Average temperature rise in chip due to frictional heating
θ_{max}	Maximum temperature in the chip
θ_m	Maximum temperature rise in chip passing friction zone
θs	Temperature rise in chip passing primary zone
θ_0	Initial temperature
H_c	Heat transfer through the chip
H_w	Heat transfer through the workpiece
H_t	Heat transfer through the tool
ω_c	Chip rotation on the drill axis
ω_z	Side curling for the chip (z-direction)
ω_x	Another curling direction (x-direction)
ω_h	Angular velocity (resultant of the three angular velocity components)
SFPM	Surface feet per minute
RPM	Number of revolutions per minute
Drillcircumference	Distance around the drill periphery in feet
Pi	Constant =3.1416
D	Drill diameter in inches
IPR	Inches per revolution
IPM	Inches per minutes
UNC	Coarse thread series

UNF	Fine thread series
T6 or T7	Solution treatment, quenching and artificial aging
α and α_{ss}	Primary phase and supersaturated solid solution in 356 and 319 alloys
θ or β	Equilibrium phases in 319 and 356 alloys
θ', θ'', β' and β''	intermediate phases in 319 and 356 alloys
PFZ	Precipitate free zones in 356 alloys
T	Yied stress
M	Shear modulus
B	Burger vector
L	Inter-particle separation distance
A	Si-particle area
L	Si-particle length
A.R	Si-particle aspect ratio
R	Si-particle roundness
D	Si-particle density
Fx, Fy and Fz	Cutting force components in drilling and tapping
Mx, My and Mz	Cutting moment components in drilling and tapping
F_{x1+2} and F_{x3+4}	Cutting forces coming from sensor 1, 2, 3 and 4 in x-direction
F_{y1+4} and F_{y2+3}	Cutting forces coming from sensor 1, 2, 3 and 4 in y-direction
F_{z1},F_{z2},F_{z3} and F_{z4}	Cutting forces coming from sensor 1, 2, 3 and 4 in z-direction
nlevel,	Number of filteration =9
Diff k	1^{st} –difference for filterd Fz (k)
Difff k	2^{ed} –difference for filterd Fz (k)
nmin	Miniumum number of points in filtered signal per cycle =5
ind, indd, tt, tt1, n, m, z, N, M, Z, time1,time2, and time3	Matlab variables in drilling and tapping
timeup and timedown,	Matlab variables in drilling
timeup1,timedown1,timedown2 and ind1	Matlab variables in tapping
NN,MM and ZZ	Range of Data for calculation in both drilling and tapping
min, max, mean, std,buffer,ones, length,filter, find and zeros	Matlab Functions (www.mathworks.com)
mFx, mFy and mFz	Mean cutting force calculated within cutting period in each cycle during the drilling (with error treatment)
mMx, mMy and mMz	Mean cutting moment calculated within cutting period in each

	cycle during the drilling (with error treatment)
mFxup, mFyup and mFzup	Mean cutting force calculated within cutting period in each cycle during the drilling (without error treatment)
mMxup, mMyup and mMzup	Mean cutting moment calculated within cutting period in each cycle during the drilling (without error treatment)
mFxdown, mFydown and mFzdown	Mean cutting force calculated within non-cutting period in each cycle during the drilling (represent error)
mMxdown, mMydown and mMzdown	Mean cutting moment calculated within non-cutting period in each cycle during the drilling (represent error)
sFx, sFy and sFz ,smMx,smMy and smMz	Standard deviation for force and moment calculated within cutting period in each cycle during the drilling
mFxup, mFyup and mFzup	Mean cutting force calculated within cutting period in each cycle when the tap enter (with error treatment)
mMxup, mMyup and mMzup	Mean cutting moment calculated within cutting period in each cycle when the tap enter (with error treatment)
mFxdown, mFydown and mFzdown	Mean cutting force calculated within cutting period in each cycle when the tap exist (with error treatment)
mMxdown, mMydown and mMzdown	Mean cutting moment calculated within cutting period in each cycle when the tap exist (with error treatment)
mFxup1,mFyup1 and mFzup1	Mean cutting force calculated within cutting period in each cycle when the tap enter (without error treatment)
mMxup1,mMyup1 and mMzup1	Mean cutting moment calculated within cutting period in each cycle when the tap enter (without error treatment)
mFxdown1,mFydown1 and mFzdown1	Mean cutting force calculated within cutting period in each cycle when the tap exist (without error treatment)
mMxdown1,mMydown1 and mMzdown1	Mean cutting moment calculated within non-cutting period in each cycle when the tap exist (without error treatment)
mFxdown2,mFydown2 and mFzdown2	Mean cutting force calculated within non-cutting period in each cycle during tapping (represent error)
mMxdown2,mMydown2 and mMzdown2	Mean cutting moment calculated within non-cutting period in each cycle during tapping (represent error)
sFxup, sFyup and sFzup	Standard deviation for force calculated within cutting period in each cycle when the tap enter
smMxup, smMyup and smMzup	Standard deviation for moment calculated within cutting period in each cycle when the tap enter
sFxdown, sFydown and sFzdown	Standard deviation for force calculated within cutting period in each cycle when the tap exist
smMxdown, smMydown and smMzdown	Standard deviation for force calculated within cutting period in each cycle when the tap exist
σ_f	Standard deviation combined functions

μ_f	Combined functions (total force or moment)
μ_x, μ_y and μ_z	Standard deviation components
F_t	Total cutting force in drilling or tapping
M_t	Total cutting moment in drilling or tapping
$\delta Ft/\delta x$, $\delta Ft/\delta y$ and $\delta Ft/\delta z$	Partial derivation of total cutting force respect to x, y and z
$\delta Mt/\delta x$, $\delta Mt/\delta y$ and $\delta Mt/\delta z$	Partial derivation of total cutting moment respect to x, y and z
σ_{ff}	Standard deviation for combined function (total force)
σ_{fm}	Standard deviation for combined function (total moment)
σx , σy and σz	Standard deviation for force or moment components (x,y and z)
F	Any variable functions
BUE	Heat build-up on the cutting edge
%V.F, %Mg, Sr-ppm, At, and AT	Metallurgical parameters (volume fractions of α-Fe intermetallics, magnesium %, strontium modification, aging time and temperature
HB	Hardness Brinell
$H_{predicted}$ or $F_{predicted}$	Predicted hardness regression equation or cutting force, moment and heat build up area, depth and width regression equations
MF_1 , MF_2 and MF_3	Main effect for each metallurgical parameters (1, 2 and 3)
IF_{1*2} , IF_{1*3} and IF_{2*3}	Interaction effect between each two metallurgical parameters
IF_{1*2*3}	Interaction effect between the three metallurgical parameters
$Y_{i\ i=1-8}$	Response variable functions
R_1 and R_2	Peak-to-valley for cutting force and moment
F_t and $M_{t\ predicted}$	Estimated total cutting force and moment (empirical models)

CHAPTER 1

DEFINITION OF THE PROBLEM

CHAPTER 1

DEFINITION OF THE PROBLEM

1.1. INTRODUCTION

In this work, Al-Si-Cu, Al-Si-Cu-Mg and Al-Si-Mg cast alloys, belonging to the Al-Si alloy system and represented respectively by 319 and 356 alloys, were selected for a machinability study, due to the high demand of these alloys in the automobile industry. Any metallurgical adjustment that can be made to the aluminum alloys which allows them to enhance the effectiveness of the coolant or reduce the amount of heat generated can be considered an improvement in the overall machinability of the product.

Although all aluminum materials tend toward difficult chip formation and material sticking to the tool, the demand on the cutting tool of soft deformable alloys for the electrical industry is very different to the demands of high strength alloys and Al-Si cast alloys for the aerospace and automotive industries. A range of drilling and tapping tools for aluminum machining, which contend with these difficulties are available to cover all applications. General purpose tools, high performance tools as well as special tools are available for both drilling and tapping operations.

Machinability, by definition, is a system property that indicates how easily material can be machined at low cost. It may be described in terms of tool life, ease of metal removal, and workpiece quality. The most important factors that determine the condition of the work material that can influence the outcome of the machinability are: [6]

- Alloy chemistry, additions,
- Morphology, size and volume fraction of the constituent phases,

- Microstructure (grain refining and modification),
- Porosity,
- Heat treatment, and
- Physical and mechanical properties.

Chemistry, microstructure, bulk strength, hardness and work-hardenability all combine to determine the machining characteristics of an alloy. Some elements are traditionally thought to provide a degree of natural lubricity, other elements are known to increase matrix hardness and still others result in the formation of hard intermetallic phases. Copper and Mg increase alloy hardness and by doing so improve the machined surface finish and decreases the tendency of an alloy to build up on a cutting tool edge.[7]

The heavy elements (Mn and Cr) tend to combine with Al, Fe, Si, and sometimes Cu to form hard complex intermetallics phases (sludge or fall-out) that cause hard spots and have a most dramatic effect on the tool edge build-up problems. Iron, manganese, and chromium, when present even in moderate quantities in most aluminium casting alloys, tend to combine with each other and with aluminium and silicon to form hard, complex, intermetallic phases. The microhardness of such phases is usually in the 500-900 KHN range compared to the alloy matrix hardness range of 70 to 180 KHN. Such phases act as abrasives in a relatively soft alloy matrix, and reduce the tool life.

All important automotive casting alloys contain Si, Cu, and Mg as a major alloying element. Silicon, like the heavy-element, intermetallic, impurity phases of iron, manganese, and chromium, is an abrasive material in an otherwise soft matrix and is the element that singularly has the greatest tendency to decrease cutting tool life. Silicon

crystal hardness ranges from 1000-1300 KHN, while that of the alloy matrix seldom exceeds 180 KHN.

Sodium and strontium modify the eutectic silicon phase, especially in the case of sand and permanent mold casting (coarse grain size) than die casting (which already provides a fine microstructure due to the high cooling rates). The finer the grain size the better the overall machining characteristics. Tool life decreases with the coarse eutectic silicon structure.[8] Smearing effect or built-up edge occurs during the machining process for Si percentages up to 12%. As the Si % increases, the abrasive wear mechanisms dominate and result in shorter tool life.

Porosity can cause problems particularly in those workpiece areas where holes are to be drilled or tapped. Excess porosity due to improper gating, venting and injection can result in poor machining characteristics. Porosity due to entrapped air can be minimized by proper gating and venting while porosity resulting from excess lubricant in the die can be reduced by use of minimum and suitable lubricants.

In fact, aluminium alloys differ from many other metals, in that, machinability of aluminium generally improves as strength and hardness increase. Typical automotive machining techniques, however, usually require some minimum workpiece hardness in order to avoid difficulties associated with built-up-edge (BUE) on the cutting tool. According to a previous study [7] on the effects of minor and impurity elements on the machining characteristics of 380 alloy die castings, it was found that built-up-edge was affected quite dramatically by the matrix microhardness of the workpiece alloy, and perhaps also by its work-hardenability.

Heat treatments that increase the hardness will reduce the built-up-edge on the cutting tool and improve the surface finish of the machined part. Strength and hardness both affect the machinability of aluminum alloys. A minimum hardness of 80 BHN for the alloy casting is desirable to avoid difficulties associated with built-up-edge (BUE) on the cutting tool.[7] The BUE is affected quite dramatically by the matrix microhardness and by the work hardening response of the alloy. In drilling and turning, the added cutting temperature is detrimental to tool life, since it produces excess heat causing accelerated edge wear. In milling, increased material hardness produces higher impact loads as inserts enter the cut, which often leads to a premature breakdown of the cutting edge.

Metals with high thermal conductivity are helpful for more heat dissipation. As the thermal conductivity increases, the rate of heat dissipation increases and hence, the rise in the temperature will decrease during machining. High temperature can promote the diffusion of elements and chemical reactions at the interface and finally result in tool damage.

Heat build-up on the cutting tools is the biggest drawback for maintaining material machining characteristics and productivity of the machining operations. Once the cutting temperature reaches a point in which the metal actually begins to weld itself to the cutting tool, BUE occurs. Essentially, what happens is that the aluminum begins to be cut by the aluminum welded to the cutting edge. The effort placed toward improving the machinability of a material is actually an effort to reduce the heat build-up on the cutting edge of the tool, and hence improvement in: chip size, tool life, surface finish, and part dimensional control.

In a collective sense, the more important terms as related to the subject of machinability are: tool wear, chip formation (characteristics), burring tendency and finish of machined surface. The rate, at which the tool wears, under a given set of machining parameters, determines the frequency of required tool adjustment and replacement. Chips, their length and curl and the ease or difficulty associated with their removal and handling influence the surface finish. Surface finish relates to the relative difficulty of achieving a desired degree of smoothness on a machined surface.

1.2. OBJECTIVES

1.2.1. Metallurgical Characterization of 356 and 319 Alloys

A thorough understanding of all the metallurgical factors affecting alloy machinability would help in selecting a metallurgical design that would achieve the optimum machining combinations critical to maximizing productivity at high speed machining. A preliminary study for hardness and microstructural characterization was made for both 356 and 319 alloys. Hardness measurements were carried out on specimens prepared from 356 and 319 alloys in the as-cast and heat-treated conditions, using different combinations of grain refining, Sr-modification, and alloying additions. Aging treatments were carried out at different temperatures and times to determine conditions under which specific hardness levels viz., 85 and 115 HBN could be obtained. Iron intermetallic volume fractions were measured for the as-cast and solution heat-treated samples of such alloys in order to determine which conditions provided volume fractions of 2% and 5%. Silicon particle characterizations for both 356 and 319 alloys in

the unmodified and Sr-modified conditions when solution heat-treated at 540°C/8h and at 495 °C/8h were made.

1.2.2. Drilling and Tapping Study for 356 and 319 Alloys

The present study was undertaken to investigate the effect of metallurgical parameters on the machining performance of the heat treated 356 and 319 alloys. The most important factors undertaken in the present study that determine the condition of the work material that can influence the outcome of the machinability are:

- Alloy chemistry and additions
    1. Role of Cu-intermetallics when machining 356 (without Cu- aged at 180°C/2h) and 319 (with Cu- aged at 220°C/2h) alloys, both have the same level of hardness (100 HB).
    2. Role of Mg addition to 319 alloys at two levels of Mg content (0.1 and 0.28%) given the same aging treatment (220°C/2h) that yields different levels of hardness (90 and 100 HB) and given different aging treatments (180°C/2h and 220°C/2h) that yield the same level of hardness (100 HB).
    3. Effect of increasing α-Fe intermetallic volume fractions to 319 alloys (2 and 5%) when aging carried out at 220°C/2h and at 180°C/2h that yields hardness of (90 HB) and (100 HB), respectively.
- Solidification time (25-45)s and quenching rate (100-145)°C/s
- Hardness (100 ±10 HB).

CHAPTER 2

LITERATURE REVIEW

CHAPTER 2

LITERATURE REVIEW

2.1. INTRODUCTION

Aluminum alloys containing silicon as the major alloying element offer excellent castability, high thermal conductivity, low specific gravity, high wear and corrosion resistance, and good weldability. Due to their excellent strength to weight ratio, Al-Si castings are being adapted extensively in applications in the automobile industry, where there is a high demand for greater fuel efficiency and higher performance. The high thermal conductivity of aluminum is advantageous for thermally loaded parts such as pistons, cylinder blocks and heads.

Aluminum has replaced steel in automobile wheels, because of its superior heat dissipation during braking, which allows for improved road handling and decreased tie wear. Also due to the lighter weight, Al-Si casting has gradually replaced automobile parts such as transmission cases, intake manifolds, and certain engine blocks and cylinder heads, which were formerly monopolized by cast iron. The relatively high strength-to-weight ratio, coupled with the availability in a variety of forms made aluminum alloys the ideal choice for many engineering applications. Both medium-and high-strength aluminum alloys are widely used in the aerospace and transportation industries in a variety of forms such as sheet, plate, extrusion, and casting.

Aluminum alloys can be divided into two major groups: wrought and cast alloys, depending on their method of fabrication. Wrought alloys, which are manufactured into

different shapes by hot deformation, have compositions and microstructures significantly different from cast alloys, because they have less segregation and structural inhomogeneities. Within each group, we can divide the alloys into two subgroups: heat treatable and non-heat treatable alloys. While 1xxx, 3xxx, and 5xxx series of the wrought Al alloys are not age hardenable, the 2xxx, 6xxx and 7xxx series are heat-treatable.[9]

The most commonly used designation system for aluminum casting alloys is the three digit system (i.e., 1xx.x, 2xx.x, etc.) proposed by the Aluminum Association (AA).[9] The first digit indicates the alloy group. The second and third digits identify the specific aluminum alloy according to its alloying elements, or indicate aluminum purity for the aluminum (1xx.x) series. A decimal value always follows, where decimal .0 in all cases represents chemical composition limits for casting, while decimal .1 and .2 concern chemical composition limits for ingots. Several AA alloy designations also include a prefix letter, which distinguishes alloys of a general composition (with the same alloy number) only in percentage of impurities or minor alloying elements, e.g., 319, A319 and B319. Among the most common aluminum casting alloys are 319.0 (Al-6Si-3.5Cu) and 356.0 (Al-7Si-0.3Mg). Such alloys and properties are summarized in Table 2.1.

Table 2.1 Characteristics of various aluminum-silicon casting alloys[10]

Alloy	Casting Method	Resistance To Tearing	Pressure Tightness	Fluidity	Shrinkage Tendency	Machinability
319.0	S, P	2	2	2	2	3
A356.0	S, P	1	1	1	1	3
Rating: 1- best, 5- worst; S = sand casting, P = permanent mold casting						

Backerud *et al.*[11] investigated the solidification process in various alloys, by employing the thermal analysis technique, followed by a subsequent metallographic

examination of samples sectioned from the solidified castings. The polished metallographic samples were examined using scanning electron microscopy (SEM) and energy dispersive X-ray spectrometry (EDX) for identifying the various phases. The phases were quantified using heat transport equations that included latent heat evolution.

2.1.1. Phases in Al-Si-Mg Alloys (A356.2 Alloy)

This alloy belongs to the Al-Si-Mg system with magnesium as an alloying element (0.35 wt %) and copper in the amount of 0.02 wt%. The main sequence of phase precipitation during solidification is listed in Table 2.2.

Table 2.2 Reactions observed during solidification of alloy A356.2[11]

Reaction No.	Reactions	Suggested temperature, °C
1	Development of dendritic network	615
2a	Liq.→ Al + Si	575
2b	Liq.→ Al +Al_5FeSi	575
3a	Liq.→ Al + Si + Al_5FeSi	575
3b	Liq. + Al_5FeSi → Al +Si + $Al_8Mg_3FeSi_6$	567
4	Liq.→ Al +Mg_2Si + Si	555
5	Liq.→ Al + Mg_2Si + Si + $Al_8Mg_3FeSi_6$	554

Table 2.3 Phases observed by optical microscopy/SEM/EDX in alloy A356.2[11]

Phase	α-Al	Si	$Al_8Mg_3FeSi_6$	Mg_2Si	Al_5FeSi
Char.	Dendrite	Gray	Brown Script	Black	Needle

The corresponding phases and their characteristics are given in Table 2.3. Due to the high purity of A356 alloy, it is difficult to nucleate the silicon crystals after the development of dendritic networks, thus some Al_5FeSi phase may precipitate before the start of the main eutectic reaction, as indicated by reaction 2b in Table 2.2. Some of this

phase later transforms into $Al_8Mg_3FeSi_6$ via a peritectic reaction.[11] Particles of the secondary eutectic phase, Mg_2Si, also appear in the microstructure on account of the high Mg content of the alloy.

2.1.2. Phases in Al-Si-Cu (319.2 Alloy)

During the solidification of 319 alloys, the main sequence of phase precipitation that occurs is as follows. First, there is the formation of the dendritic network of α-aluminum, the aluminum-silicon eutectic reaction and the precipitation of secondary eutectic phases like $CuAl_2$. In addition, the precipitation of iron- and manganese-containing phases, e.g., the α-Al_{15} $(Mn, Fe)_3Si_2$ and β-Al_5FeSi intermetallics also takes place. These α- and β-iron intermetallics normally precipitate after the initial dendrites have formed but before the appearance of the Al-Si eutectic, i.e., in a pre-eutectic reaction. However, the β-iron phase can also precipitate as a co-eutectic phase. $CuAl_2$ and other more complex phases with low melting points will precipitate from the remaining liquid, in which any Si, Fe, Mg, Cu and Zn left over may precipitate.[11] If high iron and manganese levels are present in the alloy, and the cooling rate is low, the α-Al_{15} $(Mn, Fe)_3Si_2$ phase will precipitate as a primary phase, in the form of coarse particles termed "sludge," having polygonal or star-like morphologies.

Backerud *et al.* [11] have listed the reactions that occur during the solidification of alloy 319.1 and 319.2. The sequence of reactions during solidification and the phases observed in both alloys are listed in Table 2.4.[11] The characteristics and compositions of these phases are provided in Table 2.5.

Table 2.4 Reactions observed during solidification of alloy 319.2[11]

Reaction No.	Reactions	Suggested Temperature (°C)
1	Development of dendritic network	609
2a	Liq.→ Al + $Al_{15}Mn_3Si_2$	590
2b	Liq.→ Al +Al_5FeSi+ $Al_{15}Mn_3Si_2$	590
3	Liq.→ Al + Si+ Al_5FeSi	575
4	Liq.→ Al +$CuAl_2$+ Si+ Al_5FeSi	525
5	Liq.→ Al + $CuAl_2$ + Si + $Al_5Mg_8Cu_2Si_6$	507

Table 2.5 Phases observed by optical microscopy/SEM/EDX in alloy A319.2[11]

Phase	α-Al*	Si*	$CuAl_2$*	Al_5FeSi*	$Al_{15}Mn_3Si_2$	$Al_5Mg_8Cu_2Si_6$
Char.	Dendrite	Gray	Pink particle	Needle	Brown Chinese script	Brown bulk
* Confirmed by X-Ray Diffraction (XRD)						

2.1.3. Phases in Al-Si-Cu (B319.2 Alloy)

This alloy is very similar to alloy 319.2, except for its higher magnesium content. According to Backerud *et al.*,[11] the increased level of magnesium does not change the solidification process significantly, except that an increased amount of the $Al_5Mg_8Cu_2Si_6$ phase is observed, see Table 2.4 and Table 2.5.[11] Copper intermetallics ($CuAl_2$) precipitation is caused by a divorced eutectic reaction coupled with segregation in the remaining areas shaped by the advancing eutectic Si-containing inter-dendritic regions.

The mechanism of Al_2Cu precipitation in modified 319 alloys may be represented schematically by the model depicted in Figure 2.1.[12] During the first stages of solidification, the formation of the α-Al dendritic network is associated with segregation of Si and Cu in the liquid, ahead of the progressing dendrite interfaces. When the solidification temperature approaches the eutectic temperature, rounded/fibrous Si

particles precipitate, leading to a local concentration of Cu in the remaining areas. Depending on the cooling rate, Al_2Cu may precipitate as a mixture of eutectic-like and block-like form or mainly in the block-like form in the presence of β-Al_5FeSi needles. It was noted that precipitation of the Cu phase is strongly dependent on the possible sites available for nucleation, which is determined by the amount and nature of the β-iron phase precipitation and the cooling rate.[12]

Grain refining plays an important role in reducing the degree of $CuAl_2$ segregation and in refining the block-like $CuAl_2$ particles in the Sr-modified alloys, particularly at low cooling rates. It is a well-established fact that the addition of small quantities of TiB_2 refines the grain size and reduces the pore sizes, which improves the mechanical properties.[13]

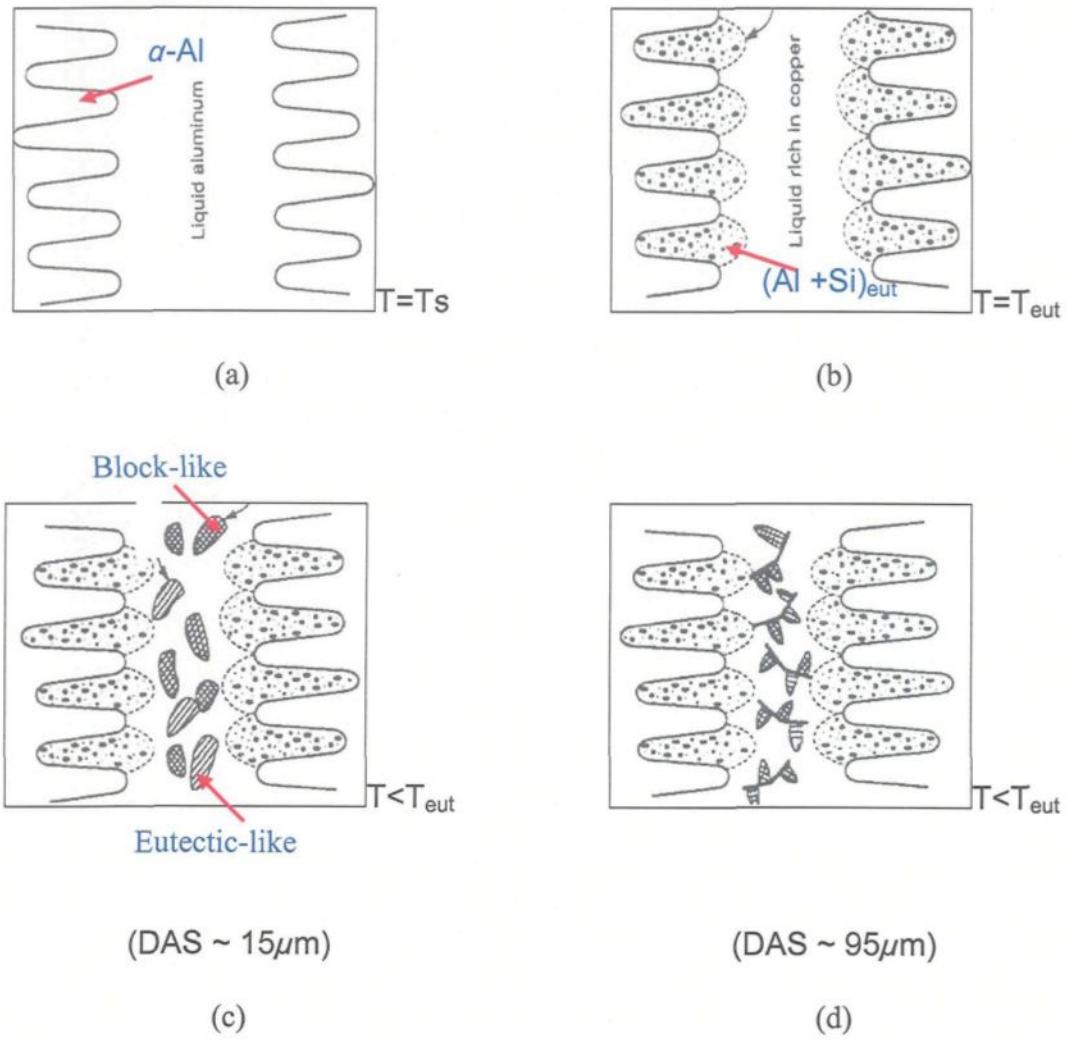

Figure 2.1 Schematic diagram demonstrating different solidification stages of modified 319.1 alloy a) formation of α-Al dendritic network, b) formation of eutectic Si, c) precipitation of both blocky and eutectic Al_2Cu, DAS~15 μm and d) dominance of blocky Al_2Cu, DAS~95μm.[12]

2.1.4. Iron Intermetallics in Al-Si Alloys

Iron is one of the most common impurities normally present in Al-Si cast alloys.[14] Iron has a high solubility in molten aluminum and is therefore readily dissolved at all molten stages in production. The solubility of iron in the solid state is, however, very low

(only~ 0.05 wt% at 600°C, and even less at room temperature [14]). Common sources of iron pick-up in foundry processing are from melting equipment and from remelted scrap castings. Iron level is usually restricted to below 0.15% Fe, in commercial casting alloys such as 356, 357, 358, and 359. However, increased activity in the recycling of spent automobiles, in order to cut down the alloy production cost, causes iron levels to soar as high as 1.5-2.0%. On the other hand, iron content up to 1.3% is beneficial to die cast parts in terms of improved strength, hardness and low tendency toward hot cracking.[15] Iron reduces the tendency of the metal to weld or solder to the die surface, which can cause tearing of the casting surface.

There is an abundant amount of literature dealing with the effect of iron on the mechanical properties of Al-Si alloys. Courture[16] in his review reported that the addition of iron to aluminum-silicon alloys is detrimental to the mechanical properties. Vorobev *et al.*[17] claimed that, even a small Fe addition to Al-Si alloys seriously diminishes tensile strength and elongation. This is due to the formation of the brittle intermetallic compound, Al_5FeSi (β-phase) at cooling rates normally employed in sand and permanent mold castings. This compound tends to form thin plates, which are very hard and brittle and have relatively low bond strength with the matrix.[18]

According to Bonsack[19] any amount of Fe over 0.5% will be present as Al-Fe silicide in large needles which, up to about 0.8% Fe, increases strength and hardness but slightly reduces ductility. Above 0.8 %Fe, both strength and elongation deteriorate rapidly, and there is a deleterious effect on the machinability.

2.1.5. α- AlFeSi and β-AlFeSi Intermetallics

Amongst the many AlFeSi intermetallics, the most important are generally thought to be α- and β- Fe intermetallic phases. The α-AlFeSi phase has the composition of Al_8Fe_2Si (31.6 %Fe, 7.8%Si) and is often reported as $Al_{15}Fe_3Si_2$ (30.7%Fe, 10.2%Si), with a probable composition range of 30~33% Fe, 6~12%Si. It is reported as having a hexagonal structure with parameters a = 12.3 Å, c =26.3 Å, a density 3.58 g/cm^3 and appears in the form Chinese script particles.[20]

There are two types of β-Al_5FeSi platelets: pre-eutectic particles, characterized by their large size, and co- or post-eutectic particles, which are relatively thin. The difference in their sizes is directly related to the rates of diffusion of the iron atoms with respect to the temperatures at which the two particle types precipitate. The composition of the β-AlFeSi phase is Al_5FeSi (25.6 %Fe, 12.8% Si), with a range 25~30 %Fe, 12~15%Si. It has a monoclinic structure with parameters a = b = 6.12 Å, c =41.5 Å, α = 91°, density of 3.30~3.35 g/cm^3, and appears in the form of thin platelets in the microstructure.

The α-AlFeSi phase shows an irregular, curved crystal growth conforming to the complicated shape of the interdendritic spaces during solidification. It has a nonfaceted interface with the aluminum matrix, exhibits no growth twinning, which allows for a better bonding with the aluminum matrix. This type of growth occurs at high driving forces of solidification or rapid cooling, i.e., at high degree of undercooling, ΔT. On the other hand, the β-AlFeSi phase grows in a lateral or faceted mode which is poorly bonded to the aluminum matrix and contains multiple (001) growth twins parallel to the growth

direction. This type of growth occurs at low driving forces or at slow cooling, i.e., at low degrees of undercooling, ΔT.

When the melt is superheated to a high temperature (about 200-300°C above the liquidus temperature), the iron compound crystallizes in α phase at high cooling rate[21]. It has also been reported that at low cooling rates, Al_5FeSi plates are coarse and concentrated at grain boundaries, where they promote a brittle fracture. At higher cooling rates, Al_5FeSi particles are quite small and interspersed more uniformly. Consequently, Fe levels tolerable in permanent mold casting alloys are greater than in sand casting alloys.[22]

2.1.6. Modification and Dissolution of Iron Intermetallics

The negative effects of iron in aluminum-silicon alloys can be minimized or overcome through the following techniques:

- Rapid solidification
- Addition of neutralizing elements such as Mn, Cr, Be, and Ca
- Melt superheating
- Strontium modification
- Non-equilibrium solution heat treatment.

All of these techniques convert the crystallization of needle-like β-AlFeSi phase to the less harmful Chinese script form (α-AlFeSi), or dissolve partially or completely the β-AlFeSi phase in the matrix hence improving the mechanical properties and alloy machinability.

The solidification rate of the casting is perhaps the most important of the various parameters influencing the microstructure, as it directly or indirectly affects almost all the

microstructural parameters such as the dendrite arm spacing (DAS), the degree of eutectic silicon modification and grain refinement, and the amount of microporosity, intermetallics and inclusions observed in the microstructure. The rapid solidification technique involves solidifying the melt at a very high cooling rate so that Fe will be retained in solid solution or provide finely distributed Fe phase. In the presence of Mn, the iron crystallizes in the form of the α-$Al_{15}(Fe, Mn)_3Si_2$ script phase at low and intermediate cooling rates (0.1 to 10 °C/s), and in both α and β (Al_5FeSi) iron phases at high cooling rates (> 20 °C/s).

Manganese is the common alloying addition which is used to neutralize the effect of iron and to modify the morphology and type of intermetallic phases.[16, 18] Small amounts of manganese (usually Mn: Fe ratio of 1:2) play a positive role in combining with iron to form the Chinese script structure instead of a plate-like structure; however, when present at higher ratios of Mn: Fe and/or in the presence of chromium, a complex multicomponent sludge is produced. The beneficial influence of Mn additions in Al-Si alloys is attributed to the formation of a quaternary intermetallic phase of iron and manganese with the main components of Al-Si alloys. This phase crystallizes in three distinctly different morphologies.[23]

- As needles or thin platelets (β- phase)
- As Chinese script (α- phase)
- As polyhedral or star- like crystals (primary α-phases)

The crystallization and volume fraction of these three different morphologies depend on the Fe: Mn ratio, the cooling rate, and the melt holding temperature. The volume fraction of Fe- intermetallics decreases with increasing cooling rates. However,

the size and volume fraction of β- plates increases with increasing iron content and decreasing solidification rate. In their study of Al-Si-Cu (319) foundry alloys, Samuel *et al.*[24] have also pointed out that increasing the iron content results in the precipitation of long, thick plates of the β-AlFeSi phase. They also observed that these plates are often branched into several plates, and that large shrinkage cavities can be formed within the casting due to the inability of liquid metal to feed into the spaces between the branched plates.

Recently, studies have been carried out on Sr modification of 1xxx and 6xxx DC alloys. Mulazimoglu *et al.* [25] claim that β-Al_5FeSi occurs by peritectic decomposition of α-Al_8Fe_2Si phase. Strontium "adsorbs" to the α-Al_8Fe_2Si interface, prevents the diffusion of Si into this phase, and hence there is an "absence" of β-Al_5FeSi plates in the microstructure. A similar effect of Sr on Cu segregation in 319 alloys during the solidification has been reported.[26] Samuel *et al.*[27] showed that Sr addition leads to dissolution of the β-iron phase (without conversion to the α-phase).

An increase in the addition of Mg content depresses the silicon eutectic temperature, rendering it more difficult to avoid β-phase crystallization in high Mg-content 319 alloys, even at high melt superheat. The length of the primary β-phase platelets greatly depends on the time interval between the β-phase start temperature and the silicon eutectic temperature, an increase in the plate length being observed with time. The above noted time interval is found to increase with a decrease in cooling rate and melt superheat and an increase in Fe and Mg content.[28]

Addition of Mg to 319 type alloys leads to transformation of a large proportion of the β-platelets into the compacted α-Fe script phase ($Al_8Mg_3FeSi_6$), precipitation of

Mg_2Si, and precipitation of $Al_5Mg_8Cu_2Si_6$ in the form of branched crystals or ultra-fine eutectic growing out of Al_2Cu particles during the complex eutectic reaction that takes place in the final stages of solidification. The dissolution of both $Al_8Mg_3FeSi_6$ and $Al_5Mg_8Cu_2Si_6$ during solution treatment is fairly slow (regardless of Sr modification). This, in turn, decreases the amounts of free Mg and Cu available for further hardening during the aging process. [29, 30]

Eutectic silicon morphology, *viz.*, particle size and shape, plays an important role in determining the mechanical properties of Al-Si alloy castings. The silicon particles, appearing as coarse, acicular needles under normal cooling conditions, act as crack initiators, lowering the mechanical properties. Strontium modification changes the silicon morphology from acicular to fibrous, resulting in a significant decrease in the size of the Si particles, and a corresponding increase in the particle count per unit area. Zhu *et al.*[31, 32] have proposed that changes in Si morphology occur in two stages: in the first stage, the Si particles separate into segments at corners or thin growth steps, but they retain their flake morphology. In the second stage, the broken segments spheroidize and the aspect ratio decreases.

When an eutectic structure is subjected to a thermal treatment at elevated temperatures, shape perturbations in the second phase increase and ultimately the particles are broken into a series of nearly spherical crystals. Theoretical analyses suggest that interfacial instabilities cannot readily occur in plate-like eutectics (unmodified case) and consequently, the structure is resistant to spherodization.[33] Fibrous eutectics, however, are susceptible to shape perturbations and the particles are easily fragmented.

2.2. HEAT TREATMENT

Heat treatment is one of the major factors used to enhance the mechanical properties of heat-treatable Al-Si alloys. The solution treatment homogenizes the cast structure and minimizes segregation of alloying elements in the casting. The time required for homogenization is determined by the solution temperature and by the dendrite arm spacing. Dissolution of Mg_2Si and homogenization of the casting occur very rapidly while altering the Si particle morphology takes time. Silicon particles undergo fragmentation, necking, spheroidization, and coarsening. The β-Fe needles gradually undergo necking and fragmentation, while the α-Fe Chinese script particles are not affected.[34] Due to their compact form, the α-Fe-intermetallics are less harmful to the mechanical properties and, hence, preferable to the β-Fe in the casting microstructure.

2.2.1. Solution Heat Treatment

In precipitation-strengthened alloys, more than one phase may be precipitated in a matrix of the predominant phase. To achieve the best result, the precipitate phase should be hard and discontinuous, its particles small and numerous, the morphology round rather than sharp-edged. On the other hand, the matrix phase should be soft and ductile so that if cracks were to nucleate, it would be much safer for them to take place in the particle rather than in the matrix. A solution and an aging treatment are needed for such a microstructure to be evolved. The basic requirements of age hardening of an alloy system are: decreasing solubility with decreasing temperature, and formation of clusters of solute atoms coherent with the matrix. In other words, there should be an orientation relationship between the precipitates and the matrix.

An alloy made up of an abundant primary (α) phase and a smaller quantity of secondary (θ) phase is heated to the single-phase region and held there for the proper time. During that time the secondary phase dissolves completely leaving a solid solution single phase, see Figure 2.2. When the alloy is quenched from the α-region, no time will be available for atomic diffusion to take place and the product resulting from the quench will be a supersaturated solid solution (αss).[35] In general, the higher the solution treatment temperature, the more the chemical heterogeneities are dissolved, and a homogenized structure is obtained, thereby, leading to wider property changes during subsequent aging.[36] The optimum solution treatment time and temperature depend upon the chemical composition and prior thermal and mechanical treatment of the alloy. [36]

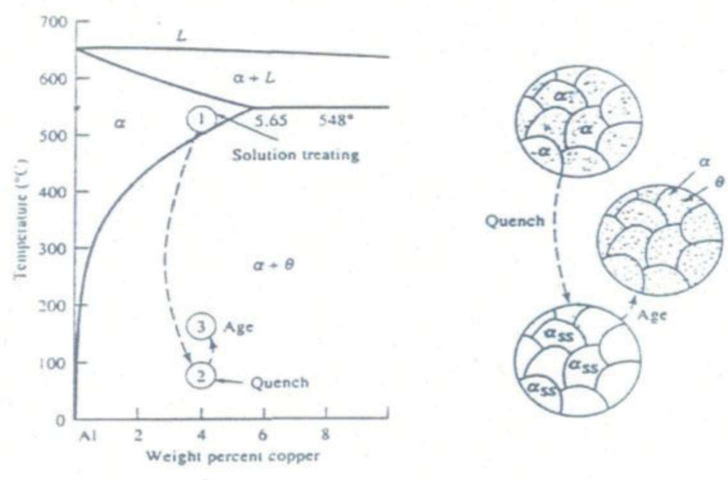

Figure 2.2 The Al-rich end of the Al-Cu phase diagram showing the two age hardening heat treatments and the microstructures involved.[35]

The influence of processing parameters on microstructural changes occurring during heat treatment and their influence on mechanical properties of as-cast Al-Si-Mg alloys (356 and 357) was reviewed by Apelian *et al.*[37] They found that the modified state

showed a higher spherodization rate than the unmodified one. The optimum solution temperature was found to be 540^0C for 356 alloys. Grain boundary melting was observed in the temperature range 560 to 563^0C. They have also established that chemical modification may be used in conjunction with thermal modification to achieve substantial savings in the heat treatment costs.

Earlier studies by Gauthier *et al.*[38] on the solution heat treatment and aging behavior of 319.2 alloy over a temperature range of 480°C to 540°C, for solution times of up to 24 hours, showed that the best combination of mechanical properties was obtained when the alloy was solution heat-treated at 505 °C for 8-16 h, followed by quenching in warm water at 60°C. Garcia-Celis *et al.*[39] found that the aging behavior of heat-treatable cast aluminum alloys depends on the quenching rate. Hot water quenching is recommended for both 356 and 319 alloys since it minimizes quenching stresses and distortion.

Samuel *et al.*[40] reported that solution treatment at 500°C for 8 to 10 hours appeared to be the best solution heat treatment recommended for high Mg-content 319 alloys. In another study[41] on the dissolution and melting of Al_2Cu phase in solution heat-treated unmodified 319.2 alloy solidified at ~10 °C/s, two forms of Al_2Cu were observed, i.e., block-like and eutectic-like. They observed that dissolution of the (Al-Al_2Cu) eutectic takes place at temperatures close to 480°C through fragmentation and dissolution of these phases in the Al matrix. The dissolution is seen to accelerate with increasing solution temperature form 505°C to 515°C. It is essential to avoid too high a solution temperature to prevent any appearance of liquid phase (i.e., incipient melting), which can be detrimental to the mechanical properties.

Gloria *et al.*[42] investigated the dimensional changes during heat treatment of an automotive 319 alloy through T6 and T7 tempers (solution treatment, quenching and artificial aging). They observed that increasing the solution temperature has the greatest influence in the dimensional change of samples due to dissolution of Al-Cu (θ) eutectic phase. However increasing aging temperatures produce expansion due to the transformation of the metastable phases to the equilibrium ones.

2.2.2. Aging Treatment

Any rise in aging temperature will allow atoms to diffuse with time to potential nucleation sites because the supersaturated solid solution αss is unstable. This results in successive precipitation events, starting with the formation of very small clusters of solute atoms fully coherent with the matrix, called Guinier-Preston or G.P zones, followed by one or more intermediate phases, and ending eventually with the equilibrium phase (θ and/or β) in Al-Si alloys. During aging below the G.P zone solvus line, G.P zones and intermediate phases (β' (356 alloys) or θ' (319 alloys) are formed within the matrix. The B' or θ' are heterogeneously nucleated on dislocations if aging is carried out above the G.P zones solvus line. The equilibrium phase β (Mg_2Si) or θ (Al_2Cu) will nucleate and grow at grain boundaries if aging is carried out above the β' or θ' solvus line. This equilibrium precipitate is incoherent with the matrix and its formation always leads to softening, since coherency strains disappear. The properties of a given age-hardening alloy can be greatly varied by controlling the temperature and time of aging. It has also been established that diffusion takes place faster at higher temperatures, but the driving energy for precipitation is less, therefore, precipitation is most rapid at an intermediate aging temperature.

Murayama *et al.*[43] showed that preaging Al-0.65Mg-0.70Si alloy (Si-excess) at 70°C somehow causes a higher density of nucleation sites for the β" precipitates during artificial aging, whereas the nucleation of the β" precipitates during artificial aging is significantly suppressed after room temperature preaging. Preaging (24 hr at room temperature) for 356 alloys is recommended to refine the microstructure through fine dispersion of GP zones obtained during preaging treatment can act as heterogeneous nucleation sites for precipitation at the higher temperature. By this treatment, finer precipitate distributions are obtained.

Shivkumar *et al.*[44] studied the aging behavior of Al-Si-Mg alloys. The precipitation of very fine β'-Mg_2Si during aging leads to a pronounced improvement in strength properties. The hardness of Al-Si alloys depends mainly on the Mg content and aging conditions.[45, 46, 47] In the peak-aged condition, the Al_2Cu and β'-Mg_2Si are metastable phases, coherent with the matrix. Increasing the aging time or aging temperature increases the sizes of these particles, with a gradual change in their chemical composition. As a result, equilibrium θ (Al_2Cu) and β (Mg_2Si) phases in the form of incoherent particles are responsible for the drop in the alloy strength.[40]

Mechanisms of Hardening: the strength of an age-hardenable alloy is governed by the interaction of moving dislocations and precipitates. The obstacles in precipitation hardening alloys that hinder the motion of dislocations may be either the strain field around G P zones resulting from their coherency with the matrix, or the zones and precipitates themselves, or both. The dislocations are forced to cut through them or go around them forming loops. This means that there are three sources for age hardening: strain field hardening, chemical hardening and dispersion hardening.

Dispersion hardening is what happens when the dislocation loops around the precipitate. In dispersion hardening, the yield stress (τ) is the stress necessary to expand a loop of dislocations between the precipitates, see equation (Eq. 3.1);

$$\tau = \frac{2\alpha\mu b}{l} \qquad \text{Eq. 3.1}$$

where α a constant, μ is the shear modulus, b is the Burgers vectors, and l is the separation of the precipitates.

2.2.3. Heat-Treatable Cast Aluminum Alloys

Cast aluminum alloys that contain Cu and Mg are age hardenable alloys. Among them, Al-Si-Mg, Al-Si-Cu and Al-Cu-Mg-Si alloys are those that can be heat-treated to improve the alloy strength. Two of the most commonly used alloys by the automotive industry are 356 and 319 Al-Si alloys, belonging to the Al-Si-Mg, Al-Si-Cu systems respectively.

2.2.3.1. Al-Si-Mg (356) Cast Alloys

Al-Si-Mg alloys are widely used for load-bearing structural components, as well as in less high stress applications. The 356.0 cast alloys are typically used in the production of aircraft pump parts, automotive transmission cases, aircraft fitting and control parts, water-cooled cylinder blocks, and in other applications where excellent castability, good weldability, pressure tightness and resistance to corrosion are required. A356.0 cast alloys are typically used in aircraft structures and engine controls, nuclear engine installations, etc., where high strength permanent mold or investment castings are required. Compared to 319 alloys, 356 alloys have a stricter control over impurities,

especially iron, which is detrimental to the mechanical properties of the alloy. High copper or nickel levels decrease ductility and resistance to corrosion, whereas a high iron level decrease strength and ductility, so limitation control or neutralization of these elements is essential.[48]

Chemical Composition: The chemical composition specification limits for the 356 type alloys are listed in Table 2.6.

Table 2.6 Chemical composition limits of 356 type alloys[48]

AA Alloy	Element (%)										
	Si	Fe	Cu	Mn	Mg	Ni	Zn	Ti	Others		Al
									each	Tot.	
356.0	6.5-7.5	0.6	0.25	0.35	0.20-0.45	...	0.35	0.25	0.05	0.15	Bal
356.1	6.5-7.5	0.5	0.25	0.35	0.25-0.45	...	0.35	0.25	0.05	0.15	Bal
356.2	6.5-7.5	0.2	0.1	0.05	0.30-0.45	...	0.05	0.2	0.05	0.15	Bal
A356.0	6.5-7.5	0.2	0.2	0.1	0.25-0.45	...	0.10	0.2	0.05	0.15	Bal
A356.1	6.5-7.5	0.15	0.2	0.1	0.30-0.45	...	0.10	0.2	0.05	0.15	Bal
A356.2	6.5-7.5	0.12	0.1	0.05	0.30-0.45	...	0.05	0.2	0.05	0.15	Bal
B356.0	6.5-7.5	0.09	0.05	0.05	0.25-0.45	...	0.05	0.15	0.05	0.15	Bal
B356.2	6.5-7.5	0.06	0.03	0.03	0.30-0.45	...	0.03	0.15	0.05	0.10	Bal
C356.0	6.5-7.5	0.07	0.05	0.05	0.25-0.45	...	0.05	0.15	0.05	0.15	Bal
C356.2	6.5-7.5	0.04	0.03	0.03	0.30-0.45	...	0.03	0.15	0.05	0.10	Bal

Physical Properties of 356 Alloy:[48]

Density (at 20 °C)	2685 kg/m^3
Liquidus temperature	615°C
Solidus temperature	555°C
Coefficient of linear thermal expansion (at 20-200°C)	22.5 μm/m.K
Specific heat (at 100°C)	963 J/kg.K
Latent heat of fusion	389 kJ/kg
Thermal conductivity (volumetric, at 20°C)(T6, permanent mold)	167 W/m.K

Castability and Fabrication: Both sand and permanent mold castings possess excellent resistance to hot cracking and solidification shrinkage, as well as excellent pressure tightness and fluidity common among Al-Si cast alloys. The melting temperature range is 675 °-815 °C and the casting temperature is about 675 °-790 °C. For heat treatment, sand cast alloys are given either a T5 or T6 temper treatment, while permanent mold cast alloys are usually given a T6 temper treatment. Different solution and aging treatments applied to 356 type alloys are summarized in Table 2.7. The precipitation sequence in heat-treated and aged (T6) 356 alloy conditions is as follows.[49]

$\alpha_{(SSS)}$ → G.P Zones → intermediate phase β''(Mg_2Si) together with a homogenous precipitation → intermediate phase β' (Mg_2Si) together with a heterogeneous precipitation → equilibrium phase β(Mg_2Si)

where the G P zones appear in the form of needles (~10nm length), and the β (Mg_2Si) phase has an fcc structure (a = 0.639 nm) and appears in the form of rods or plates (0.1um×1um in size).[50, 51] Typical mechanical properties for cast test bars of alloy 356.0 are summarized in Table 2.8.

Table 2.7 Heat treatment for cast test bars of alloys 356.0 and A356.0.[48]

Casting type	Solution		Aging			
			T6[c]		T7[c,d]	
	Temp.(°C)	Time(h)	Temp.(°C)	Time(h)	Temp.(°C)	Time(h)
Sand casting	535-540	12[a,b]	150-155	2-5	225-230	7-9
Permanent mold castings	535-540	8[a,b]	150-155	3-5	225-230	7-9

(a) Soaking-time periods required for average casting after load has reached specified temperature, (b) Cool in water at 65°-100 °C, (c) Start with solution heat-treatment materials, and (d) U.S. Patent 1,822,877.

Table 2.8 Typical mechanical properties of cast test bars of alloy 356.0.[48]

Property	Permanent mold cast	
	T6	T7
Tensile strength, MPa	262	221
Yield Strength, MPa	185	165
Elongation, %	5.0	6.0
Hardness, HB[b]	80	70
Shear strength. MPa	205	170
Fatigue Strength, MPa[c]	90	75
Compact Yield Strength, MPa	180	165

2.2.3.2. Al-Si-Cu (319) Cast Alloys

Al-Si-Cu alloys contain both copper and magnesium as the hardening elements, and are widely used in automotive cylinder heads, internal combustion engine crankcases and piano plates, as well as other applications where good casting characteristics, weldability, pressure tightness and moderate strength are required.

Chemical Composition: The chemical composition specification limits for the 319 type alloys are listed in Table 2.9. Alloy 319.0 refers to the composition of 319 castings, whereas 319.1 and 319.2 refer to those of the ingots. The prefixes A, B, etc. indicate the differences in impurities or minor alloying elements such as Mg. It has been reported that mechanical properties are relatively insensitive to impurities when the impurity limits are exceeded.[48]

Table 2.9 Chemical compositions limits of 319 type alloys[48]

AA Alloy	Element (%)									
	Si	Fe	Cu	Mn	Mg	Ni	Zn	Ti	Others	Al
319.0	5.5-6.5	1.0	3.0-4.0	0.50	0.1	0.35	1.0	0.25	0.50	Bal
319.1	5.5-6.5	0.8	3.0-4.0	0.50	0.1	0.35	1.0	0.25	0.50	Bal
319.2	5.5-6.5	0.6	3.0-4.0	0.10	0.1	0.10	0.10	0.2	0.20	Bal
A319.0	5.5-6.5	1.0	3.0-4.0	0.50	0.1	0.35	3.0	0.25	0.50	Bal
A319.1	5.5-6.5	0.8	3.0-4.0	0.50	0.1	0.35	3.0	0.25	0.50	Bal
B319.0	5.5-6.5	1.2	3.0-4.0	0.8	0.10-0.50	0.50	1.0	0.25	0.50	Bal
B319.1	5.5-6.5	0.9	3.0-4.0	0.8	0.15-0.50	0.50	1.0	0.25	0.50	Bal

Physical Properties of 319 Alloy:[48]

Density (at 20 °C)	2790 kg/m^3
Liquidus temperature	605°C
Solidus temperature	515°C
Coefficient of linear thermal expansion (at 20-200°C)	23.0 μm/m.K
Specific heat (at 100°C)	963 J/kg.K
Latent heat of fusion	389 kJ/kg
Thermal conductivity (volumetric, at 20°C)(T6, permanent mold)	109 W/m.K

Castability and Fabrication: Sand and permanent mold castings have excellent resistance to hot cracking and solidification shrinkage, as well as excellent pressure tightness and fluidity. The melting temperature range is 675°-815°C and the casting temperature is about 675°-790°C. Solution heat treatment is usually carried out at a temperature of 500°C to 505°C, and held for 12 h (sand casting) or 8 h (permanent mold casting) at this temperature. Quenching is accomplished in water at 65° to 100°C. Aging (for T6 temper) is done at 150° to 155°C, for times ranging from 2 to 5 h. In Al-Si-Cu alloys, the age hardening occurs through the precipitation of Al_2Cu as follows.

$\alpha_{(SSS)}$ → $G.P_{(1)}$ zones → $G.P_{(2)}$ (θ'' (Al_2Cu)) → transition phase, θ' (Al_2Cu)

→ Incoherent equilibrium phase θ (Al_2Cu)

where the $G.P_1$ zones are two-dimensional Cu-rich regions oriented parallel to {100} planes, the $G.P_2$ or θ" are considered to be three-dimensional regions having an ordered atomic arrangement, the θ' phase has the same composition as the stable phase and exhibits coherency with the solid solution lattice, while the equilibrium θ is incoherent with the lattice.[49,48]

The effect of increasing the Mg content is well known and has previously been reported by Apelian *et al.*,[37] and Kashyap *et al.*[52] A Mg level of 0.6 wt pct leads to a marked increase in strength compared to the strength obtained in alloys with only 0.2 wt pct Mg. This is related to the increased formation of the β`-Mg_2Si hardening precipitates, with the increased amount of Mg in solid solution. Increasing the Mg content up to 0.45% in A319.2 alloy considerably improves the alloy response to heat treatment in the T5 and T6 tempers, more particularly in the latter case. Typical Mechanical properties for cast test bars of alloy 319.0 are summarized in Table 2.10.

Table 2.10 Typical mechanical properties of cast test bars of alloy 319.0.[48]

Property	Sand cast		Permanent mold cast	
	As Cast	T6	As cast	T6
Tensile strength, MPa[a]	185	250	235	280
Yield Strength, MPa[a]	125	165	130	185
Elongation[a], %	2.0	2	2.5	3.0
Hardness, HB[b]	70	80	85	95
Shear strength. MPa	150	200	165	185
Fatigue Strength, MPa[c]	70	75	70	.....
Compact Yield Strength, MPa	130	170	130	.....
(a) In 50 mm or 2 in. (b) 500kg load; 10mm ball. (c) at 5×10^8 cycles; R. R. Moore type test.				

2.3. MACHINABILITY OF ALUMINIUM ALLOYS

The conditions and physical properties of the work material have a direct influence on its machinability. These conditions, individually and in combinations, directly influence and determine the alloy machinability. Machinability problems during the machining of Al alloys are related to tool wear, quality of machined surface, chip disposal and presence of burrs and all appear to be the ones restricting productivity. The available literature on the turning and drilling shows that machinability of cast alloys through the role of alloying elements, heat treatment and optimization of tool geometry, from the point of view of machined surface quality, all appear to be the dominant fields of past research of interest.[53]

A brief survey of literature on the machinability of commonly used aluminum-silicon alloys, especially for hypo-eutectic alloys (Al-Mg-Si) and (Al-Cu-Mg-Si) in heat treated conditions, is reported. Machinability studies in terms of specific alloying additives[54, 55, 56, 57, 58, 59, 60] and casting mode [63, 61] have been reported for a number of high silicon alloys. Some results on the role of dendrite arm spacing and heat treatment upon machinability have been reported.[61, 62, 63] The influence of metallurgical structural aspects characterized by dendrite arm spacing on the turning machinability of cast Al-Cu, Al-Si and Al-Mg alloys have been reported by Yamada and Tanaka.[55] Obviously refining the dendrite arm spacing reduces tool wear. The cooling rate reduction helps chip control (higher number of chips per unit weight of aluminum machined). Casting mode affects material microstructure and hence, the machinability of the alloy through cooling rate differences. Diecasting material has finer outer structure compared to the subsurface regions, while sand cast material has a coarser structure in general.

2.3.1. Effect of Metallurgical Parameters on Machinability

The most important metallurgical factors that determine the condition of the work material that can influence the outcome of the machinability are:[6]

- Alloy chemistry and alloying additions
- Morphology, size and volume fraction of the constituent phases
- Porosity
- Casting method employed
- Microstructure and properties
- Various treatments that alter the microstructure, cleanliness or strength of the alloy (e.g., grain refining and modification)
- Heat treatment temper and subsequent mechanical properties
- Thermal and Physical properties

2.3.1.1. Alloy Chemistry and Alloying Additions

Chemistry, microstructure, bulk strength, micro hardness and work-hardenability all combine to determine the machining characteristics of an alloy. Some elements are traditionally thought to provide a degree of natural lubricity, other elements are known to increase matrix hardness and still others result in the formation of hard intermetallic phases.[7]

Cast aluminium alloys mainly contain Si, Cu, and Mg as the major alloying elements. Magnesium is normally used to improve the alloy mechanical properties through the precipitation of the Mg_2Si intermetallic. Copper and Mg content in the alloys determines the precipitation strengthening and the volume fraction of Cu-rich and Mg-rich intermetallics obtained. [64] Increasing Cu and Mg content generally increased the

hardness and hence improve machined surface finish and decrease the tendency of an alloy to build up on a cutting tool edge. A small addition of Mg (about 0.3%) to primary 380 die casting alloys improves alloy machinability. Mg hardens the alloy matrix and by doing so reduces the friction between tool and workpiece, resulting in shorter and tighter chips, and providing a better surface finish.[7] Heavy elements such as Mn and Cr tend to combine with Al, Fe, Si, and sometimes Cu to form hard complex intermetallic phases (sludge or fall-out) that cause hard spots and hence increase build-up on the cutting tool edge.

2.3.1.2. Constituent Phases (Morphology, Size and Volume Fraction)

The constituents or phases that exist in the workpiece play an important role in its machinability. These phases are characterized as soluble and non-soluble types. The soluble phases contain elements that dissolve in the aluminum matrix during heat treatment and are characterized as being relatively soft particles. The insoluble phases are those that do not dissolve during heat treatment. They typically contain a large amount of iron (Fe) and consist of very hard, brittle particles when compared to the soluble phases.

The amount of insoluble phases present is also dependent upon the Fe level of the alloy. From a machinability viewpoint, the insoluble particles represent abrasive areas in the metal which can cause excessive tool wear. Lowering the Fe is very effective in suppressing the formation of the needle-like β-Fe intermetallic phase and preventing sludge formation, and hence in improving the tool life.[65] Modification of iron intermetallics by the addition of suitable "neutralizers" like Mn and Cr convert the β-Fe platelets into the more compact and less harmful α-Fe script like phase. Control of

morphology, volume fraction, and distribution of these intermetallics will improve the alloy matrix homogeneity and hence improve its machinability.

2.3.1.3. Porosity

Porosity is one of the defects normally present in Al-Si cast alloys. In commercial practice, the formation of porosity is always considered to be a function of alloy composition, melt hydrogen level, and foundry processing parameters such as cooling rate, modification, alloying elements, grain refinement, inclusions, etc. Iron also plays an important role in porosity formation and hence a deterioration of the mechanical properties and machinability of Al-Si alloys. With mechanical degassing facilities and some typical fluxes, it is possible to minimize the porosity content. Porosity is harmful to the mechanical properties of the casting, especially, the ductility, fracture toughness, fatigue life and, in some cases, the surface finish of the casting.[66] Porosity can cause problems particularly in those workpiece areas where holes are to be drilled or tapped. Excess porosity due to improper gating, venting and injection can result in poor machining characteristics. Porosity due to entrapped air can be minimized by proper gating and venting while porosity resulting from excess lubricant in the die can be reduced by use of minimum and suitable lubricants.

2.3.1.4. Casting Method and Refinement Factors

Sand castings require more machining stock and have a coarser microstructure than either permanent mold castings or diecastings and therefore are more costly to machine. Diecastings are the least expensive to machine. In permanent mold or sand casting, primary silicon is refined by the addition of a small amount of phosphorus (P) to

the molten alloy. Unrefined primary silicon is eight-to ten times the size of refined silicon crystals, and drastically affects the machinability. In conventional die casting, a refining treatment is not necessary, since the primary silicon size obtained is very small even without phosphorus refinement. The silicon size and distribution are controlled by process parameters such as melt temperature, die temperature, and die fill rate. Regardless of the casting method employed, primary silicon acts as a chip breaker.

The silicon content, in particular, affects the progressive wear on the tool and hence the choice of optimum cutting parameters.[67] Optimum machining parameters to ensure production of a good quality holes in such alloys is usually difficult due to the softness of aluminum alloys and to a lesser extent, the presence of hard particles which tend to weld onto the tool face resulting in built-up edge (BUE) formation and production of "erratic" chips and poor surface finish. These promote overheating and premature failure of the cutting tool.[68] For machining aluminum-silicon casting alloys with high silicon content a limit for the applicable cutting speed was found: the point of thermal overloading of the work material in the shear zone by means of a deceptive chip formation.

Inclusions (which could be oxide films, oxidation products or reaction products) may affect the machinability by causing tool wear and poor surface finish. Some common inclusions [69] include:

- Dross or aluminum oxide (Al_2O_3), which is the most common inclusion found in aluminum alloy castings.
- Corundum, which is chemically identical to dross, and occurs in a massive and crystalline form (alpha alumina) and can form by oxidation of melts at

high temperatures, by agglomeration of dross or by the decomposition of refractory material in the furnace.

- Spinel or $MgAl_2O_4$ occurs in alloys containing Mg and results from oxidation, similar to corundum.

Excessive tool wear can come from occluded oxides in the metal casting. Tool breakage can be caused by non-metallic inclusions such as aluminum oxide, corundum and intermetallic complexes or sludge. Sludge can cause excessive tool wear, while hard spots cause tool breakage. Adherence to good foundry practices can minimize or eliminate inclusions in aluminum castings. These include:

- Proper balance of pouring and die temperatures
- Control of Fe, Mn and Cr levels and metal temperature
- Prevention methods such as fluxing and subsequent careful skimming
- Keeping melting equipment, tools, ladles and molds clean.
- Chlorine treatment aid in removal of oxides and other non-metallic inclusions.

2.3.1.5. Microstructure, Grain Refinement and Modification

Strontium, a surface- active element, is a well-known additive in cast Al-Si alloys. It is commonly employed to modify the shape of the eutectic silicon from acicular to fibrous,[70, 71] in order to improve the mechanical properties. Silicon and other hard phases act as abrasives in the relatively soft alloy matrix and tend to reduce cutting tool life. Silicon crystal hardness ranges from 1000-1300 KHN, while that of the alloy matrix seldom exceeds 180 KHN.

A fine, well-modified eutectic silicon structure is far less detrimental to tool life than heavy element intermetallic phases, while tool life decreases with a coarse eutectic

silicon structure. Primary silicon crystals, even if well refined and distributed, are more detrimental than eutectic silicon, and large unrefined primary silicon crystals can seriously degrade tool life. Without phosphorus refinement, the primary silicon crystals are normally quite large but with the addition of 0.01 to 0.05%P will result in satisfactory refinement of the primary crystals.

Hard second phase constituents are detrimental to tool life and, if their presence is necessary, it is best to have them as spheroidized and dispersed as possible. Treatments that refine the microstructure and primary silicon or the eutectic silicon morphology substantially improve the tool life. The finer the grain size the better the overall machining characteristics. Sodium and strontium modification modify the eutectic silicon phase, especially in the case of sand and permanent mold casting, where a coarser grain size is observed than in the case of die casting which already provides a fine microstructure due to the high cooling rates involved. Rare earth additions to Al-Si alloys are found to modify the eutectic Si and improve the mechanical properties,[72] while Mg, and Sr are found to modify the eutectic silicon and Cu strengthens the alloy matrix. Addition of 1 percent Mischmetal (MM) to the 356 alloys containing 0.2 and 0.6 percent Fe was found to refine the microstructure and modify the eutectic silicon. Lanthanum, Ce, and Nd present in the MM form different intermetallic compounds with Al, Si, Fe, and Mg which improve the mechanical properties of the alloys at room and elevated temperatures.[73]

2.3.1.6. Heat Treatment and Mechanical Properties

Heat treatments that increase the hardness will reduce the built-up-edge on the cutting tool and improve the surface finish of the machined part. The specific role of heat

treatment upon the machinability of some of the common alloys is available in literature.[74, 75, 76] Where chip count (number of chips in 100 grams of work material) as a function of feed and speed was used to evaluate the machinability criteria.

Strength affects the machinability of aluminum alloys in that machined surface finish improves as strength increases. The strength level has a strong influence on machining characteristics; typically, higher strength alloys and tempers will result in brighter machined surface finishes, but can also create tool wear problems because of the poor chip formation. A material with high yield strength (force required per unit of area to create permanent deformation) requires a high level of force to initiate chip formation during machining operation. So, as yield strength increases, a stronger insert shape as well as a less positive cutting geometry is necessary to combat the additional load encountered in the cutting zone. The same can be said for increased tensile strength.

Low material hardness enhances productivity, since cutting speed is often selected based on material hardness; the lower the hardness the higher the cutting speed. For a specific cutting speed, tool life is adversely affected by the increase in the workpiece hardness, since the cutting loads and temperatures increase with increasing hardness of the material, thereby reducing tool life.

In practical milling processes, an important factor related to the dimensional accuracy is the material properties (density, modulus, strength, toughness, ductility and hardness). Although the hardness of a material is a crude measure of its strength, it has been used as a relative measure of machinability for machining steels [77] and has been used significantly as an indicator of the machinability of aluminum alloys.[78] There is a direct relationship between the unit cutting force and the Brinell hardness for cast iron,

copper and carbon steel. Thus, this permits the selection of the Brinell hardness of the workpiece as an indicator, with sufficient accuracy, in machining of different aluminum alloys.[79]

Increased material hardness produces higher impact loads as inserts enter the cut, which often leads to a premature breakdown of the cutting edge. As the fracture toughness and ductility increase, plastic deformation takes place and consequently, the cutting resistance becomes larger and the cutting heat will be higher. High temperatures can promote the diffusion of elements and chemical reactions at the interface and finally result in tool damage. So materials with high thermal conductivity increase the rate of heat dissipation and hence decrease the rise in the temperature during machining.

Heat treatment, quenching and straightening can create a large amount of stress in a rod or bar. These residual stresses can manifest themselves as dimensional control problems during machining. Mechanical stress relief is the method applied to remove residual stress without changing other machining characteristics. Residual stress can be induced by a dull cutter that cold works the surface by excessive force. The distribution resulting from machining stresses can be eliminated by employing a series of light cuts as the part approaches its finished size or by stress-relieving the part between rough and finished machining. For heat-treatable alloys, it is preferable to do all rough machining on materials in the solution-treated and aged condition, rather than in the annealed condition because a less ductile structure is more machinable. The distortion resulting from machining stress can often be minimized by purchasing the alloy in a stress-relieved condition, normally designated by T451, T651 or T851, if the metal has been stress-

relieved by stretching. The code Tx52 denotes stress relief by compression, while Tx53, and denotes stress relief by heat treating.

2.3.1.7. Physical Properties of Work Materials

Among the important physical properties of work materials that influence the machinability are; modulus of elasticity, thermal conductivity, thermal expansion and work hardening.[80] Modulus of elasticity is a fixed material property. This particular property is an indicator of the rate at which a material will deflect when subjected to an external force.

General manufacturing practice dictates that productive machining of workpiece material with a relatively moderate modulus of elasticity normally requires positive raked cutting geometries. Positive cutting geometries produce lower cutting forces and therefore, chip formation is enhanced on elastic material using these types of tools. Sharp positive cutting edges tend to bite and promote shearing of material, while blunt negative geometries have a tendency to create large cutting forces which impede chip formation by severely pushing or deflecting the part as the tool enters the cut.[80]

Metals which exhibit low thermal conductivities will not dissipate heat freely and therefore, during the machining of these materials, the cutting tool and workpiece become extremely hot. This excess heat accelerates wear at the cutting edge and reduces tool life. The proper application of sufficient amounts of coolant directly in the cutting zone (between the cutting edge and workpiece) is essential for improving tool life in metals with low thermal conductivities. For comparable mechanical properties such as hardness and strength, for machining an aluminum alloy, we need only about a third of the energy required for machining a steel alloy. This indicates the strong role of thermal properties

(melting point, thermal diffusivity) along with deformation and failure behavior upon chip forming operations.[80]

The coefficient of thermal expansion of aluminum alloys (18-25 μm/m.k) is higher than that of most commonly machined metals. Therefore, the dimensional accuracy of finished parts requires that the part be kept cool during machining. Materials with large thermal expansion coefficients will make holding close finish tolerances extremely difficult, since a small rise in workpiece temperature will result in dimensional change. The machining of these types of materials requires adequate coolant supplies for thermal and dimensional stability. In addition, the use of positive cutting geometries on these materials will also reduce machining temperatures.[80]

When materials which exhibit work hardening tendencies are subjected to increased temperature during machining, higher hardness levels will be obtained in the workpiece. Adequate coolant and positive low force cutting geometries at moderate speed and feeds are normally very effective on machining materials which exhibit both high thermal expansion coefficients and work hardening tendencies.[80]

Good machinable materials should have low ductility, low strain-hardening exponent (n), low fracture toughness, low shear and tensile strength, and low hardness. A strong metallurgical bond (adhesion) between tool and workpiece is undesirable. Very hard compounds, such as some oxides, all carbides, many intermetallic compounds, and elements such as Si embedded in the workpiece material accelerate tool wear. On the other hand, inclusions that soften at high temperatures are beneficial.

2.3.2. Machining

Machining is a term applied to material removal processes in which excess metal is removed by a harder tool, through a process of extensive plastic deformation or controlled fracture. The most common types of machining are:

- Traditional machining (Turning, Milling, Drilling, etc.) and,
- Non-traditional machining (Chemical machining, EDM, ECM, etc.)

2.3.2.1. Machinability

Machinability is an interaction phenomenon between the work piece (material type and form), cutting tool (material type and geometry) and the cutting medium (air, liquid) in a number of different removal sequences (turning, drilling, tapping, milling, sawing etc.) and cutting conditions (speeds, feed and depth of cut). In other words, machinability is a system property that indicates how easily a material can be machined at low cost. It may be described in terms of tool life, ease of metal removal, and workpiece quality.[81] In a collective sense, the most important terms as related to the subject of machinability are:

1. Tool life, wear level, fracture probability
2. Specific power consumed, forces, temperature rise
3. Chip control (chip breakability, chip shape, built-up edge)
4. Dimensional tolerances in terms of surface roughness, microstructure, burr formation etc.
5. Work requirement (machining rate) and
6. Overall cost

Some of the parameters are, however, easy to evaluate and interpret, and consequently commonly used. Tool life and tool wear come in this category along with surface roughness and dimensions. All effort related parameters are rather more difficult to evaluate, but can often provide an explanation for the observed good or bad machinability.

Recent research findings show some interrelationship among these parameters. The rate, at which the tool wears, under a given set of machining parameters, determines the frequency of required tool adjustment and replacement. Chips, their length and curl and the ease or difficulty associated with their removal and handling influence the surface finish. Edge build-up on the cutting tool involves the tendency of the workpiece to adhere to and build up on the cutting edge (relative to a set of machining parameters/conditions), and directly affects the ability to achieve critical dimensional and surface finish control. Surface finish relates to the relative difficulty of achieving a desired degree of smoothness on a machined surface. Work requirements include the forces generated during cutting affecting tool life and the power requirements of the machine tool.

2.3.2.2. Tool Materials

Many types of tool materials, ranging from high carbon steel to ceramics and diamonds, are used as cutting tools in the metal working industry. The best tool is the one that has been carefully chosen to get the job done quickly, efficiently and economically. Good tool materials should have the following properties:[81]

- Higher hardness than the workpiece
- High strength (or hardness) at high temperature
- High impact toughness

- High thermal shock resistance
- Low adhesion (to prevent wear and diffusion)
- Low coefficient of friction
- Low diffusivity to workpiece material

The main cutting tool materials are:[81]

- High Speed Steels (HSS)Cermets, Ceramic Tools, Cast Carbides, Cemented Carbides
- Polycrystalline Cubic Boron Nitride (PCBN)
- Polycrystalline Diamonds (PCD)

2.3.2.3. High Speed Machining

A high productivity cutting process, a decrease in machined surface roughness, a reduction of cutting forces and an improvement in the chip formation can be achieved when increasing cutting speed. In recent years, high speed machining has been widely recognized as one of the key processes in fabricating aluminum parts.[82, 83] This is due to the several advantages of high speed machining offers namely, good surface finish, allowing for the machining of parts with thin cross-sections.[84] However, the higher the cutting velocity, the shorter the contact time between the tool and the hole surface. So that heat produced in the tool-chip contact does not have enough time to affect the surface quality and the dimensional accuracy of the holes produced.[85]

Studies on high speed face milling of 7075-T6 aluminum using a single insert fly-cutter were carried out by Rao *et al.*[86] The results showed that a high cutting speed leads to a high chip flow angle, very low thrust forces, high shear angle, no built up edges and no burrs formation. In drilling, whether, a given drill is run at conventional speed or

"high speed," one pass still equals one hole. Fast or slow, the tool path is still the same. This is why any challenges inherent in the slower process grow more pronounced as spindle speed and feed rate are increased. Among these challenges is how to remove heat and chips as the tool feeds deeper into the hole. Also in both drilling and turning, the added cutting temperature is detrimental to tool life, since it produces excess heat causing accelerated edge wear.

According to Mathew and Oxley [87], the increase in tool-chip interface temperature at higher speeds is sufficiently large compared to the increase in strain rate. Thus, the decrease in the tool-chip interface shear flow stress due to the temperature rise exceeds the increase due to strain rate and hence, low frictional forces are obtained at the tool-chip interface.

At low speed machining, a high speed steel (HSS) drill can be used more effectively. This kind of tool provides high toughness and bending strength. However, at high speed applications, carbide or possibly ceramic are the most required tools. Both of them sacrifice toughness in favor of wear and heat resistance at high speed machining. Tools used for high speed drilling must keep their hardness at high temperatures, i.e., high heat resistance becomes more important for such kinds of tools as the holes get deeper. Ceramic tooling retains its hardness at high temperatures, and runs completely without coolant or lubricant. Unfortunately, ceramic drills can be used only where the material collapses into small and easily manageable chips, limiting its use to cast iron. These limitations make carbide tools the best choice and the most widely applicable tools for dry drilling.

2.3.2.4. Dry Machining

At present, dry cutting technology has become an important topic in the machining field because of environmental issues and the remarkable effect of cost-down[88, 89]. The improvement in the coatings of carbide tools and in chemical and mechanical properties of tool materials has caused the increase of tool working life in machining processes. This fact has allowed the use of the so-called dry machining technology and also machining with minimal quantity of lubricant. The main concern in dry machining is how to protect the tool from heat. The heat generation depends mainly on the tool geometry, the cutting conditions and the tool-chip friction.[90]

Dry drilling of aluminum alloys are mainly controlled by two main parameters; chip removal from the cutting area and heat generation. The dry drilling process is one of the most difficult machining processes due to the special characteristics of drilling process, such as 1) cutting in a closed and limited space, 2) high cutting temperature and 3) difficulty of chip removal. [91, 92] In particular, the drilling of cast aluminum alloys give rise to several unfavorable properties for dry machining including high-thermal conductivity, high-thermal expansion and low-melting point. Dry drilling problems of cast aluminum alloy also include the adhesion (welding) of the chips and the chip/flute clogging on the drill[93, 94]. Therefore, chip formation and chip removal in dry drilling can be considered as the key points in dry drilling.

Heat produced during the dry machining process is critical in terms of tool life and workpiece surface quality.[85] Tool-chip interface temperature plays a major role in determining the hole quality. The tool has to withstand extreme environments which include high temperatures, high frictional forces and large mechanical loads in dry

machining. This requires the tool to possess high hot hardness, high refractoriness (thermal stability) and low coefficients of friction.[95] Several basic causes of tool wear are abrasion, adhesion and diffusion,[96, 97] the magnitude of tool-chip interface temperature causes shift from abrasion to adhesion or from adhesion to the diffusion wear process. Significant temperatures can be obtained in dry machining of aeronautic materials and cause tool wear.[98]

Braga *et al.*[99] investigated the performance of uncoated and coated diamond carbide drills using minimal lubrication (10ml/h of oil in a flow of compressed air) and abundant soluble oil as a refrigerant/lubricant in the drilling of aluminum-silicon alloys (A356). An irregular wear in the surface of the diamond coated drill is observed as well as a decrease in the quality of the holes that it made, when compared to the uncoated one. Coating with TiAlN, or any proprietary coating that offers better insulation for the tool can improve chip evacuation. Greasing the flutes can achieve better chip removal without coolant. Soft lubricating coating which is designed only for chip transport can be applied over the tool's heat-resistant hard coating to keep the hot chip from adhering to the tool.

The effects of cutting fluids and other cutting variables on chip morphology in drilling of aluminum cast alloys were investigated [92, 100]. In drilling processes, the chip is formed within a closed space; hence it is greatly difficult to observe the process of the chip formation and the motion of the chip within the flute directly. The fan shaped chips were formed in the initial stage of the drilling process, and the curling of the chips was caused by the restriction of the flute and impact with the flute, the chip fracture was caused by the bending moment due to the chip/flute impact or chip/hole wall impact.

2.3.2.5. Heat Evolution during Machining

The energy dissipated in cutting operations is largely converted into heat, raising the temperature of the chip, tool, and workpiece. Shear processes are most effective in producing heat. There are three sources for heat development:[101]

- The shear process itself (primary shear zone plastic deformation)
- The tool-chip interface friction (secondary shear zone friction)
- The flank of the tool rubbing the workpiece (especially if the tool is dull).

For many materials it is thought that tool wear is directly linked to the influence of temperature within the primary and secondary shear zones. Interaction of the heat sources, combined with the geometry of the cutting area, results in a complex temperature distribution as shown in Figure 2.3.[80]

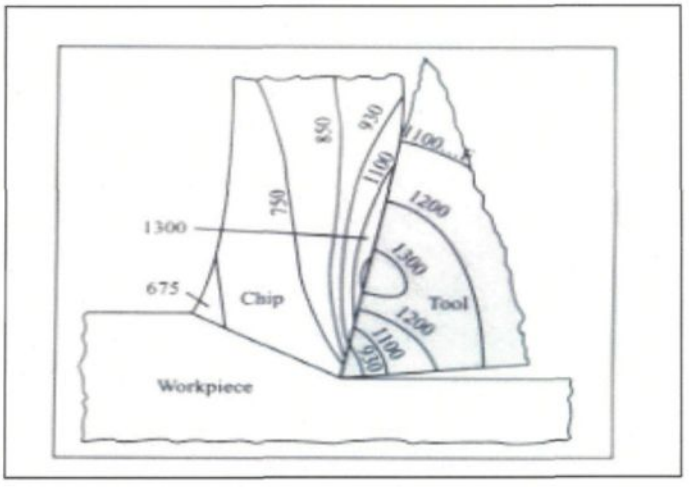

Figure 2.3 Typical temperature distribution in the cutting zone.[80]

The temperature generated in the shear plane is a function of the shear energy and the specific heat of the material. The temperature increase on the tool face mainly

depends on the friction conditions at the interface. Temperature distribution will be a function of, among other factors, the thermal conductivities of the workpiece and the tool materials, the specific heat, cutting speed, depth of cut, and the use of a cutting fluid.

The cutting temperature is the key factor which directly affects cutting tool wear, workpiece surface integrity and machining precision in the high speed machining (HSM) process. Using the infrared thermometer as a remote sensor can solve the problem of measuring the temperature in high-speed milling and also it can be used as an approach to reveal the cutting mechanism. Wang *et al.*[102] studied the temperature effects in curled chip formation, using an infrared (IR) imaging system for measuring the transient temperature distributions within curled chips. They show a great feasibility of using the IR measurement system for measuring the temperature distributions in curled chips. Also they provide a comprehensive thermal analysis of the curled chip. They observed that the temperature distributions within chips vary during their formation and reach the maximum value at the root of curled chips. This maximum value of temperature increases with the increase in cutting speed.

The temperature field developed at the tool-chip interface and the transient temperature distributions in the chip and the cutting tool play a major role in the chip formation process which strongly affects the machining performance. There is an ideal combination of tooling feed rate, speed, and application of coolant to machine the component well. The microstructure and mechanical properties of the feed castings provide information about their machinability. Chip formation also reveals information about machinability, and its form can influence the removal after cutting.

2.3.2.6. Analysis of Heat Generation During Metal Cutting

The heat generated during a cutting process can be predicted as the following:[101]

$$Pm = Fc \times V \qquad \text{Eq. 2.1}$$

where Pm is the energy consumption (or heat generated), Fc is the cutting force and V is the cutting speed. Also Pm is given by,

$$Pm = Ps + Pf \qquad \text{Eq. 2.2}$$

where Ps is the heat generated in primary shear and Pf is the heat generated in secondary shear zone (friction zone). The heat generated in the secondary shear zone can be predicted by the following equation.

$$Pf = Ff \times V0 \qquad \text{Eq. 2.3}$$

where Ff is the friction force and $V0$ is the chip velocity. Also the chip velocity can be calculated from the next equation.

$$V0 = V \times Rc \qquad \text{Eq. 2.4}$$

where Rc is the cutting ratio as expressed by the ratio of the undeformed chip thickness (ac) to the depth of cut(a0).

$$Rc = ac / a0 \qquad \text{Eq. 2.5}$$

Temperature in the primary shear zone can be predicted by the following. If we suppose that Ps is heat generation in the primary zone and Γ is the portion of Ps which

is conducted to the work piece, then, this portion will not cause a temperature increase in the chip.

$$(1-\Gamma)Ps = \theta s c \rho V a c a w$$

Eq. 2.6

where θs is the average temperature rise in shear zone, $_C$ is specific heat, ρ is the density, V is the cutting speed, ac is the undeformed chip thickness and aw is the depth of cut.

$$\theta s = (1-\Gamma)Ps / c \rho V a c a w$$

Eq. 2.7

Temperature in the secondary shear zone (friction zone) can also be predicted by the following:

$$Pf = \theta f c \rho V a c a w$$

Eq. 2.8

where θf is the average temperature rise in chip due to frictional heating and can be calculated from the following equation:

$$\theta f = Pf / c \rho V a c a w$$

Eq. 2.9

The maximum temperature in the chip can be calculated from the following equation.

$$\theta \max = \theta m + \theta s + \theta 0$$

Eq. 2.10

where $\theta \max$ is the maximum temperature of the chip and θm is the maximum temperature rise in chip passing friction zone, while θs is the temperature rise in chip

passing primary zone and $\theta 0$ is initial temperature.[101] Heat dissipation or heat generation during metal cutting can be predicted using the following equation.

$$Pm = Hc + Hw + Ht \qquad \text{Eq. 2.11}$$

where Pm is the total heat generation, Hc is the heat transfer through the chip, Hw is the heat transfer through the workpiece and Ht is the heat transfer through the tool (may be neglected).

2.3.3. Heat Built-Up on the Cutting Tool Edge (BUE)

Heat build-up on the cutting tool edge is the biggest drawback in maintaining material machining characteristics and the productivity of the machining operation. In general, the softer alloys and, to a lesser extent, some of the harder alloys are likely to form a built-up edge on the cutting lip of the tool. This edge consists of aluminum particles that have become welded to the tool edge because they were melted by the heat generated in cutting. Essentially, what happens is that the aluminum begins to be cut by the aluminum welded to the cutting edge. This results in deterioration of chip size, tool life, surface finish, part dimensional control and effectiveness of the coolant.

Built-up edge occurs during the machining process for Si up to 12% in Al-Si alloys. The BUE is one of the major sources of surface roughness and also plays an important role in tool wear. The workpiece material adheres to the rake face of the tool in two forms; Built-up Edge (BUE) and built-up layer BUL. The tool damage is mainly caused by the formation of such type of layers.

At higher rates of metal removal, i.e. at higher speed or feed, a built-up edge is no longer observed, a transition from built-up edge to flow zone is strongly influenced by

both speed and feed and occurs in a range of cutting conditions commonly encountered in industrial machining operations. The flow zone is usually more strongly bonded to the tool than the built-up edge. The flow zone is a "stable instability" or "thermoplastic shear band" as a preferred term description. The behavior of work material in the thermoplastic shear bands is probably the most important property governing its "machinability" in high speed machining.[103]

2.3.4. Chip Formation

Chip formation process is influenced by many factors including cutting conditions, cutting fluids, tool geometry, chip control devices, machine tool dynamics and tool and work material properties. In drilling and tapping, the specific type of the chip depends on a number of parameters, in particular, the drilling speed, the feed rate and mechanical and thermo-physical properties of the workpiece.

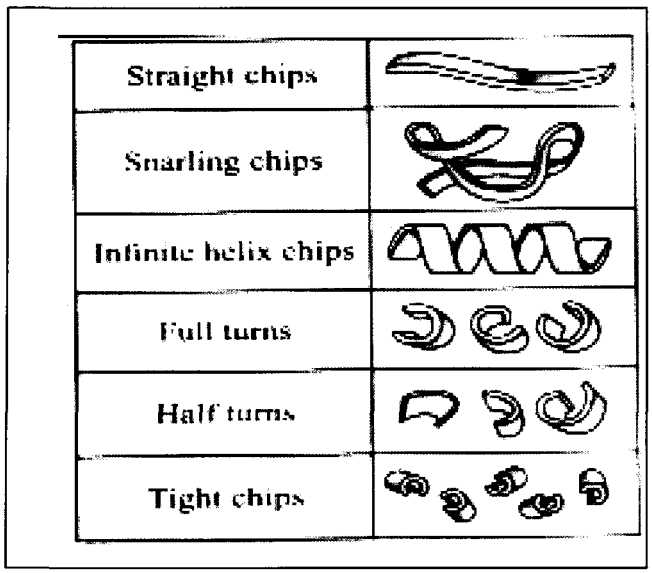

Figure 2.4 Various types of chip formations.[80]

Machinability groupings for aluminum alloys are useful in specifying tool forms. For this purpose, alloys are classified into five groups: A, B, C, D, and E, in increasing order of chip length and in decreasing order of finish quality. There are three categories of chips, namely:

- Continuous chips
- Discontinuous or segment chips
- Continuous with built-up edge chips

The most common types of continuous and discontinuous chips are namely; straight chips, snarling chips, infinite helix chips, full turn, half turn and tight chips as shown in Figure 2.4. [80] Continuous chips are observed during the machining of ductile metals. There are mainly three types of continuous chip; straight, snarling and infinite helix chips. Straight chips are usually the most troublesome. They string out all over the machine tool and get snarled in the tool, workpiece, and fixturing which cause tooling to break. They also jam up chip handling equipment and are difficult to remove as well as get more dangerous especially when they begin to whip around. Snarling chips are continuous chips much the same as straight chips. They are generally caused by the same conditions as straight chips and create the same problems. Infinite helix chips are chips that are near the breaking point. The problems this type of chip creates are similar to those created by straight chips.

Discontinuous chips are observed during machining of brittle metal and ductile metals under poor machining conditions. In these cases, the metal compresses until it reaches a point where rupture occurs and the chip separates from the unmachined portion. Full turn chips are not usually a problem as long as they are consistent and without

occasional stringers. Half turn chip is known as the classic chip form however, tight chips are a sign that poor tool life or premature tool failure may occur.

Examining the chips that are coming off from machining a workpiece will give a lot of information as to how well the job is going, how tool wear is progressing, and why premature tool failure or short tool life is occurring. Many times a straight, snarled or infinite helix chip will be generated at the start of a cutting operation, when the insert is new. As the insert begins to wear, the chip gradually becomes well shaped and properly broken. It may even progress into a tight chip and eventually cause catastrophic tool failure.

As a result of high temperature, high pressure and high frictional resistance against the flow of the chip along the chip-tool interface during machining, small particles of metal adhere to the edge of the cutting tool while the chip shears away. As the cutting process continues, more particles adhere to the cutting tool and larger build-up results, which affects the cutting action. The built-up edge increases in size and becomes more unstable. The build up and breakdown of the built-up edge occur rapidly during the cutting action and cover the machined surface with a multitude of built-up fragments. Chip formation in the drilling processes is governed by the following points[104]:

- The rake faces of the first part of the cutting lip in the straight drill are not flat and the rake angle varies along the cutting edges. The twisted rake face gives the chip a rotation, ω_c, on the axis of the drill.
- The cutting speed varies proportionally with the distance from the drill center, which cause a strong side curling, or large ω_z

- The greatly side curled chip is forced to curl in another direction by the obstruction of the web and flutes of the drill, thus chip with a large ω_x

Given the three components of angular velocity ω_c, ω_z and ω_x , the chip experiences a helical motion with the angular velocity ω_h, which is the resultant of these three angular velocity components, see Figure 2.5. As the drilling process progresses, the weight of the chip increases constantly and the center of gravity goes away from the root of the chip. The chip flow gradually becomes impeded by the web and flutes, which produce a resistance force on the chip. This force develops a bending moment, or non-uniform stress distribution, at the root of the chip, which causes unstable or fragmented chips. The fragmentation acts to decrease the bending and the resistance force. In other words, the chip changes its form to meet the external force and the constraints governing its flow. The resistance force acting on the chip contributes to the total thrust and torque on the drill.

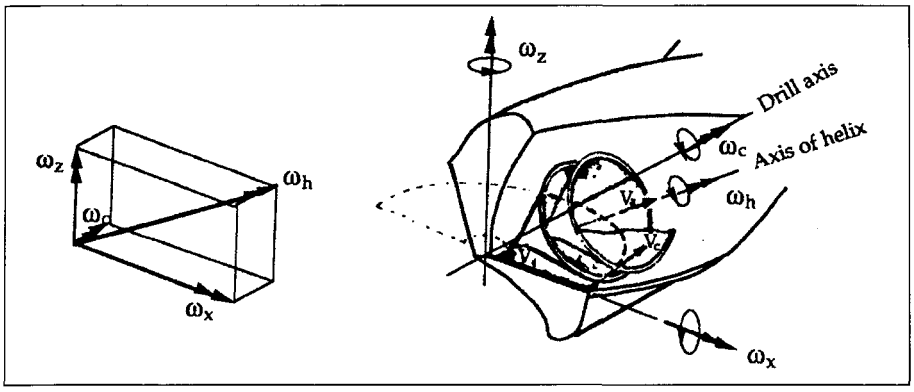

Figure 2.5 Conical helical chip produced by the twisted part of the cutting lip.[104]

2.3.4.1. Chip Formation in Drilling

In material such as aluminum, proper selection of feeds and speeds usually causes the chips to break up and allows them to be flushed out of the cut by the cutting fluid. In drilling processes, the chip is formed within a closed space; hence it is very difficult to observe the process of the chip formation and the motion of the chip within the flute directly. The fan shaped chips were formed in the initial stage of drilling process, and the curling of the chips was caused by the restriction of the flute and impact with the flute, the chip fracture was caused by the bending moment due to the chip/flute impact or chip/hole wall impact.

In drilling and tapping, the specific type of the chip depends on a number of parameters, in particular, the drilling speed, the feed rate and mechanical and thermo-physical properties of the workpiece. Discontinuous chips are observed during machining of both 356 and 319 alloys. In these cases, the metal compresses until it reaches a point where rupture occurs and the chip separates from the unmachined portion. Full, half turn and helical chips are generated at the start of a cutting operation when the drill is new (shearing process). As the drill begins to wear, the chip gradually becomes well deformed and both shearing and deformation occurs.

Studies of chip formation during the drilling process are complicated to a great extent by the peculiarities of the drilling process. One of these, a chip after its formation remains in contact with the tool and workpiece for a significantly long time during its path through the chip removing channels of the hole. And additional friction-induced heat release takes place in the course of the drilling. In a drilling operation, small well-broken chips are desirable. As the chips get larger, they cannot move easily through the flutes.

This increases torque requirements, perhaps causing drill breakage. During formation, the chips rotate with the drill and impact the hole wall or interior of the flute. This impact produces a bending moment in the chip and causes fracture.[105]

Kruzhanov and Zeitz [106] investigated the mechanism of chip formation during high speed drilling of steel, titanium and aluminum alloys. They observed that a transition from continuous ribbon to a segmented chip could take place when drilling in aluminum alloy, which has greater thermal conductivity than the titanium alloy. They also observed that increasing cutting speed as well as feed rate caused the formation of single segments. Batzer *et al.*[100] investigated the effect of cutting fluids and other process variables on chip morphology when drilling cast aluminum alloys. Their results show that the significant variables affecting chip size are the feed, material, drill type and to a lesser extent, cutting fluid presence and drill speed.

A squeezing of the chip, caused by the geometry of the drill, was accompanied by the formation of extended segments and separated by shear bands. The state of ductility/brittleness of a curled chip is greatly influenced by the temperature fields generated and transmitted through the chip. The breakability of the curled chip is mainly dependent upon the brittleness of a curled chip and the mechanical forces, bending moment and torque, etc. applied on the pre-curled chip.

A simulation using fracture criteria to obtain discontinuous chip formation was presented by Marusich and Oritiz.[107] Exceeding a "critical effective plastic strain", a crack is initiated on the free surface of the chip and propagates into the interior. This approach is interesting especially for the simulation of machining brittle workpiece materials. The two main chip formation mechanisms .i.e. the two physical processes of

material separation which are shearing and cracking, were established by Poulachon and Moisan.[108] They observed that a competition exists between work hardening and thermal softening during chip formation in high speed cutting of hardened steel. Haan et al [109] studied the function of cutting fluid in drilling of aluminum alloys. Their results indicate that cutting fluids act as lubrication at the margins of the drill and assist in the evacuation of chips out of the hole and therefore, affect both surface finish and hole quality.

Transmission electron microscopy examination of the body of chips shows that shear strain takes place by dislocation movement with the formation of cells or subgrains elongated in the direction of shear strain. Strain on the shear plane is concentrated in a narrow zone where, recovery processes annihilate the strain hardening. Thermoplastic instabilities with the high temperature rise promote recovery processes. This then deforms by dislocation movement with strain hardening until the next instability is generated; a cyclical process reflected in the shape of the chip. Chip formation is achieved by dislocation movement and periodic fracture.[103]

2.3.5. Tool Geometry and Coating

Tool material, coating and geometry exercise an indirect effect on the alloy machinability and can be used to overcome difficult conditions presented by the work material. The right choice of coating can extend the life of the carbide tool considerably by offering an additional line of defense against the friction and the heat of the high-speed machining process.[80] Titanium aluminum nitride (Ti, Al) N can be deposited on the tool surface by the PVD process, and can act as a thermal barrier between the tool and the chip (thermal conductivity is about (0.05kW/mK). This type of coating has advanced wear resistance and oxidation resistance and offers an advantage for dry machining of

cast iron, alloyed steels and aluminum alloys with 10% of Si. Titanium carbon nitride (Ti, C) N coating guards the tool against wear, particularly when machining steel. Though TiN cannot match the performance of the previous two coatings in their ideal applications, it is generally cost-effective and universally applicable. Diamond is the ideal coating when machining aluminum alloys without any coolant where high wear-resistant cutting tools are required.

2.3.6. Cutting Fluids

In machining, coolants and lubricants improve machinability, increase productivity by reducing the tool wear and extend the tool life. Shaw[110] lists the functions of cutting fluids; it acts as lubrication at low cutting speeds and heat removal at high cutting speed. Cassin and Boothroyed[111] suggest that the functions of the cutting fluids are; extracting the heat and reducing the tool wear, providing lubrication, improving the surface finish and modifying the shear flow properties of the material in the primary and secondary deformation zones. Burant and Skingle[112] observed that the cutting fluid reduced the smearing and galling effect on the cutting tool, thereby assisting in the evacuation of chips.

2.3.7. Tool Wear

Cutting tool life is one of the most important economic considerations in metal cutting. Cutting tools must afford extreme heat, high pressure, abrasion, and thermal or mechanical shock. Extreme heat degrades binders and other tool constituents, and can also trigger detrimental chemical reactions between tool and workpiece. Basic failure

mechanisms include crater wear, thermal deformation and cracking, nose wear, depth-of-cut notching, built-up edge, chipping, fracture, and flank wear.

Clearly, any tool or work material improvements that increase tool life without causing unacceptable drops in production will be beneficial. In order to form a basis for such improvements, efforts have been made to understand the behavior of the tool, how it physically wears, the wear mechanisms, and forms of tool failure. Tool wear vs. time at different cutting speed is shown in Figure 2.6.[113]

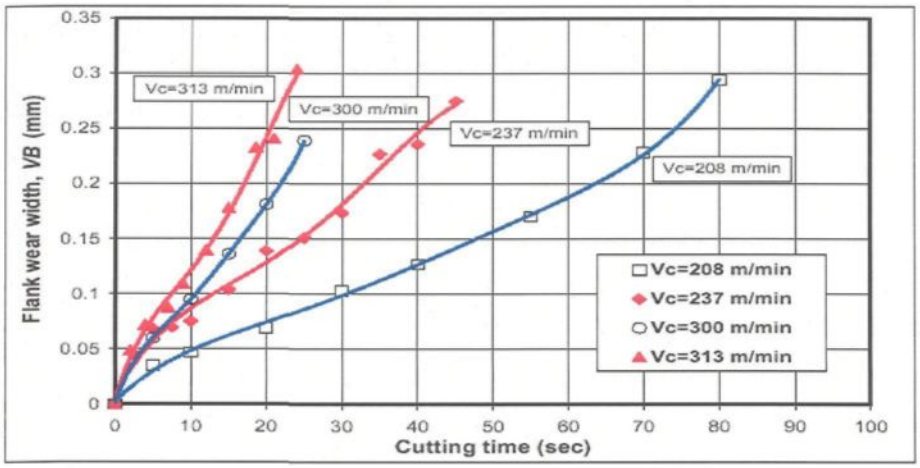

Figure 2.6 Tool wear vs. time.[113]

First, the cutting edge loses its sharpness rapidly following by a uniform wear and ending in rapid wear due to the high-temperature generated. Crater wear may occur on the rake face or on the top of the insert, where chemical interaction between the hot chip and the tool material can occur. At high speeds, the tool material may dissolve into the chip; tiny particles of the tool may adhere to the chip and get carried away. Excessive cratering weakens the cutting edge, inhibits proper chip flow, and increases heat and pressure on the tool. At very high speed machining conditions and when machining tough materials, crater wear can be the factor which determines the tool life.

Excessive heat softens the tools (edge depression and body bulging) and makes it flow plastically at high stress. Insert material is actually worn away and the nose of the insert becomes distorted. One of the best solutions to minimize the thermal deformation of the carbide insert is to select the carbide with low cobalt content and fine grain size.

Thermal and/or mechanical shock also plays an important role in tool failure. Thermal shock, by definition is a rapid heating and cooling of the tool, this is more common in milling operations, in which the insert heats up during cutting and cools down while away from the cut. Large differences in temperature between the cutting edge and the bulk of the insert cause evenly spaced cracks perpendicular to the cutting edge. Cracks will slowly progress, leading to chipping and eventually the fracture of the tool. Mechanical shock is also a factor in milling, as well as in machining interrupted surfaces in turning, depending on the operation involved and the condition of the workpiece.

Selection of carbide grade insert with high cobalt content provides high toughness and high resistance to thermal shocks as well as resistance to cracking. Rubbing or abrasion and local deformation of the tools leads to nose wear during machining hard alloy steel. As the tool nose wear occurs, part size changes and surface finish deteriorates. ***Gradual Wear Mechanisms:*** The four basic wear mechanisms affecting tool material have been categorized as:[114]

- Abrasion
- Adhesion
- Diffusion
- Oxidation

Hard inclusions in the workpiece microstructure cause abrasion of the tool. This kind of wear predominates at relatively low cutting temperatures. Adhesion is commonly observed as built-up edge (BUE) on the top face of the tool. High pressure/temperature causes adhesion of asperities between the tool and the chip. Diffusion wear, micro-transfer on the atomic scale takes place at high temperatures and pressures. In the exchange of atoms across the contact boundary between the chip and the tool, hard atoms may be loosened from the tool side. The rate of diffusion increases exponentially with increases in temperature. At elevated temperatures, the oxidation of the tool material can induce high tool wear rates. The oxides that are formed are easily carried away, leading to more wear. The different wear mechanisms as well as the different phenomena contributing to the attritions wear of the cutting tool are dependent on a multitude of cutting conditions and especially on the cutting speeds and cutting fluids.

The machine operator can observe several indications of the progression of the physical wear prior to total rupture of the edge. Among such indications are:[114]

- Increase in the flank wear size above a predetermined value;
- Increase in the crater depth and width of the crater, in the rake face;
- Increase in the power consumption, or cutting forces required to perform the cut;
- Failure to maintain the dimensional quality of the machined part within a specified tolerance limit;
- Significant increase in the surface roughness of the machined part;
- Change in the chip formation due to increased crater wear or excessive heat generation.

2.3.8. Drilling

Drilling is one of the most complex machining processes and most commonly associated with producing machined holes. The chief characteristic that distinguishes it from other machining operations is the combined cutting and extrusion of metal at the chisel edge in the center of the drill. Although many other processes contribute to the production of holes, including boring, reaming, broaching, and internal grinding, it is drilling that accounts for the majority of holes produced in the machine shop. Drilling is the most simple, quick and economical method of hole production.

The high thrust force caused by the feeding motion first extrudes metal under the chisel edge. Then it tends to shear under the action of a negative rake angle tool. The cutting action along the lips of the drill is not unlike that in other machining processes due to variable rake angle and inclination angle and hence, there are differences in cutting action at various radii on the cutting edges. Both lips for the twist drill (cutting edges) operate with variable rake angle, inclination angle, and clearance angle along the cutting edge. The flutes of the drill play the important role of conveying the chips out of the hole and the helix angle of the drill is important in this connection.[80]

The machine settings used in drilling reveal some important features of this hole producing operation. Depth of cut, a fundamental dimension in other cutting processes, corresponds most closely to the drill radius. The undeformed chip width is equivalent to the length of the drill lip, which depends on the point angle as well as the drill size. For a given set-up, the undeformed chip width is constant in drilling. The feed dimension specified for drilling is the feed per revolution of the spindle. A more fundamental quantity is the feed per lip. For the common two flute drill, it is half the feed per

revolution. The undeformed chip thickness differs from the feed per lip depending on the point angle. The spindle speed is constant for any one operation, while the cutting speed varies all along the cutting edge. Cutting speed is normally computed for the outside diameter. At the center of the chisel edge the cutting speed is zero; at any point on the lip it is proportional to the radius of that point. This variation in cutting speed along the cutting edges is an important characteristic of drilling.[80]

In drilling, whether, a given drill is run at conventional speed or "high speed," one pass still equals one hole. Fast or slow, the tool path is still the same. This is why any challenges inherent to a slower process grow more pronounced as spindle speed and feed rate are increased. Among these challenges is how to remove heat and chips as the tool feeds deeper into the hole.

2.3.8.1. Drill Nomenclature

A drill is an end cutting tool for producing holes. It has one or more cutting edges, and flutes to allow fluids to enter and chips to be ejected. There are many different types of drills. Examples are twist drills for general machining, rock drills for mining minerals, laser drills for extremely small holes, spade drills for large holes, and gun drills for deep holes. The most important type of drill is the twist drill. Important nomenclature is illustrated in Figure 2.7.

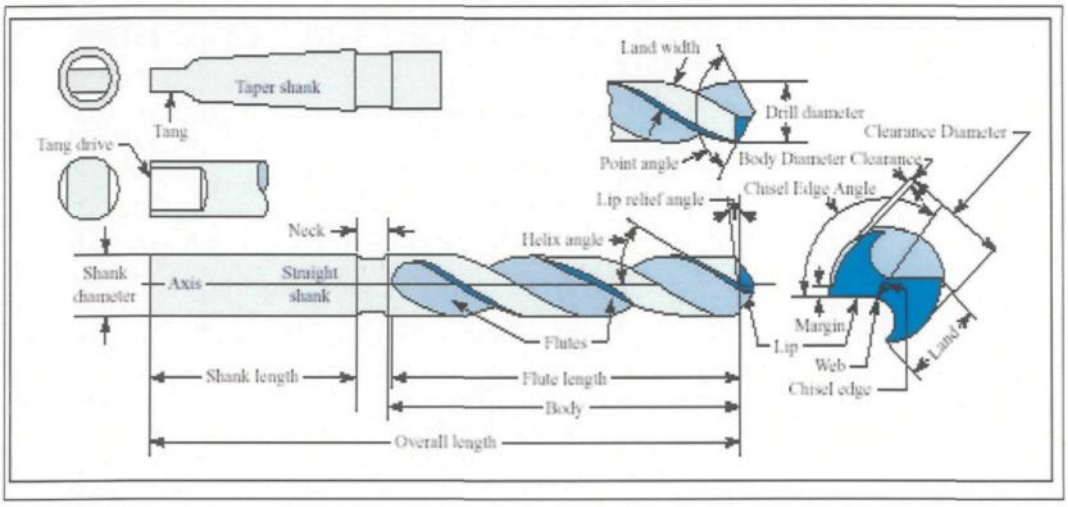

Figure 2.7 Nomenclature of a twist drill shown with taper and tang drives.[115]

It was reported that the first and second drilling machines were developed in 1801 by an engineer at Soho Foundry.[116] The first machine-made twist drill development actually began with the introduction of high-speed steels around the year 1900.[117] A variety of drills, such as split-point, helicon and multifaceted, were developed for specific functions around 1950.[118]

The drill is composed of a shank, body, and point. The shank is the part of the drill that is held and driven. It may be straight or tapered. The body of the drill extends from the shank to the point, and contains the flutes. Flutes are grooves that are cut or formed in the body of the drill to allow fluids to reach the point and chips to reach the workpiece surface. Although straight flutes are used in some cases, they are normally helical. The land is the remainder of the outside of the drill body after the flutes is cut. The land is cut back somewhat from the outside drill diameter in order to provide clearance. The margin is a short portion of the land not cut away for clearance; it preserves the full drill diameter. The web is the central portion of the drill body that connects the lands. The edge ground on the tool point along the web is called the chisel

edge, it connects the cutting lips. Drills with various helix angles are available for different operational requirements. The included angle between the drill lips is called the point angle. It is varied for different workpiece materials.[115]

To understand the mechanics of the drilling process, one must understand two types of cutting processes: orthogonal cutting and oblique cutting. The main difference between the two cutting processes is the orientation of the tool's cutting edge with respect to the direction of the cutting velocity. According to Merchant's description of orthogonal cutting [119] ," the tool is set so that its cutting edge is perpendicular to the direction of relative motion of the tool and workpiece and generates a plane surface parallel to the original work surface". The second type of cutting process is oblique cutting. In oblique cutting processes, the cutting edge is rotated at an angle (90°-i) relative to the direction of tool motion. The drilling process is treated as double oblique-cutting process by the lips, with varying inclination angles and geometry along the cutting edges.

During the drilling process, the observable forces are the thrust applied by the rotating drill to the workpiece and the torque supplied by the spindle to maintain the drill rotation. The trust and torque of a general drilling process are caused by drill point. The drill point is the main cutting region and consists of the web and lips. Besides thrust and torque, a drill is subjected to a cutting force in the lateral direction due to unsymmetrical lips or misalignment of the drill axis. A drill subjected to this kind of force will change the thrust and torque magnitudes, which is an indication of tool wear or system instability.

2.3.8.2. Operating Conditions

Drill manufacturers and a variety of reference texts provide recommendations for proper speeds and feeds for drilling a variety of materials. Cutting speed may be referred to as the rate that a point on a circumference of a drill will travel in 1 minute. It is expressed in surface feet per minute (SFPM). At low speed, the drill might chip or break; high speed dulls the cutting lips.[115]

Cutting speeds depend on the following seven variables:

- Type of workpiece material,
- Cutting tool material and diameter,
- Type and use of the cutting fluids,
- Rigidity of the drill press,
- Rigidity of the drill,
- Rigidity of the work setup, and
- Quality of the hole required.

Work material and cutting speed are the most important variables and should be considered prior to the drilling process. Hard cutting tool material can be used at high speeds. Large drill diameters must revolve at low cutting speeds and a short drill has a better rigidity. The formula normally used to calculate cutting speed is as follows:

$$SFPM = (Drill\ Circumference) \times (RPM) \qquad \text{Eq. 2.12}$$

where, *SFPM* are equal to surface feet per minute, or the distance traveled by a point on the drill periphery in feet each minute. *Drill Circumference* is equal to the distance

around the drill periphery in feet and *RPM* are equal to the number of revolutions per minute. In the case of a drill, the circumference is:

$$Drill\ Circumference = Pi/12 \times (d) = 0.262 \times d \quad \text{Eq. 2.13}$$

where, *Drill Circumference* = the distance around the drill periphery in feet, Pi is a constant of 3.1416 and d is the drill diameter in inches. By substituting for the drill circumference, the cutting speed can be written as:

$$SFPM = 0.262 \times d \times RPM \quad \text{Eq. 2.14}$$

Feed in drilling operations is expressed in inches per revolution, or IPR, which is the distance the drill moves in inches for each revolution of the drill. The feed may also be expressed as the distance traveled by the drill in a single minute, or IPM (inches per minute), which is the product of the RPM and IPR of the drill. It can be calculated as follows:

$$IPM = IPR \times RPM \quad \text{Eq. 2.15}$$

Where, *IPM* are equal to inches per minute, *IPR* are equal to inches per revolution and *RPM* are equal to revolutions per minute.[115]

2.3.9. Tapping

Tapping is defined as a process for producing internal threads using a tool that has teeth on its periphery to cut threads in a pre-drilled hole. A combined rotary and axial relative motion between tap and workpiece forms threads. Tap nomenclature is shown in Figure 2.8.

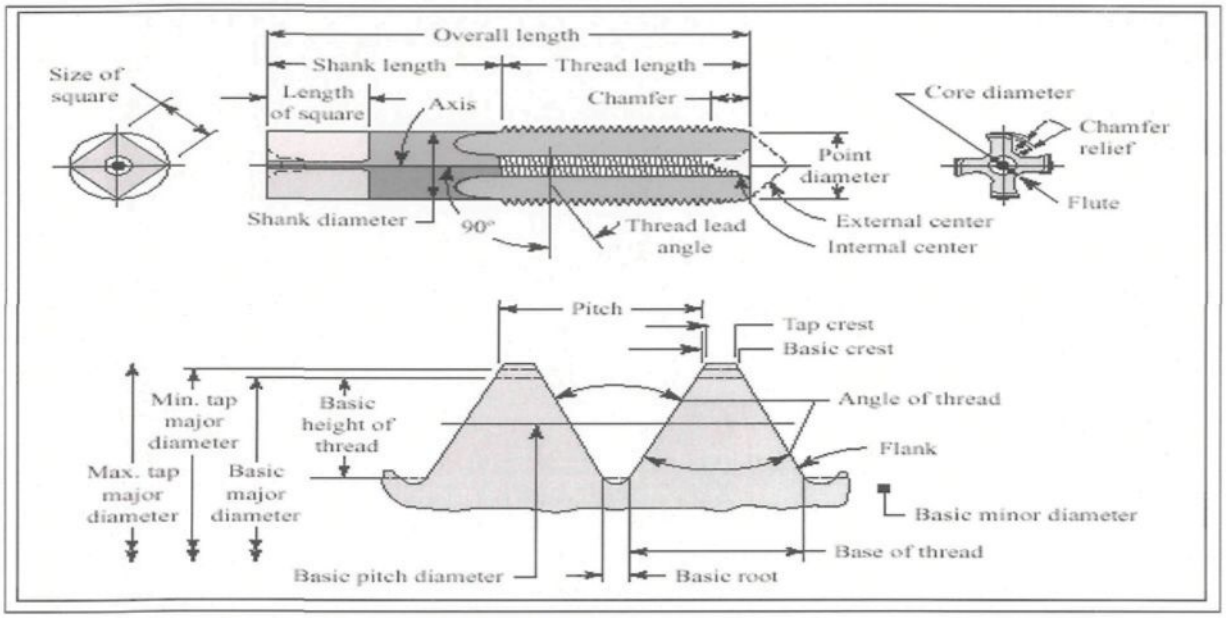

Figure 2.8 Tap and Thread Nomenclature.[120]

Tap Nomenclature: In modern manufacturing, it is important to have a working knowledge of screw thread terminology. A 'right-hand thread' is a screw thread that requires right-hand or clockwise rotation to tighten it. A 'left-hand thread' is a screw thread that requires left-hand or counterclockwise rotation to tighten it. 'Thread fit' is the range of tightness or looseness between external and internal mating threads. 'Thread series' are groups of diameter and pitch combinations that are distinguished from each other by the number of threads per inch applied to a specific diameter. The two common thread series used in industry are the coarse and fine series, specified as UNC and UNF.[120]

Chamfer is the tapering of the threads at the front end of each land of a chaser, tap, or die by cutting away and relieving the crest of the first few teeth to distribute the cutting action over several teeth. Crest is the surface of the thread which joins the flanks of the thread. Flank is the part of a helical thread surface which connects the crest and the

root, and which is theoretically a straight line in an axial plane section. Flute is the longitudinal channel formed in a tap to create cutting edges on the thread profile and to provide chip spaces and cutting fluid passage. The land is one of the threaded sections between the flutes of a tap. The lead of thread is the distance a screw thread advances axially in one complete turn. Pitch diameter is the diameter of an imaginary cylinder or cone, at a given point on the axis of such a diameter and location of its axis. The spiral flute-bottoming tap is made in regular and fast spirals, that is, with small or large helix angle. The use of these taps has been increasing since they pull the chip up out of the hole and produce good threads in soft metals.[120]

Taps are made in many styles, but a few styles do 90 percent of the work. Material used for taps is usually high-speed steel in the M1, M2, M7, and sometimes the M40 series of cobalt high-speed steels. A few taps are made of solid tungsten carbide. A tap drill is merely a convenient way to refer to the proper size drill to be used before using a tap. The trend today in many factories, in order to save taps, time and rejects, is to use 60 to 65 percent of thread to determine tap drill sizes. The deeper the hole is threaded, the longer it takes to drill and tap and the more likely it is that the tap will break.[120]

CHAPTER 3

EXPERIMENTAL PROCEDURES

CHAPTER 3

EXPERIMENTAL PROCEDURES

3.1. INTRODUCTION

In the present study, 356 and 319 type alloys were selected as representing the Al-Si-Mg and Al-Si-Cu alloy systems, respectively. The iron levels were varied from 0.2 to 1 wt % in both alloys, covering the Fe levels normally observed in industry. The alloy melts were also modified with Sr, in keeping with regular melt treatment practices, to study the effect of modification on the hardness and machinability of such alloys.

Casting was carried out using four preheated (450°C) rectangular graphite-coated metallic molds to prepare samples for adjusting all the metallurgical parameters required before preparing castings for the machinability part of the work. Identical castings were prepared for metallographic analysis, in order to correlate the microstructural characteristics with the properties observed. Microstructural observations of Fe-intermetallic characteristics were carried out using optical microscopy in conjunction with image analysis.

3.2. EXPERIMENTAL PROCEDURE

The base A356.2 and 319.0 base alloys were supplied in the form of 12.5 kg ingots. The compositions representing the average of three spectrometric analyses are listed in Table 3.1.

Table 3.1 Chemical compositions for 356 and 319 alloys used in the present work: a) 356 alloys, b) 319 alloys

Alloy Code a) 356 Alloys	Element (wt %)								
	Si	Fe	Mn	Mg	Cu	Ti	Sr	Mn/Fe	Al
1-356-base alloy	6.55	0.11	0.03	0.27	0.03	0.09	0.0000	0.29	92.8
1S-356-base alloy	6.96	0.14	0.03	0.33	0.14	0.10	0.0177	0.25	92.1
2	6.72	0.25	0.03	0.25	0.01	0.10	0.0000	0.13	92.5
2S	7.08	0.23	0.04	0.34	0.17	0.11	0.0148	0.18	91.9
3	6.78	0.43	0.03	0.31	0.01	0.10	0.0000	0.08	92.2
3S	6.52	0.35	0.00	0.36	0.06	0.14	0.0147	0.00	92.5
4	6.79	0.87	0.03	0.30	0.01	0.10	0.0000	0.04	91.8
4S	6.89	0.92	0.01	0.35	0.04	0.14	0.0163	0.01	91.6
5	6.42	0.24	0.1	0.33	0.00	0.14	0.0000	0.43	92.7
5S	7.64	0.22	0.13	0.36	0.04	0.11	0.0172	0.62	91.3
6	6.5	0.44	0.21	0.31	0.00	0.13	0.0000	0.47	92.3
6S	7.12	0.37	0.23	0.35	0.02	0.11	0.0176	0.61	91.6
7	6.52	0.85	0.41	0.30	0.01	0.11	0.0000	0.48	91.7
7S	6.99	0.9	0.42	0.32	0.03	0.11	0.0186	0.46	91.1
b) 319	Element (wt %)								
Alloy Code	Si	Fe	Mn	Mg	Cu	Ti	Sr	Mn/Fe	Al
8	6.12	0.40	0.01	0.01	3.33	0.13	0.0000	0.02	89.9
8S	6.03	0.33	0.00	0.02	3.18	0.12	0.0160	0.02	90.2
9	5.85	0.62	0.00	0.00	3.34	0.14	0.0000	0.00	90.0
9S	6.26	0.67	0.01	0.02	3.41	0.14	0.0118	0.02	89.4
10	5.81	1.03	0.01	0.01	3.07	0.13	0.0000	0.01	89.8
10S	6.03	1.07	0.00	0.00	3.32	0.13	0.0150	0.00	89.4
11	5.85	0.39	0.09	0.00	3.32	0.13	0.0000	0.23	90.1
11S	6.24	0.36	0.09	0.00	3.66	0.14	0.0158	0.25	89.6
12	5.79	0.64	0.18	0.00	3.35	0.14	0.0000	0.29	89.8
12S	5.80	0.64	0.19	0.00	3.24	0.13	0.0165	0.30	89.9
13	5.66	1.08	0.38	0.00	3.20	0.14	0.0000	0.35	89.5
13S	5.99	1.07	0.37	0.01	3.23	0.17	0.0340	0.35	89.0
14	5.81	0.37	0.00	0.09	3.35	0.12	0.0000	0.01	90.2
14S	5.87	0.33	0.00	0.09	3.22	0.13	0.0179	0.02	90.3
15	5.81	1.10	0.01	0.08	3.28	0.13	0.0000	0.01	89.5
15S	6.75	1.00	0.02	0.14	2.93	0.12	0.0131	0.02	86.8

Alloy Code	Si	Fe	Mn	Mg	Cu	Ti	Sr	Mn/Fe	Al
16	5.81	0.36	0.00	0.27	3.30	0.13	0.0000	0.00	90.1
16S	5.99	0.33	0.00	0.28	3.31	0.13	0.0178	0.00	89.9
17	5.61	1.05	0.00	0.27	3.20	0.13	0.0000	0.00	89.7
17S	5.89	1.11	0.00	0.27	3.22	0.13	0.0185	0.00	89.3
18	5.94	0.42	0.09	0.09	3.42	0.13	0.0000	0.22	89.8
18S	6.01	0.35	0.09	0.1	3.30	0.14	0.0196	0.25	89.9
19	5.57	1.00	0.36	0.09	3.18	0.13	0.0000	0.36	89.6
19S	5.79	1.06	0.38	0.10	3.20	0.14	0.0193	0.36	89.2
20	6.00	0.39	0.09	0.27	3.44	0.14	0.0000	0.24	89.6
20S	6.05	0.35	0.1	0.28	3.35	0.13	0.0209	0.27	89.6
21	5.42	1.04	0.37	0.29	3.06	0.17	0.0000	0.36	89.6
21S	5.66	1.06	0.39	0.27	3.09	0.13	0.0200	0.36	89.3
22-319 base alloy	5.99	0.22	0.00	0.01	3.45	0.14	0.0000	0.03	90.1
22S	6.01	0.18	0.00	0.01	3.27	0.19	0.0248	0.03	90.2
S = Sr-modified									

3.2.1. Melt Preparation and Casting Procedures

The ingots were cut into smaller pieces, dried and melted in charges of 6-kg each to prepare the various alloys. Melting was carried out using a SiC crucible of 7 kg capacity, and an electrical resistance furnace. The melting temperature was kept at 750 ± 5^0C.

Measured Sr, Mg, Fe and Mn additions were made to the melt using a perforated graphite bell. Strontium was added in the form of Al-10 wt% Sr master alloy, whereas Mg was added as pure metal. Iron and Mn were added in the form of Al-25%Fe and Al-25%Mn master alloys, respectively. The melts were degassed using pure dry argon for ~15-20 min, by means of a graphite rotary impeller (~130 rpm). The melt was poured at ~ 740^{0}C into four preheated (450^{0}C) rectangular graphite-coated metallic molds to prepare samples for adjusting all the metallurgical parameters required prior to preparing castings for the machinability part of the work. Samples for chemical analysis were also taken simultaneously for each melt condition.

3.2.2. Metallography

Samples for metallographic examination were sectioned from the castings corresponding to each condition, mounted and polished, using a BUEHLER Variable Speed Grinder- Poliser to the desired fine finish (1 μm diamond paste). Details of the grinding and polishing procedure are shown in Table 3.2. In each stage of the procedure, the coolant used also acted as lubricant and ensured constant cleaning of the paper and the specimen simultaneously. Care was taken to see that pressure exerted on the specimen was high enough to ensure proper cutting by the abrasive and a sufficient rate of abrasion, without unwanted production of heat and premature wear and tear of the abrasive.

Table 3.2 Grinding and polishing procedure of metallographic samples.

Stage	Abrasive	Particle Size (μm)	Coolant	Pressure(lb)	Time (min)
1	SiC (120)	100	Running Water	15	2:30
2	SiC (240)	50	Running Water	15	3:45
3	SiC (320)	35	Running Water	15	4:00
4	SiC (400)	26	Running Water	15	4:45
5	Diamond	6	Special Oil	32	3:30
6	Diamond	1	Special Oil	32	3:30
7	Diamond	0.25	Special Oil Running Water	25 1	2:30 5:00
Note: *Special oil* means *BUEHLER Metadi Fluid*					

3.2.3. Microstructural Characterization (Microstructure and Hardness Study)

In the present work involving both qualitative and quantitative aspects of the microstructure of the different alloy conditions, metallographic observations were carried out using optical microscopy in conjunction with image analysis as well as scanning electron microscopy.

3.2.3.1. Metallography and Image Analysis

The microstructures were analyzed using an optical microscope (Olympus PMG3). The eutectic Si particle characteristics were quantified using a Leco 2001 image analyzer in conjunction with the optical microscope, following the usual procedures employed for volume fraction or other measurements of any specified phase. The various phases observed in these samples were identified using electron probe microanalysis (EPMA) coupled with energy dispersive X-ray (EDX) and wavelength dispersive spectroscopic (WDS) analysis, employing a Noran Instruments microanalyzer operating at 15 KV and 20 nA, using an electron beam of diameter~1 μm. In each case, at least 5-6 measurements were taken (using a point count of 20 sec for each reading) to obtain the

average composition. Mapping of some specific areas of the polished sample surfaces was carried out to show the distribution of alloying elements in the phases. Peak-hardness samples from T6-tempered 356 and 319 (with Mg) alloys were etched (using 1 ml HF (48%)+ 200 ml distilled water) to examine the precipitate distribution, using both optical and scanning electron microscopy.

3.2.3.2. Mechanical Testing (Hardness)

Specimens (1 in ×1 in ×3 in) were cut from the metallic mold castings. These were heat-treated in a Blue M Electric furnace equipped with a programmable temperature controller (± 2 °C) for both solution and aging treatments. The solution heat treatments were carried out for 8 h at 540°C and at 495 °C for the 356 and 319 alloys respectively. The solution heat treated samples were quenched in warm water (65°C), followed by aging at 155°C, 180°C, 200°C and 220°C for 4hr. Aging was also carried out for different times (2, 4, 6, and 8 hr) at temperatures of 180°C and 220°C. A summary of the heat treatment procedures is provided in Table 3.3.

Hardness measurements were carried out on the heat-treated samples using a Brinell hardness tester (10 mm diameter ball; 500 kgf applied load). Each data point on the plots of hardness measurements represents the average of at least eight indentation readings taken from two perpendicular faces (each one four indentations), see Figure 3.1.

(a) (b)

Figure 3.1 Preliminary test sample (a) rectangular horizontal mold samples with dimension of 1 in ×1 in ×3 in are used for Hardness (HB) test and b) hardness indentation

Table 3.3 Heat treatment procedures used

Alloys	SHT [a]	Aging Treatment		Samples obtained
356 alloys	1.SHT (540°C, 8h) 2. water Quenching (65°C) 3. stabilization treatment 25°C /24h	4. Aging		12 samples (1 as cast, 1 as SHT [a] and 10 as AA [c])× 2 ×7 **Total =168 samples**
Alloy codes 1 to 7 and 1S to7S [b] in Table 3.1		Temp.	Time	
		150 °C 180 °C 200 °C 220 °C	4h 2,4,6 and 8h 4h 2,4,6 and 8h	
Mg-free 319 alloys	1.SHT (495°C, 8h) 2. water Quenching (65°C)	3. Aging		12 samples (1 as cast, 1 as SHT [a] and 10 as AA [c]) × 2 ×7 **Total= 168 samples**
Alloy codes (8 to 13 and 8S to 13S [b]) + (base alloy 22 and 22S [b]) in Table 3.1		Temp.	Time	
		150 °C 180 °C 200 °C 220 °C	4h 2,4,6 and 8h 4h 2,4,6 and 8h	
Mg-containing 319 alloys	1.SHT (495°C, 8h) 2. water Quenching (65°C)	3. Aging		12 samples (1 as Cast,1 as SHT [a] and 10 as AA [c])× 2 ×8 **Total =168 samples** ..... **Total= 528 samples**
Alloy codes (14 to 21 and 14S to 21S [b]) in Table 3.1		Temp.	Time	
		150 °C 180 °C 200 °C 220 °C	4h 2,4,6 and 8h 4h 2,4,6 and 8h	
a: Solution heat treatment, b: S = Sr-modified, and c: AA = artificial aging				

3.2.4. Machinability Study (Drilling and Tapping)

Chemical compositions of Al-Si-Mg (alloy code M1) and Al-Si-Cu-Mg (M2, M3, M4 and M5) are listed in Table 3.4. Conditions of 356 and 319 alloys containing mainly α-Fe-intermetallic and related to different levels of hardness (90, 100 and110 HB) were selected for the machinability study. The α-Fe-intermetallic volume fraction was set at two levels i.e. 2 and 5 percent for low and high Mg content 319 alloys (0.1 and 0.28% Mg), respectively. On the other hand, one condition from 356 alloys (2% α-Fe-intermetallic volume fraction) was undertaken for comparison with 319 alloys. Hardness and α-Fe intermetallic volume fractions measurements for 356 and 319 alloys at different aging treatments are listed in Table 3.5. Porosity can cause problems particularly in those workpiece areas where holes are to be drilled or tapped. A very low level of porosity is apparent in 356 alloys (M1-condition) however it is more than the sounder 319 alloys (M4-condition) as can be seen in Figure 3.2.

For the machinability test sample, it was founded that the external ribs have higher cooling rates than the internal ones. Solidification times in the range of (25-45 sec) were measured by using five thermocouples fixed in the center within each rib in the machinability test sample, see Figure 3.3. Following solutionizing, the castings were quenched in warm water (65 °C); the quench media and quench interval were the most important parameters controlling the effectiveness of the treatment. The quench media had sufficient volume and heat extracting capacity to produce rapid cooling. The quench was attained within less than 10 seconds. Differences in the quenching rates were observed within the five ribs, Figure 3.3 (b).

Carbide "G" drills of 6.5 mm diam. and with minimum 30 mm length, straight flute and coolant fed were used to drill two rows of through-holes in each rib of the waffle plate with 4 mm between rows. TiN coated HSS cutting taps, M8*1.25-6H, with three spiral flutes and radial coolant hole were used in subsequent tapping process. Tapping was made simultaneously for the drilled holes of the full plate. Optimum drilling and tapping conditions are listed in Table 3.6.

The experimental setup which consisted of an A88E machine, electric furnaces for the heating cycle, tool-holder setup, sample coupled with electronic dynamometer cable positions, workpiece-tool setup (i.e. horizontal machining) and electric furnaces for the cooling cycle are shown in Figure 3.4. Chemical emulsion concentrate VHP® E210 (5% cutting fluid +95% liquid) was applied to avoid the effects of the heat generated during machining. The machinability test sample, drill and tap geometry are displayed in Figure 3.5.

Chips were collected at the middle and the end of each sample tested for more examinations. A Go-No-Go gauge test was periodically checked and was taken as an assessment characteristic for dimensional accuracy control for both drilled and tapped holes. The reference diameter of Go-No-Go gauge test (6.5024-6.5278 mm and 7.02056-7.15518 mm) was used for drilling and tapping respectively. Heat built-up depth (i.e. aluminum layer thickness accumulated on the cutting tool edge) was measured during each machining test using a toolmakers microscope (TM-505 types) with 30X magnification.

DRILLING AND TAPPING PROCEDURES For each new drill or tap an optical micrograph was taken before testing. After drilling the first group of holes (115-holes), the chips were

collected and the drill was examined for heat built-up measurements. This was followed by drilling the second group of holes (115-holes). Again the chips were collected and the drill was examined after the first sample block was drilled (230-holes). The Go-No-Go gauge test was checked using reference diameter (> 6.5 mm) of 6.5024 for Go-gage test and 6.5278 mm for No-Go-gauge test for drilled holes. A machinability test sample, after 230 holes had been drilled (first and second group of holes) is shown in Figure 3.5 (a).

Tapping was done simultaneously for the first 115 drilled holes for the same sample. After tapping of the first group of holes (115-holes), the tap was examined for heat built-up measurement and was checked for 1^{st} and 2^{nd} teeth failure. Tapping of the second group of holes (115-holes) was then carried out. There were no chips produced in the tapping tests. Again the tap was examined after the first sample block (230-holes). The Go-No-Go gage test for tapping was checked using reference diameter of 7.02056 for Go-gage test and 7.15518 for No-Go-gage test for tapped holes. After drilling and tapping were done for the first block, another one of the same condition (same series) was placed for drilling and tapping test according to the same procedure as mention above. The same procedures for drilling and tapping were repeated for the subsequent blocks.

Each alloy/heat treatment condition was tested with the same drill or tap. When the drill was broken during the drilling, two options were followed: 1) drilling was stopped and tapping was continued to the position where drill was broken then the test was changed for another condition or series, 2) in the case the drill was broken due to the presence of a defect or a large inclusion, the test was resumed with a new drill on the same block according to the same above procedure.

Table 3.4 Chemical compositions for 356 and 319 alloys used for the machinability test

Alloy Code	Element (wt %)								
	Si	Fe	Mn	Mg	Cu	Ti	Sr	Mn/Fe	Al
356 alloy- M1	6.85	0.44	0.30	0.33	0.05	0.15	0.0218	0.69	91.7
319 alloys- M2	6.20	0.40	0.29	0.10	3.40	0.15	0.0234	0.73	89.3
M3	6.20	0.97	0.39	0.10	3.40	0.14	0.0236	0.40	88.6
M4	6.25	0.42	0.30	0.28	3.50	0.15	0.0133	0.72	88.7
M5	6.30	1.02	0.39	0.28	3.40	0.15	0.0260	0.38	88.3

Table 3.5 Hardness and α-Fe intermetallic surface fractions measurements for 356 and 319 alloys used in drilling and tapping study

Alloy Code	Alloy type	Hardness (HB)	Fe- intermetallic S.F %
M1	356	100	~2 %
M2	319	90 and 100	~2 %
M3	319	90 and 100	~5 %
M4	319	88, 100 and 110	~2 %
M5	319	100	~5 %

Table 3.6 Optimum drilling and tapping conditions

Parameters	Drilling	Tapping
Cutting Speed	234.458 m/min or 11000 rpm.	12.57 m/min or 500 rpm.
Cutting Drill Dia.	Carbide "G" drills 6.5 mm	TiN coated HSS cutting taps, M8*1.25-6H
Cutting Depth	31.75 mm	Depth ≤3×D (19 mm)
Cutting Feed Rate	44 IPM (0.1016 mm/rev)	27.8 IPM (1.41224 mm/rev)
Lubricant/Coolant	Chemical emulsion concentrate VHP® E210 (5% cutting fluid +95% liquid)	

(a)

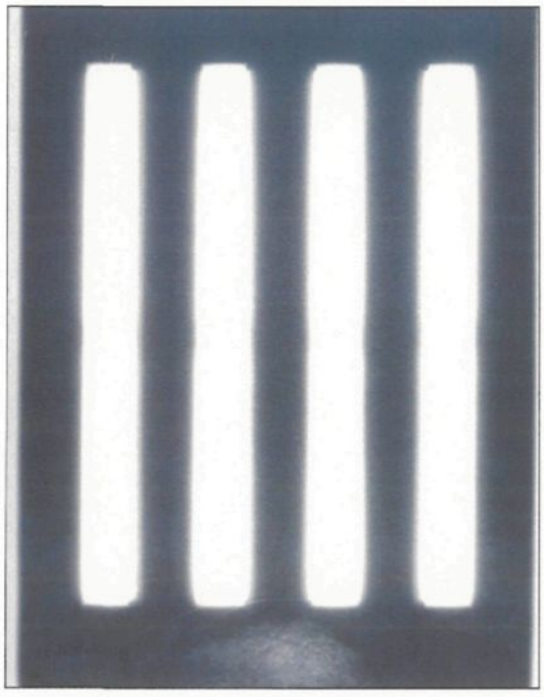

(b)

Figure 3.2 Radiography results showing the sound casting of 356 (M1) and 319 (M4) alloys

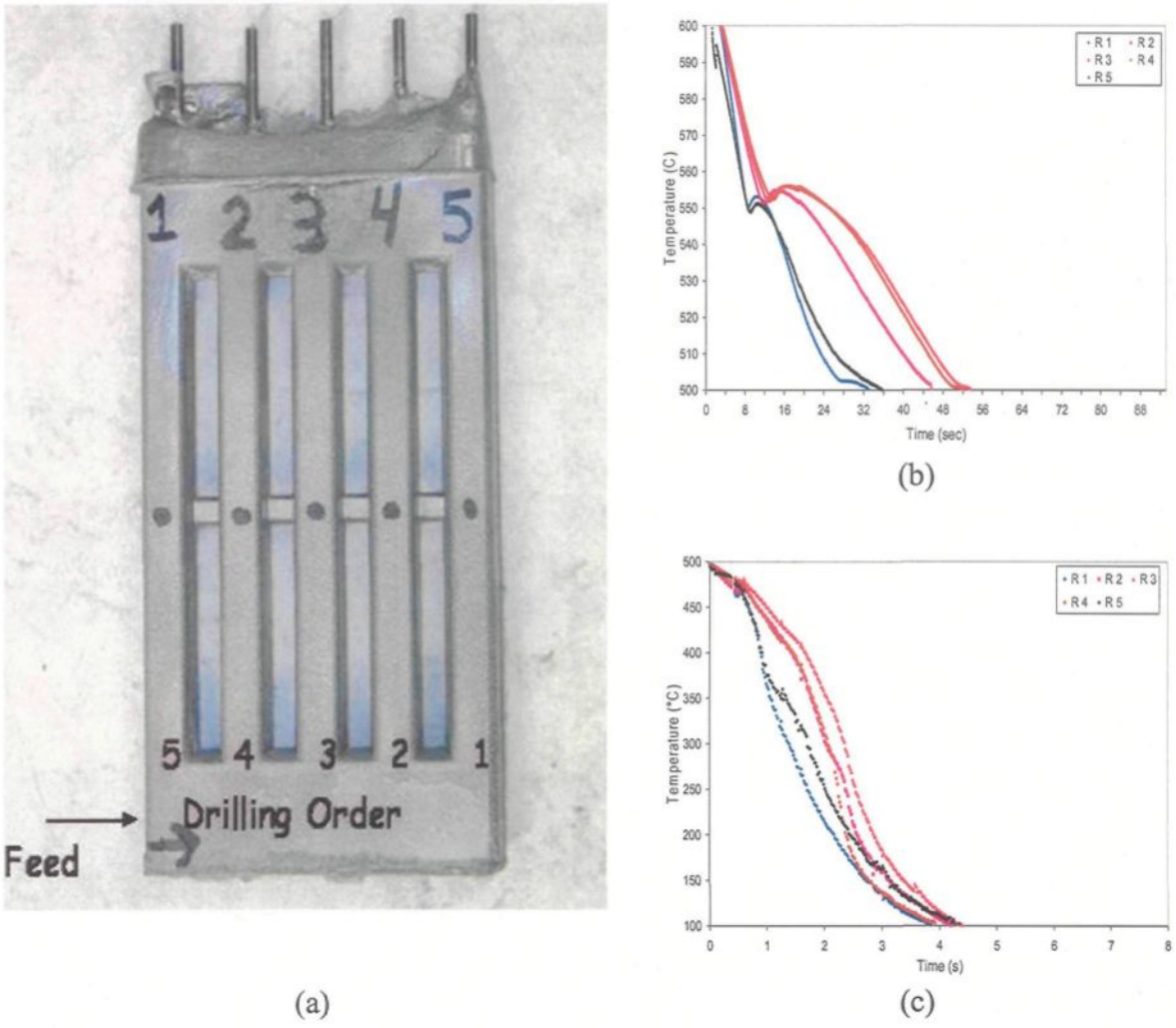

Figure 3.3 Solidification and quenching rate measurements a) machinability test sample with the five thermocouples, b) solidification time for the five ribs and c) quenching rates for the five ribs

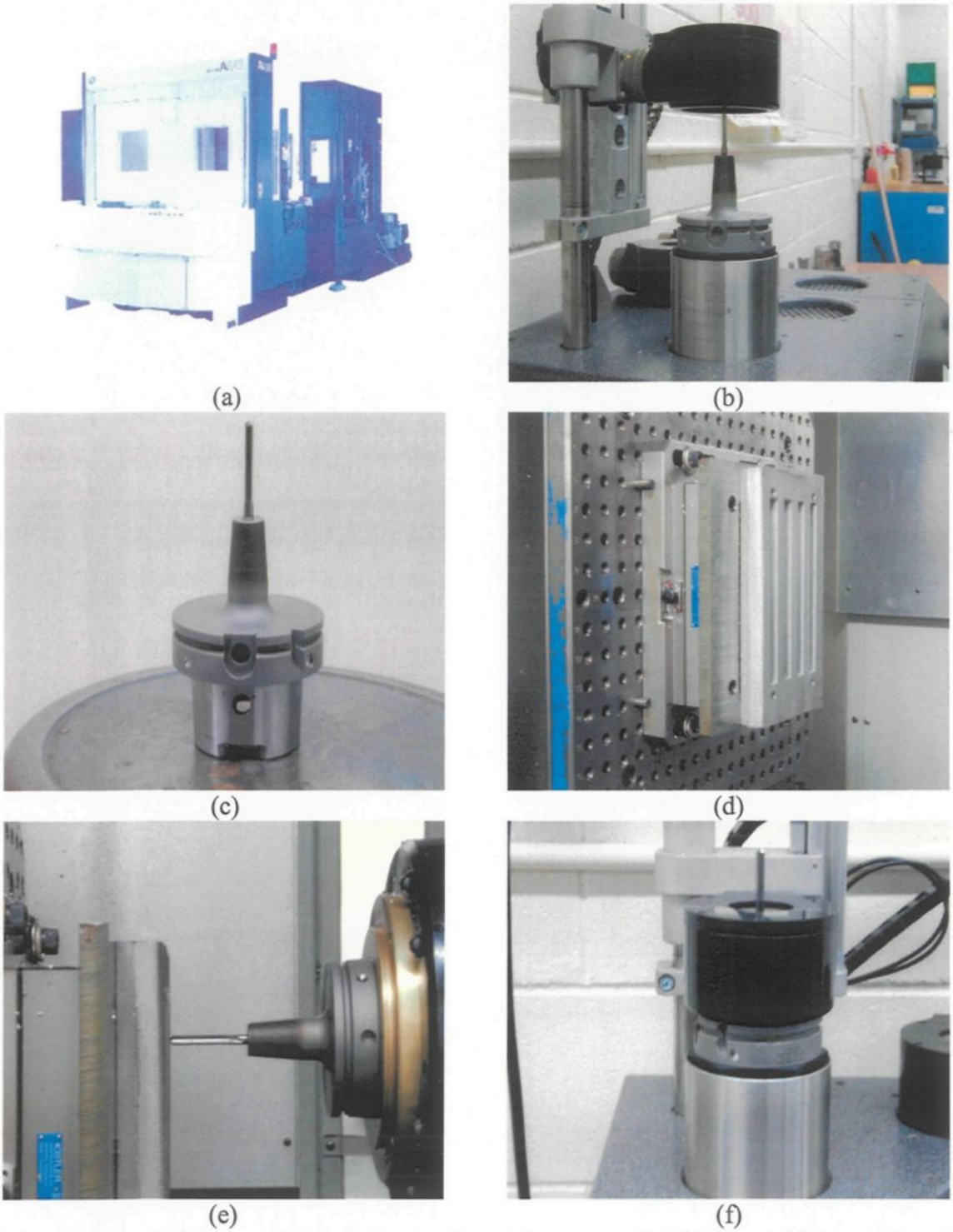

Figure 3.4 Drilling and tapping experimental set-up; a) Makino A88E machine, b) Tool set-up during heating cycle, c) Tool set-up, d) Sample and dynamometer cable set-up and e) horizontal machining set-up f) Tool removal during cooling cycle.

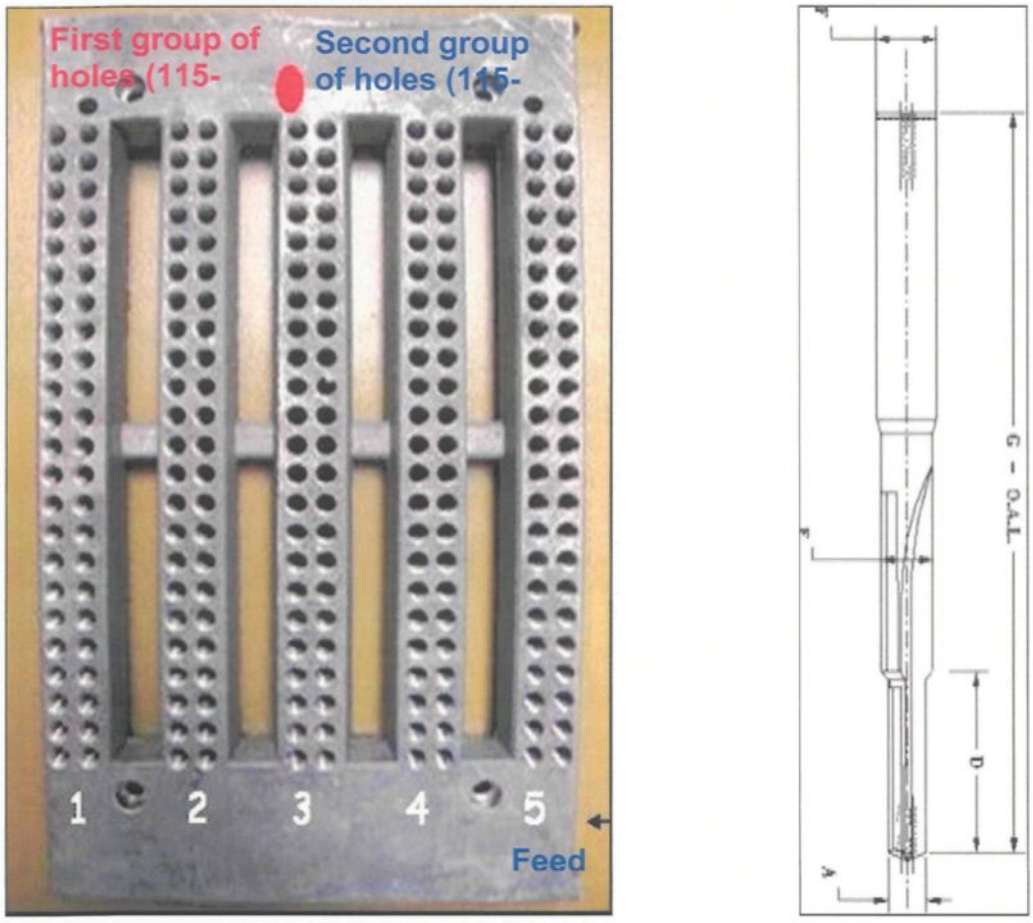

(a) (b)

(c)

Figure 3.5 Machinability test Sample, Drill and tap geometry, a) Machinability test sample after drilling, b) Carbide G (RT 150) drill (O.A.L= 103mm, F.L=28mm and drill dia= 6.5mm) and c)HSS-E tap (UNC-DIN 371, Class to Fit 2B, Helix 40°RH)

CHAPTER 4

HARDNESS AND MICROSTRUCTURE

CHAPTER 4

HARDNESS AND MICROSTRUCTURE

4.1. INTRODUCTION

Al-Si-Cu, Al-Si-Cu-Mg, and Al-Si-Mg cast alloys, belonging to the Al-Si alloy system were selected for the present study, represented respectively by 319 and 356 alloys. The Aluminium Association has summarized the variables that affect the mechanical properties in an aluminium alloy casting, namely, chemical composition, solidification rate, metal soundness, and heat treatment.[121] In 356 and 319 alloys, the iron- and copper- intermetallics, the porosity size and distribution, the eutectic silicon particle morphology (size, shape, and distribution), and the degree of supersaturation of Mg and Cu in the α-Al matrix after solution heat-treatment are the main parameters expect to control the mechanical properties.

The effect of these metallurgical parameters on the hardness and microstructural characteristics of as-cast and heat-treated 356 and 319 alloys was investigated, with the aim of adjusting these parameters to produce castings of suitable hardness and Fe-intermetallic volume fractions for subsequent use in studies relating to the machinability of these alloys. The hardness, Fe- and Cu-intermetallic volume fractions and eutectic Si-particle characteristics were measured for the as-cast and T6 heat-treated samples prepared from the grain refined 356 and 319 alloys using different combinations of Sr-modification and alloying additions. An understanding of these parameters would help in selecting the metallurgical conditions required to achieve the optimum and maximum productivity at high speed machining. The range of hardness and Fe-intermetallic volume

fractions used in this study conforms to the levels commonly observed in commercial applications of these alloys.

Hardness measurements were carried out on specimens prepared from 356 and 319 (with and without Mg) alloys in the as-cast and heat-treated conditions. Aging treatments were carried out at 155°C, 180°C, 200°C, and 220°C for 4 h, followed by air cooling, as well as at 180°C and 220°C for 2, 4, 6, and 8 h to determine the conditions under which specific hardness levels *viz.*, 85 and 115 (HB) could be obtained.

4.2. RESULTS AND DISCUSSION

4.2.1. Hardness Testing

Hardness measurements were performed on all heat-treated specimens prepared from the various 356 and 319 alloys. The different solution and aging treatments employed were used to estimate conditions under which hardness levels of 85 and 115 HBN could be obtained for the two alloys. The results are provided in Table 4 1.

4.2.2. Aging Behavior

4.2.2.1. Al-Si-Mg (356) Alloys

During the early aging stages of an Al-Si-Mg alloy (155˚C/ 4 h), the saturated solid solution first develops solute clusters. However, the supersaturation of vacancies allows diffusion, thus leading to the formation of GP zones.[122] A state of underaging can be maintained. This state is known to be associated with a microstructure consisting primarily of needle-shaped [123] or spherical[124] GP zones, needle-like β" (Mg_2Si), and rod-like β' (Mg_2Si) transitional phases.[124] All of these are fully coherent with the matrix. A behavior that can be attributed to extensive precipitation of well-developed GP zones and which cannot progress any further because of a lack of thermal activation energy at 155˚C. The hardness increases with aging temperature up to 180˚C (peak temperature) for 356 alloys in the unmodified and modified conditions, followed by a decrease at 200˚C and 220˚C of hardness (overaging), see Figure 4.1. At 200ºC and 220˚C, corresponding to the overaged conditions, the coherent rods or needles of β' (Mg_2Si) and incoherent equilibrium β phase dominates the microstructure.[125]

4.2.2.2. Al-Si-Cu and Al-Si-Cu-Mg (319 Alloys)

The hardening of Al-4%Cu alloy during aging is attributed to the formation of GP1 and GP2 or θ" (Al_2Cu) zones, θ' (Al_2Cu), and the equilibrium Al_2Cu phase, where the GP1 zones are two-dimensional Cu-rich regions oriented parallel to {100} planes, the GP2 (or θ") zones are considered to be three-dimensional regions having an ordered atomic arrangement, the θ' phase has the same composition as the stable phase and exhibits coherency with the solid solution lattice, while the equilibrium θ is incoherent with the lattice. Addition of Mg to Al-Cu alloys accelerates and intensifies the age-hardening process.

Similarly, when aging is carried out for Al-Si-Cu (319 type) alloys at 155°C or 180°C for 4 h, a microstructure consisting primarily of GP1, GP2 or θ" (Al_2Cu) zones and θ' (Al_2Cu) is developed. The composition of the quenched and aged aluminum matrix changes with aging time due to the precipitation of the θ' (Al_2Cu) phase, which is responsible for the increase in hardness.[126] The decrease in hardness is bound with the growth of the θ' phase and the transition of the Al_2Cu phase into large, stable precipitates.

In the case of Mg-free 319 alloys, both modified and unmodified alloys reveal similar trends and show lower hardness values than 356 alloys when aging is carried out at 180°C. However, the opposite is observed when aging is carried out at 220°C, for all aging times, Figure 4.1. In the Al-Si-Cu-Mg system (319 alloys), hardening may be caused by the precipitation of Al_2Cu, Mg_2Si, Al_2CuMg and $Al_4CuMg_5Si_4$ phases.

Table 4 1 Hardness as a function of alloy and heat treatment conditions.

356 alloys			Aging Treatment Conditions									
Sample Code	As-cast	SHT	155^{0}C	200^{0}C	180 ^{0}C				220 ^{0}C			
			4hr	4hr	2hr	4hr	6hr	8hr	2hr	4hr	6hr	8hr
1	56.0	65.5	85.5	86.0	93.5	91.5	95.0	92.0	77.5	72.0	67.5	68.0
2	58.0	65.0	85.0	89.0	90.5	91.5	93.5	91.0	78.5	72.0	68.5	65.5
3	63.0	72.5	97.0	95.5	102.0	100.0	103.5	103.5	88.5	78.5	75.0	77.0
4	61.0	74.0	96.0	97.5	103.5	103.5	105.0	102.0	89.0	84.0	79.5	79.0
5	59.0	68.5	85.0	92.5	104.0	98.5	100.5	97.5	85.5	73.5	69.5	70.0
6	61.0	72.5	96.5	98.5	104.0	98.0	106.5	104.0	87.0	79.0	70.5	69.5
7	64.0	74.0	100.0	100.0	107.0	109.0	110.0	107.0	92.0	84.0	76.5	76.0
1S	59.0	66.0	91.5	94.5	100.0	100.0	100.0	99.5	85.0	77.0	76.5	73.5
2S	59.5	71.5	88.0	95.5	100.5	101.5	100.0	99.5	86.5	80.5	76.0	74.5
3S	59.0	68.0	99.0	97.0	102.0	100.0	105.5	104.5	86.0	77.5	75.6	75.0
4S	60.0	70.0	98.0	101.0	104.5	104.5	104.0	107.0	90.0	82.5	73.5	74.0
5S	59.0	67.5	92.0	93.5	100.0	99	99.5	96.5	85.5	74.0	73.0	72.0
6S	60.0	71.0	93.5	93.5	98.5	104.5	106.5	98.0	85.0	76.5	71.5	68.5
7S	60.0	71.5	87.5	90.5	103.0	92.5	102.5	97.5	84.5	72.0	75.0	72.0
319 alloys			Aging Treatment Conditions									
	As cast	SHT	155^{0}C	200^{0}C	180 ^{0}C				220 ^{0}C			
			4hr	4hr	2hr	4hr	6hr	8hr	2hr	4hr	6hr	8hr
8	72.0	74.0	79.5	93.5	82.5	82.0	84.0	92.5	99.0	97.5	95.5	95.5
9	70.0	74.0	73.0	72.5	80.5	73.0	84.0	90.5	89.5	97.0	95.5	95.5
10	76.5	75.5	79.0	97.0	81.5	78.5	83.4	76.5	99.0	103.5	93.5	95.5
11	69.5	76.5	71.5	93.0	80.5	79.0	82.5	89.0	104.0	103.0	98.5	95.5
12	76.5	75.5	73.0	98.0	79.0	75.5	83.5	86.0	96.0	89.0	91.0	89.5
13	72.0	71.5	76.5	99.0	80.0	82.5	79.0	87.5	100.5	93.0	91.5	91.5
14	84.0	93.5	101.0	113.5	116.5	115.0	117.5	121.0	104.5	101.5	100.0	96.5
15	80.5	92.5	102.5	117.0	112.5	118.0	117.5	120.0	104.0	102.0	102.0	101.0
16	85.0	84.0	106.5	125.0	130.0	130.0	128.5	132.0	120.5	115.5	113.0	110.0
17	87.0	98.0	105.5	125.0	131.5	126.0	133.0	133.5	120.5	116.5	111.5	114.0
18	79.5	92.5	104.5	116.0	117.0	124.5	122.5	119.0	108.0	104.5	106.5	103.0
19	78.5	94.0	101.5	115.0	117.5	117.5	120.0	123.0	106.0	104.0	99.0	101.0
20	84.0	98.5	105.0	128.5	131.5	133.5	135.0	132.5	119.0	115.0	112.5	116.0
21	85.5	98.0	107.0	130.0	137.5	134.0	137.5	133.5	127.0	115.0	116.5	112.0

	As cast	SHT	155^{0}C	200^{0}C	180 ^{0}C				220 ^{0}C			
			4hr	4hr	2hr	4hr	6hr	8hr	2hr	4hr	6hr	8hr
22	69.5	72.0	79.5	89.5	81.0	80.5	80.0	90.0	96.5	96.0	92.5	92.0
8S	72.5	69.5	84.5	83.0	80.0	77.5	82.5	79.5	92.5	84.5	83.0	83.5
9S	71.5	71.0	80.0	87.0	78.0	77.0	78.0	79.5	88.5	93.5	86.0	86.5
10S	77.5	69.0	77.0	85.5	77.0	78.0	81.5	74.0	87.0	91.0	89.5	96.0
11S	70.0	69.5	70.0	92.5	73.5	73.5	74.5	77.5	92.0	89.0	88.0	85.0
12S	77.5	72.0	70.0	86.0	79.0	78.5	80.0	85.0	96.0	91.0	88.0	88.0
13S	71.5	75.5	74.5	89.0	78.5	76.5	78.5	82.0	96.5	87.0	84.0	92.5
14S	74.0	84.0	94.5	100.0	104.0	109.0	106.5	114.5	97.5	99.0	92.0	89.0
15S	82.5	87.0	99.5	106.5	112.5	113.5	112.5	109.5	99.5	97.5	103.5	95.5
16S	80.5	88.0	100.0	113.5	121.0	119.0	121.0	119.5	108.5	102.5	101.5	107.0
17S	88.0	92.5	100.5	119.0	128.0	125.0	131.5	126.5	111.5	106.0	104.5	109.5
18S	74.0	85.0	94.5	104.5	108.5	109.0	116.5	109.0	94.0	99.5	94.0	96.5
19S	76.0	83.0	96.0	103.5	117.5	108.0	119.0	115.0	96.0	93.0	91.5	95.5
20S	80.5	87.5	97.5	113.0	120.5	118.0	123.0	119.0	114.0	112.0	100.0	99.0
21S	86.5	95.0	103.5	122.0	127.0	123.5	128.0	128.5	116.0	107.5	102.5	101.5
22S	64.5	68.5	71.5	79.0	75.5	72.0	78.5	76.2	88.0	85.0	83.0	87.0

SHT : solution heat treatment @ 540^{0}C/8h for 356 alloys and @ 495^{0}C/8h for 319 alloys

4.2.3. Effect of Fe-Intermetallic Morphology and Sr-Modification on Hardness and Aging Behavior of 356 and 319 Alloys

The effect of Fe-intermetallic type/morphology on the aging behavior of both 356 and 319 alloys (Mg-free) with increasing aging temperature (at 4h aging time) can be observed from Figure 4.1. The results show that for the unmodified 356 alloys, those containing mainly α-Fe intermetallics display slightly higher hardness values than those containing β-Fe intermetallics. In the modified condition, the reverse is observed. In the case of 319 alloys containing both α-Fe and β-Fe intermetallics, and in the α-Fe intermetallic-containing 356 alloys, their Sr-modified alloys exhibit lower hardness levels compared to the unmodified alloys. Only in the case of the β-Fe intermetallic-containing 356 alloys do the modified alloys display hardness values that are equal to or slightly higher than those obtained for the unmodified alloys.

Peak hardness was observed in 319 alloys containing mainly α-Fe intermetallics when aging was carried out at 200°C/4h. On the other hand, hardness still increases up to 220°C for 319 alloys containing β-Fe intermetallics in the unmodified and modified conditions, Figure 4.1. Unlike the Mg_2Si precipitates that strengthen Al-Mg-Si alloys and are easily cut by dislocations even when the alloy is overaged,[127, 128] the Cu-rich precipitates become increasingly resistant to cutting by dislocations, leading to increased strain hardening rates.

In 356 and 319 Mg-content alloys, the 319 alloys exhibit higher hardness levels than do the 356 alloys at the two aging temperatures regardless of the modification condition. The hardness values in the modified alloys are lower than the unmodified one at both aging temperatures i.e. 180°C and 220°C for all aging times. This may be

explained on the basis of the combined effect of Cu-and Mg in the 319 alloys, where hardening occurs by the cooperative precipitation of Al_2Cu and Mg_2Si phase particles,[129] compared to only Mg_2Si precipitation in the case of 356 alloys, see Figure 4.2. Aging at 180°C over a period of 8h, presented in Figure 4.2, revealed a sharp rise in hardness during the first two hours of aging, followed thereafter by a broad peak or plateau between 2h and 8h. for the 356 alloys and Mg-containing 319 alloys. At 220°C aging temperature, hardness peaks were clearly observed at 2h of aging in both alloys.

In the peak-aged condition, the higher hardness of 319 Mg-containing alloys is clearly due to the high concentration of $CuAl_2$ (θ') plates and Mg_2Si (β') needle-like metastable phases, where the thermal activation energy is enough to nucleate these intermediate phases that are coherent with the matrix, leading to a sharp rise in hardness at both 180°C and 220°C when aging is carried out for two hours. Increasing the aging time or aging temperature increases the size of these particles, with a gradual change in their chemical composition, resulting in the equilibrium θ (Al_2Cu) and β (Mg_2Si) phases in the form of incoherent particles, which are responsible for the observed drop in the alloy hardness.

Addition of Mg to unmodified or modified 319 alloys containing β-Fe and/or α-Fe intermetallics produced a remarkable increase in hardness at all aging temperatures. The effect of increasing the Mg content on the hardness of 319 alloys containing mostly β-Fe intermetallics is displayed in Figure 4.3(a) A similar trend was observed for alloys containing mostly α-Fe intermetallics, independent of aging temperature as shown in Figure 4.3(b). The high level of hardness in Mg containing alloys (0.28%) can be

explained due to the high volume fraction of Mg-intermetallics or precipitates that can formed within the alloy matrix.

Aging at180°C and 220°C for 356 and Mg-containing 319 alloys with both α-Fe and β-Fe intermetallics corresponding to the peak hardness and overaging conditions was carried out over the 2-8 h aging period. In both alloys, aging at 180°C up to 8h produced a sharp rise in hardness during the first two hours of aging, followed by a broad peak or plateau over the 2-8 h aging period. However, aging at 220°C revealed a hardness peak at 2h. Figure 4.4 shows the hardness dependence on the aging time at the two aging temperatures in the unmodified and modified 319 alloys containing mainly β-Fe intermetallics at different levels of Mg content. Similar results are observed for 319 alloys containing mainly α-Fe intermetallics, as shown in Figure 4.5.

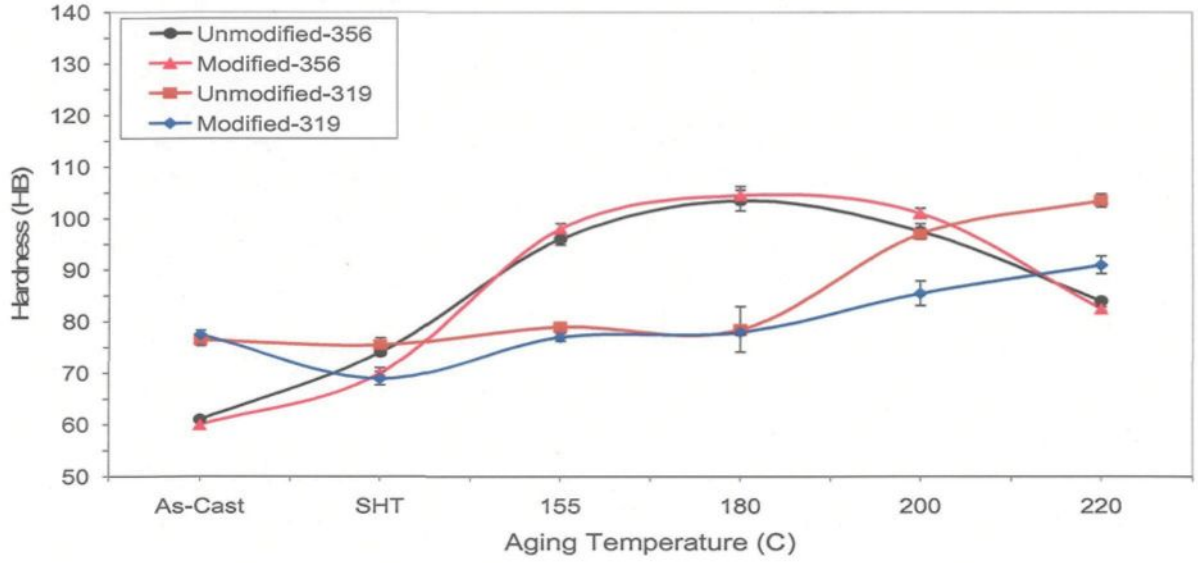

(a)

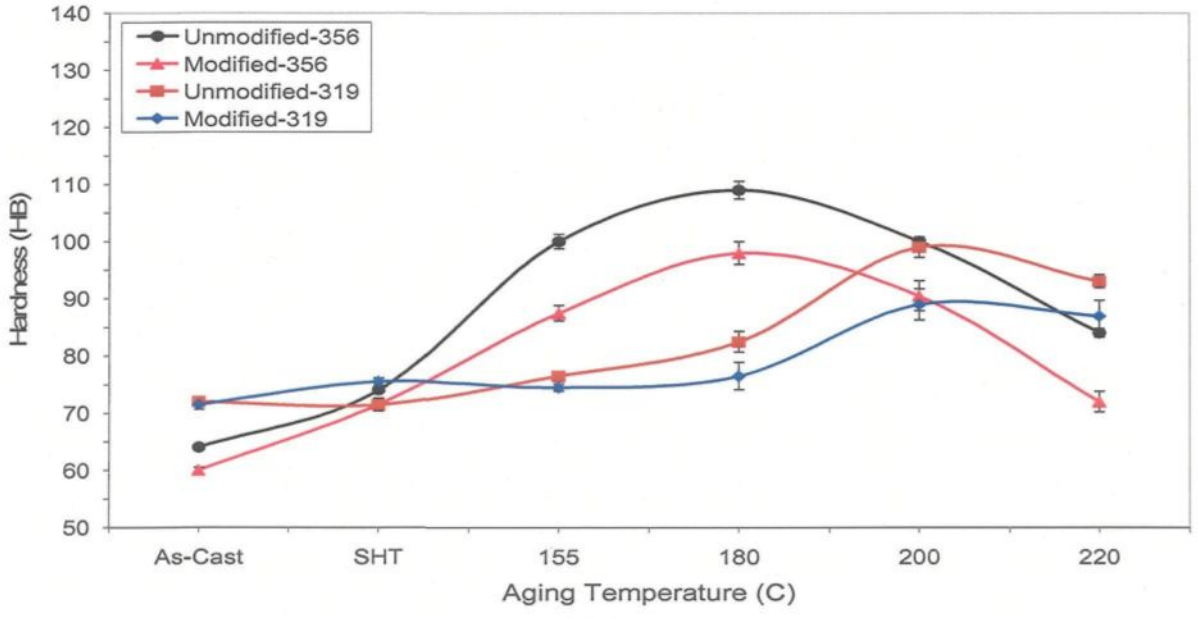

(b)

Figure 4.1 Effect of aging temperature on the hardness of 356 and 319 alloys following aging at 4 h for alloys containing: (a) β–Fe intermetallics (1%Fe), (b) α-Fe intermetallics (1%Fe-0.4%Mn)(aging time :4h).

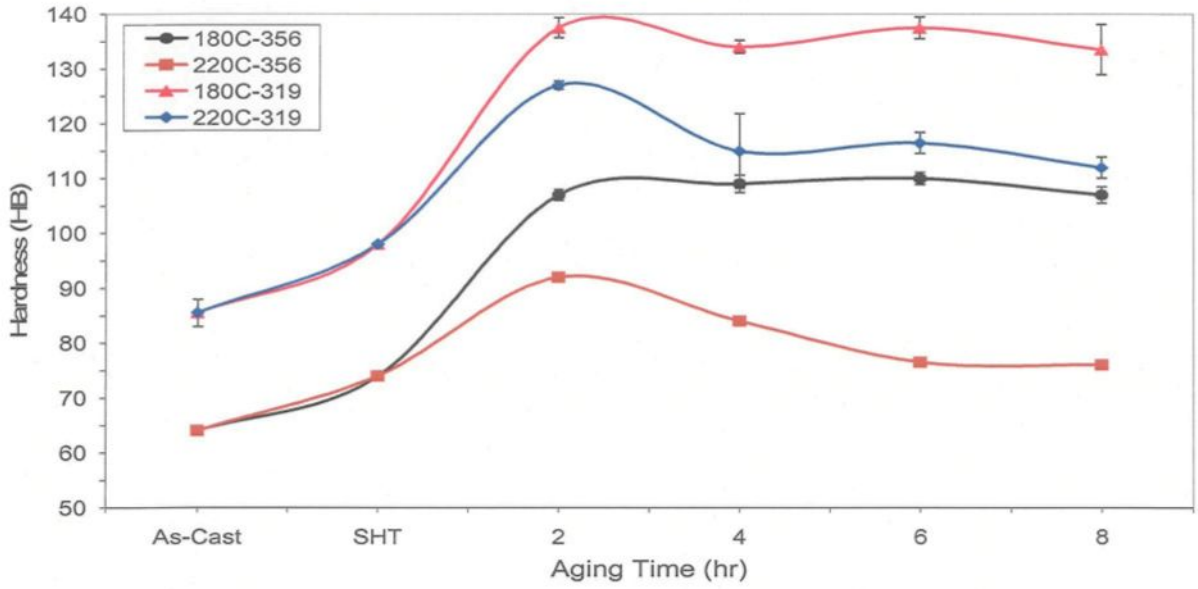

(a)

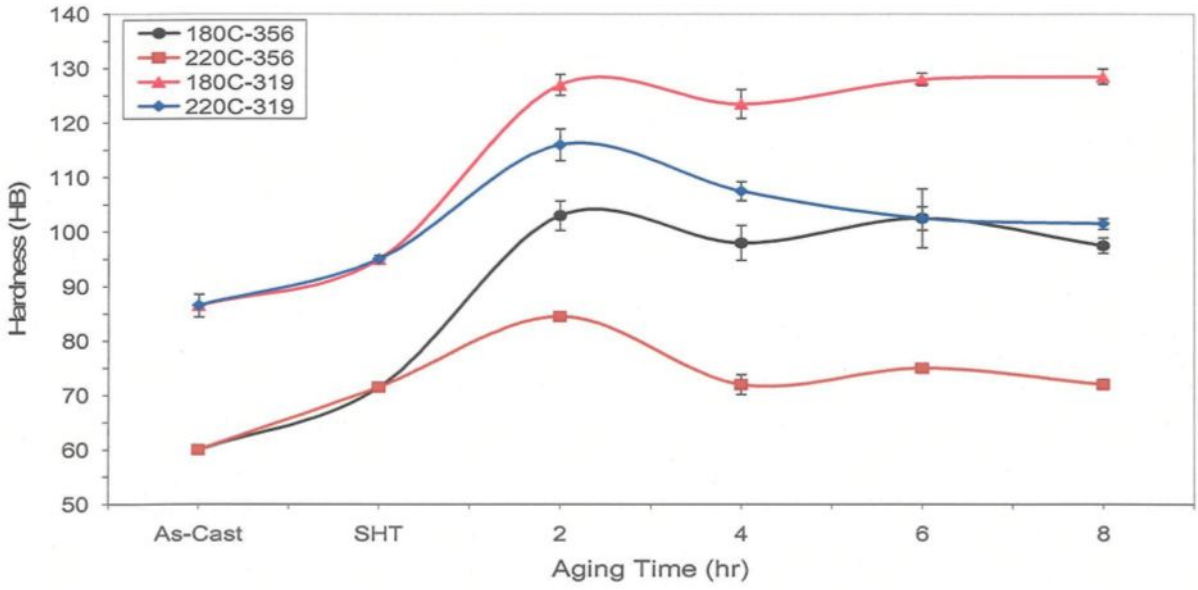

(b)

Figure 4.2 Hardness as a function of aging time at aging temperatures of 180° and 220°C for 356 and 319 alloys containing mainly α-Fe intermetallics and having similar Mg content (a) unmodified alloys, and (b) Sr-modified alloys.

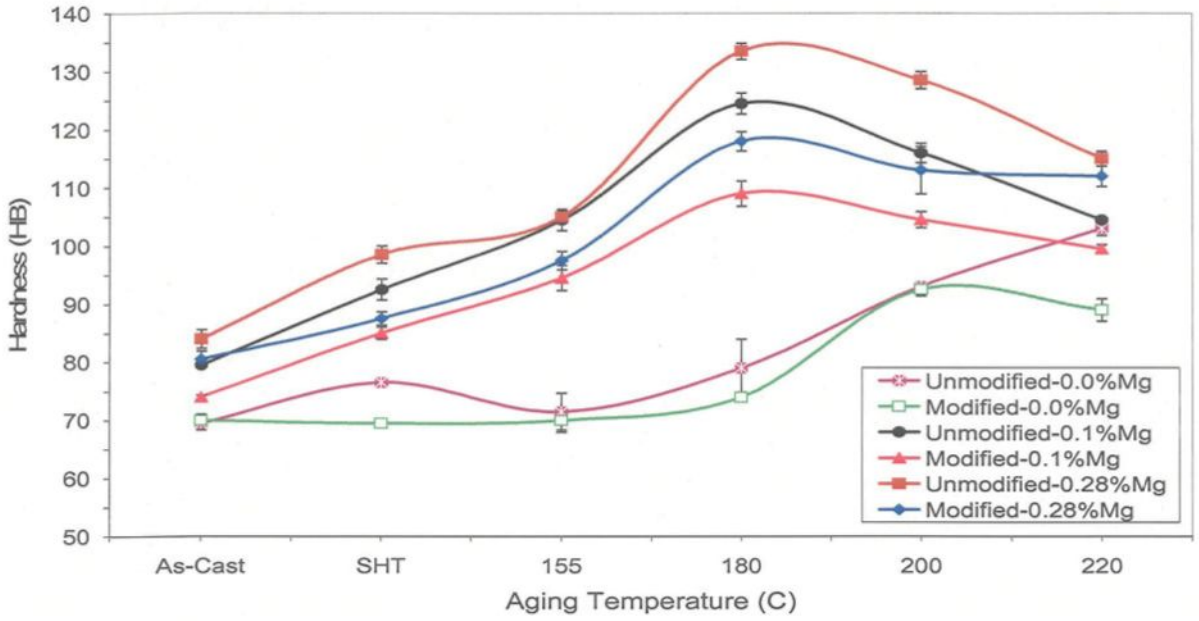

(a)

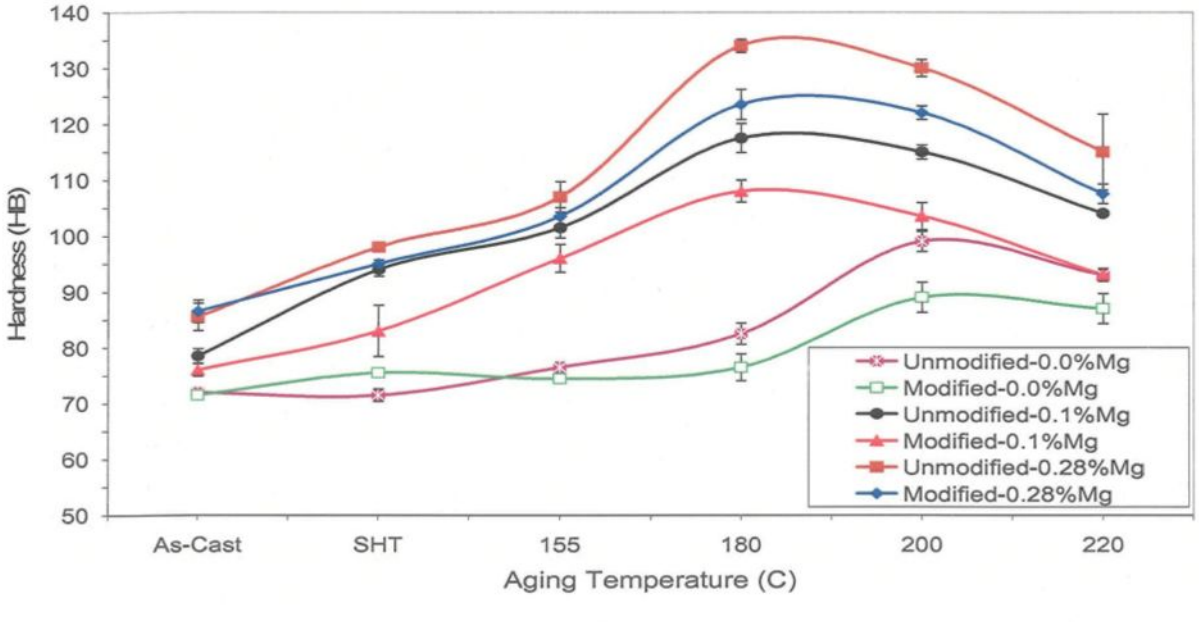

(b)

Figure 4.3 Hardness as a function of aging temperature for unmodified and Sr-modified 319 alloys containing different Mg levels and exhibiting (a) mainly β-Fe, and (b) mainly α-Fe intermetallics (aging time :4h).

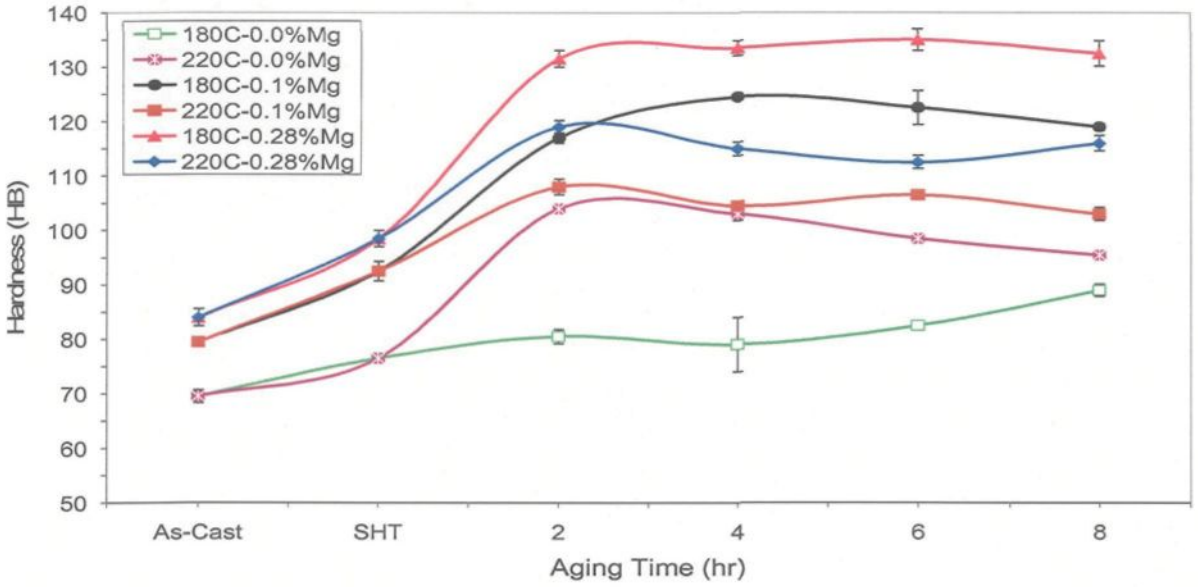

(a)

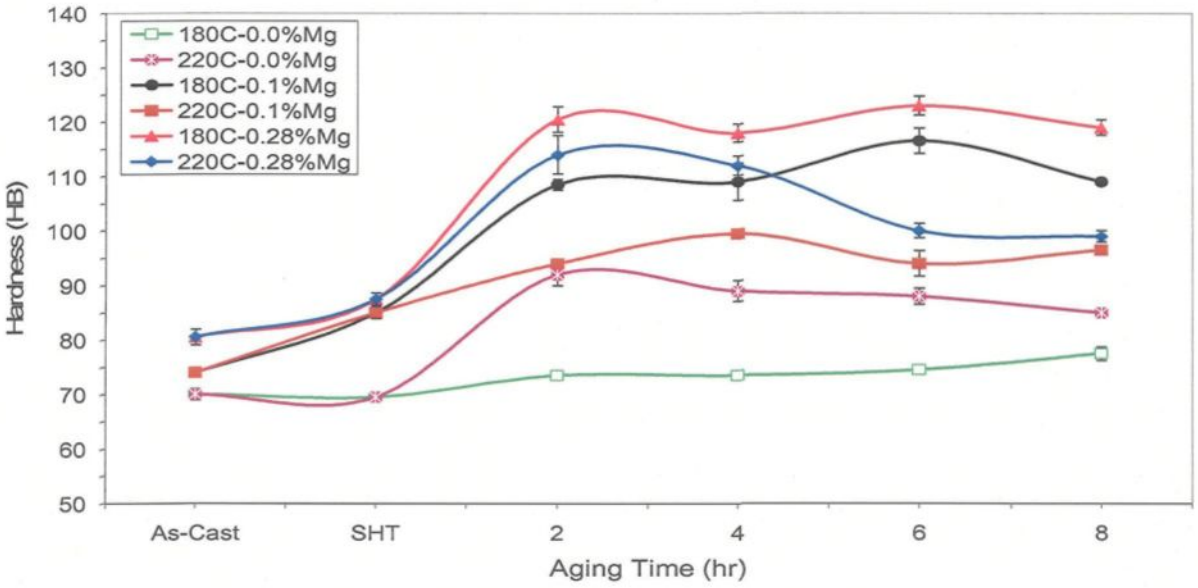

(b)

Figure 4.4 Hardness as a function of aging time at aging temperatures of 180° and 220°C for 319 alloys containing different Mg levels, and exhibiting mainly β-Fe intermetallics: (a) unmodified alloys, and (b) Sr-modified alloys.

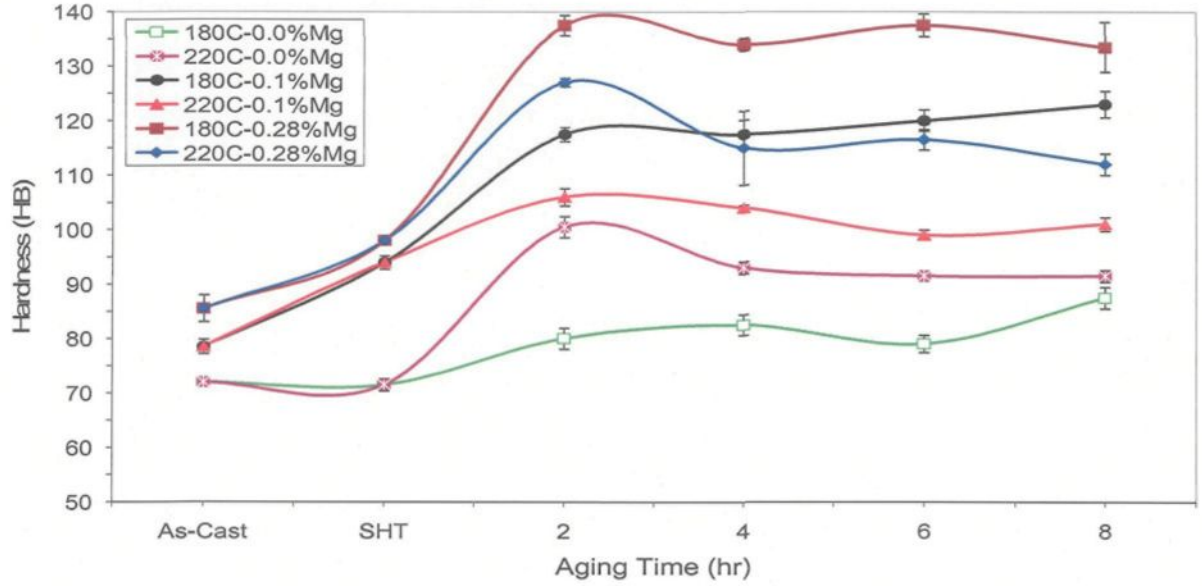

(a)

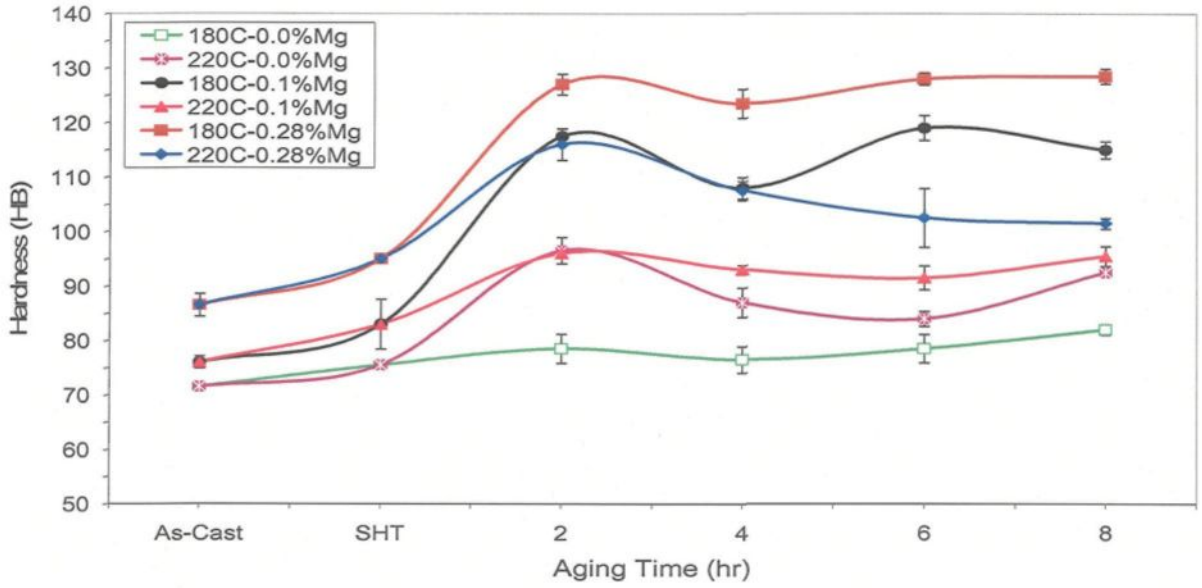

(b)

Figure 4.5 Hardness as a function of aging time at aging temperatures of 180° and 220°C for 319 alloys containing different Mg levels and exhibiting mainly α -Fe intermetallics: (a) unmodified alloys, and (b) Sr-modified alloys.

4.2.4. Effect of Additions on Hardness and Fe-Intermetallic of 356 and 319 alloys

The effect of alloying content on the hardness and Fe-intermetallic surface fractions observed in 356 and 319 alloys which exhibited mainly β-Fe or β-Fe and/or α-Fe intermetallics after aging at 180°C or 220°C for 2h is shown in Figure 4.6 through Figure 4.9. The alloying content is expressed in terms of the Fe content or the Fe-Mn content, depending on the type of Fe-intermetallics formed. Figure 4.10 and Figure 4.11 show the effect of Mg content on the hardness and Fe-intermetallic surface fraction obtained in the case of 319 alloys exhibiting low and high levels of β-Fe and α-Fe intermetallics, respectively, following the same aging conditions (viz., 180°C/2h or 220°C/2h). Similar plots when aging is carried out at different conditions of temperature and time (viz., as cast, as SHT, 155°C/4h, 200°C/4h, 180°C at 4, 6 and 8h and 220°C at 4, 6 and 8h) are not presented in this thesis but have been produced.

From the hardness and Fe-intermetallic volume fractions result for the 356 and 319 alloys in both unmodified and modified conditions Table 4 1 and Table A.1 (in the Appendix), it is found that both hardness and Fe-intermetallic surface fractions increase slightly with the Fe and Fe-Mn contents. However, a remarkable increase in hardness is observed with increasing Mg content when aging carried out at 180°C (peak condition) than at 220°C (overaging condition). The Fe-intermetallics surface fractions were found to be higher in the unmodified alloys compared to the modified alloys, regardless of the intermetallic type (α-Fe or β-Fe). The lower surface fractions exhibited by the modified alloys may be explained by the combined effect of both Sr-modification and solution heat treatment on the dissolution/ fragmentation in the heat-treated samples, see Figure 4.6 through Figure 4.11.

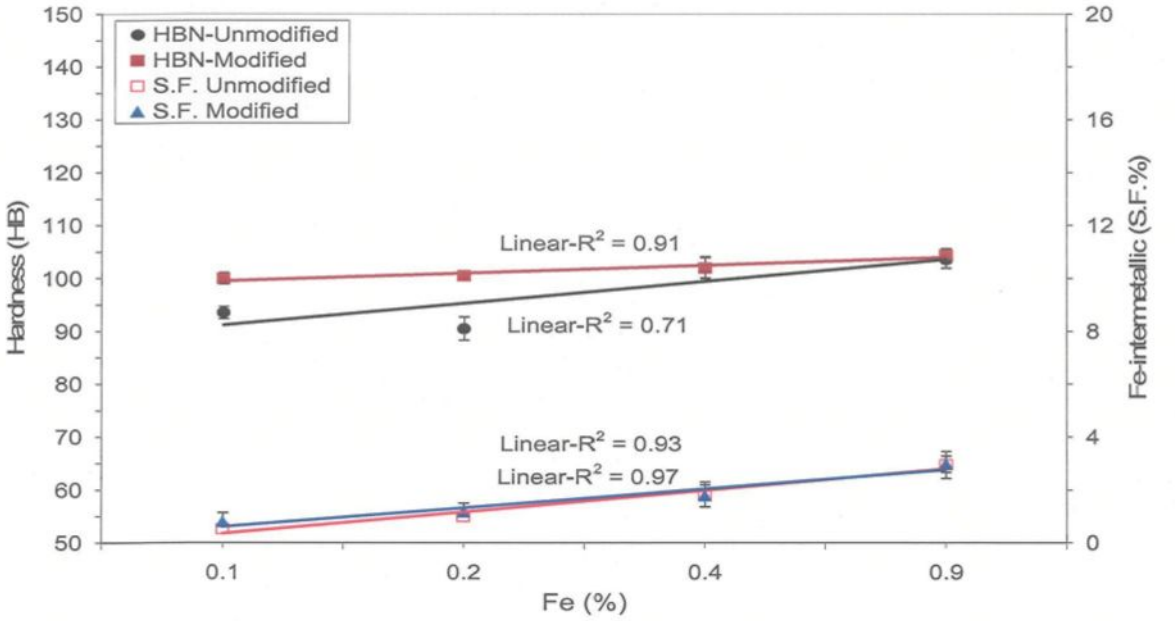

(a)

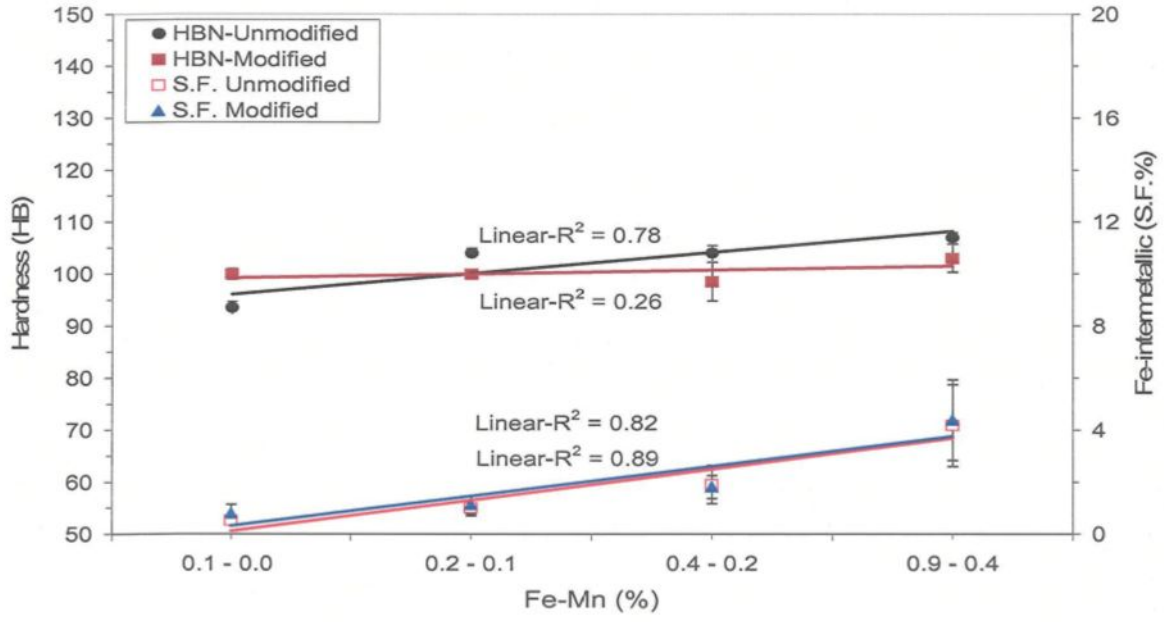

(b)

Figure 4.6 Dependence of hardness and Fe-intermetallics surface fraction on alloying content in 356 alloys aged at 180°C/2h and exhibiting (a) β-Fe, and (b) β-Fe and/or α-Fe intermetallics.

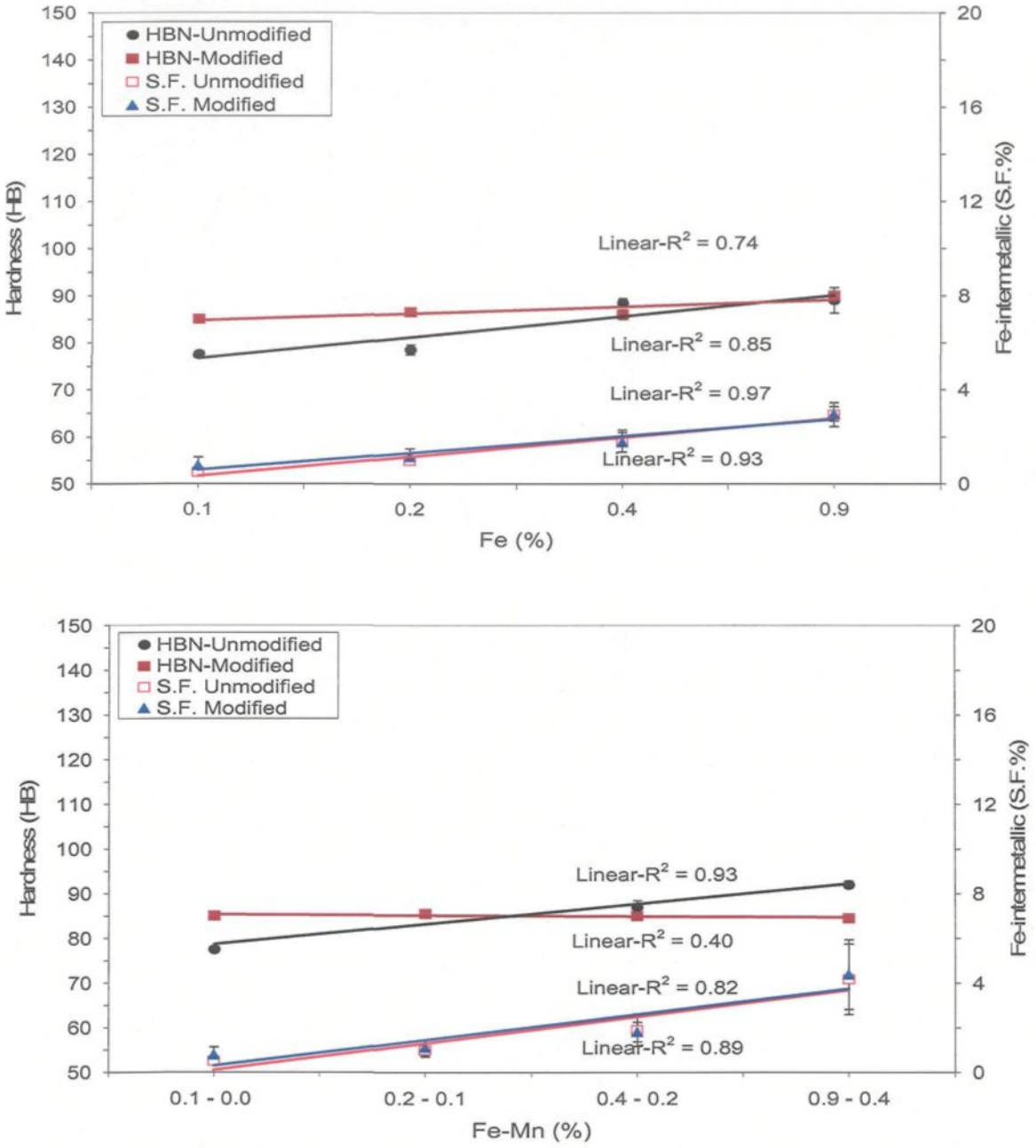

Figure 4.7 Dependence of hardness and Fe-intermetallics surface fraction on alloying content in 356 alloys aged at 220°C/2h and exhibiting (a) β-Fe, and (b) β-Fe and/or α-Fe intermetallics.

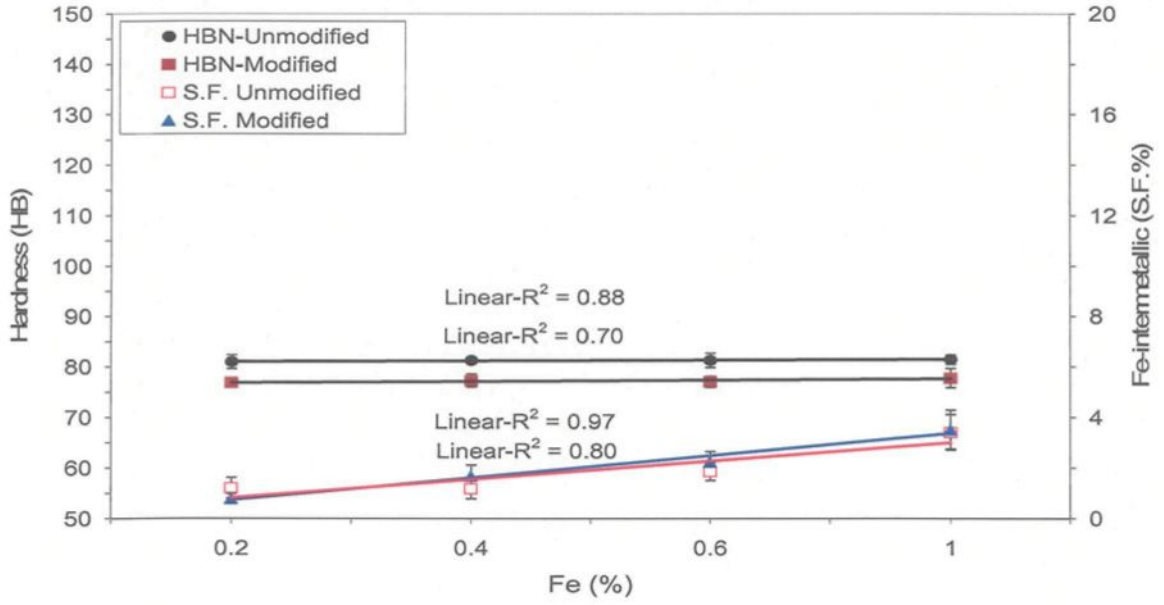

(a)

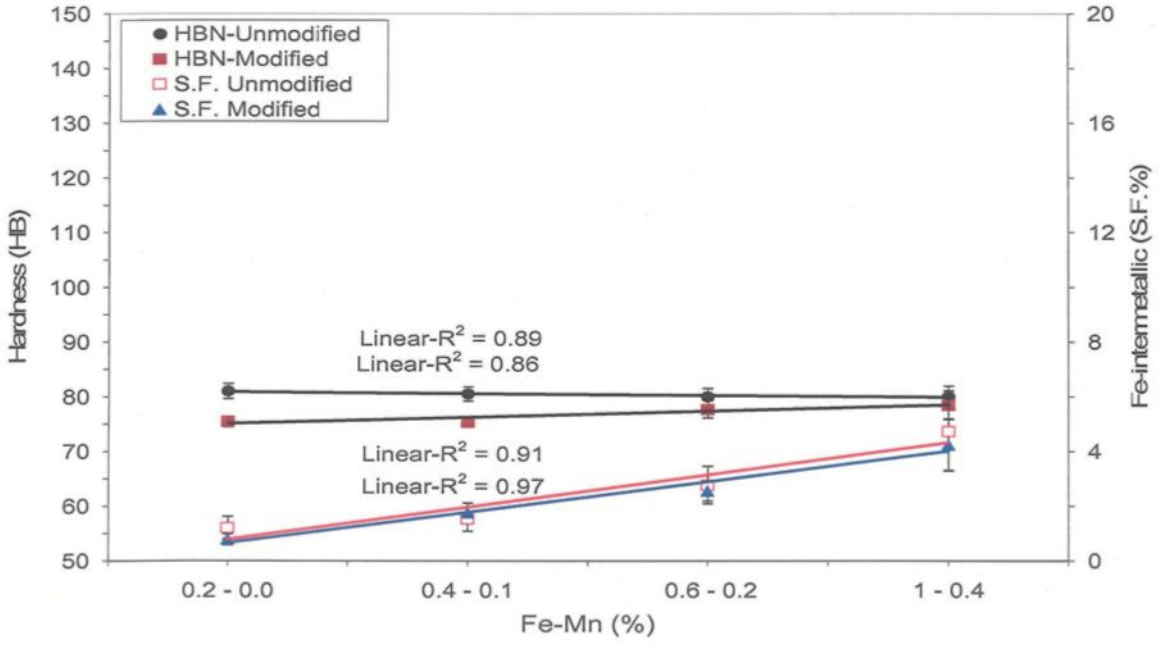

(b)

Figure 4.8 Dependence of hardness and Fe-intermetallics surface fraction on alloying content in 319 alloys aged at 180°C/2h and exhibiting (a) β-Fe, and (b) β-Fe and/or α-Fe intermetallics.

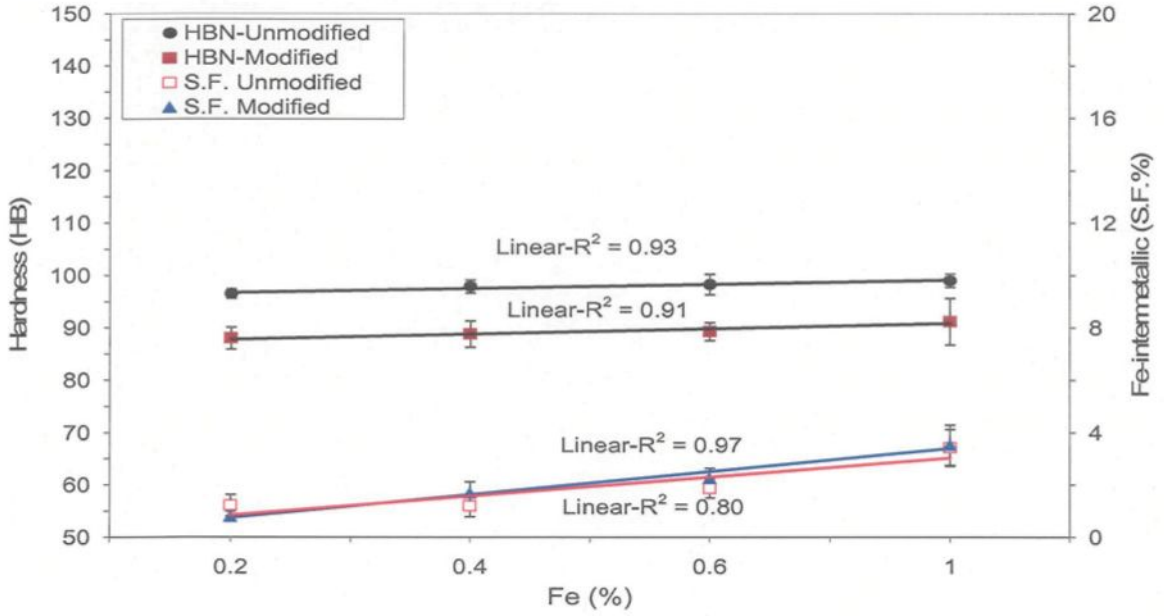

(a)

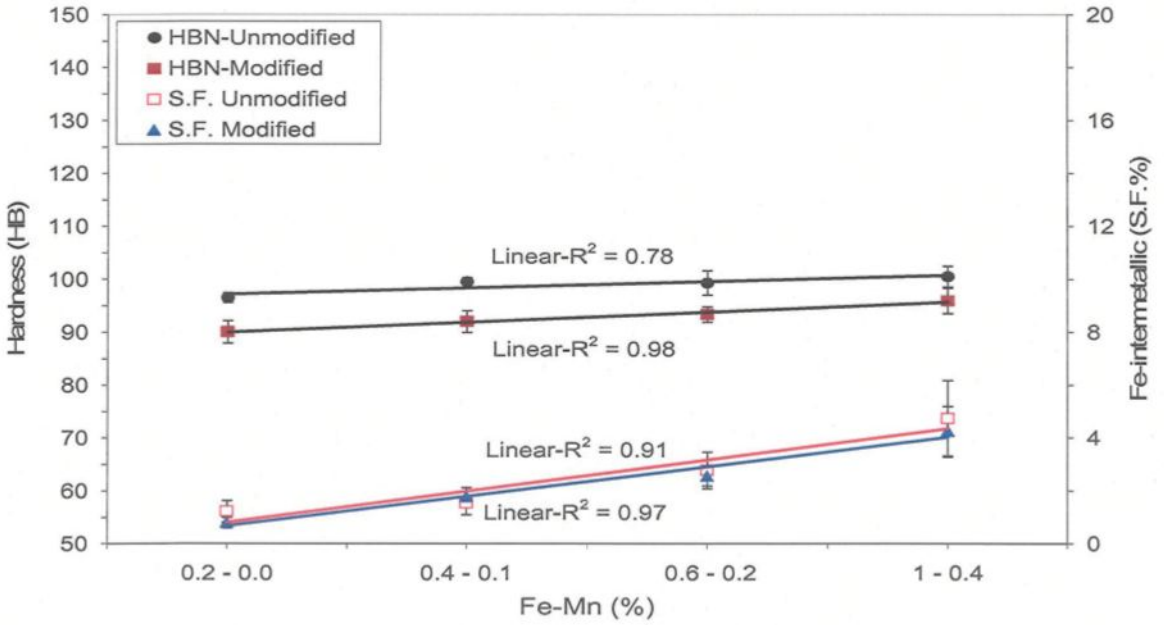

(b)

Figure 4.9 Dependence of hardness and Fe-intermetallics surface fraction on alloying content in 319 alloys aged at 220°C/2h and exhibiting (a) β-Fe, and (b) β-Fe and/or α-Fe intermetallics.

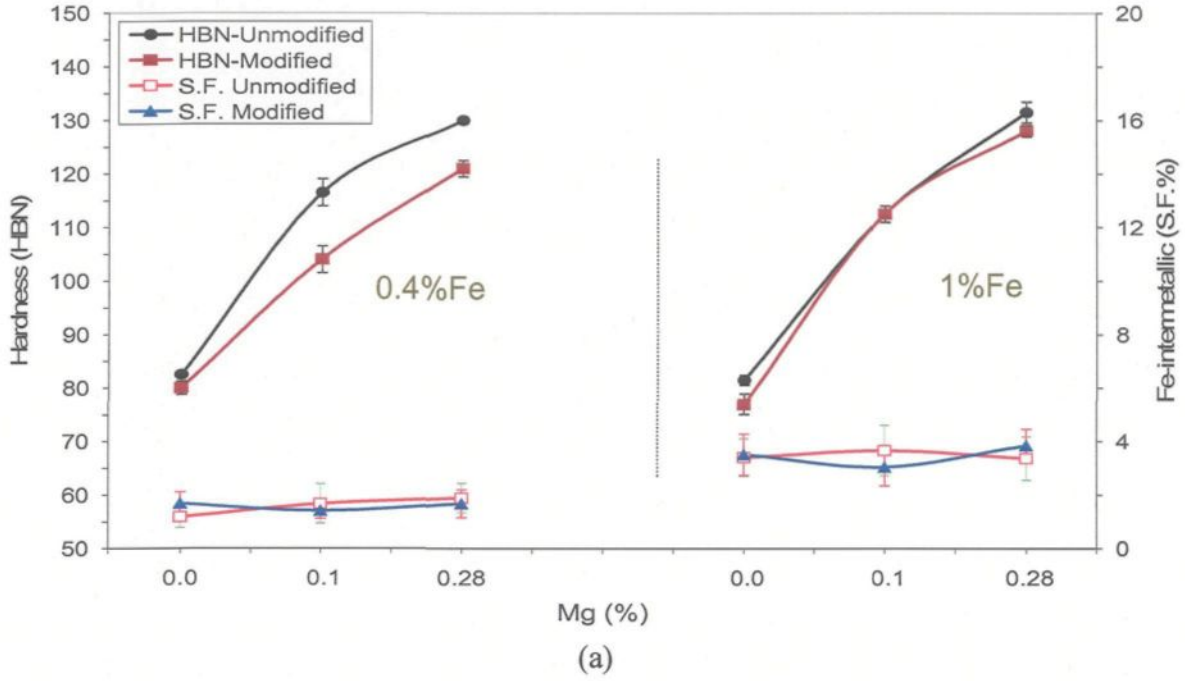

(a)

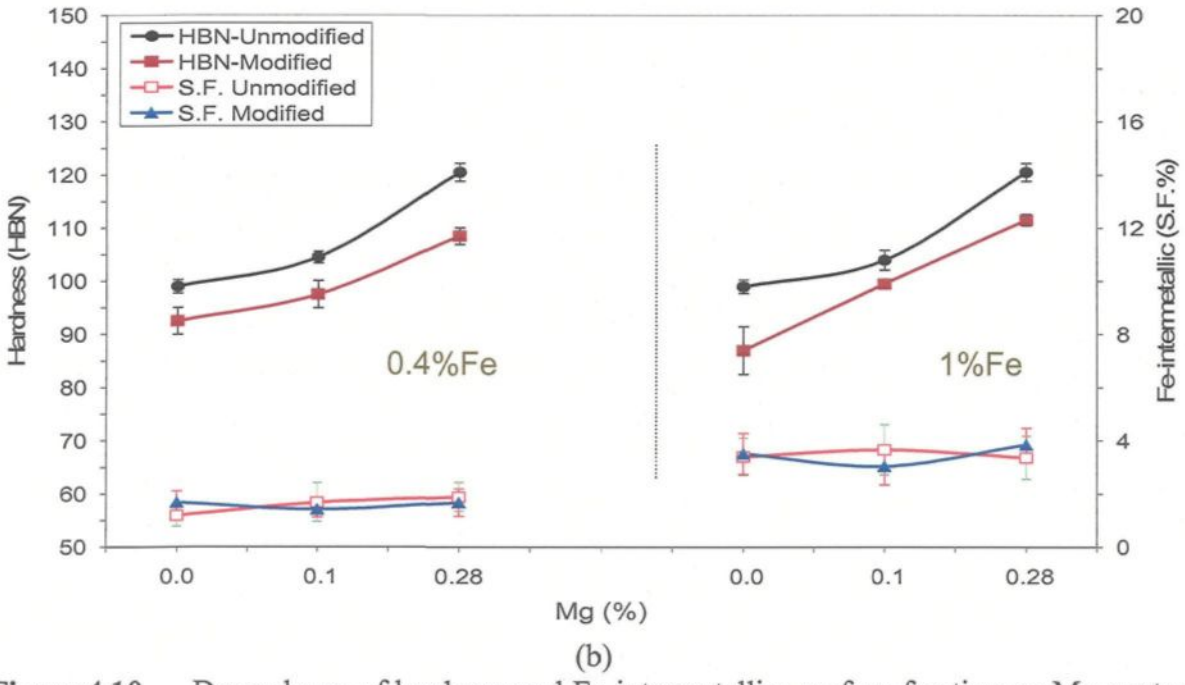

(b)

Figure 4.10 Dependence of hardness and Fe-intermetallics surface fraction on Mg content in 319 alloys exhibiting β-Fe intermetallics and aged for 2h at (a) 180˚C, and (b) 220˚C.

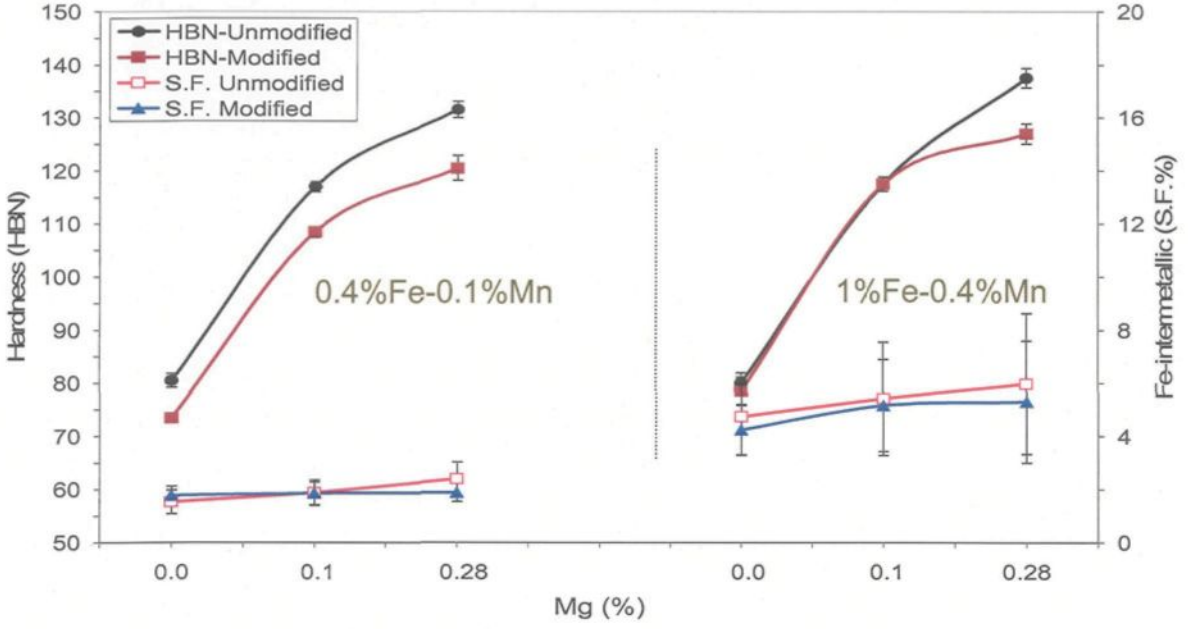

(a)

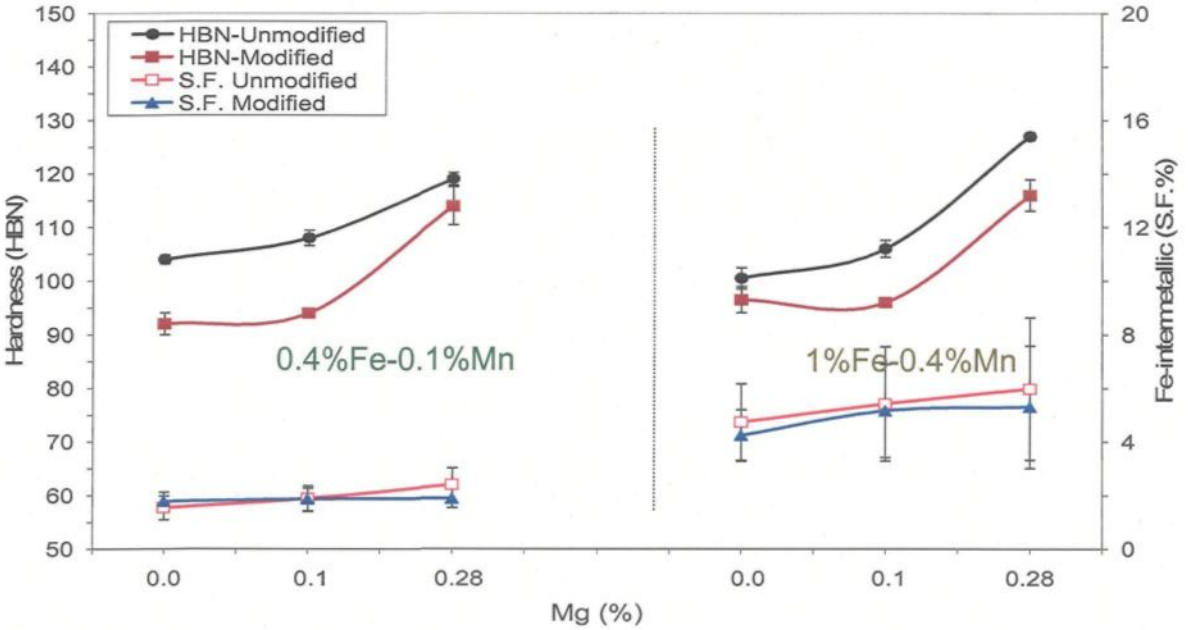

(b)

Figure 4.11 Dependence of hardness and Fe-intermetallics surface fraction on Mg content in 319 alloys exhibiting mainly α and/or β intermetallics in the (a) 180°C/2, (b) 220°C/2 aged conditions.

4.2.5. Microstructure

4.2.5.1. Iron and Copper Intermetallic Volume Fractions

Iron-intermetallic volume fractions were measured for the as-cast and solution heat-treated samples of 356 and 319 alloys in order to determine which conditions provided volume fractions of 2% and 5% (i.e. low and high levels) The corresponding data are provided in Table A.1.in the Appendix, and also are displayed graphically in Figure 4.12(a) and Figure 4.13(a), respectively. The lower surface fractions exhibited by the modified alloys may be explained by the effect of Sr-modification on the fragmentation and dissolution of the β-Fe-intermetallics in the as-cast samples, and to the combined effect of both Sr-modification and solution heat treatment on the dissolution/ fragmentation in the heat-treated samples.

Copper-intermetallic volume fractions for the as-cast and solution heat-treated samples of 319 alloys in the modified and unmodified conditions are presented in Table A.1 in the appendix and also in Figure 4.12(b) and Figure 4.13(b). It is observed that the undissolved Cu-intermetallic volume fractions is higher in 319 alloys containing β-Fe intermetallic compared to those containing α-Fe intermetallic and in the modified than the unmodified conditions (Table A.1 in the appendix). The high level of the undissolved Cu-intermetallic volume fractions exhibited by the Sr-modified and β-Fe intermetallic containing alloys can be attributed to the segregation of the undissolved $AlCu_2$ phase by Sr-modification. On the other hand, β-Fe intermetallic act as nucleation sites for the $AlCu_2$ phase.

The compositions of these Fe-intermetallics were analyzed using wavelength dispersive spectroscopy (WDS) and the average compositions are listed in Table 4.2. At

least 5 to 6 measurements were taken in each case to obtain these values. As expected, and depending upon the Fe/Mn ratio the presence of Mn enhances the formation of the α-Fe intermetallic (rather than the β-Fe).

Table 4.2 Compositions obtained from WDS analysis (at %) of Fe-intermetallics observed in different 356 and 319 alloys

Alloy-Alloy Code.		Element (at %)					Approximate Formula	Phase
		Al	Si	Fe	Mn	Cu		
356	4S	66.0	18.0	15.0	----	----	$Al_{4.4}FeSi_{1.2}$	β-Fe
356	7S	72.0	11.0	10.5	6.0	----	$Al_{11}(Fe_{0.63}, Mn_{0.36}, Cr_{0.004})_{2.64}Si_{1.68}$	α-Fe
356	7S	64.5	20.0	13.0	2.0	----	$Al_{4.3}(Fe_{0.85}, Mn_{0.15})Si_{1.33}$	β-Fe
319	15S	67.0	18.0	14.0	----	----	$Al_{4.8}FeSi_{1.3}$	β-Fe
319	19S	70.0	11.0	12.0	5	1.5	$Al_{11}(Fe_{0.647}, Mn_{0.27}, Cu_{0.081})_{2.9}Si_{1.73}$	α-Fe
319	19S	66.0	19.0	13.0	1.5	----	$Al_{4.55}(Fe_{0.9}, Mn_{0.1})Si_{1.31}$	β-Fe
319	19S	65.5	19.0	13.0	2.0	0.5	$Al_{4.23}(Fe_{0.84}, Mn_{0.13}, Cu_{0.03})Si_{1.23}$	β-Fe

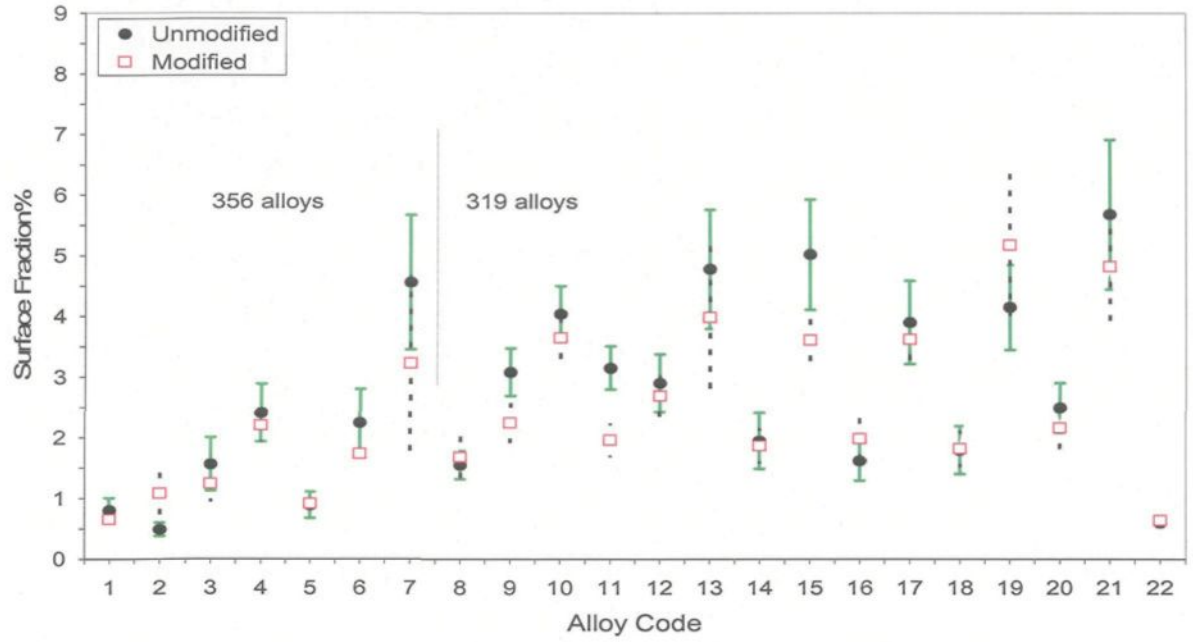

(a)

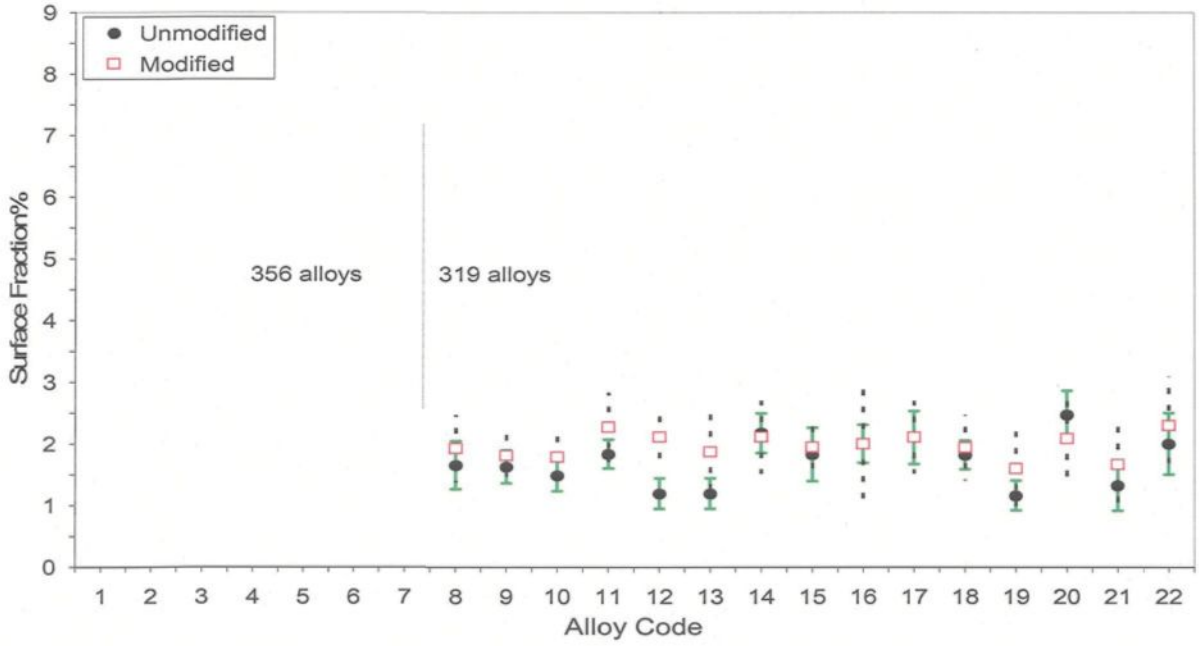

(b)

Figure 4.12 Surface fractions (%) of intermetallics observed in the various 356 (alloy codes 1-7) and 319 (alloy codes 8-22) alloys in the as-cast condition: (a) Fe-intermetallics, (b) Cu-intermetallics.

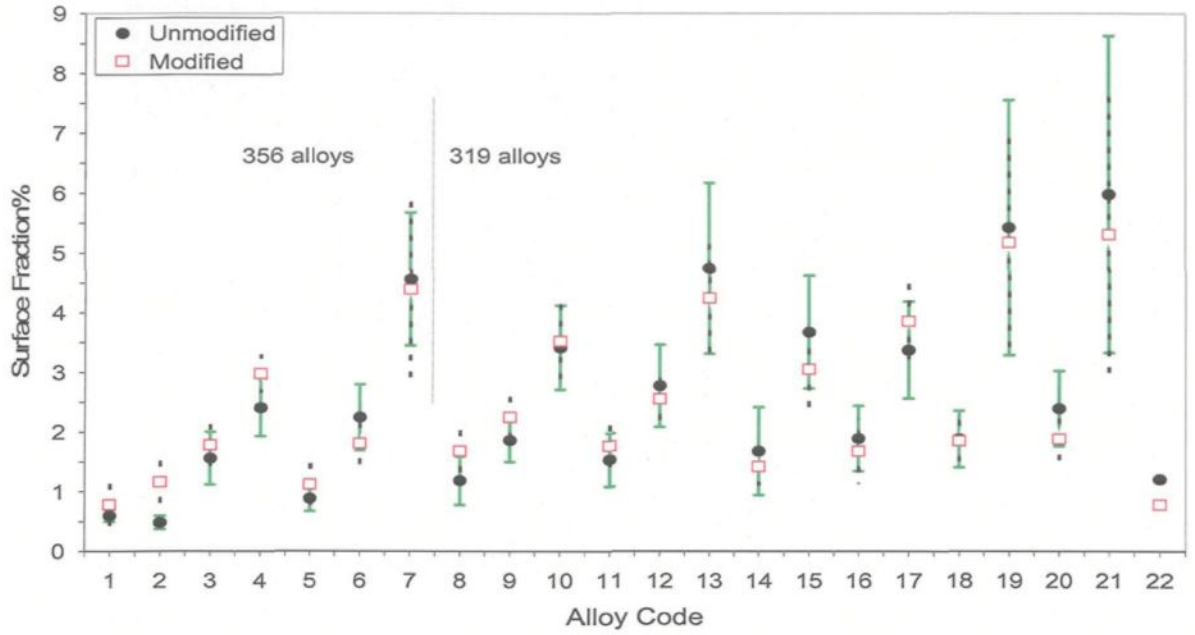

(a)

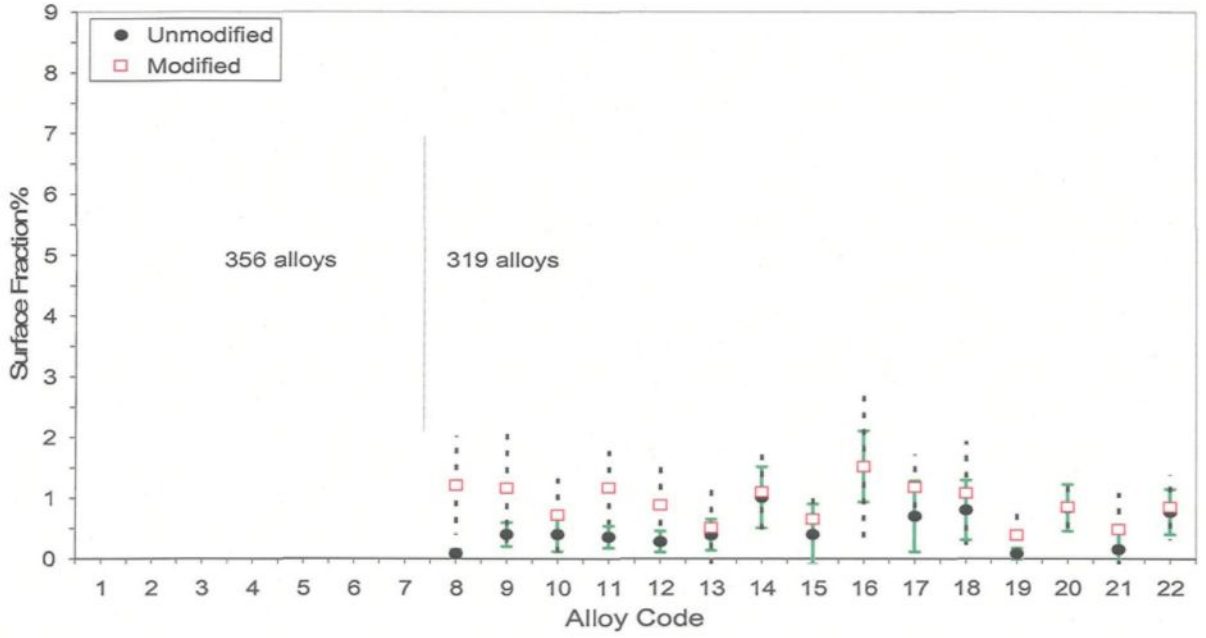

(b)

Figure 4.13 Surface fractions (%) of intermetallics observed in the various 356 (alloy codes 1-7) and 319 (alloy codes 8-22) alloys in the solution heat treated condition: (a) Fe-intermetallics, (b) Cu-intermetallics.

Figure 4.14 shows the backscattered (BS) image and the corresponding elements in the α-Fe intermetallics observed in the microstructure of the 319 alloy 19S sample (containing 1% Fe, 0.4%Mn and 0.1%Mg) in the as-cast condition. Similarly, Figure 4.15 shows the BS image and element distribution corresponding to the β-Fe intermetallics observed in the same alloy sample.

Figure 4.16 compares the morphology of the β-Fe and α-Fe intermetallics observed in backscattered images obtained from 319 and 356 alloy samples, where the higher magnification micrographs of Figure 4.16(b) and (d) clearly reveal the plate-like and script-like morphologies of the two types. The presence of these intermetallics near pores assists in revealing the 3-D aspects of their morphologies. Other interesting aspects of the Fe-intermetallics observed in 356 alloy samples are provided by the optical micrographs of Figure 4.17(a) and (b), which reveal the presence of sludge particles (a), the existence of α-Fe intermetallic particles within the α-Al dendrite (b), modified eutectic silicon regions (c, d) and long platelets (or needles) of the β-Fe intermetallics in the 7S and 4S samples of the Sr-modified 356 alloy, respectively.

Figure 4.18 shows examples of optical microstructures obtained from various high Mg-containing 319 alloy samples, viz., samples 17 (1%Fe-0.28%Mg) and 21 (1%Fe-0.4%Mn-0.28%Mg) and their modified counterparts,17S and 21S. The presence of β-Fe platelets in both samples is observed, Figure 4.18 (a) and (c), while the Sr-modified 17S sample displays a large pre-eutectic β-Fe platelet. The presence of 0.4% Mn in the alloy sample 21 (giving an Fe: Mn ratio of 1.05: 0.38) leads to the formation of mainly α-Fe intermetallics in this case, compared to sample 17 (containing no Mn). The presence of a $CuAl_2$ intermetallic particle is also observed in Figure 4.18(c).

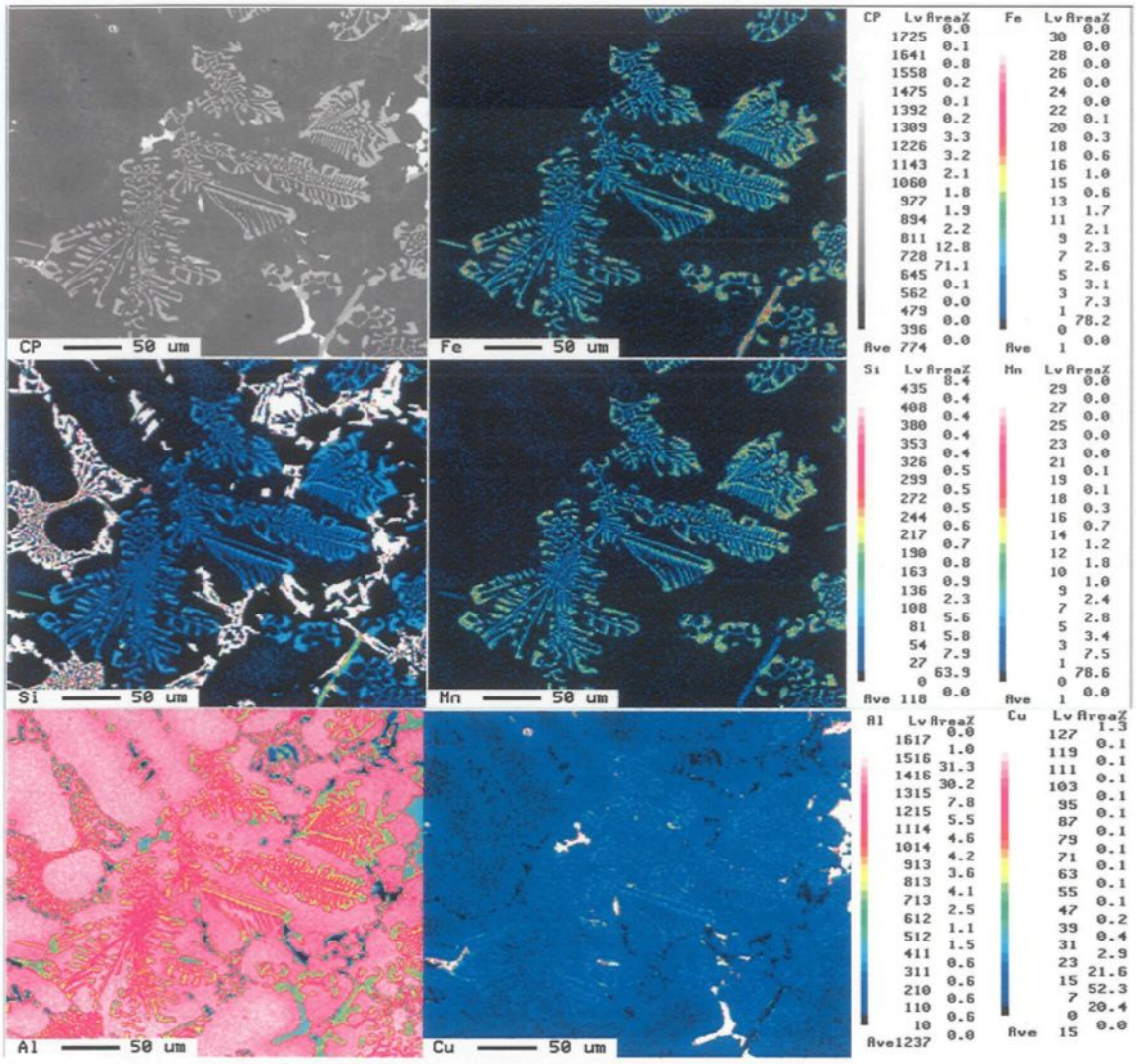

Figure 4.14 Backscattered image (cp) taken from the 19S alloy sample (319 alloy, as-cast condition), showing the α-Fe intermetallic phase and the corresponding X-ray images of Fe, Si, Mn, Al and Cu.

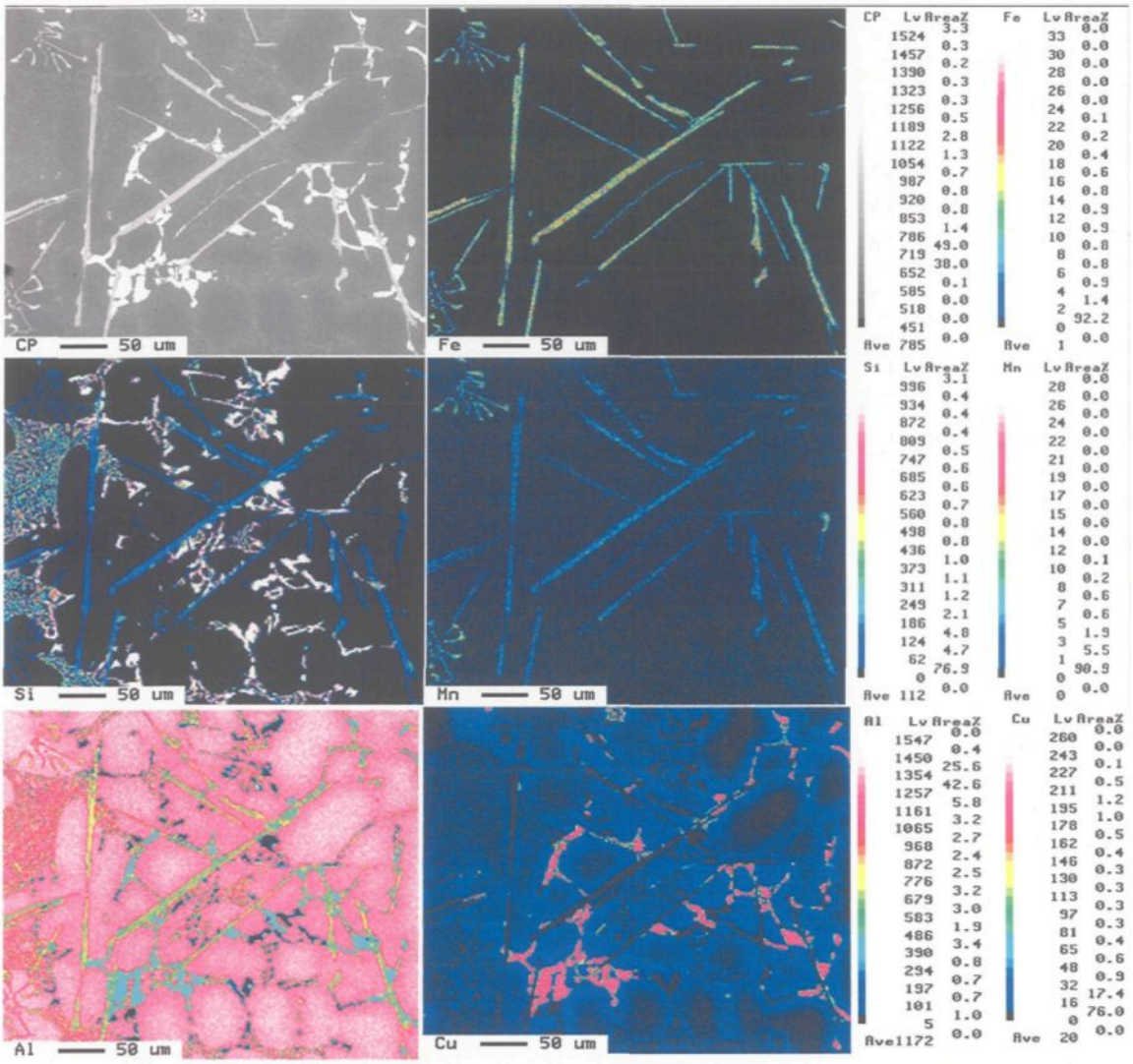

Figure 4.15 Backscattered image (cp) taken from the 19S alloy sample (319 alloy, as-cast condition), showing the β-Fe intermetallic phase and the corresponding X-ray images of Fe, Si, Mn, Al and Cu.

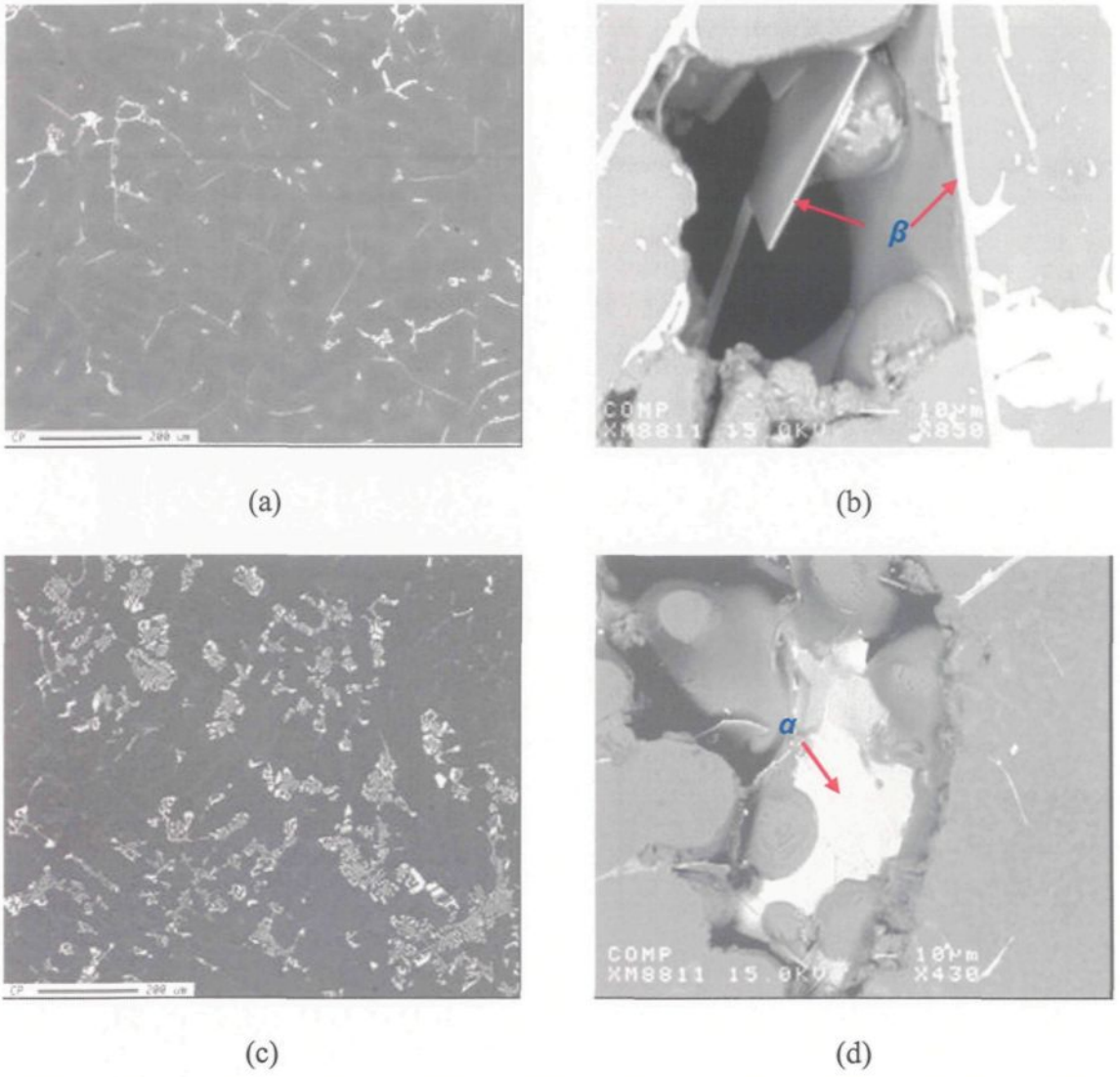

(a) (b)

(c) (d)

Figure 4.16 Backscattered images taken from alloy samples 8S (319 alloy) and 7S (356 alloy) showing (a, b) plate-like β-Fe intermetallics, and (c, d) script-like α-Fe intermetallics observed in the two samples, respectively.

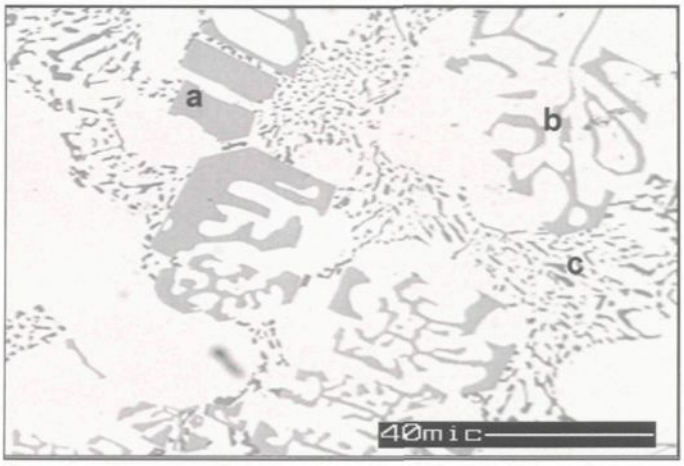

(a)

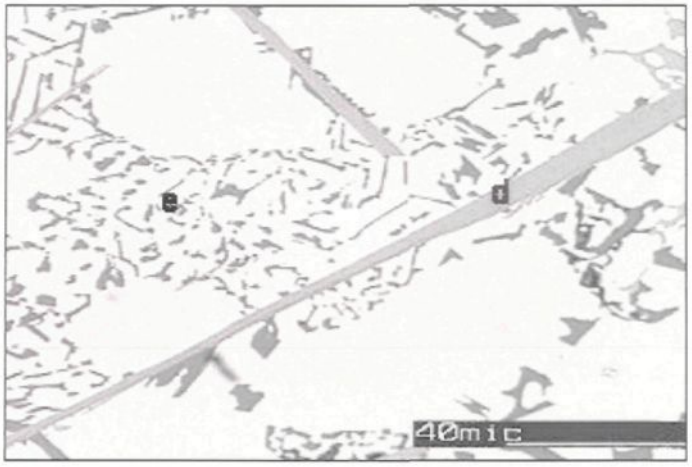

(b)

Figure 4.17 Optical micrographs corresponding to (a) 7S and (b) 4S Sr-modified 356 alloy samples, showing the presence of sludge particles (a), α-Fe intermetallic particles within the α-Al dendrite (b), modified eutectic Si regions (c, e), and plate-like β-Fe intermetallics (d).

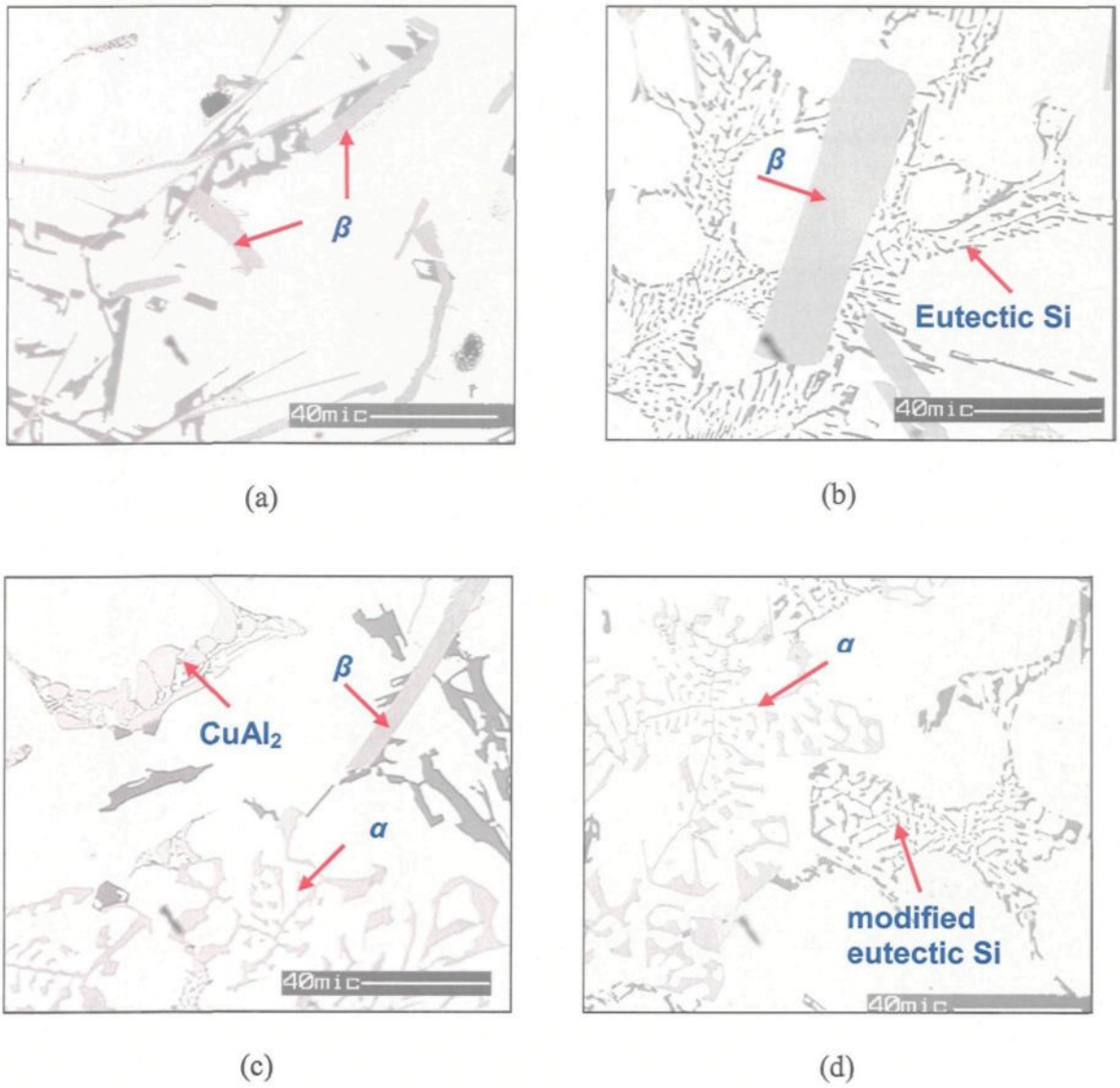

Figure 4.18 Optical micrographs obtained from as-cast 319 (a, b) 17 and 17S, and (c, d) 21 and 21S alloy samples, showing the presence of β-Fe, α-Fe and $CuAl_2$ intermetallics, and acicular and modified eutectic Si particles.

4.2.5.2. Effect of Chemical Modification and Solution Heat Treatment

Modification of eutectic Si particles can be achieved chemically (Sr-modification) and/or thermally (through solution heat treatment process). Strontium modification has been observed to lower solution treatment times considerably.[130] The variations in Si particle size and morphology for the unmodified and Sr-modified 356 and 319 alloys in the as-cast and solution heat treated conditions (540°C/8h and 495°C/8h, respectively) are shown in Table 4.3.

Strontium modification changes the silicon morphology from acicular to fibrous, resulting in a significant decrease in the size of the Si particles, and a corresponding increase in the particle count per unit area. As Table 4.3 shows, the as-cast Sr-modified 356 and 319 alloy samples exhibit a decrease in both particle area and length and an increase in the particle roundness and density (particles/mm^2), indicating fragmentation of the particles. Magnesium is reported as having either a modifying or a coarsening effect on the eutectic Si.[131, 132] While magnesium is observed to refine the eutectic silicon particles in the as-cast unmodified 319 alloys containing mainly β-Fe intermetallics (0.4%Fe and 1%Fe), however, it has a negative effect in the Sr-modified alloys due to the Mg-Sr interaction. These effects are more pronounced in the unmodified and modified (Sr >185 ppm) 319 alloys containing mainly α-Fe intermetallics (0.4%Fe-0.1%Mn and 1% Fe-0.4%Mn). This may be explained by the formation of the complex intermetallic compound $Mg_2SrAl_4Si_3$ prior to the eutectic reaction, whereby the amount of strontium in solution and hence its modifying effect are reduced.

Solution heat treatment spheroidises and coalesces the fine modified silicon particles into coarser particles. However these coarser particles are still smaller in size

than the unmodified acicular silicon particles. Unlike 356 alloys, 319 alloys are observed to be more resistant to spheroidization, Table 4.3. This can be attributed to the lower solution treatment temperature in 319 alloys (495°C) compared to that of 356 alloys (540°C).

Examples of acicular and modified Si particles in as-cast samples of 319 alloys are already shown in Figure 4.18(a, c) and Figure 4.18(b, d), respectively. As expected, the unmodified alloys samples 17 and 21 exhibit acicular eutectic Si particles, while the 17S and 21S modified alloy samples display refined eutectic Si regions. Figure 4.19. and Figure 4.20 show examples of the effect of solution treatment in various unmodified and Sr-modified 356 and 319 alloys.

Figure 4.21 shows backscattered images obtained from non-modified and Sr-modified 356 alloy samples aged at 180°C/4h. In this case, well defined Mg_2Si precipitates and precipitate-free zones (PFZ) can be observed within the alloy matrix in each case, regardless of the Fe-intermetallic type present. Yet other examples are provided in the optical micrographs of Figure 4.22, taken from the non-modified and Sr-modified 319 17 and 21, and 17S and 21S alloy samples, respectively, aged at 180°C for 4h.

Table 4.3 Silicon particle characteristics of a) 356 alloys and b) 319 alloys showing the effect of chemical modification (Sr and Mg additions) and Solution heat treatment

a) 356 alloys (as cast and SHT- 8h @540°C)										
Alloy (Mg, Sr levels)	**Silicon Particle characteristics.**									
	A	**S.D.**	**L**	**S.D.**	**A. R**	**S.D.**	**R**	**S.D.**	**D**	**S.D**
4- (0.3%Mg)	10.0	23.0	5.5	8.0	2.32	1.2	60.0	31.5	5971	4
4S- (163 ppm Sr)	4.0	9.0	3.5	4.0	2.23	1.0	67.0	26.5	10752	3
4–T6	17.0	29.5	6.5	8.5	2.17	1.2	68.0	27.0	3022	1
4S-T6	9.5	15.0	4.5	5.0	2.01	1.0	74.5	23.0	4333	0
Mostly β-Fe intermetallic-containing alloy (0.9%Fe)										
6- (0.3%Mg)	8.5	21.0	4.5	7.5	2.28	1.2	64.0	30.0	5216	3
6S– (176 ppm Sr)	2.0	6.0	2.5	2.5	2.12	0.9	74.0	24.5	16121	2
7- (0.3%Mg)	7.5	20.0	4.5	7.0	2.18	1.2	66.0	30.0	6106	6
7S– (186 ppm Sr)	3.5	8.0	3.0	3.5	2.13	0.9	70.0	26.0	12703	1
7- T6	13.0	31.0	6.0	9.0	2.15	1.3	68.0	27.0	2800	2
7S-T6	10.5	14.5	5.5	5.0	2.10	1.0	70.5	24.0	3666	1
α-Fe intermetallic-containing alloys (0.4%Fe-0.2%Mn and 0.9%Fe-0.4%Mn), respectively										
b) 319 alloys (as cast and SHT- 8h@495°C)										
Alloy (Mg, Sr levels)	**Silicon Particle characteristics.**									
	A	**S.D.**	**L**	**S.D.**	**A. R**	**S.D.**	**R**	**S.D.**	**D**	**S.D**
8- (0.0%Mg)	11.5	29.0	5.5	9.5	2.21	1.24	64.0	31.0	4225	11
8S- (160 ppm Sr)	7.5	16.0	4.5	5.5	2.14	1.01	66.0	27.0	6030	20
14- (0.1%Mg)	11.0	31.0	5.0	9.5	2.00	1.02	70.0	30.0	4299	7
14S- (179 ppm Sr)	7.0	15.0	4.5	6.0	2.24	1.08	64.0	28.0	5550	17
16- (0.3%Mg)	10.0	30.0	4.5	9.5	2.16	1.13	70.5	30.0	3985	9
16S- (178 ppm Sr)	6.5	14.5	4.0	6.0	2.12	1.04	69.0	28.0	6306	13
Mostly β-Fe intermetallic-containing alloys (0.4%Fe)										
10- (0.0%Mg)	12.0	28.5	5.5	9.0	2.32	1.2	63.5	31.0	4071	3
10S- (150 ppm Sr)	6.0	13.0	4.0	5.0	2.13	1.0	69.5	27.0	9063	10
15- (0.1%Mg)	11.0	29.0	5.0	9.0	2.14	1.1	66.5	30.0	3910	6
15S- (131 ppm Sr)	5.5	12.0	3.5	4.5	2.00	0.8	70.0	25.5	7645	6
17- (0.3%Mg)	10.5	26.0	5.0	8.5	2.16	1.1	66.5	30.0	3331	3
17S- (185 ppm Sr)	7.5	16.0	5.0	6.0	2.26	1.0	63.5	28.0	5224	11
17-T6	14.5	32.5	5.5	9.0	1.96	0.9	75.0	25.5	3120	5
17S-T6	7.5	15.5	4.5	5.0	2.10	1.0	72.0	24.5	5232	1
Mostly β-Fe intermetallic-containing alloys (1%Fe)										

Alloy (Mg, Sr levels)	Silicon Particle characteristics.									
	A	S.D.	L	S.D.	A. R	S.D.	R	S.D.	D	S.D
11- (0.0%Mg)	11.5	29.5	5.5	10.0	2.27	1.2	66.5	30.5	3988	4
11S- (158 ppm Sr)	6.0	13.0	4.0	4.5	2.00	0.9	69.0	26.0	8015	11
18-(0.1%Mg)	18.0	41.0	7.5	12.0	2.36	1.3	63.0	31.0	2111	9
18S- (196 ppm Sr)	7.0	14.5	4.5	6.0	2.17	1.0	65.5	28.5	5692	9
20- (0.3%Mg)	18.0	39.0	7.5	11.0	2.31	1.2	62.0	31.5	2550	7
20S- (209 ppm Sr)	9.0	18.0	5.5	7.0	2.29	1.1	62.5	28.5	4614	15
20-T6	23.0	39.5	8.5	11.0	2.22	1.2	65.0	29	1850	5
20S- T6	12.0	22.5	6.0	6.5	2.21	1.1	66.5	26.5	3462	1
Mostly β-Fe intermetallic-containing alloys, little α-Fe (0.4 %Fe-0.1%Mn)										
19- (0.1%Mg)	13.5	28.5	6.5	9.5	2.39	1.3	62.5	30.5	2963	3
19S- (193 ppm Sr)	7.0	14.5	4.5	5.5	2.23	1.0	65.5	27.0	4782	8
19-T6	15.0	28.0	6.5	8.5	2.18	1.2	69.5	27.5	2714	2
19S-T6	8.5	18.0	4.5	5.5	1.99	0.9	73.5	24.0	4369	1
21- (0.3%Mg)	16.0	33.0	7.0	10.5	2.40	1.3	61.0	31.0	2005	3
21S- (200 ppm Sr)	6.0	14.5	4.0	5.5	2.00	0.9	70.0	27.0	7312	19
21-T6	20.0	38.5	7.5	10.5	2.12	1.1	69.5	28.5	1950	5
21S- T6	11.0	20.0	5.5	5.5	2.11	1.0	68.5	25.0	3935	1
Mostly α-Fe intermetallic-containing 319 alloys (1%Fe-0.4%Mn)										

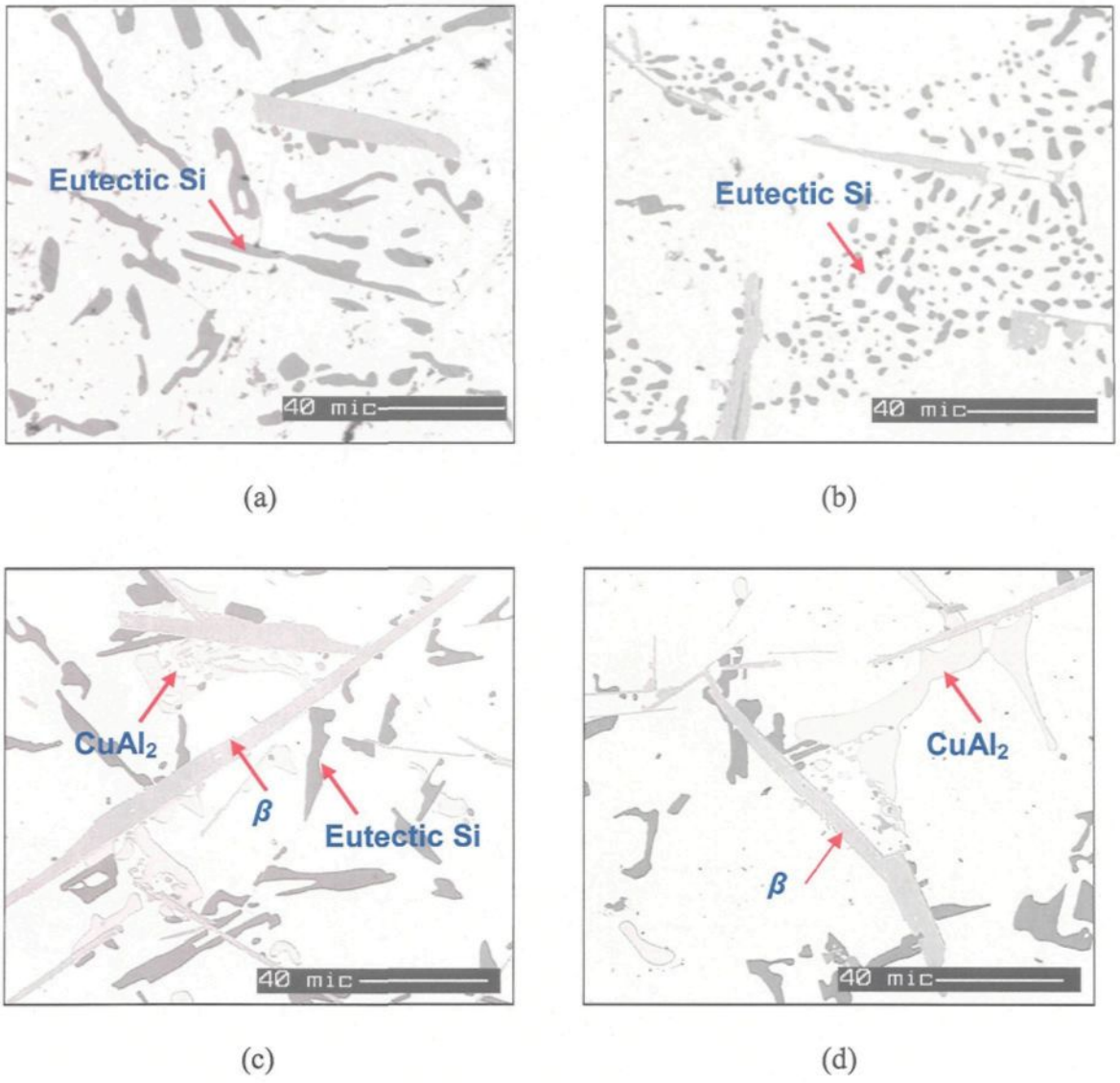

Figure 4.19 Optical micrographs obtained from (a, b) 6 and 6S 356 alloy samples, and (c, d) 20 and 20S 319 alloy samples in the SHT condition, showing the presence of β-Fe and $CuAl_2$ intermetallics, and acicular and fibrous eutectic silicon particles.

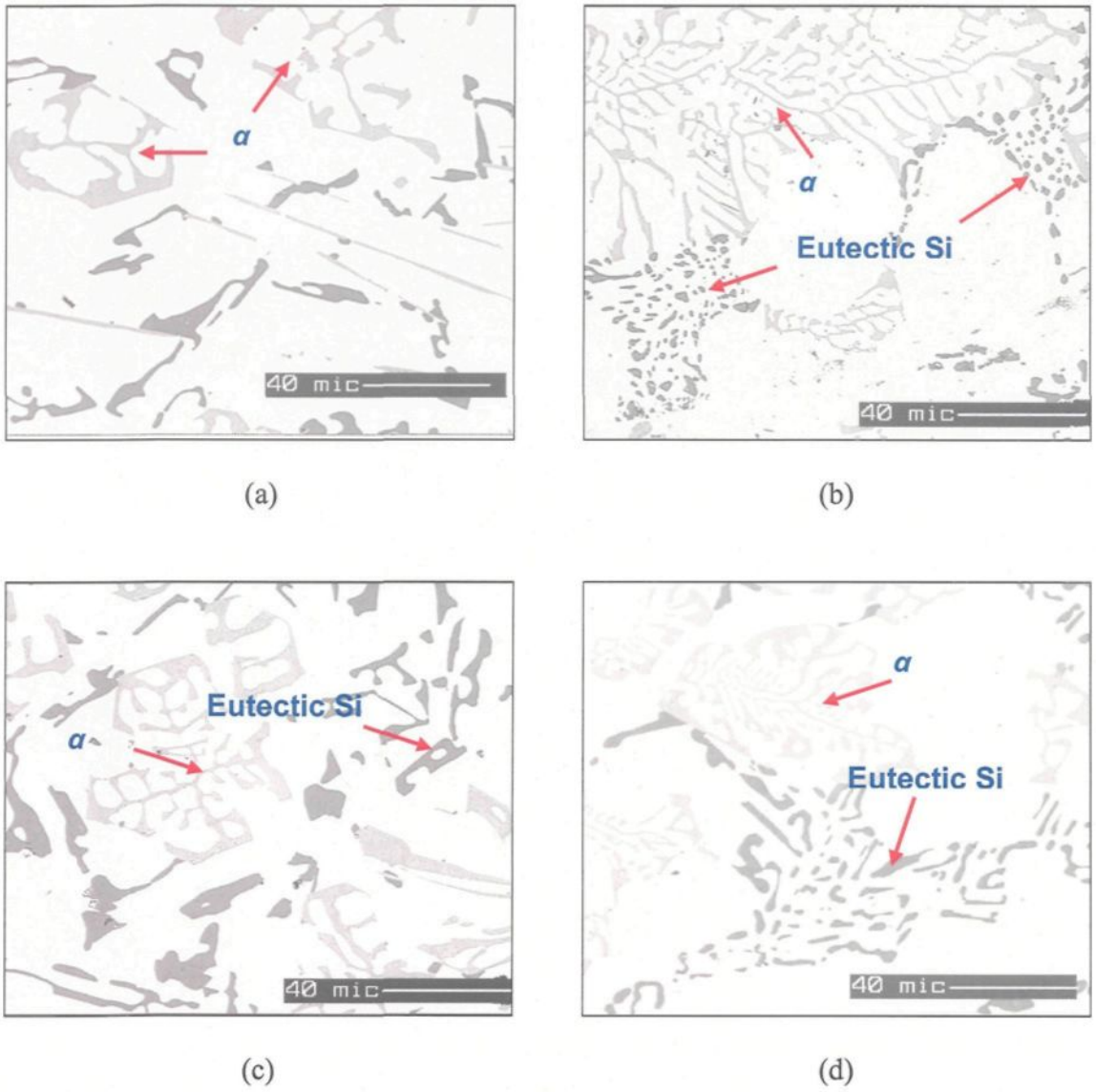

Figure 4.20 Optical micrographs obtained from solution heat-treated 319 alloy samples corresponding to alloy conditions 19 and 19S (a, b), 21 and 21S (c, d), showing acicular Si particles (a, c) and α-Fe intermetallics in the Mn-containing 19, 19S, 21 and 21S alloys (a, b, c, d).

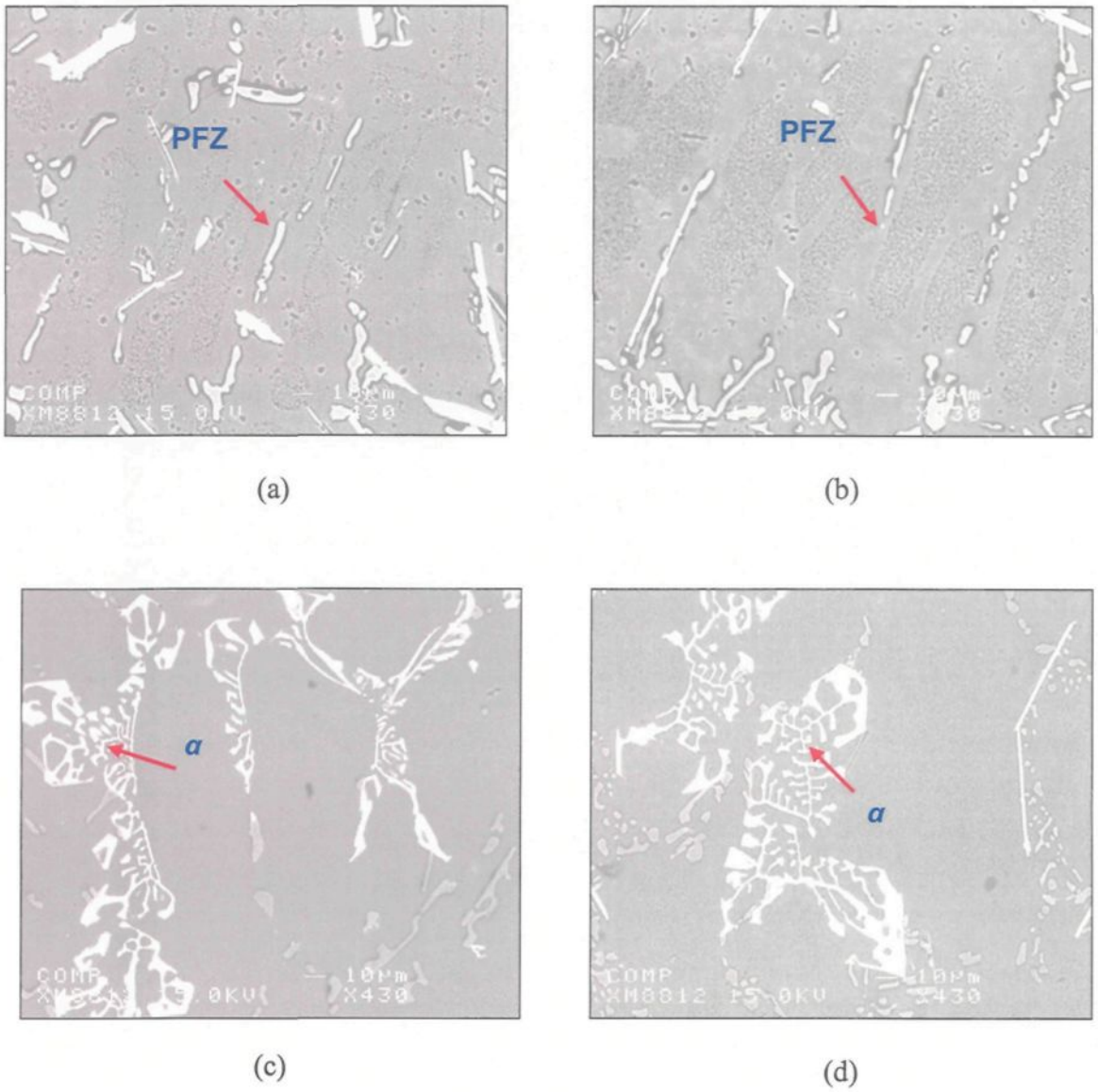

Figure 4.21 Backscattered images taken from etched 356-T6 (180°C/4h) 4 and 4S (a, b), and 7 and 7S (c, d) alloy samples, showing precipitates-free zones (PFZs) in the vicinity of (a, b) the β-Fe intermetallics in the Mn-free 4 and 4S samples, and (c, d) the α-Fe intermetallics in the Mn-containing 7 and 7S samples, respectively.

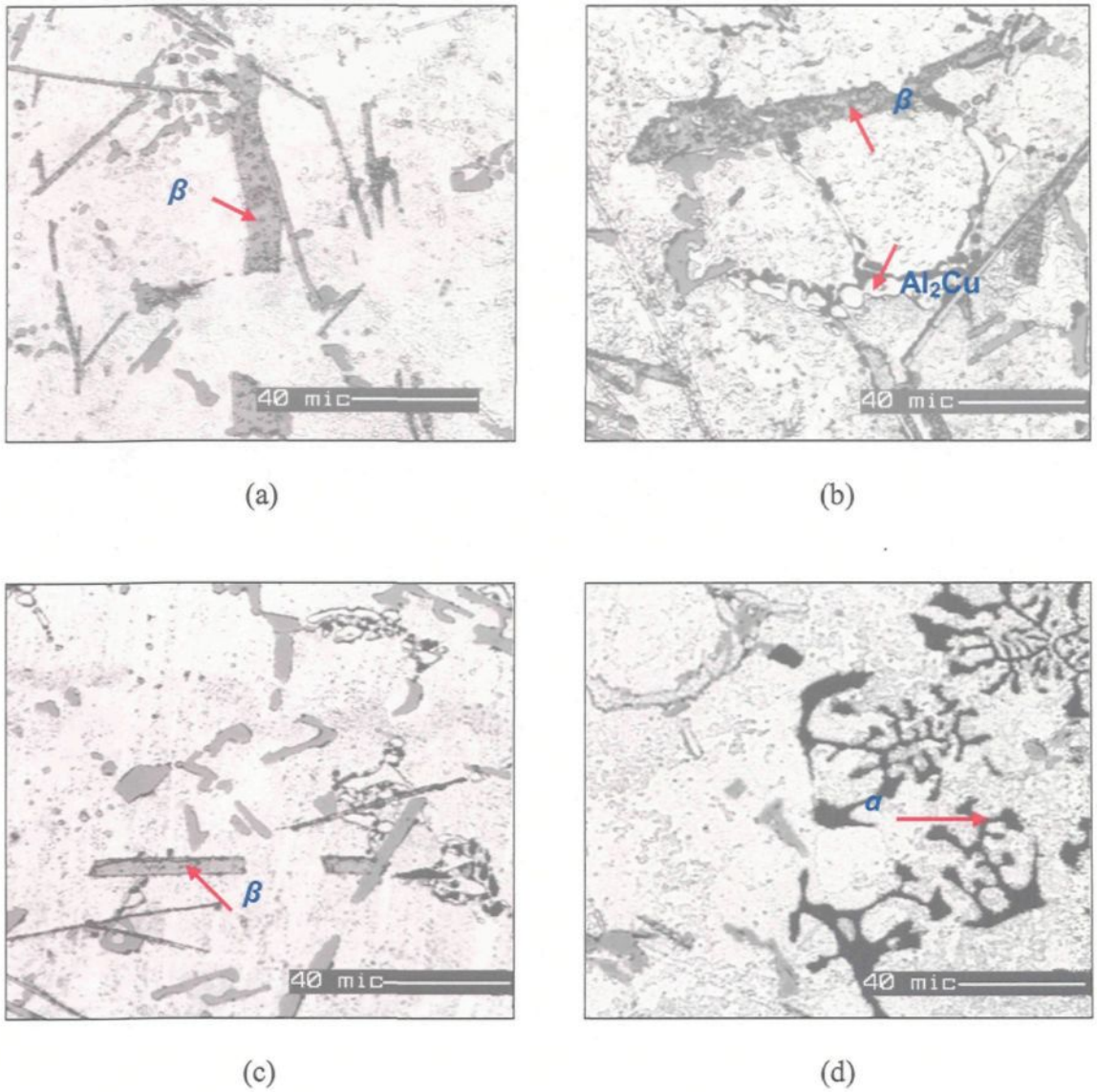

Figure 4.22 Optical micrographs obtained from etched 319-T6 (180°C/4h) 17 and 17S (a, b), and 21 and 21S (c, d) alloy samples, showing a massive β-Fe platelet in (a), β-Fe and $CuAl_2$ intermetallics in (b), and β-Fe and α-Fe intermetallics (black) in the Mn-containing 21 and 21S alloy samples, (c) and (d) Note that, etching reveals the Mg_2Si precipitation within the α-Al matrix, it also attacks the surface of β-Fe intermetallic platelets.

4.3. SUMMARY

The present study was undertaken to investigate the effect of metallurgical parameters on the hardness and microstructural characterisations of as-cast and heat-treated 356 and 319 alloys, with the aim of adjusting these parameters to produce castings of suitable hardness (85-115 HBN) and Fe-intermetallic volume fractions (2-5%) for subsequent use in studies relating to the machinability of these alloys. Hardness measurements were carried out on specimens prepared from 356 and 319 alloys in the as-cast and heat-treated conditions, using different combinations of grain refining, Sr-modification, and alloying additions. Aging treatments were carried out at 155°C, 180°C, 200°C, and 220°C for 4 h, followed by air cooling, as well as at 180°C and 220°C for 2, 4, 6, and 8 h to determine conditions under which specific hardness levels *viz.*, 85 and 115 HBN could be obtained.

Peak hardness was observed in 356 alloys containing both α-Fe and β-Fe intermetallics when aging was carried out at 180°C/4h. In the case of unmodified or modified 356 alloys containing mostly α-Fe intermetallics, aging at 180°C up to 8h produced a sharp rise in hardness during the first two hours of aging, followed by a broad peak or plateau over the 2-8 h aging period. Aging at 220°C revealed a hardness peak at 2h aging time for both 356 and 319 alloys. Addition of Mg to unmodified or modified 319 alloys containing β-Fe and/or α-Fe intermetallics produced a remarkable increase in hardness at all aging temperatures.

4.3.1. SELECTION OF ALLOY CONDITIONS FOR MACHINABILITY STUDIES

By measuring the amount of iron- and copper-intermetallics formed and the changes in the eutectic Si particle characteristics resulting from alloying additions (Fe, Mn, Mg), Sr modification, and heat treatment of the 356 and 319 alloys, and the corresponding hardness values, it was possible to determine which conditions or metallurgical parameters yielded Fe intermetallic surface fractions between 2% and 5%, and hardness levels of 85-115 HBN. These values correspond to those considered suitable for (and commonly observed in) commercial applications of these alloys.

This formed the basis for selecting the following 356 and 319 alloys-listed as M1 through M5 in Table 4.4 below, for conducting the machinability part of the work presented in Chapters 5, 6 and 7.

Table 4.4 Alloys Selected for Machinability Studies (All Containing α-Fe Intermetallic)

Mach. Casting No.	Alloy Type	Alloy code	Mg (%)	Sr (ppm)	Fe-Int. S.F (%)	Mn/Fe ratio	Cu-Int. S.F (%)	Aging Treatment	Hardness (HB)
M1	356	6S	0.3%	218	2%	0.75	0.0%	180°C/2h	100
M2	319	18S	0.1%	234	2%	0.75	1.0%	220°C/2h 180°C/2h	90 100
M3	319	19S	0.1%	236	5%	0.4	0.5%	180°C/2h 220°C/2h	100 90
M4	319	20S	0.28%	133	2%	0.75	1.0%	As-cast 220°C/2h 180°C/2h	88 100 110
M5	319	21S	0.28%	260	5%	0.4	0.5%	180°C/2h	100

Note: Mn level (0.2% in 6S alloy adjusted to 0.3% in M1 alloy
Mn level (0.1%) in 18S and 20S alloys to 0.3% in M2 and M4 alloys
S.F (%) surface fraction percent

4.3.2. Machinability Approach

From the point of view of machinability, it is expected that heat treatment that increase the hardness will reduce the built-up edge on the cutting tool and improve the surface finish of the machined part. A minimum hardness of 80 HBN for an alloy casting is desirable to avoid difficulties associated with built-up edge (BUE) on the cutting tool.[7] Thus those 356 and 319 Sr-modified alloys containing mainly α-Fe intermetallics and possessing hardness levels of 100±10 (HB) were selected for the drilling and tapping studies presented in the following chapters i.e. Ch. 5, 6 and 7.

In selecting the above alloys, viz. one 356 alloy and four 319 alloys, the machinability studies will elaborate upon the following.

i) Effect of Mg and α-Fe-intermetallic surface fraction on the machinability of heat treated 319 alloys at two levels of Mg (0.1% and 0.28%) and two levels of α-Fe-intermetallic surface fractions (2 and 5%).

j) Compare the machinability characteristics of 356 and 319 alloys (with comparable Mg levels) to determine the effect of Cu on the machinability.

CHAPTER 5
METHODOLOGY FOR DATA PROCESSSING: CALCULATION OF CUTTING FORCE, MOMENT AND PEAK-TO-VALLEY RANGE DURING DRILLING AND TAPPING PROCESSES

CHAPTER 5
METHODOLOGY FOR DATA PROCESSSING: CALCULATION OF CUTTING FORCE, MOMENT AND PEAK-TO-VALLEY RANGE DURING DRILLING AND TAPPING PROCESSES

5.1. INTRODUCTION

In this chapter is presented an introduction to the force and moment calculations which are used as a way of evaluating different kinds of machining processes such as drilling and tapping. An assessment of these processes will be made in the following chapters. Evaluating machinability based on the cutting forces requires adequate piezoelectric sensor technology. The piezoelectric force measuring system differs considerably from other methods of measurement. The forces acting on the quartz crystal element are converted to a proportional electric charge. The charge amplifier converts this charge into standardized voltage and current signals, which can then be evaluated by signal processing.

A Kistler 6-component piezoelectric quartz crystal dynamometer (type 9255B) was used for 6-component force and moment (Fx, Fy, Fz, Mx, My and Mz) measurement during drilling and tapping tests. A Kistler multi-channel charge amplifier type (5017B18) with 8 independent measuring channels was used in combined force and moment measurement using piezoelectric multi-component dynamometers. The eight output signals were fed directly to the eight charge amplifiers by the eight-core connecting cable type 1677A5/1679A5, see Figure 5.1. All signals were independently monitored, digitized and

recorded into Lab View where DynoWare software was used for force measurements and data processing of cutting forces and moments.

Drilling moment (M_z) and Feed force (F_f) are of particular interest for analyzing the drilling process. Deflective forces Fx, Fy perpendicular to the rotary axis provide additional information on the machining process. The three forces Fx, Fy, Fz and the three moments Mx, My, Mz were calculated from the 8-channel force components by the following set of equations (Eq. 5.1).[133]

$$Fx = Fx_{1+2} + Fx_{3+4}$$

$$Fy = Fy_{1+4} + Fy_{2+3}$$

$$Fz = Fz_1 + Fz_2 + Fz_3 + Fz_4$$

$$Mx = b\,(Fz_1 + Fz_2 - Fz_3 - Fz_4)$$

$$My = a\,(-Fz_1 + Fz_2 + Fz_3 - Fz_4)$$

$$Mz = b\,(-Fx_{1+2} + Fx_{3+4}) + a\,(Fy_{1+4} - Fy_{2+3})$$

Eq. 5.1

where a and b are constants (a=b=80mm) representing the location of the four sensors from the symmetry axes, see Figure 5.1(a).

According to specification of the 9255B type, see Table 5.1, there are two types of drift; normal drift and contamination drift. The normal drift was 0.03 pC/s (pC= pico coulomb= 1×10^{-12} Coulomb) and for each cycle period (340 seconds) the total drift was 10.2 pC. The sensitivity for Fx, Fy and Fz channels was 7.87, 7.86 and 3.87 pC/N respectively. So for each cycle which consisted of 115 holes in drilling and 65 holes in

tapping, the normal drift in Fx, Fy, and Fz were 1.3 N, 1.3 N and 2.64 N respectively. In general, a 6-component measuring system provides:

- The 3 components of the resultants of all applied forces, their direction but not their location in space.
- The 3 components of the resulting moment vector related to the coordinate origin.

Table 5.1 Dynamometer and charge amplifier specifications[133]

Dynamometer specifications	
Type	9255B
Measuring range	Fx, Fy kN ±20 Fz kN –10 ... 40
Sensitivity	Fx, Fy pC/N ≈–8 Fz pC/N ≈–3,7
Natural frequency	fnx kHz ≈2 fny kHz ≈2 fnz kHz ≈3,3
Operating temperature	range °C 0 ... 70
Length, Width and Height	L=260 mm, W=260 mm and H=95 mm
Weight	52 Kg
Multi-channel charge amplifier specifications	
Type	5017B... No. of channels 3 ... 8
Measuring range for F_S	pC ±10 ... ±999 000
Frequency	range –3 dB kHz ≈0 ... 200
Output	range V ±10
Supply	V/ AC 115/230

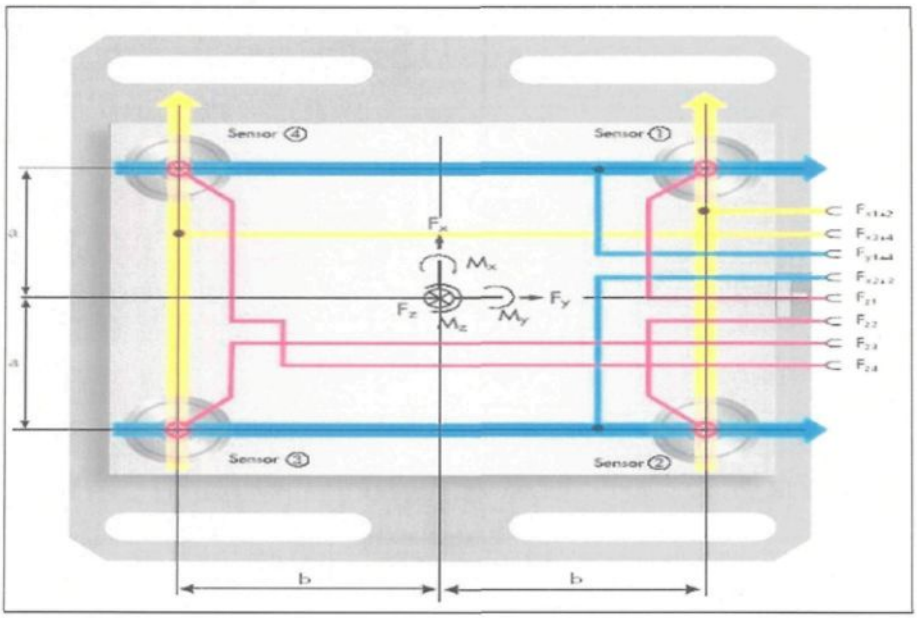

(a)

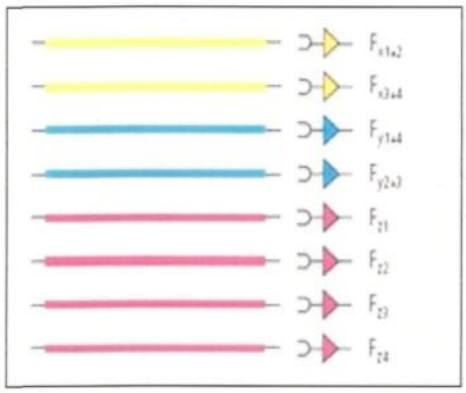

(b)

(c)

Figure 5.1 Kistler 6-component electronic dynamometer a) dynamometer with the four sensor as well as the measuring chains for the 6-cmponent force and moment measurement b) 8-core connecting cable as well as 8 charge amplifier channels c) 8-component channels.[133]

5.2. DRILLING AND TAPPING DATA PROCESSING

Matlab[1] programs were developed for processing the drilling and tapping data for all metallurgical conditions (M1 to M5). As an example of data processing, the drilling and tapping data of the 356 alloy machinability test sample number 8 ((M1-T6 condition) are presented in this chapter to show the methodology for the first group of holes (115 holes-half block). The complete programs can be found in Appendix B. The data were first separated according to each component of force and moment followed by an application of signal processing procedure for calculating the mean value of force and moment and their standard deviations. The sampling rate was 1000 Hz. Drilling was carried out at high speed machining. On the other hand, tapping was carried out at low speed, so that data for only 130 holes were processed (out of 230 holes) for each block sample in tapping, while all data was processed for drilling tests. From the signal results, it was observed that the contamination drift was more significant. This drift came from oxidation and the coolant and also from the finger impressions during handling. In addition, the long period of acquisition can also amplify such kinds of drift.

5.2.1. Drilling Data Processing Methodology and Matlab Results

Matlab graphs representing the steps of data processing for the drilling force and moment are displayed in Figure 5.2 to Figure 5.4. All components of force and moment are displayed in Figure 5.2 (a). Drilling feed force (Fz component) was separated and its data was analysed and processed. The Fz component signal was filtered nine times by using a

[1] A software for mathematical calculations and programming

low pass filter (Filter (b, 1, Fz), b= [1 1]; b= b/sum) and a smooth signal was produced, see Figure 5.3 (a). Slow changes were removed after taking the first difference for the filtered signal, Figure 5.3 (b).

Different threshold levels (i.e. 100, 120, 150 and 170) were used in point detection within each cycle in the signal for different metallurgical conditions. The threshold level should cover all the range of data in all cycles in the signal. In this example, all data points in the 1st difference signal (Figure 5.3 (b) below the threshold level (i.e. 170) was presented by zero and all data points above zero was presented by 350 as the following equations (Eq 5.2).

$$\text{diffk(diffk<Threshold=0)}$$

$$\text{diffk(diffk>0=350)} \ldots\ldots \qquad \text{Eq. 5.2}$$

where k=mFz (filtered signal) and the threshold equal to 170. In most of the cycles, triangle peaks with constant value of 350 were obtained in the signal see Figure 5.4 (a). Also, a plateau (rectangle peaks) were obtained in some of the cycles (not shown). The second difference was taken for the peak or plateau signal to detect one point at constant intervals within the signal (i.e. one peak data point within each cycle was obtained) see the blue dotted signal in Figure 5.4 (a).

Two points were determined within each cycle relative to the detected points in Figure 5.4 (a). The first one (square point) represents the mean cutting feed force (Fz_{up}) without error treatment and the second (triangle point) represents the error (Fz_{down}), see Figure 5.4 (b). 1600 sample points per cycle were acquired for calculating the mean value

of the cutting feed force (800 data points left and 800 data points right from the squared point) and 1200 sample points per cycle for the other five components of force and moment (Fx_{up}, Fy_{up}, Mx_{up}, My_{up}, and Mz_{up}) in each signal (600 data points left and 600 data points right from the same point) however, only 200 sample points per cycle were used for standard deviation or peak-to-valley calculations (100 data points left and 100 data points right from the circled point).

Output of results for all components of drilling force and moment with (Fx, Fy, Fz, Mx, My, and Mz) and without (Fx_{up}, Fy_{up}, Fz_{up}, Mx_{up}, My_{up}, and Mz_{up}) error treatment for the first group of holes and only ($Fz-Fz_{up}$, $Mx-Mx_{up}$ and $My-My_{up}$) for the second group of holes are displayed in Figure 5.5 and Figure 5.6, respectively. The error was taken into consideration and was incorporated into the Matlab drilling program as the following set of equations; 1) $Fx= Fx_{up}-Fx_{down}$, 2) $Fy= Fy_{up}-Fy_{down}$, 3) $Fz= Fz_{up}-Fz_{down}$, 4) $Mx= Mx_{up}-Mx_{down}$, 5) $My= My_{up}-My_{down}$, and 6) $Mz= Mz_{up}-Mz_{down}$.

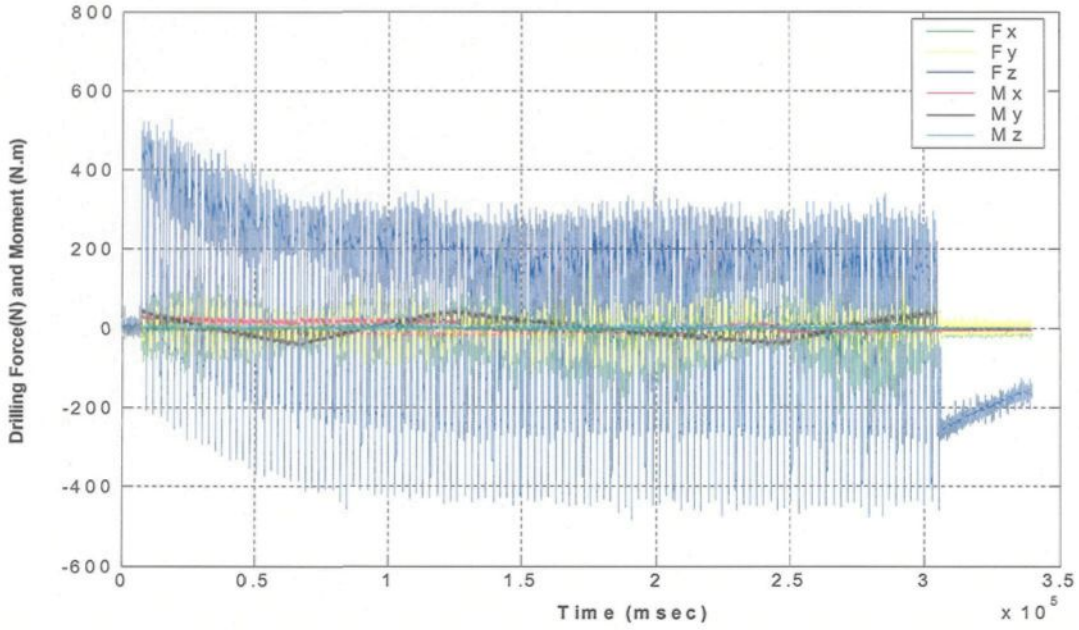

(a)

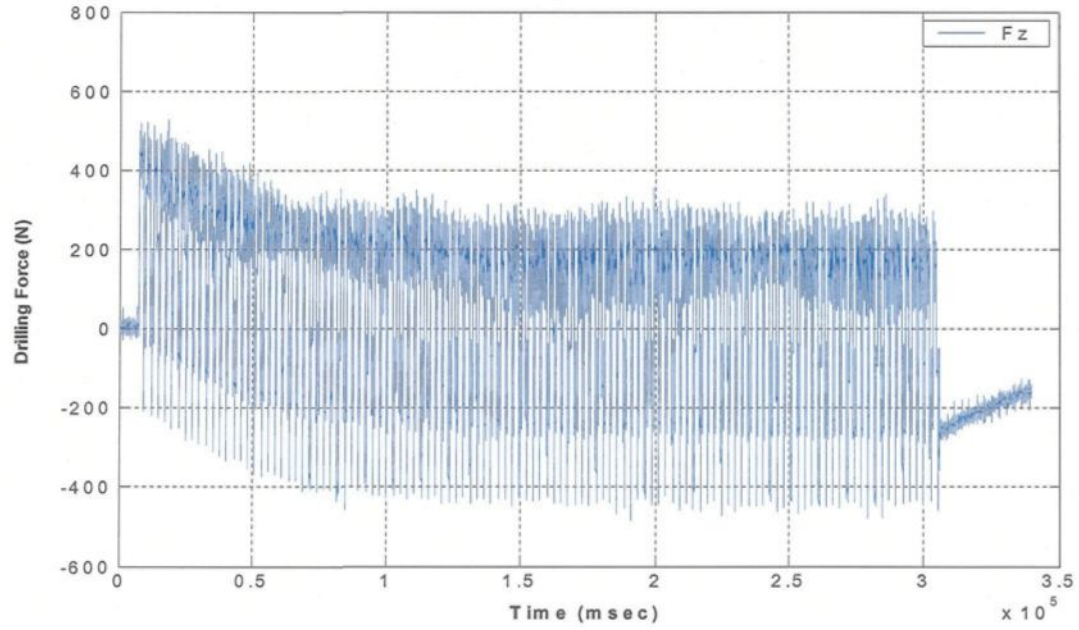

(b)

Figure 5.2 Data processing for drilling force and moment of the first group of holes (115-holes) a) original six component of force and moment b) Fz component.

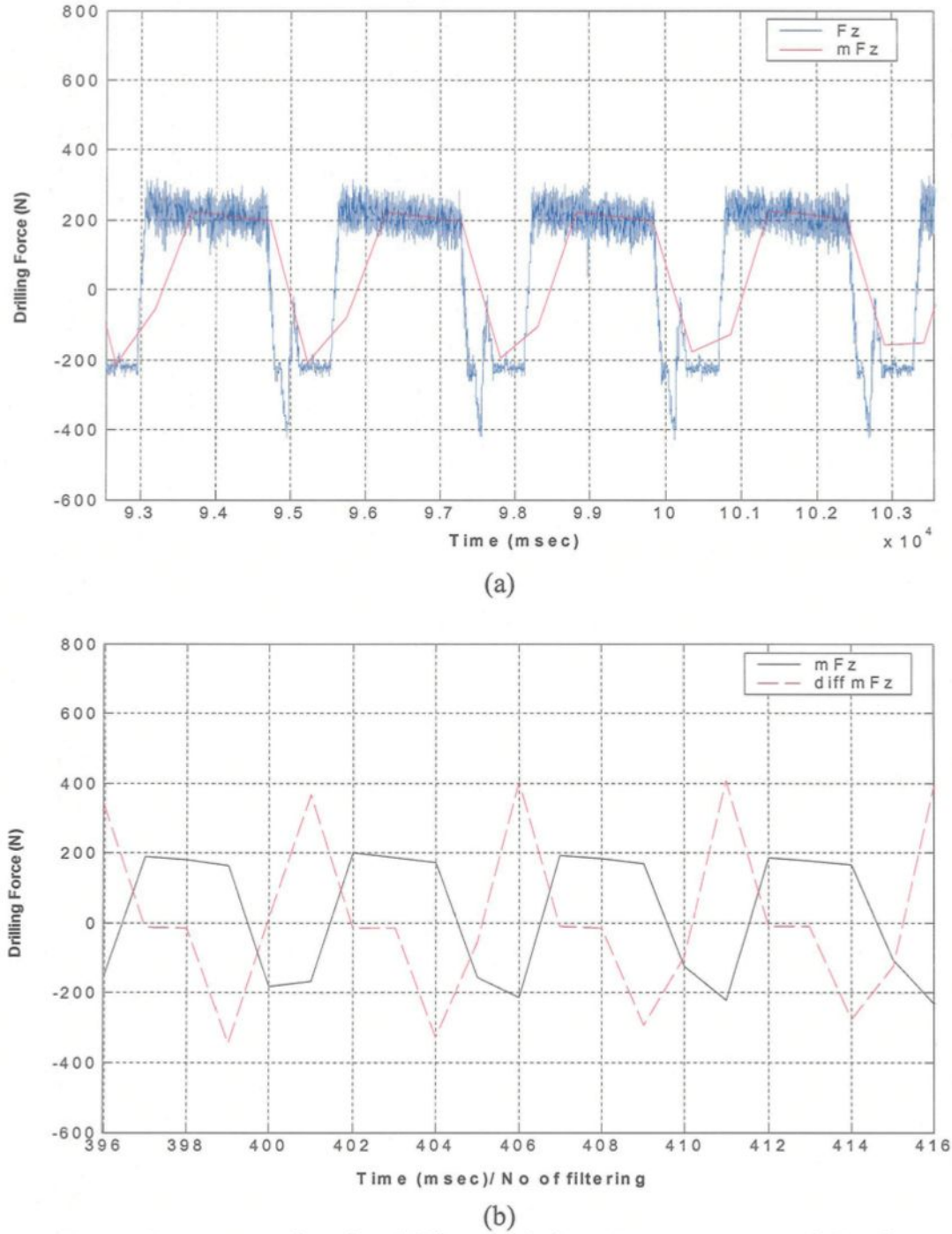

Figure 5.3 Data processing for drilling feed force-Fz component of the first group of holes (115-holes) for Fz component a) filtration (9-times) b) point detection within each cycle-first difference of the filtered Fz.

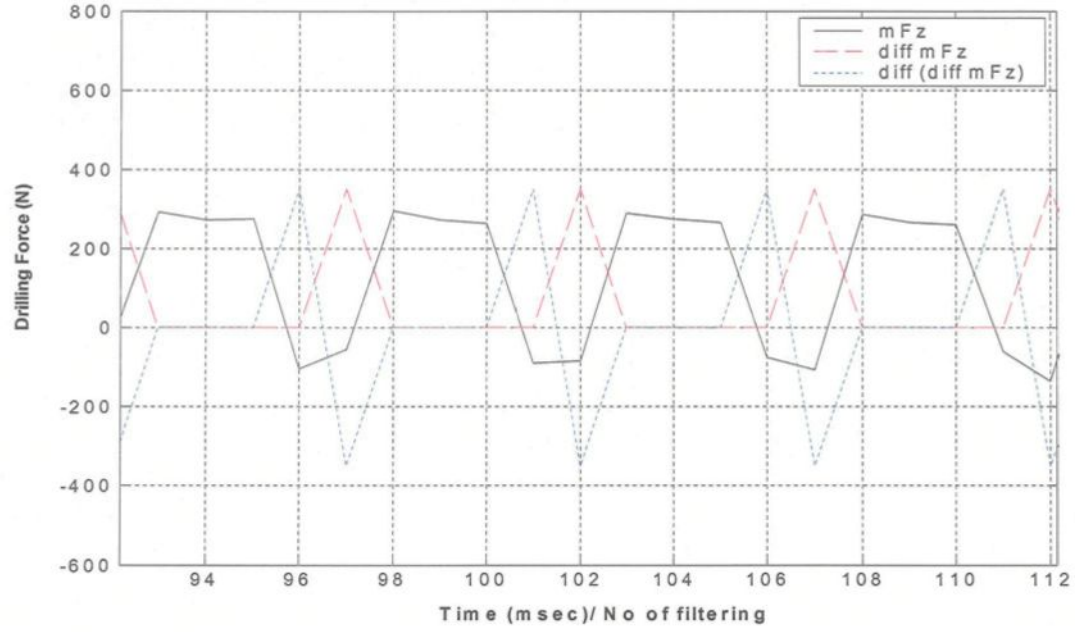

(a)

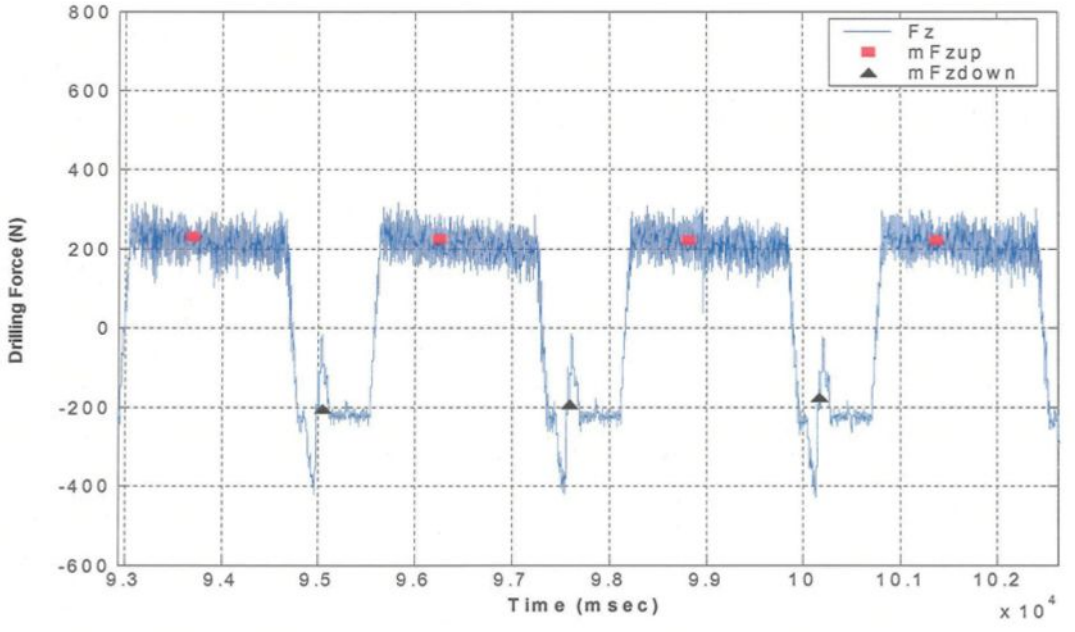

(b)

Figure 5.4 Data processing for drilling feed force-Fz component of the first group of holes (115-holes)- point detection within each cycle a) first and second difference of the filtered Fz and b) points within each cycle one represent mean Fz without error consideration and another represent the error value.

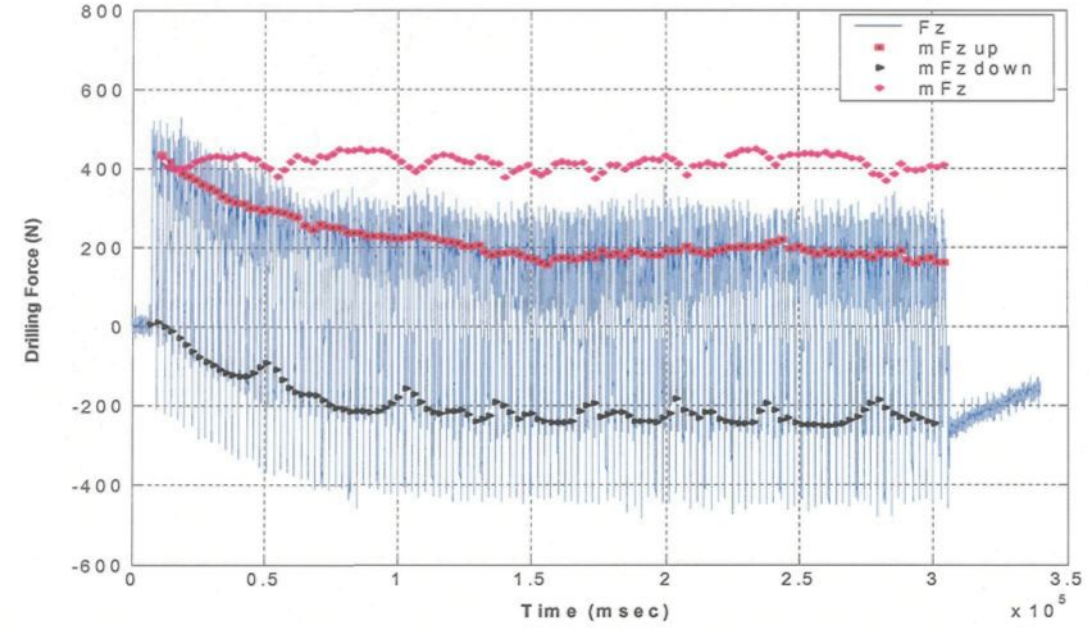

(a)

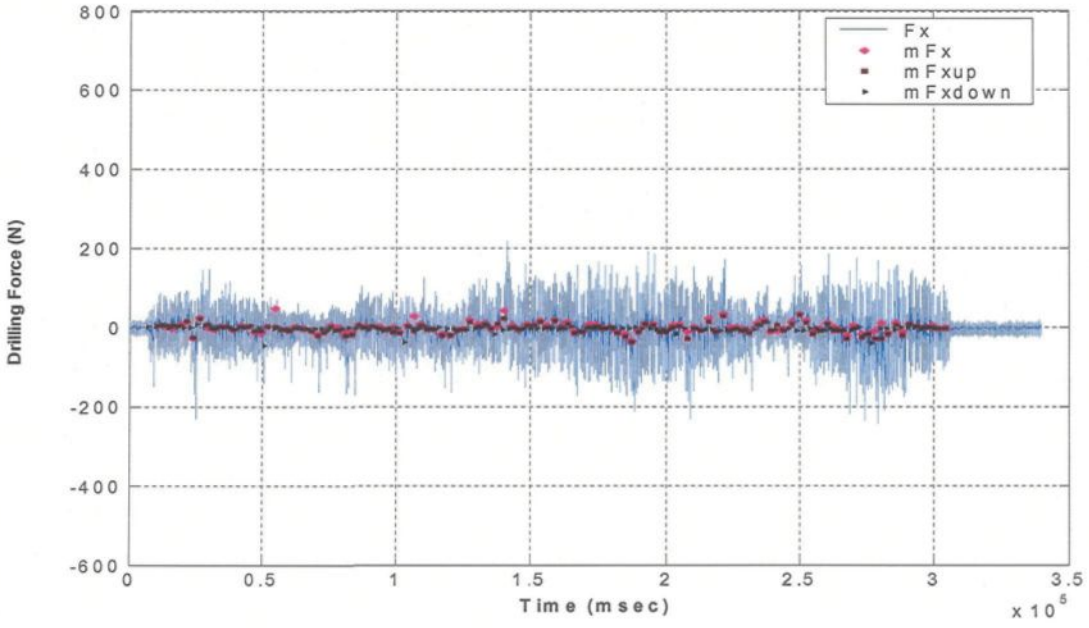

(b)

Figure 5.5 Output results for drilling force and moment of the first group of holes (115-holes)-plots with and without error treatment a) Fz, b) Fx, c) Fy , d) Mz, e) Mx and f) My.

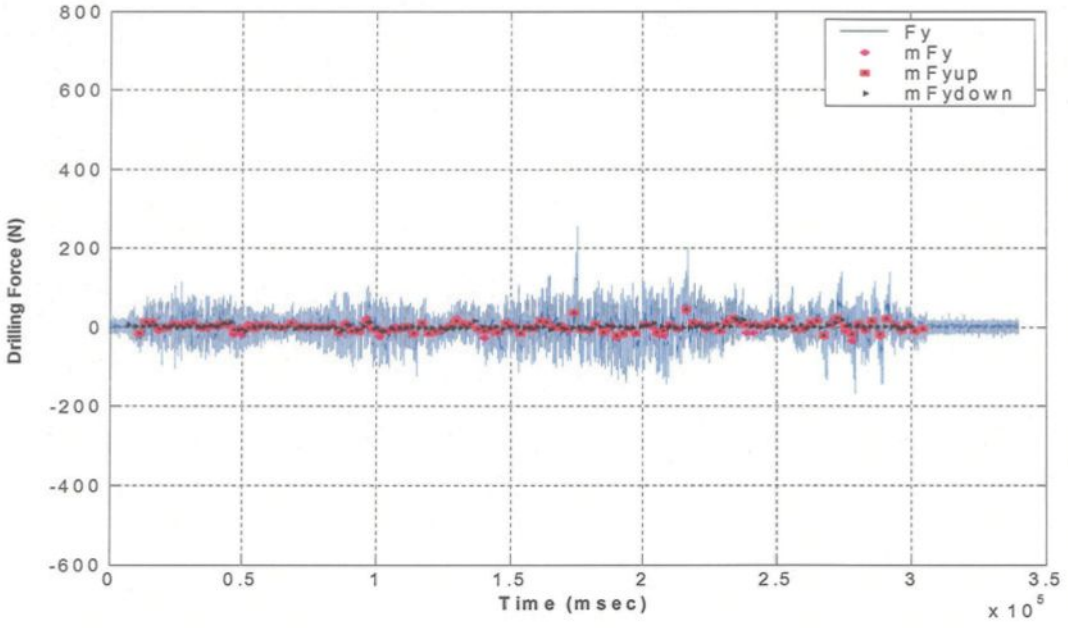

(c)

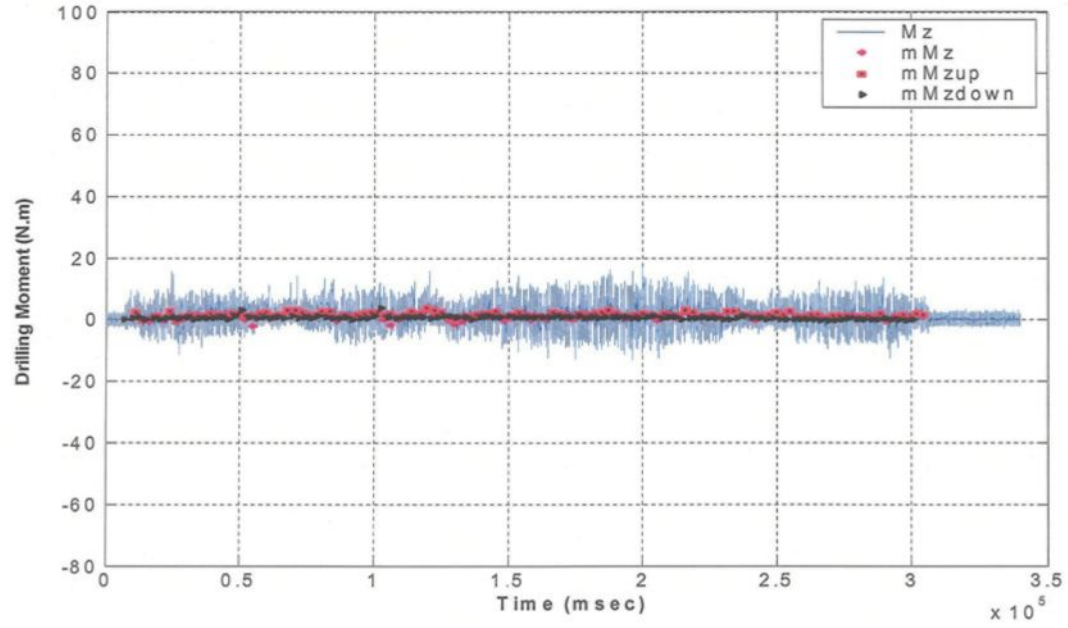

(d)

Figure 5.5 Output results for drilling force and moment of the first group of holes (115-holes)-plots with and without error treatment a) Fz, b) Fx, c) Fy , d) Mz, e) Mx and f) My.

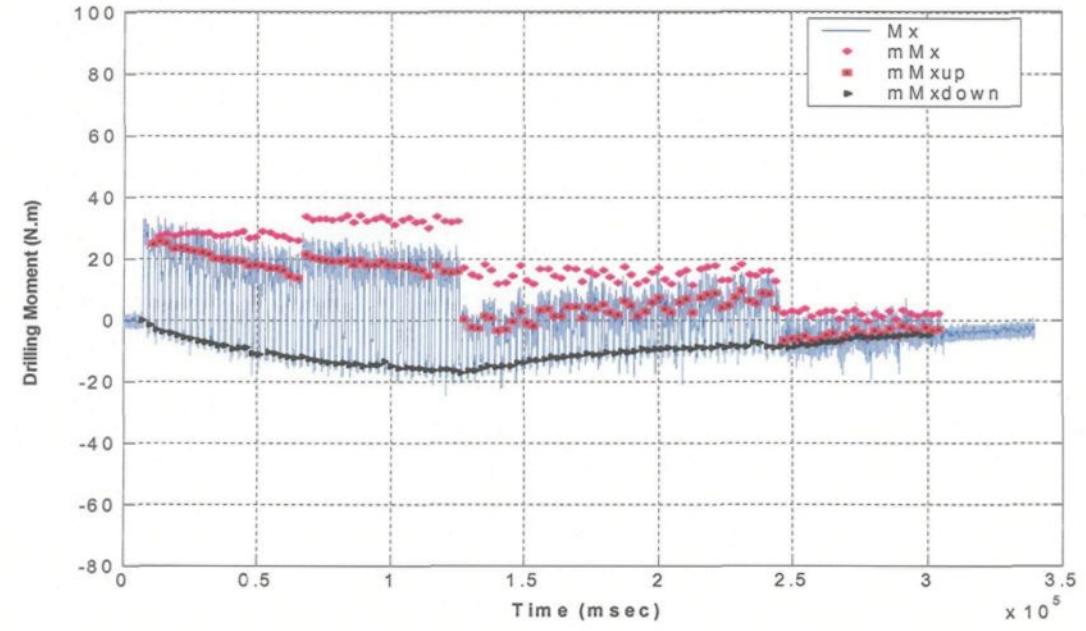

(e)

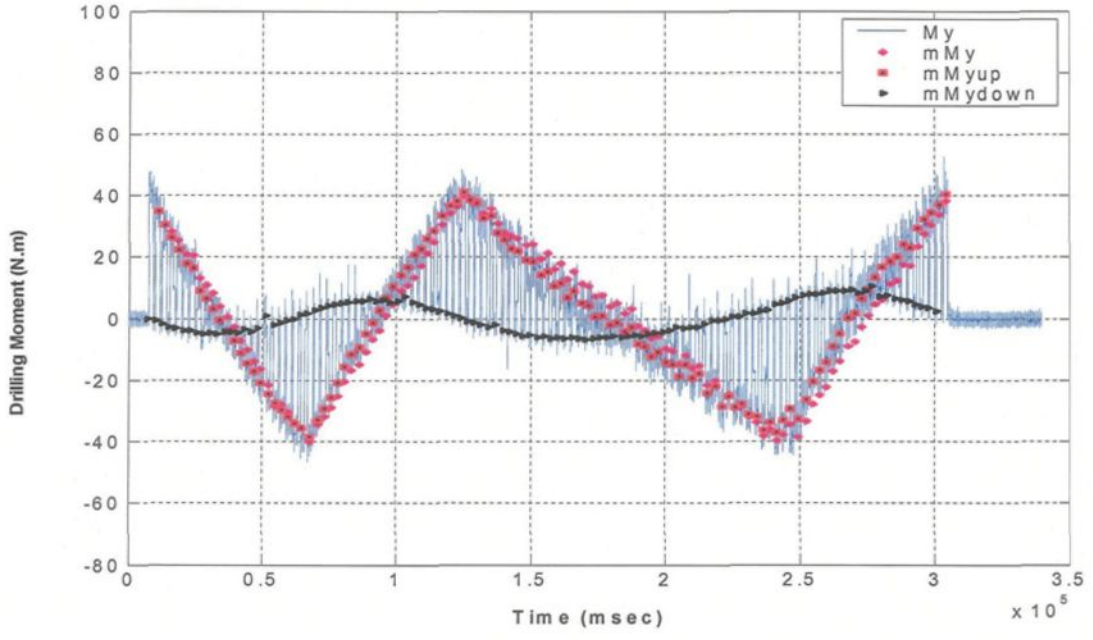

(f)

Figure 5.5 Output results for drilling force and moment of the first group of holes (115-holes)-plots with and without error treatment a) Fz, b) Fx, c) Fy , d) Mz, e) Mx and f) My.

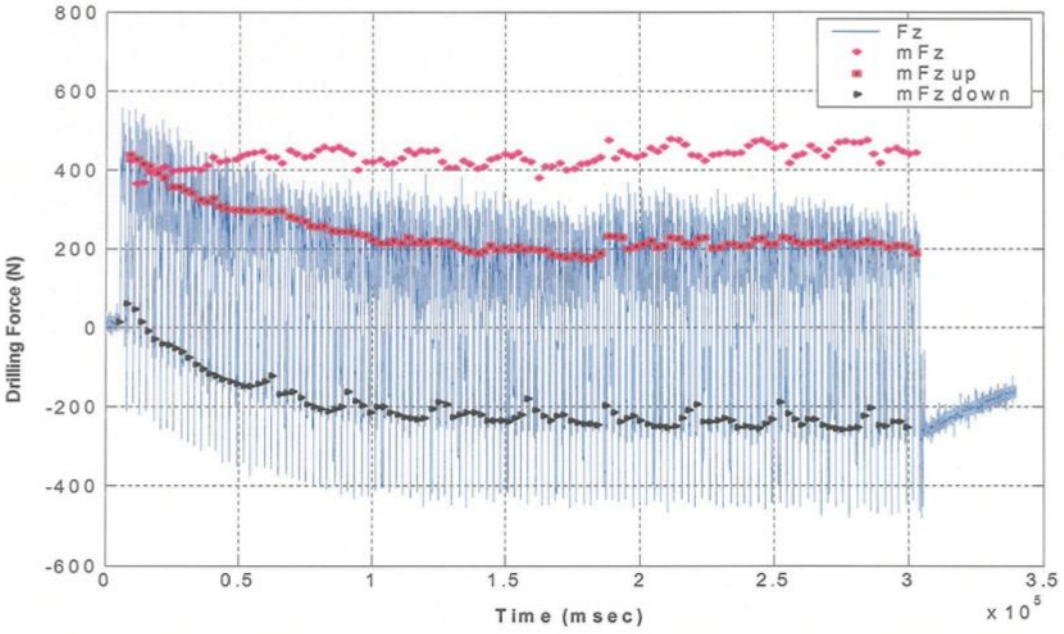

(a)

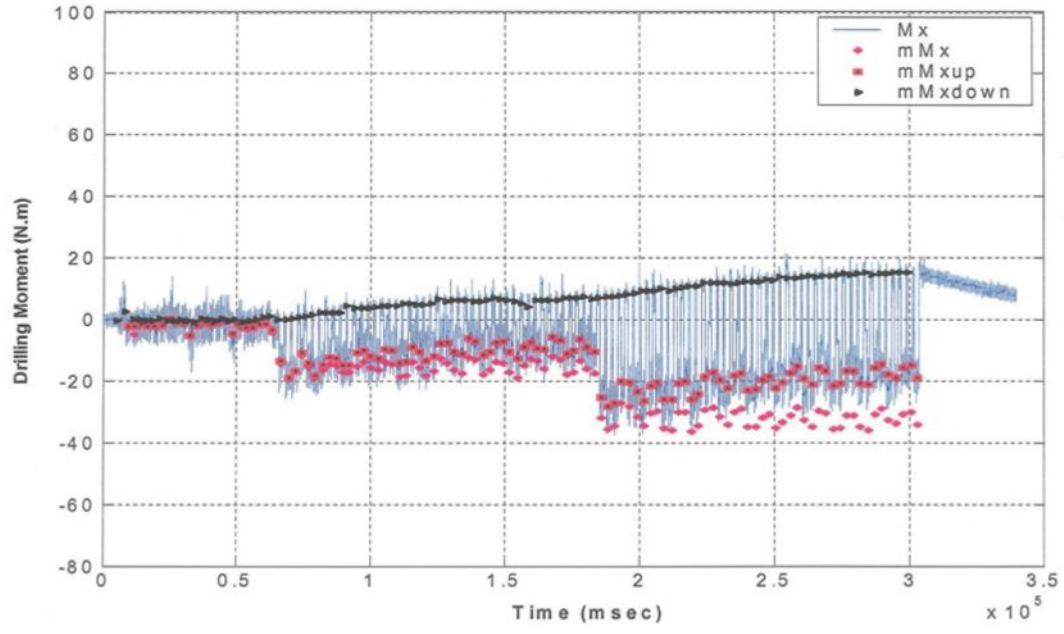

(b)

Figure 5.6 Output results for drilling force and moment of the second group of holes (115-holes)-plots with and without error treatment a) cutting feed force (Fz), b) radial cutting moments (My) and c) (Mx) and d) mean cutting feed force (mFz) vs. no. of drilled holes.

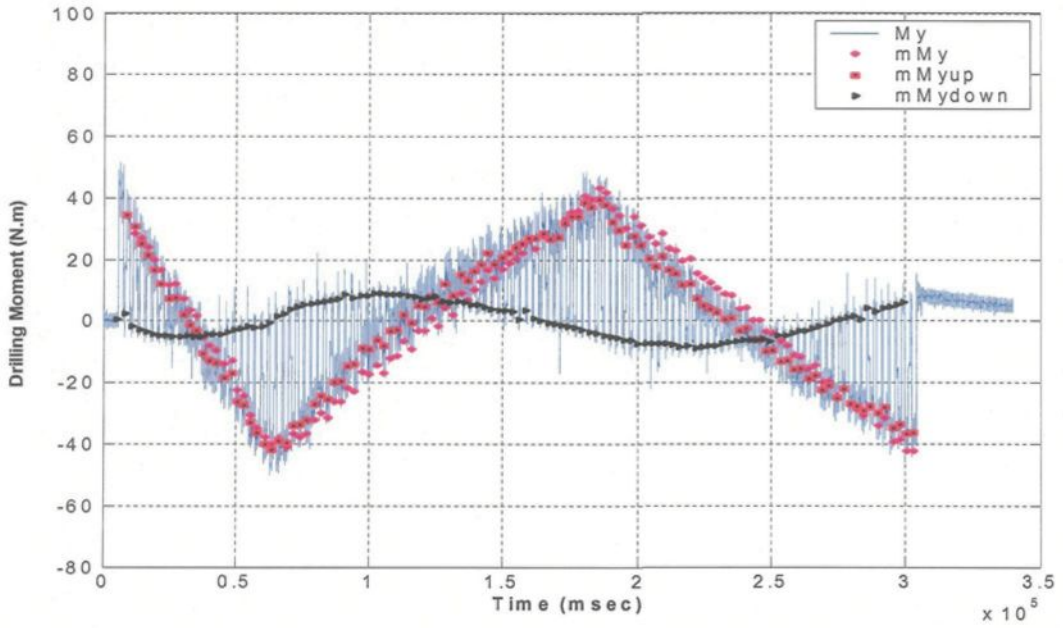

(c)

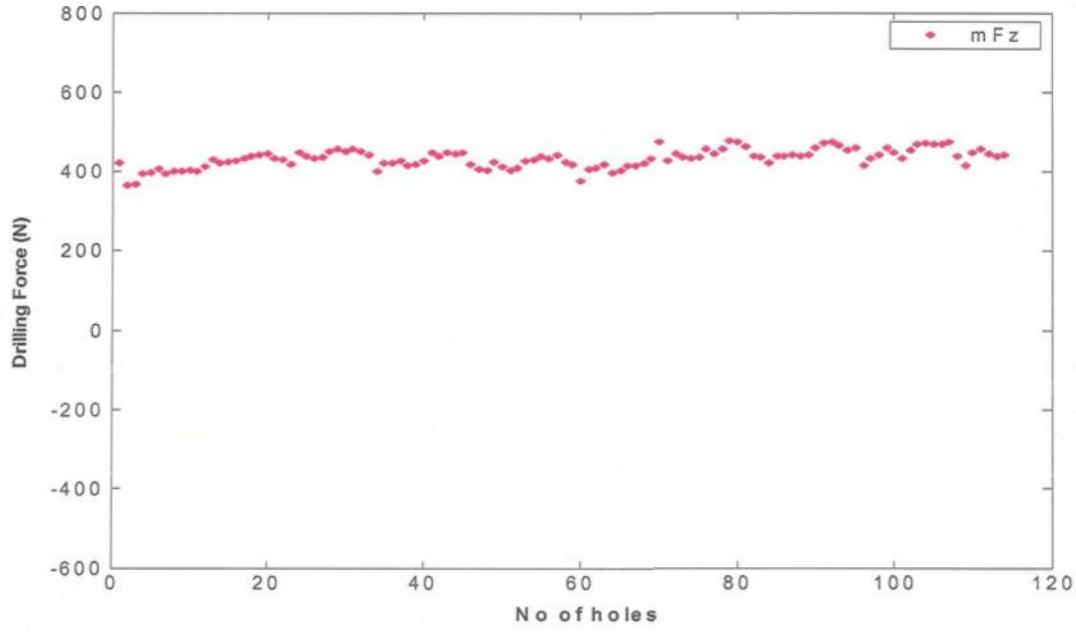

(d)

Figure 5.6 Output results for drilling force and moment of the second group of holes (115-holes)-plots with and without error treatment a) cutting feed force (Fz), b) radial cutting moments (My) and c) (Mx) and d) mean cutting feed force (mFz) vs. no. of drilled holes.

5.2.2. Tapping Data Processing Methodology and Matlab Results

The same methodology for data processing was applied for tapping force and moment calculations. It was applied to two metallurgical conditions (M1-T6 and M5-T7), where the level of forces is high and the signal is uniform. On the other hand, it was also used with special treatment for the M3-T6 condition. Only 130 holes of data were processed (out of 230 holes) for each machinability test sample in tapping because of the large size of data for each file (the time for the tapping cycle was nearly twice that for the drilling one). All components of tapping force and moment for 356 alloy (M1-number 8) are displayed in Figure 5.7 (a). Tapping feed force (Fz component) was separated and data was processed according to the same procedure used in drilling tests, Figure 5.7 (b). A smooth signal was obtained by using the same filter as in drilling tests, Figure 5.8 (a). Slow changes within the signal were removed by taking the first difference for the filtered signal, Figure 5.8 (b).

Different threshold levels (i.e. -20,-40, -50, and -60) were used in point detections within each cycle in the signal for all metallurgical conditions. The threshold level should cover all the range of data in all cycles in the signal. In this example, all data points in the 1st difference signal (Figure 5.8 (b)) above the threshold level was presented by zero and all data points below zero was presented by -250 as the following equations (Eq 5.3).

diffk(diffk>Threshold=0)

diffk(diffk<0= -250) .....

Eq. 5.3

where k=mFz (filtered signal) and the threshold equal to -50. In the negative part of most of the cycles, triangle peaks with constant value of -250 were obtained in the signal see Figure 5.9 (a). Also, a plateaus (rectangle peaks) were obtained in some of the cycles, Figure 5.9 (a). The second difference was taken for the peak or plateau signal to detect one point at constant intervals within the signal (i.e. indices of the minimum point position of the blue dotted signal was obtained in Figure 5.9 (a).

Three points were determined within each cycle relative to the detected points in Figure 5.9 (a). The first one (square point) represents the mean cutting feed force (Fz_{up1}) where the tap enters the drilled hole and the second (circle point) for mean cutting feed force (Fz_{down1}) where the tap exits, both without error treatment. The third one (triangle point) represents the error value (Fz_{down2}), see Figure 5.9 (b). 2000 sample points per cycle (1000-up and 1000-down) were used in calculating the mean value of the tapping force and moment and their standard deviation or peak-to-valley range (500 data points left and 500 data points right around the determined points).

Output results for all components of tapping force and moment with and without error treatment for the first group of holes are displayed in Figure 5.10 when the tap entered the drilled hole and in Figure 5.11 when the tap exited from the drilled hole, respectively. Results for the mean tapping feed force after error treatment for the first group of holes while the tap entered (Fz_{up}) and exited (Fz_{down}) from the drilled holes are displayed in Figure 5.12 (a) and Figure 5.12 (b), respectively. In the two cases i.e. where the tap entered and exited the drilled holes, the error was taken into consideration and was incorporated into the Matlab tapping program as the following set of equations; 1) $Fx_{up}= Fx_{up1}-Fx_{down2}$,

2) $Fy_{up}= Fy_{up1}-Fy_{down2}$, 3) $Fz_{up}= Fz_{up1}-Fz_{down2}$, 4) $Mx_{up}= Mx_{up1}-Mx_{down2}$, 5) $My_{up}= My_{up1}-My_{down2}$, and 6) $Mz_{up}= Mz_{up1}-Mz_{down2}$ and 7) $Fx_{down}= Fx_{down1}-Fx_{down2}$, 8) $Fy_{down}= Fy_{down1}-Fy_{down2}$, 9) $Fz_{down}= Fz_{down1}-Fz_{down2}$, 10) $Mx_{down}= Mx_{down1}-Mx_{down2}$, 11) $My_{down}= My_{down1}-My_{down2}$, and 12) $Mz_{down}= Mz_{down1}-Mz_{down2}$, respectively.

Similarly, all components of the mean drilling cutting force and moment for all conditions (M1 to M5 ~60 machinability test samples each 230 holes) were obtained. All components of the mean tapping cutting force and moment for all machining tests were obtained for M1, M3 and M5 conditions (~ 28 samples). The total mean cutting force and moment, their peak-to-valley range in both drilling and tapping were calculated (section 5.2.5) and were used as a way of evaluating drilling and tapping processes which will be assessed in the following chapters (Ch. 6 and Ch. 7).

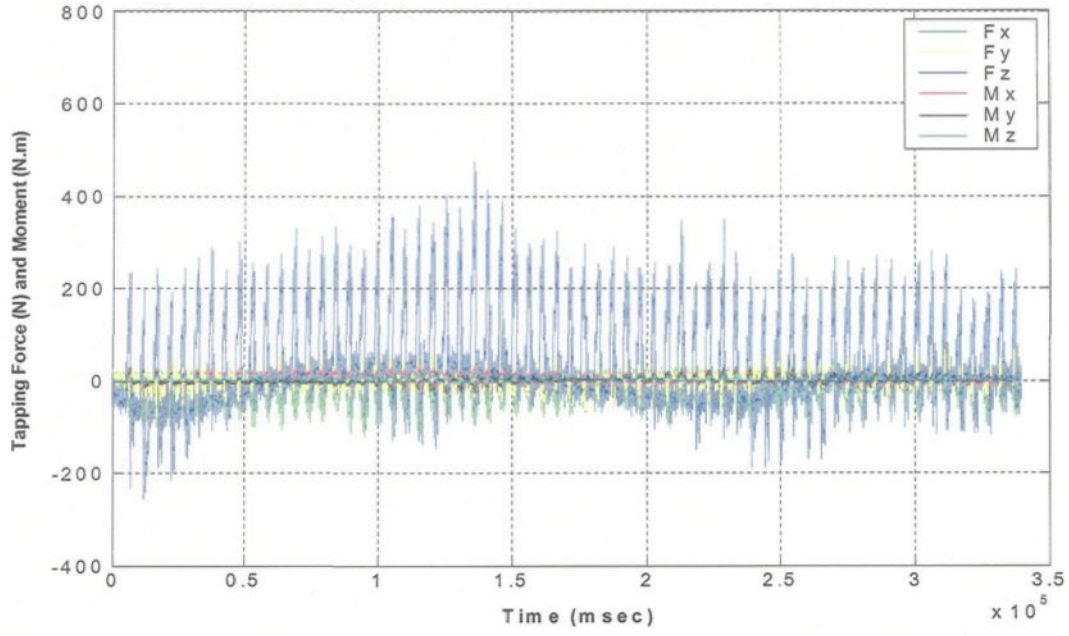

(a)

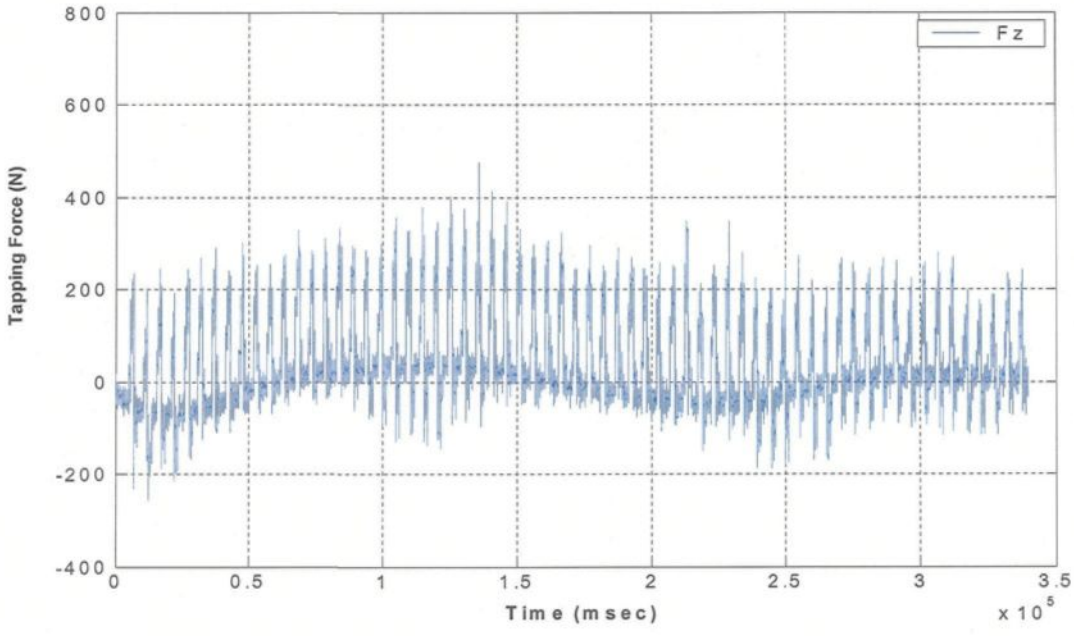

(b)

Figure 5.7 Data processing for tapping force and moment of the first group of holes (65 from115-holes) a) original six component of force and moment b) Fz component.

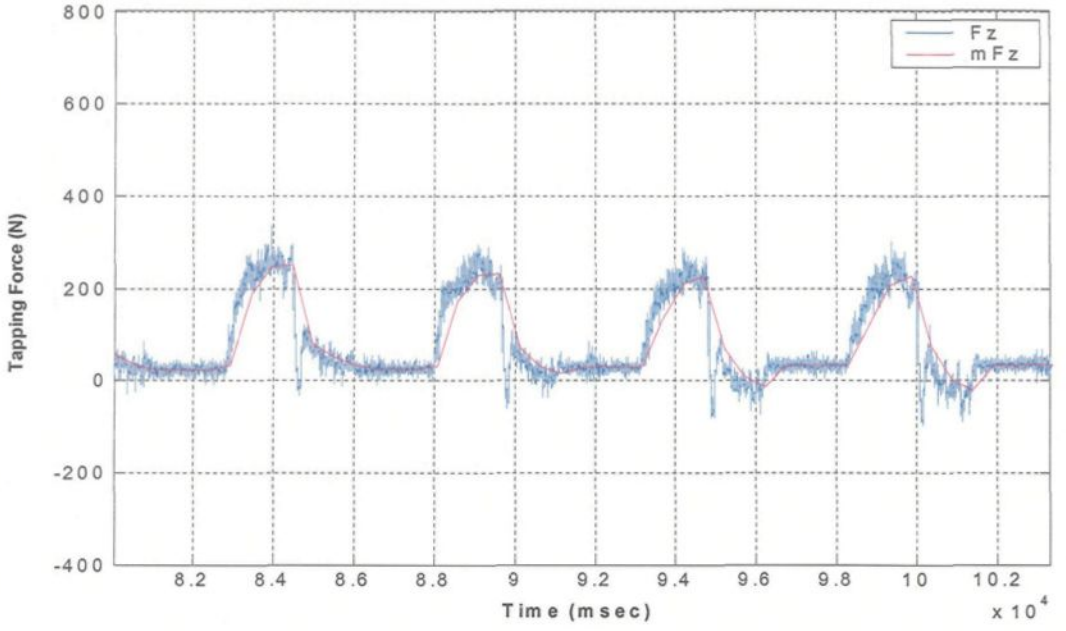

(a)

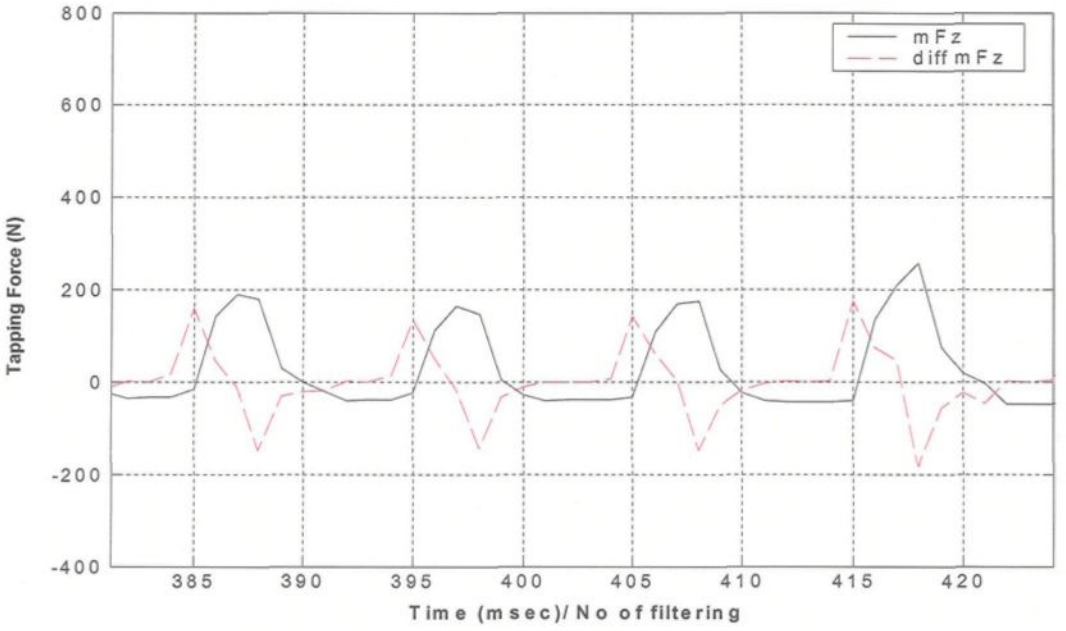

(b)

Figure 5.8 Data processing for tapping feed force-Fz component of the first group of holes (65 from 115-holes) for Fz component a) filtration (9-times) b) point detection within each cycle-first difference of the filtered Fz.

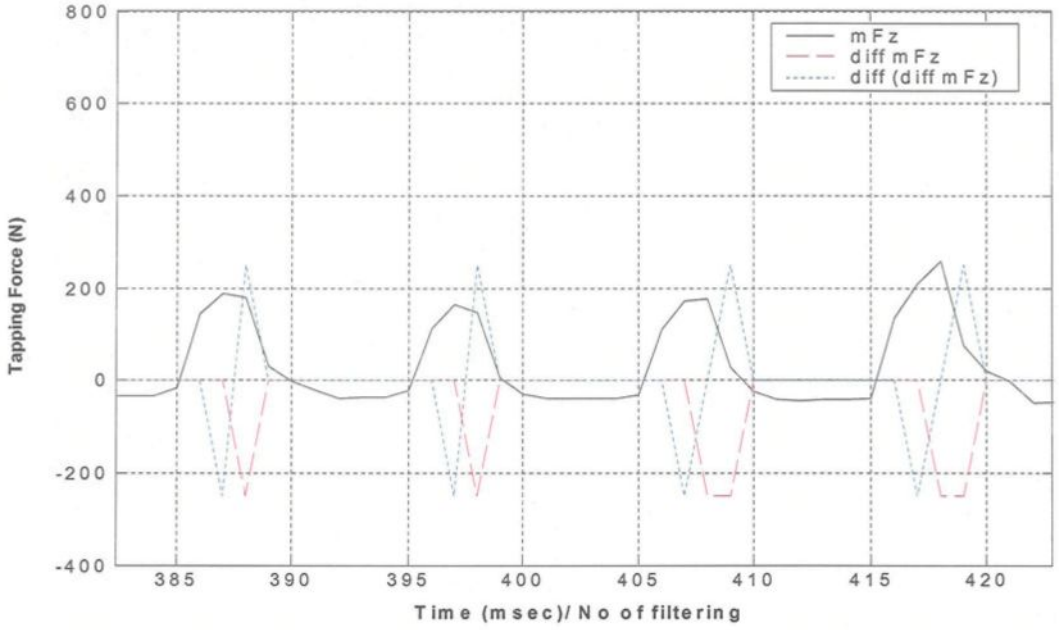

(a)

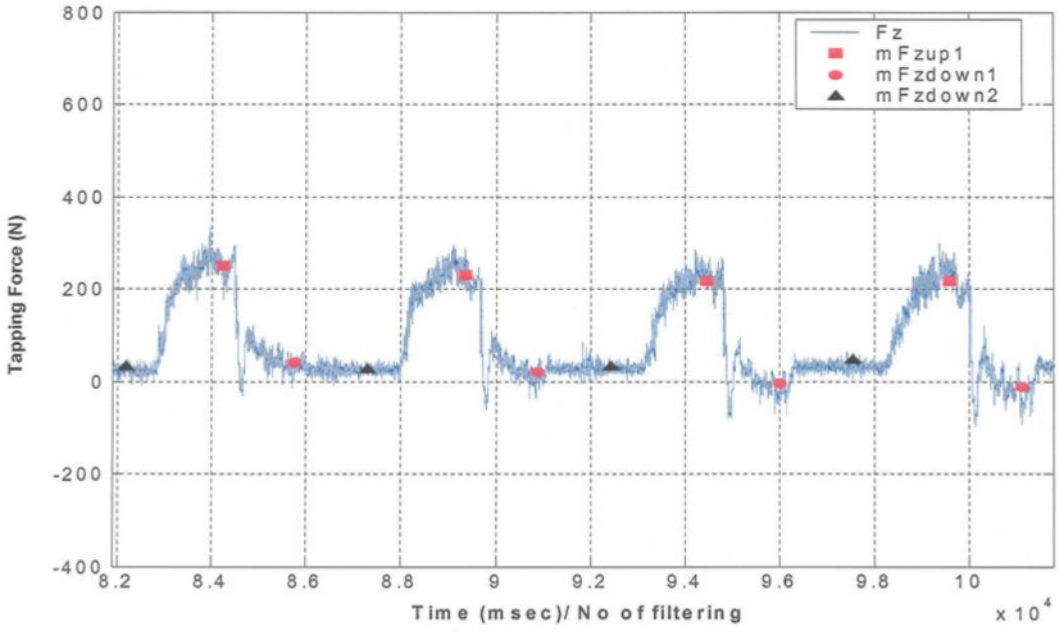

(b)

Figure 5.9 Data processing for tapping feed force-Fz component of the first group of holes (115-holes)- point detection within each cycle a) first and second difference of the filtered Fz and b) points within each cycle one represent mean Fzup and one for Fzdown and another represent the error value.

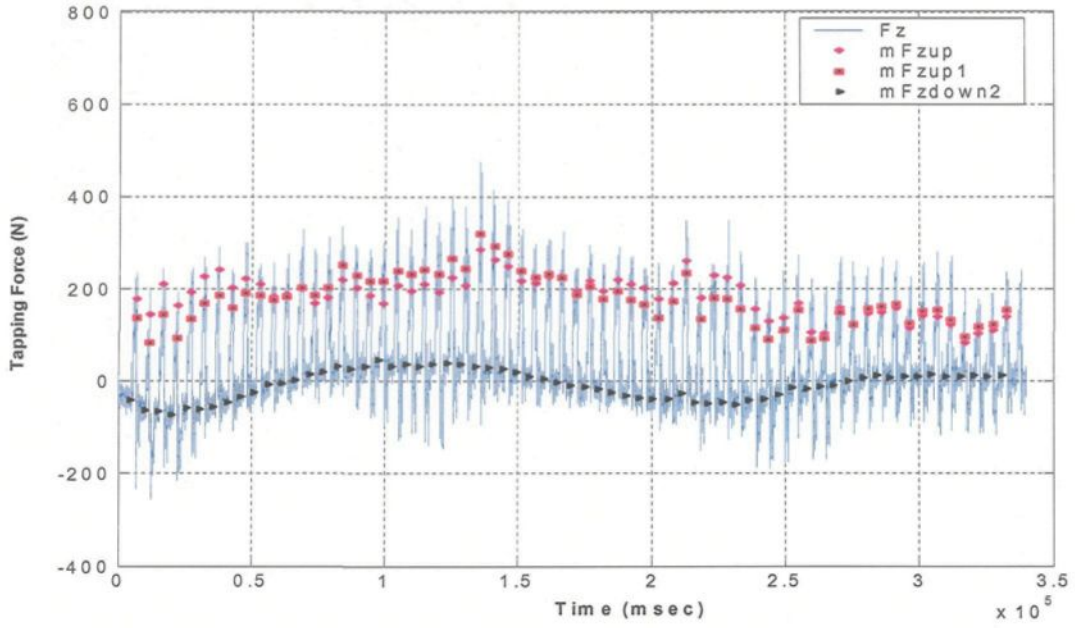

(a)

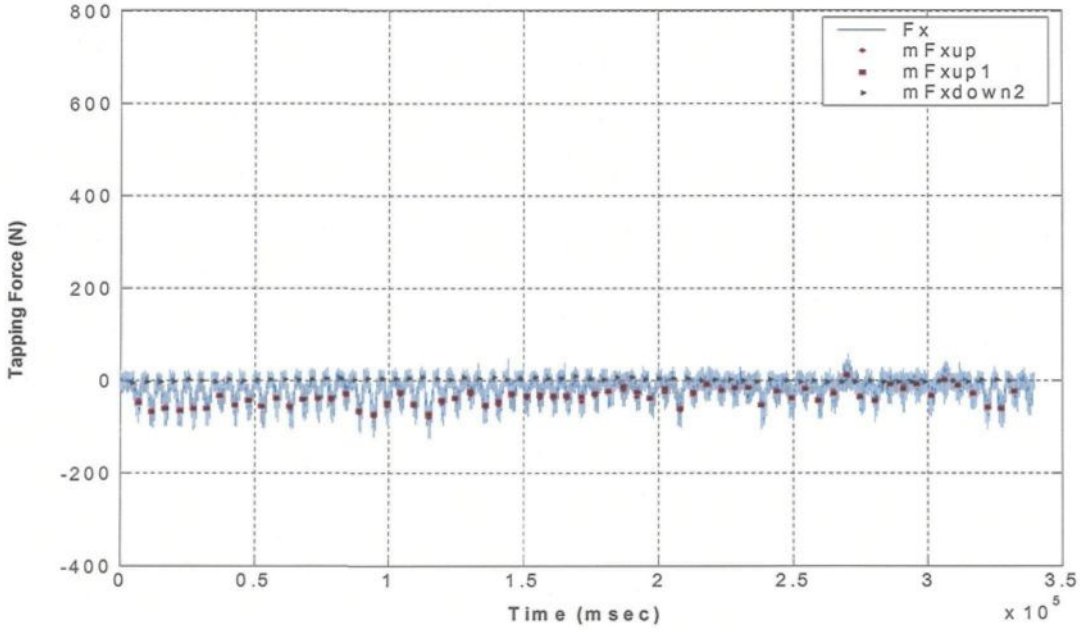

(b)

Figure 5.10 Output results for tapping force and moment of the first group of holes (65 from 115-holes)-plots with and without error treatment when the tap enter the drilled holes a) Fzup, b) Fxup, c) Fyup , d) Mzup, e) Mxup and f) Myup.

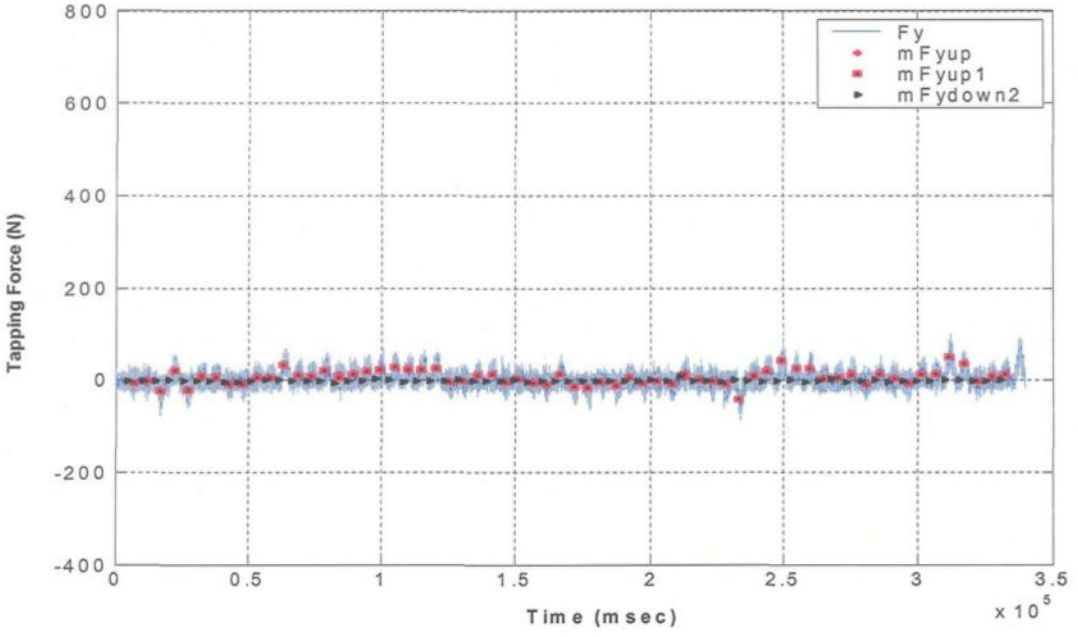

(c)

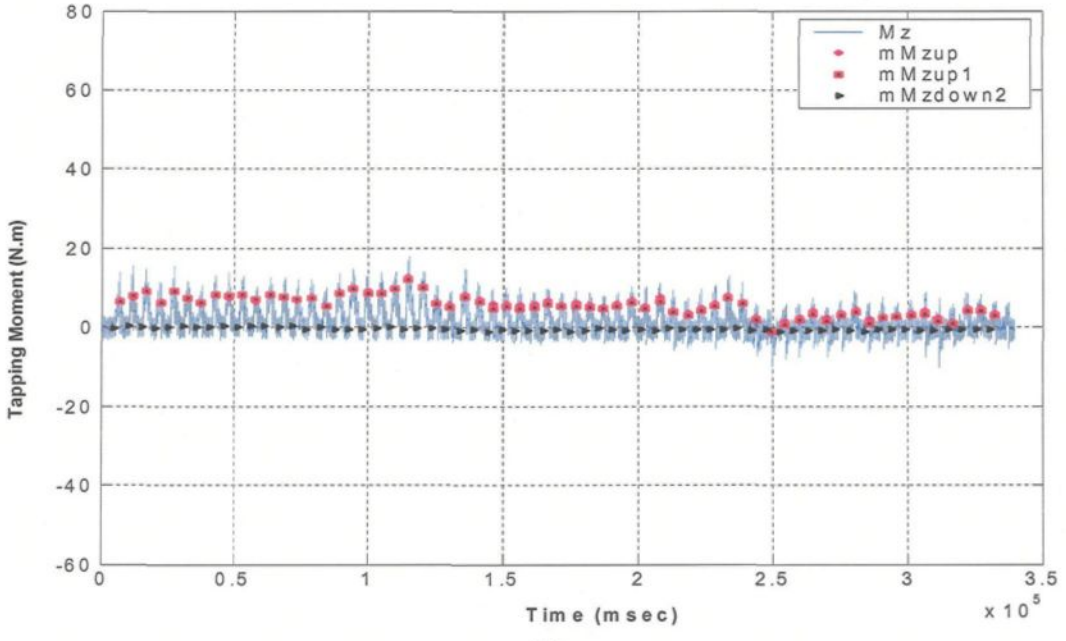

(d)

Figure 5.10 Output results for tapping force and moment of the first group of holes (65 from 115-holes)-plots with and without error treatment when the tap enter the drilled holes a) Fzup, b) Fxup, c) Fyup , d) Mzup, e) Mxup and f) Myup.

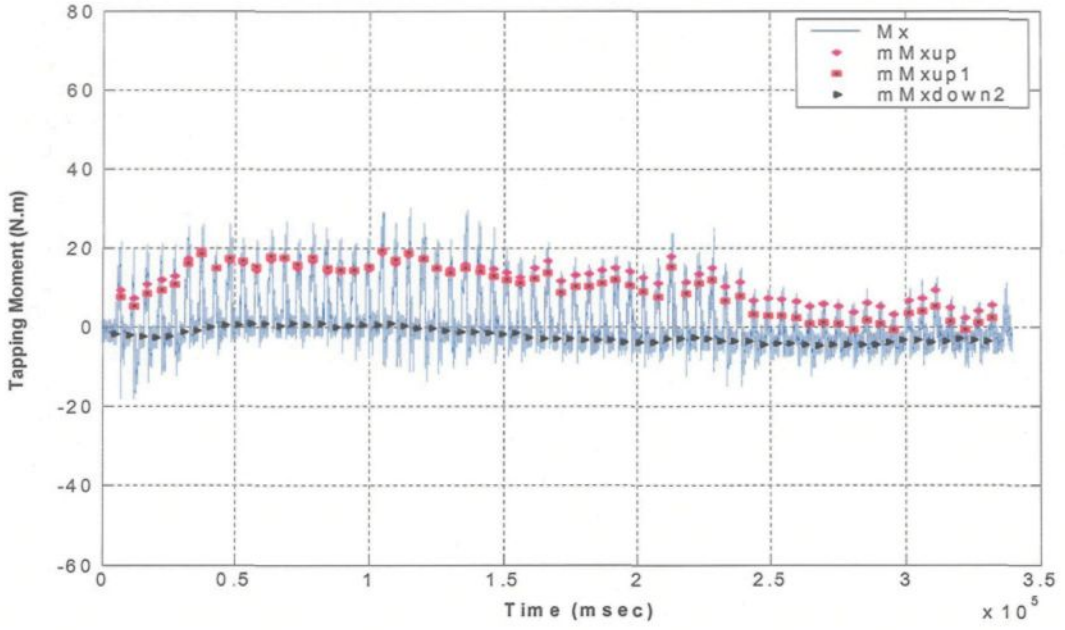

(e)

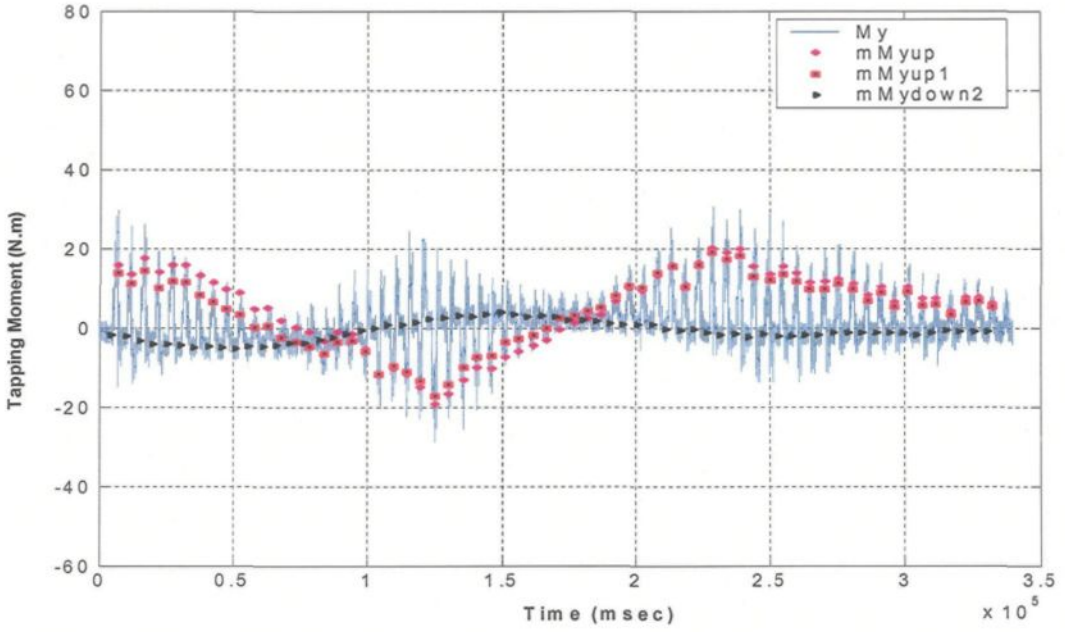

(f)

Figure 5.10 Output results for tapping force and moment of the first group of holes (65 from 115-holes)-plots with and without error treatment when the tap enter the drilled holes a) Fzup, b) Fxup, c) Fyup , d) Mzup, e) Mxup and f) Myup.

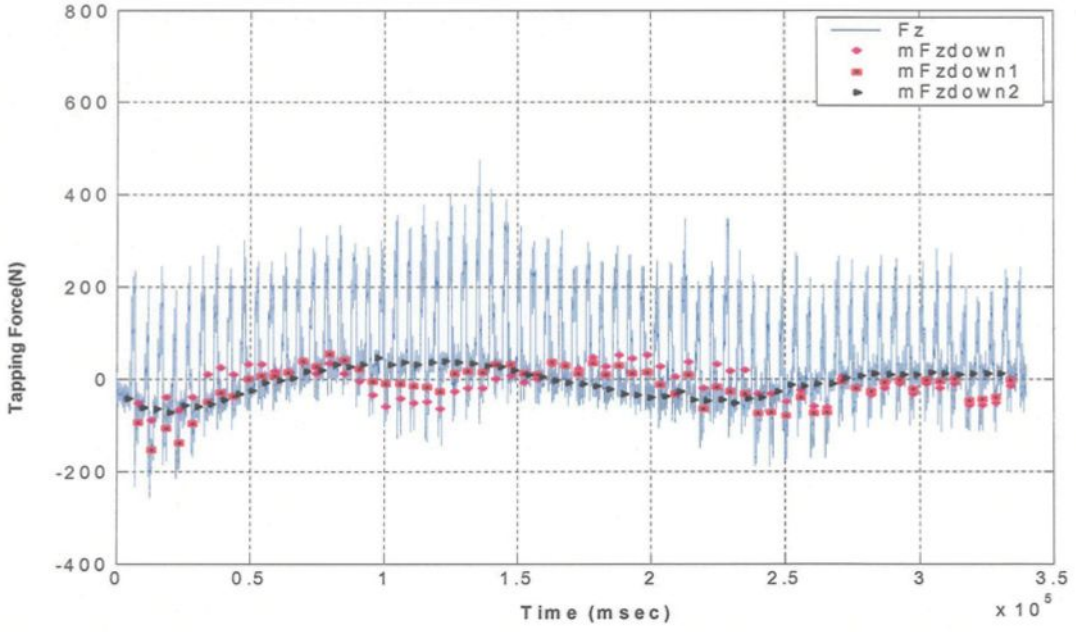

(a)

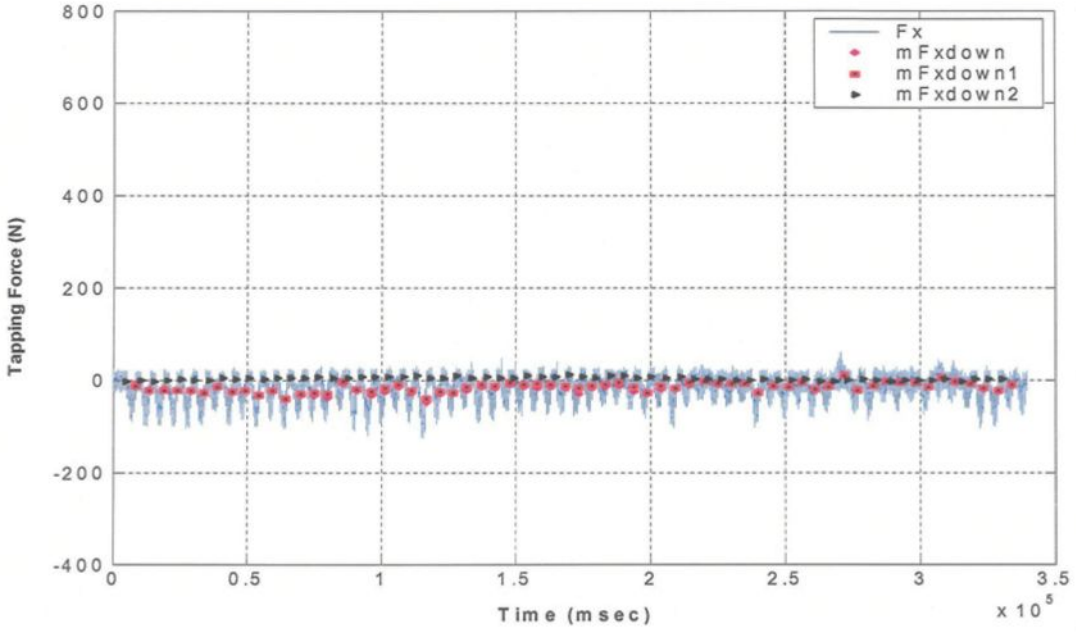

(b)

Figure 5.11 Output results for tapping force and moment of the first group of holes (65 from 115-holes)-plots with and without error treatment when the tap exist the drilled holes a) Fzdown, b) Fxdown, c) Fydown , d) Mzdown, e) Mxdown and f) Mydown.

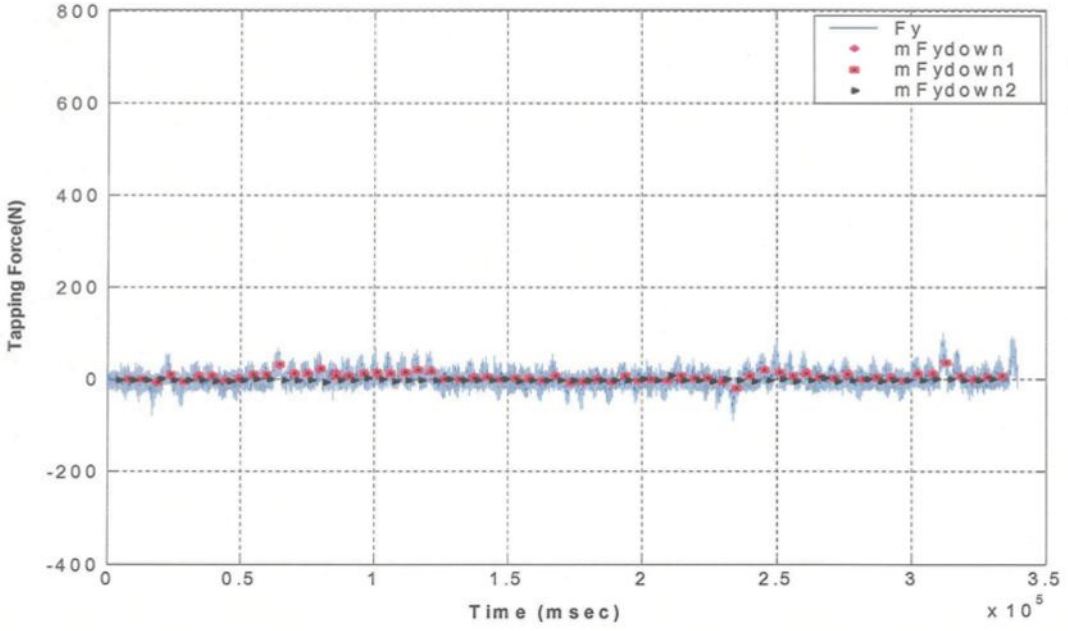

(c)

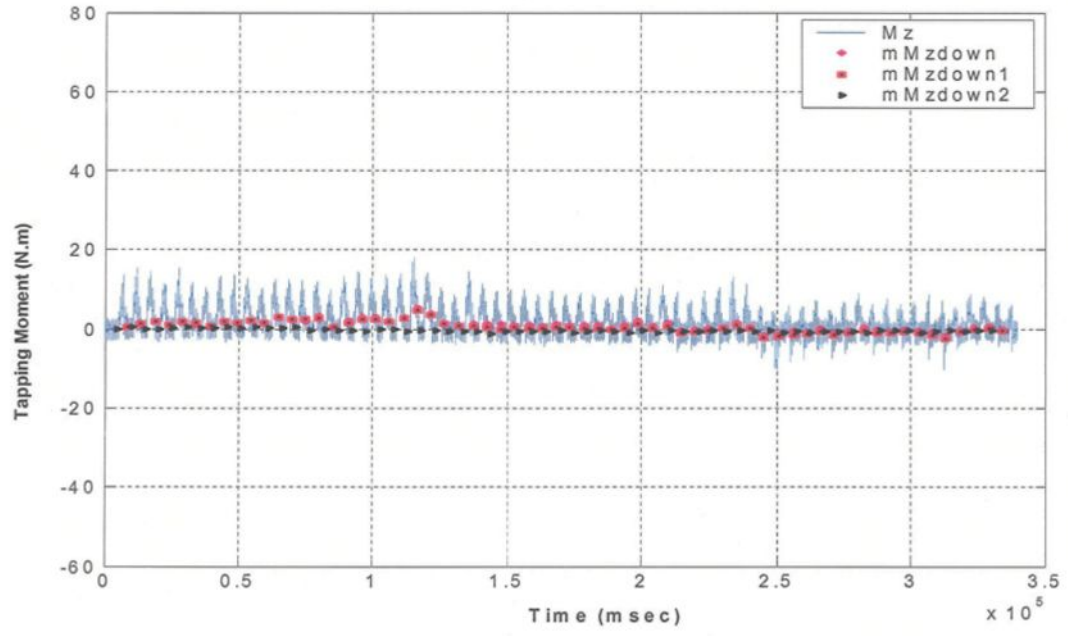

(d)

Figure 5.11 Output results for tapping force and moment of the first group of holes (65 from 115-holes)-plots with and without error treatment when the tap exist the drilled holes a) Fzdown, b) Fxdown, c) Fydown , d) Mzdown, e) Mxdown and f) Mydown.

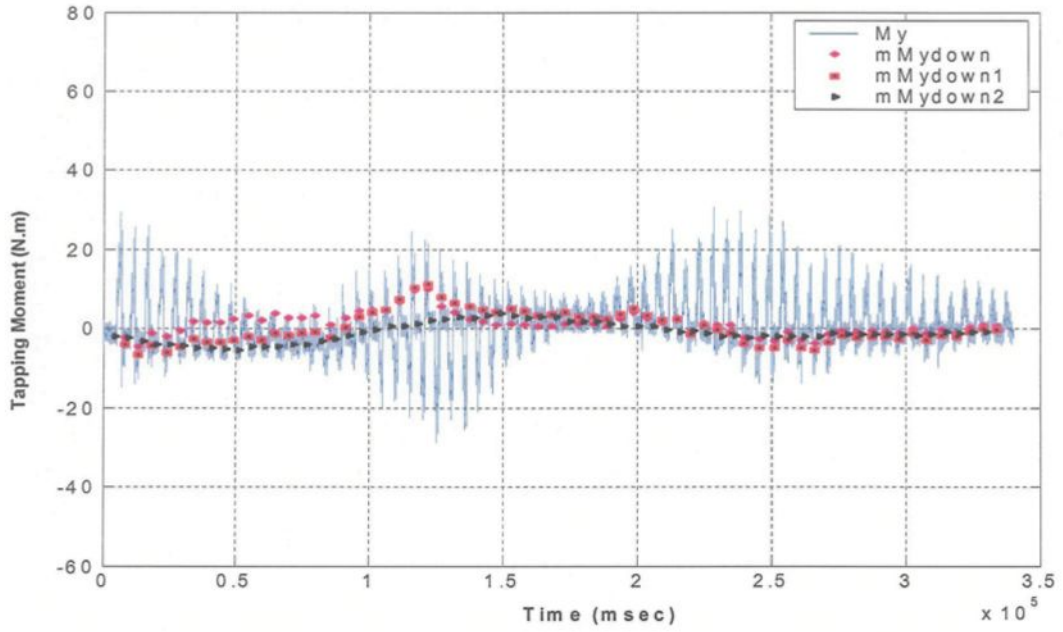

(e)

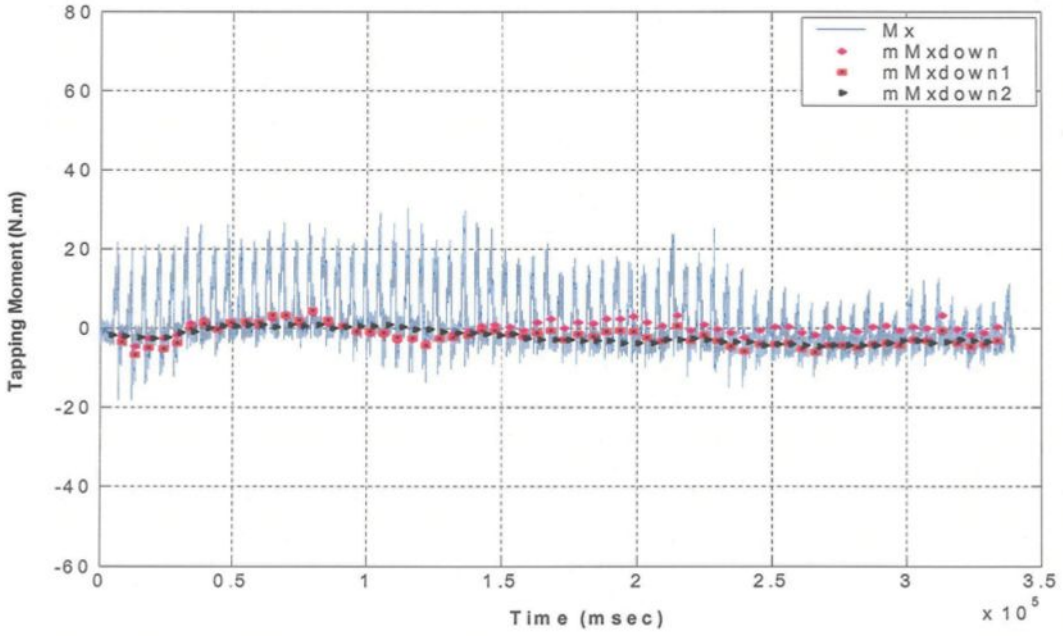

(f)

Figure 5.11 Output results for tapping force and moment of the first group of holes (65 from 115-holes)-plots with and without error treatment when the tap exist the drilled holes a) Fzdown, b) Fxdown, c) Fydown , d) Mzdown, e) Mxdown and f) Mydown.

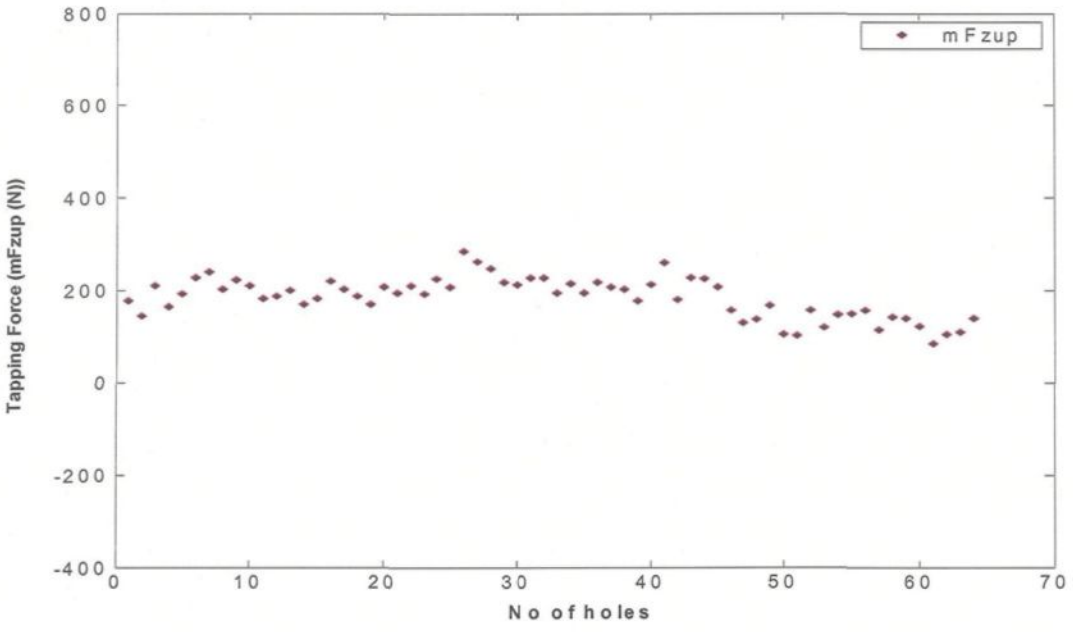

(a)

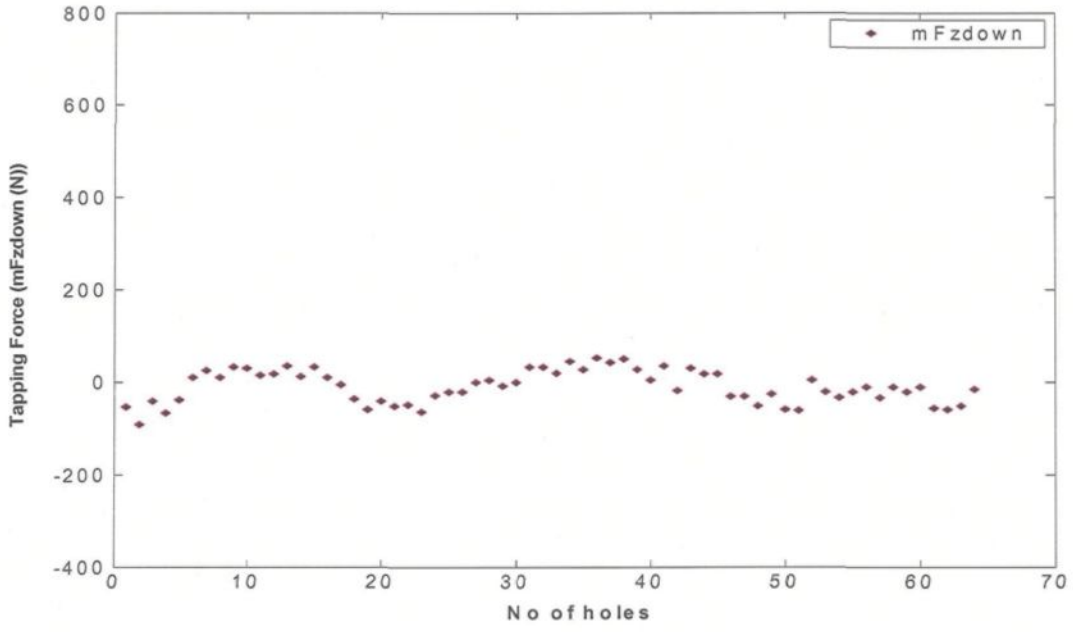

(b)

Figure 5.12 Output results for the mean tapping feed force vs. no of drilled holes of the first group of holes (65 from 115-holes) a) when the tap enter the drilled holes and b) when the tap exist.

5.2.3. Mean Total Cutting Force, Moment and Peak-to-Valley Calculations

After obtaining each component of the mean cutting force and moment as shown above, the total mean cutting force and moment, their standard deviations as well as the peak-to-valley range in both drilling and tapping were calculated. These were computed from the following set of equations. Standard deviation calculations for the total cutting force and total cutting moment were carried out by the following three methods. Method 1 was adopted in our calculations.

Method 1:[134]

$$\sigma_f = \left((\partial F_t / \partial x * \partial x)^2 + (\partial F_t / \partial y * \partial y)^2 + (\partial F_t / \partial z * \partial z)^2 \right)^{1/2}$$
$$\mu_f = (\mu_x + \mu_y + \mu_z)^{1/2}$$

Eq. 5.4

And the total cutting force and total cutting moment are calculated;

$$F_t = (F_x^{\,2} + F_y^{\,2} + F_z^{\,2})^{1/2}$$
$$M_t = (M_x^{\,2} + M_y^{\,2} + M_z^{\,2})^{1/2}$$

Eq. 5.5

The different derivatives can be estimated as the following;

$$\partial F_t / \partial x = 1/2 * 2F_x / (F_x^{\,2} + F_y^{\,2} + F_z^{\,2})^{1/2}$$
$$\partial F_t / \partial y = 1/2 * 2F_y / (F_x^{\,2} + F_y^{\,2} + F_z^{\,2})^{1/2}$$
$$\partial F_t / \partial z = 1/2 * 2F_z / (F_x^{\,2} + F_y^{\,2} + F_z^{\,2})^{1/2}$$
$$\partial M_t / \partial x = 1/2 * 2M_x / (M_x^{\,2} + M_y^{\,2} + M_z^{\,2})^{1/2}$$
$$\partial M_t / \partial y = 1/2 * 2M_y / (M_x^{\,2} + M_y^{\,2} + M_z^{\,2})^{1/2}$$
$$\partial M_t / \partial z = 1/2 * 2M_z / (M_x^{\,2} + M_y^{\,2} + M_z^{\,2})^{1/2}$$

Eq. 5.6

By substituting Eq. 5.6 into Eq. 5.4, the standard deviation for force and moment can be obtained;

$$\sigma_{ff} = \left(Fx^2 * \sigma_x{}^2 + Fy^2 * \sigma_y{}^2 + Fz^2 * \sigma_z{}^2\right)^{1/2} / (F_x{}^2 + F_y{}^2 + F_z{}^2)^{1/2}$$
$$\sigma_{fm} = \left(Mx^2 * \sigma_x{}^2 + My^2 * \sigma_y{}^2 + Mz^2 * \sigma_z{}^2\right)^{1/2} / (M_x{}^2 + M_y{}^2 + M_z{}^2)^{1/2}$$

Eq. 5.7

Method 2:

$$\sigma_{ff}{}^2 = \left(\begin{array}{l}(\partial F_t / \partial x * \partial x)^2 + (\partial F_t / \partial y * \partial y)^2 + (\partial F_t / \partial z * \partial z)^2 + (2 * \partial F_t / \partial x * \partial F_t / \partial y * \partial x \partial y) + \\ (2 * \partial F_t / \partial x * \partial F_t / \partial z * \partial x \partial z) + (2 * \partial F_t / \partial y * \partial f / \partial z * \partial y \partial z)\end{array}\right)$$
$$\sigma_{fm}{}^2 = (\partial M_t / \partial x * \partial x)^2 + (\partial M_t / \partial y * \partial y)^2 + (\partial M_t / \partial z * \partial z)^2 + (2 * \partial M_t / \partial x * \partial M_t / \partial y * \partial x \partial y) +$$
$$(2 * \partial M_t / \partial x * \partial M_t / \partial z * \partial x \partial z) + (2 * \partial M_t / \partial y * \partial f / \partial z * \partial y \partial z)$$
$$\mu_f = (\mu_x + \mu_y + \mu_z)^{1/2}$$

Eq. 5.8

Again the different derivatives as in equations (Eq. 5.8) and following the above procedures, total cutting force and total cutting moment and their standard deviation can be obtained;

$$F_t = (F_x{}^2 + F_y{}^2 + F_z{}^2)^{1/2}$$
$$M_t = (M_x{}^2 + M_y{}^2 + M_z{}^2)^{1/2}$$

Eq. 5.5

$$\sigma_{ff} = \left(\left(Fx * \sigma_x + Fy * \sigma_y + Fz * \sigma_z\right)^2 / (F_x{}^2 + F_y{}^2 + F_z{}^2)\right)^{1/2}$$
$$\sigma_{fm} = \left(\left(Mx * \sigma_x + My * \sigma_y + Mz * \sigma_z\right)^2 / (M_x{}^2 + M_y{}^2 + M_z{}^2)\right)^{1/2}$$

Eq. 5.9

Method 3:[134]

The total cutting force and moment and their standard deviation can be obtained as the following (developed method from error propagation subject)

$$F_t = F^{1/2}$$

$$F = F_x^{\,2} + F_y^{\,2} + F_z^{\,2}$$

$$\sigma_f/F = 1/2 * \sigma_f/F$$

$$F + \sigma_f = F_x^{\,2} + F_y^{\,2} + F_z^{\,2} + 2\sigma_x * F_x + 2\sigma_y * F_y + 2\sigma_z * F_z + \sigma_x^{\,2} + \sigma_y^{\,2} + \sigma_z^{\,2}$$

$$\sigma_f/F = (2\sigma_x * F_x + 2\sigma_y * F_y + 2\sigma_z * F_z + \sigma_x^{\,2} + \sigma_y^{\,2} + \sigma_z^{\,2})/(F_x^{\,2} + F_y^{\,2} + F_z^{\,2})$$

$$1/2 * \sigma_f/F = 1/2 * (2\sigma_x * F_x + 2\sigma_y * F_y + 2\sigma_z * F_z + \sigma_x^{\,2} + \sigma_y^{\,2} + \sigma_z^{\,2})/(F_x^{\,2} + F_y^{\,2} + F_z^{\,2})$$

$$\sigma_{ff} = \sigma_f = (\sigma_x * F_x + \sigma_y * F_y + \sigma_z * F_z + \sigma_x^{\,2}/2 + \sigma_y^{\,2}/2 + \sigma_z^{\,2}/2)/(F_x^{\,2} + F_y^{\,2} + F_z^{\,2})^{1/2}$$

Eq. 5.10

Similarly;

$$M_t = (M_x^{\,2} + M_y^{\,2} + M_z^{\,2})^{1/2}$$

$$\sigma_{fm} = (\sigma_x * M_x + \sigma_y * M_y + \sigma_z * M_z + \sigma_x^{\,2}/2 + \sigma_y^{\,2}/2 + \sigma_z^{\,2}/2)/(M_x^{\,2} + M_y^{\,2} + M_z^{\,2})^{1/2}$$

Eq. 5.11

5.3. SUMMARY

In this chapter, one was provided with an introduction to the force and moment calculations that were used to evaluate the different kinds of machining processes (i.e. drilling and tapping) as are outlined in a subsequent chapter. A new technique was developed whereby a low pass filter was incorporated in the signal processing algorithm which was used in calculating the mean cutting force and moment during both the drilling and tapping processes. All signals were independently monitored, digitized and recorded into Lab View. Universal Kistler DynoWare software was used for force measurements and data processing of cutting force and moments. Matlab programs were developed for data processing and for calculating the mean value of cutting force and moment and their standard deviations in both drilling and tapping tests.

The raw cutting force data were analysed using the application of a low pass filter and following the detection of points within each cycle in the signal in the drilling and tapping tests. The sampling rate was 1000Hz. For the drilling cases, 1600 sample points per cycle were acquired for calculating the mean value of cutting feed force (Fz) and 1200 sample points per cycle for the other five components of force and moment (Fx, Fy, Mx, My, and Mz) in each signal (115 cycle or hole/signal) however, only 200 sample points per cycle were used for standard deviation or peak-to-valley calculations.

On the other hand, for the tapping tests, 2000 sample points per cycle (1000 for the start when the tap enters the drilled hole and 1000 for the end when the tap exits) were used for calculating the mean value of the tapping force and moment (Fx, Fy, Fz, Mx, My and

Mz) and their standard deviations or peak-to-valley range in each signal (65 cycle or hole/signal). Contamination drift was treated in the Matlab programs.

All components of the mean drilling cutting force and moment for all conditions (M1 to M5 ~60 machinability test samples each 230 holes) were determined. All components of the mean tapping cutting force and moment for all machining tests were obtained for M1, M3 and M5 conditions (~ 28 samples). The Matlab output results for all components of force and moment and their standard deviations in both drilling and tapping tests were put into an Excel data sheet and followed by calculations to arrive at the total mean cutting force and moment, and their standard deviations as well as the peak-to-valley range in both drilling and tapping (section 5.2.5) that were used as a way of evaluating drilling and tapping processes in the following chapters (Ch. 6 and Ch. 7).

CHAPTER 6

MACHINABILITY EVALUATIONS (DRILLING AND TAPPING)

CHAPTER 6
MACHINABILITY EVALUATIONS (DRILLING AND TAPPING)

6.1. INTRODUCTION

In this work, the heat treated and Sr-modified (200-250 ppm) Al-Si-Mg and Al-Si-Cu-Mg cast alloys, belonging to the Al-Si alloy system and represented respectively by 356 (M1) and 319 (M2, M3, M4 and M5) alloys containing mainly α-Fe-intermetallic and related to hardness levels of (100±10 HB), were selected for the machinability study, due to the high demand of these alloys in the automobile industry. Additions of Mg to 319 alloys which help to accelerate and intensify age hardening during the T6 temper coupled with different heat treatment conditions of both 356 and 319 alloys were carried out to get similar levels of hardness for all alloy conditions, Table 6.1.

Table 6.1 Condition of Mg, Fe- and Cu-intermetallic surface (volume) fraction and hardness for 356 and 319 alloys used for drilling and tapping study.

Alloy code	Alloy type	%Mg	Fe-Int. (S.F. %)	Hardness (HB)	Solidification time & Quenching rate
M1	356	0.3%	2%	100	.....
M2	319	0.10%	2%	90 and 100	.....
M3	319	0.10%	5%	90 and 100	.....
M4	319	0.28%	2%	88, 100 and 110	25-45 s and 100-145°C/s
M5	319	0.28%	5%	100	.....

Difference in microstructural constituent (i.e. Cu, Mg and α-Fe-intermetallic volume fractions) of 356 and 319 alloys because of normal differences in chemistry and additions can affect their machinability. Strontium modification in the presence of Mn causes the formation of α-Fe intermetallic within the dendritic area which improves the matrix hardness homogeneity and hence the overall alloy machinability for both 356 and 319 alloys. Both drilling and tapping operations were carried out at affixed machining conditions to study the machining performance of the Sr-modified and heat treated 356 and 319 alloys through the following parameters;

1. Role of Cu-intermetallics when machining 356 (without Cu- aged at 180°C/2h) and 319 (with Cu- aged at 220°C/2h) alloys, both have the same level of hardness (100 HB).
2. Role of Mg addition to 319 alloys at two levels of Mg content (0.1 and 0.28%) given the same aging treatment (220°C/2h) that yields different levels of hardness (90 and 100 HB) and given different aging treatment (180°C/2h and 220°C/2h) that yield the same level of hardness (100 HB).
3. Effect of increasing α-Fe intermetallic volume fractions to 319 alloys (2 and 5%) when aging carried out at 220°C/2h and at 180°C/2h that yields hardness of (90 HB) and (100 HB), respectively.

6.2. RESULTS AND DISCUSSION

6.2.1. Chemistry and Additions (Cu, Mg and α-Fe Volume Fractions)

The mean total cutting force and moment and the corresponding peak-to-valley range (standard deviation bars) based on the mean value of 46 holes (one rib) and 230 holes (one sample) were used as a way of evaluating the effect of metallurgical conditions on the drilling processes. On the other hand, each data point in tapping results represents the mean total cutting force or moment of 120 holes in each sample.

The effect of Cu and Mg on the drilling and tapping (force and moment) of Sr-modified 356 (M1) and 319 (M3 and M5) alloys containing mainly α-Fe- intermetallics are shown in Figure 6.1 and Figure 6.2, respectively. The effect of both Mg content and α-Fe-intermetallic surface fraction on the cutting force and moment viz. M2-319 alloy (low α-Fe-intermetallic volume fractions 2% and Mg content 0.1%) and M5-319 alloy (high α-Fe-intermetallic volume fraction 5% and high Mg content 0.28%) when both alloys given the same aging treatment (220°C/2h) are displayed in Figure 6.1 (plot(4) and (2), respectively).

Drilling force and moment of low and high Mg content 319 alloys i.e. M3 and M5 conditions when aging carried out at 180° and 220°C for two hours are shown in Figure 6.1 (trend line 3 and 2, respectively). A small addition of 0.1% Mg to the M3-condition improves the alloy machinability, lowers cutting force and moment compared with M5 (0.28% Mg). Similar behaviour was observed in tapping results, Figure 6.2.

Comparison of M3 and M5 drilling and tapping results (in terms of number of holes made) shows that the M5-condition is more sensitive to tool wear than the M3-one i.e.,

there were more than 3000 holes drilled and tapped in the M3-conditions compared with less than 2000 holes in the case of M5-conditions. In tapping results of M3-319 (0.1%Mg) alloy, only the cutting force and moment for 1840 holes (8 machinability test sample) out of 3220 holes (14 machinability test sample) are shown in Figure 6.2. The M2-319 alloy gave similar drilling results to those of the M3-319 alloy (>3500 holes) when aging was carried out for M3 at 180°C/2h and for M2 at 220°C /2h.

In drilling results, it was found that the lower copper content (i.e. M1-356 alloy) results in higher cutting force compared to M5-319 alloys (~ the same level of Mg-intermetallics), with both alloys given different aging treatments but having the same hardness level (100 HB). On the other hand, the softer M1-356 alloy gave the best results in tapping processes i.e. lower tapping force and moment and hence higher number of tapped holes than the M5-319 alloy. The higher cutting force and moment observed in 356 alloy can attributed to the ductility, the presence of precipitates free zones (PFZs) and the non uniform micro-hardness and hence more heat generation during high speed drilling processes. On the other hand, 356 alloy give best results during low speed tapping processes.

The morphology of iron intermetallics affected the cutting force results when the aging was carried out for two hour at 180° and not at 220°C for 319 alloys. Higher Mn/Fe ratio (0.75) in the M2 alloy (α Fe) display lower cutting force and moment than the lower Mn/Fe ratio (0.4) in the M3 alloy (α and β-Fe), Figure 6.3. There is no effect of iron intermetallic morphology in the T7 condition. Also, the low level of undissolved Cu in M3 alloy increase the cutting force and moment compared to M2 alloy (high undissolved Cu).

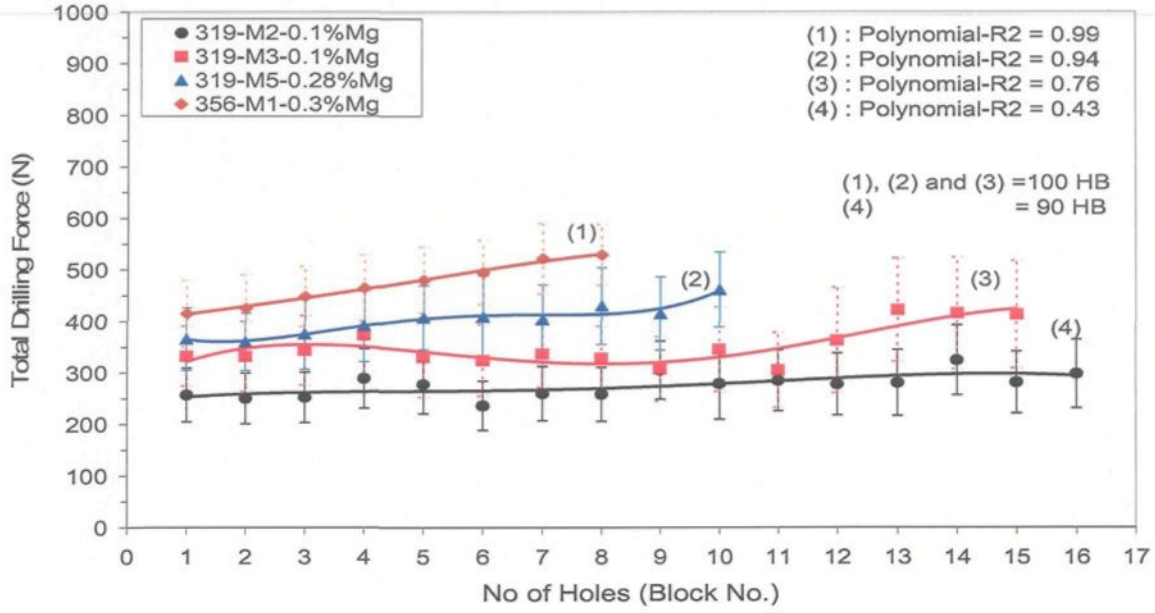

(a)

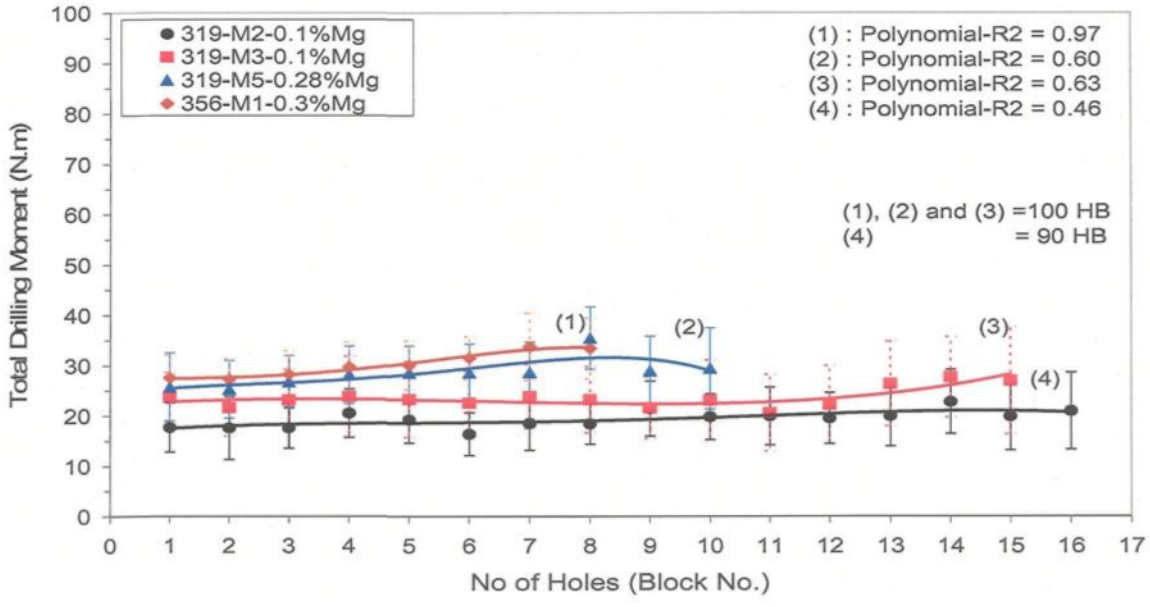

(b)

Figure 6.1 The effect of Cu, Mg and α-Fe- intermetallic volume fraction on the machinability of Sr-modified 356 and 319 alloys containing mainly α-Fe-intermetallics corresponding to alloy codes M1 (356 alloy), M2, M3 and M5 (319 alloys): (a) average total drilling force of 230 holes (one block), (b) average total drilling moment of 230 holes (one block).

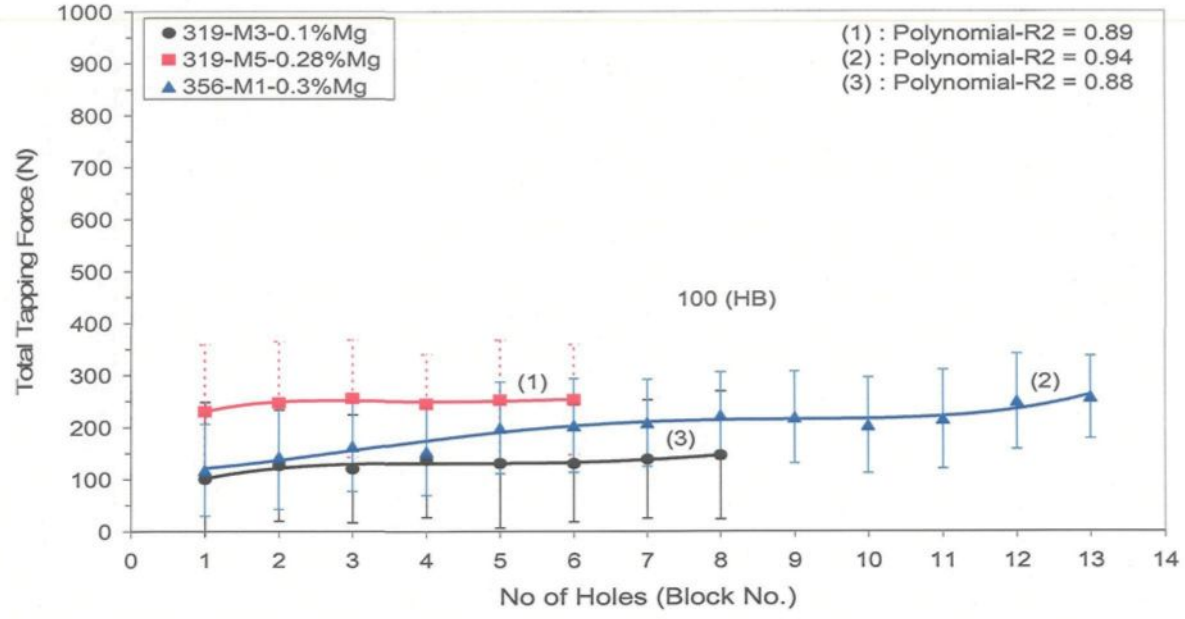

(a)

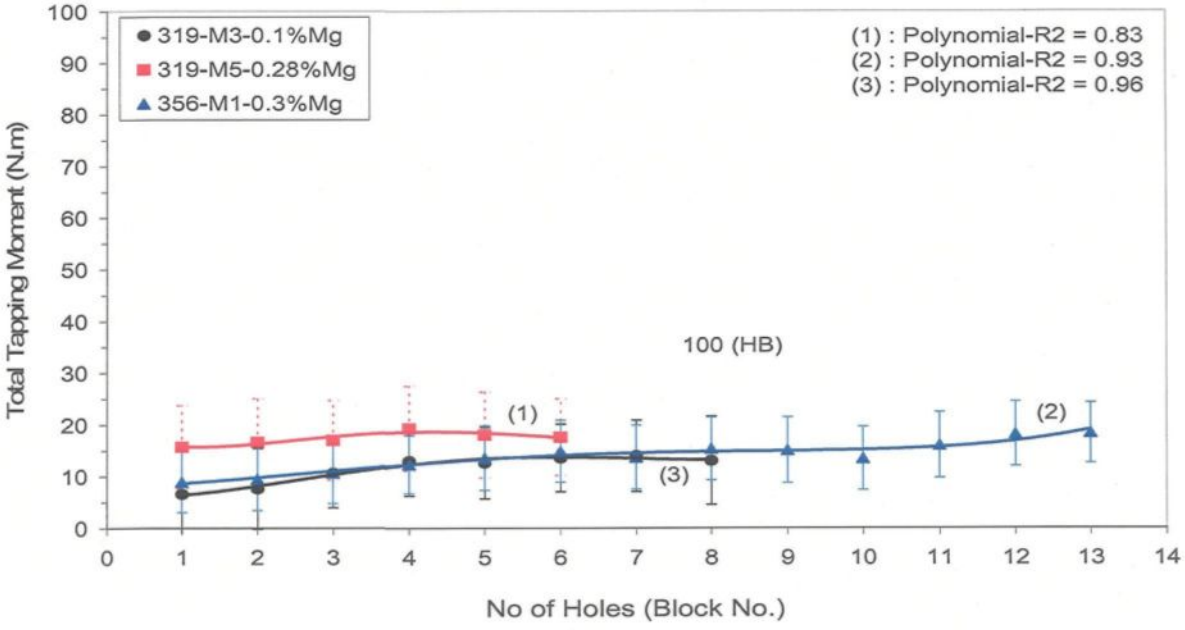

(b)

Figure 6.2 The effect of Cu and Mg on the machinability of Sr-modified 356 and 319 alloys containing mainly α-Fe- intermetallics corresponding to alloy codes M1 (356 alloy), M3 and M5 (319 alloys): (a) average total tapping force of 230 holes (one block), (b) average total tapping moment of 230 holes (one block).

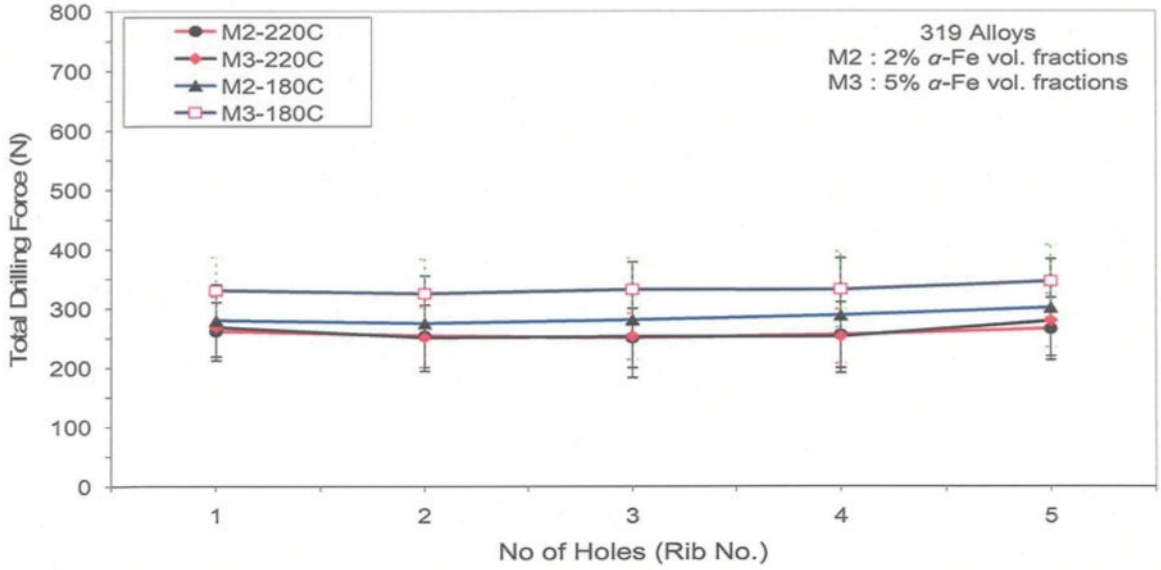

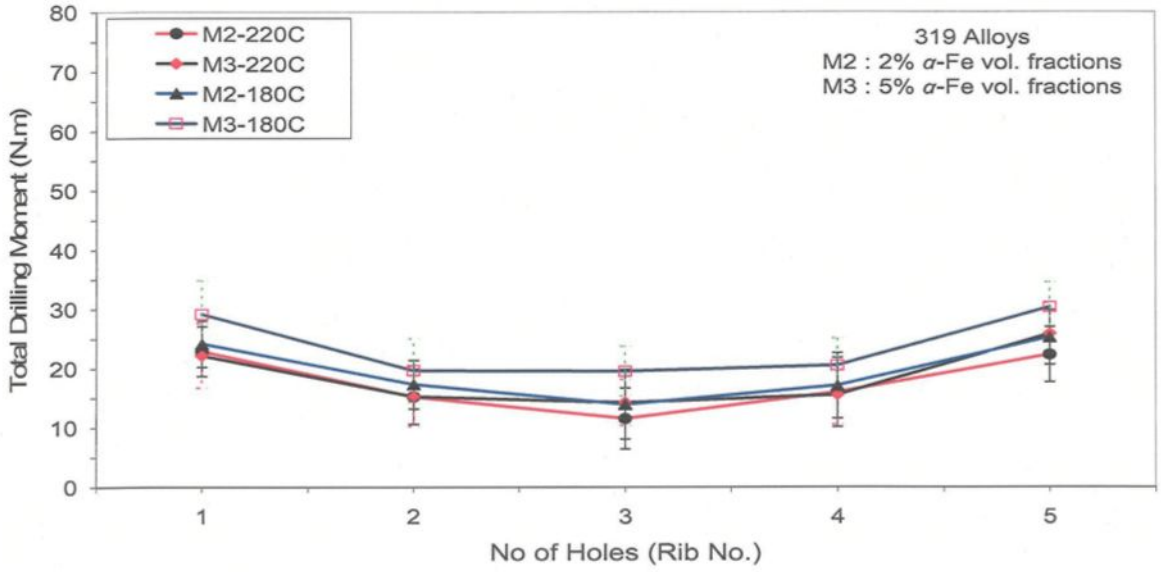

Figure 6.3 The effect of α-Fe-intermetallic volume fraction on the machinability of Sr-modified 319 alloys corresponding to alloy codes M2 (90HB-0.1%Mg) and M3 (100HB-0.1%Mg) after 2h aging at 220°C and 180°C, respectively: (a) average total drilling force of 46 holes (one rib), (b) average total drilling moment of 46 holes (one rib).

From the above drilling and tapping results, three main conclusions can be formulated:

1. Higher Mg content results in a higher cutting force at the same level of hardness. This can be explained by the fact that a high volume fraction of Mg-intermetallics or precipitates can be formed within the alloy matrix in the high Mg content 319 alloy conditions (M4 and M5) compared to the low Mg content one (M2 and M3).
2. Lower copper content (i.e. 356 alloy) results in higher cutting force compared to 319 alloys at the same level of hardness. This may be explained by the improvement in the homogeneity of the alloy matrix hardness in 319 alloys on the basis of the combined effect of Cu-and Mg-intermetallics, whereas hardening occurs by cooperative precipitation of Al_2Cu and Mg_2Si phase particles compared to only Mg_2Si precipitation in the case of 356 alloys.
3. The morphology of iron intermetallics affected the cutting force results when the aging was carried out for two hour at 180° and not at 220°C.

6.2.2. Effect of Solidification Time and Quenching Rate

Lower solidification rate materials have a coarser microstructure than the higher ones. For the machinability test sample, it was found that the external ribs have higher cooling rates than the internal one. Solidification times in the range of (25-45 sec) were measured by using five thermocouples fixed in the center of each rib in the machinability test sample, see Figure 3.2(a). Following solutionizing, the castings were quenched in warm water (65 °C); Differences in the quenching rates were observed within the five ribs, Figure 3.5(b). The quench media and quench interval are the most important parameters controlling the effectiveness of the treatment. The quench media had sufficient volume and heat extracting capacity to produce rapid cooling. The quench was attained within less than 10 seconds. Uniform dispersion of Mg_2Si and maximum properties are obtained if the quench can be attained within 10 seconds.[135]

The effect of solidification time in the range of (25-45 sec) on the cutting force and cutting moment is shown in Figure 6.4. It appears that both cutting force and moment are slightly influenced by solidification time. Similar behavior is observed for the quenching rate when aging was carried out at 220°C for two hours (see Figure 6.5). In all cutting moment results (total value), there is a geometry effect from the symmetry of the machinability test sample. This effect can participate in increasing the difference in cutting moment results between the external and internal ribs. For all metallurgical conditions tested, the total moment was higher for rib numbers (1 and 5) than rib numbers (2 and 4) and rib number 3.

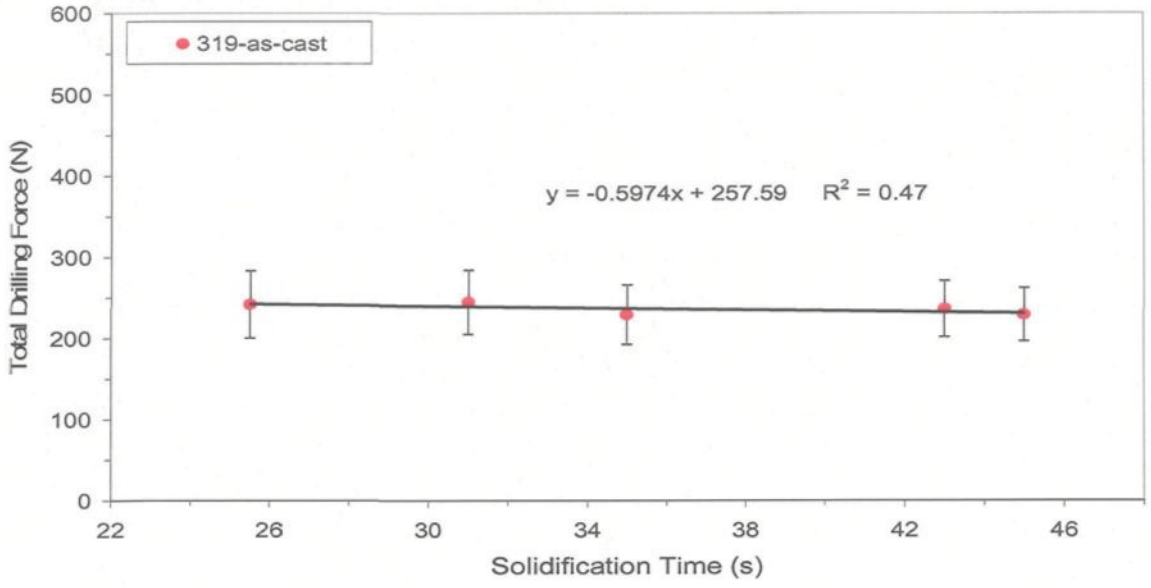

(a)

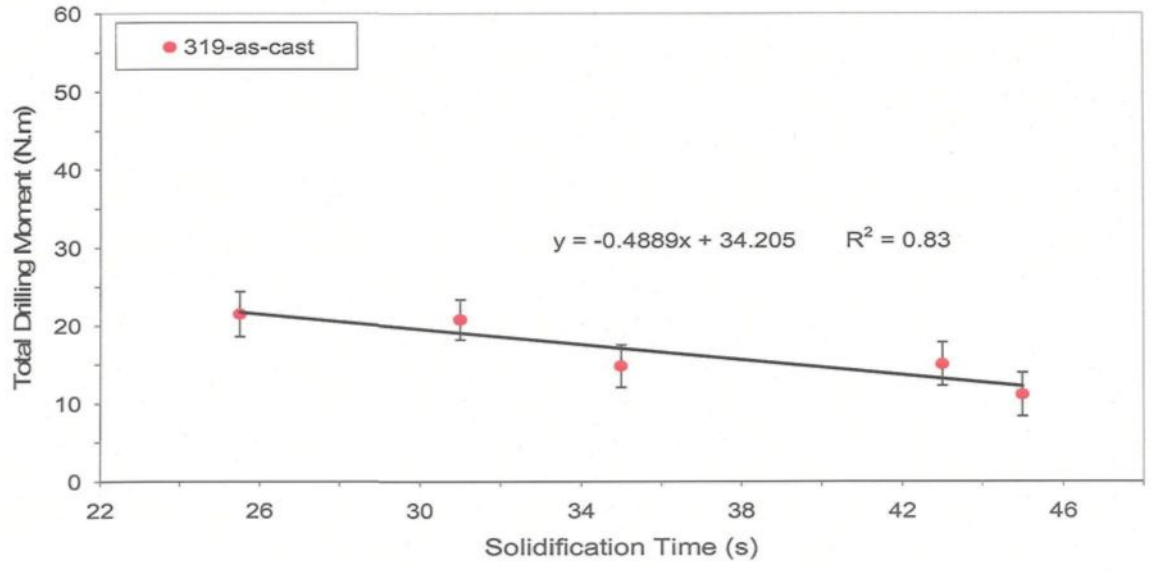

(b)

Figure 6.4 The effect of solidification time on the machinability of as-cast Sr-modified 319 alloy corresponding to alloy code M4 (88 HB-0.28%Mg): (a) average total drilling force of 46 holes (one rib), (b) average total drilling moment of 46 holes (one rib).

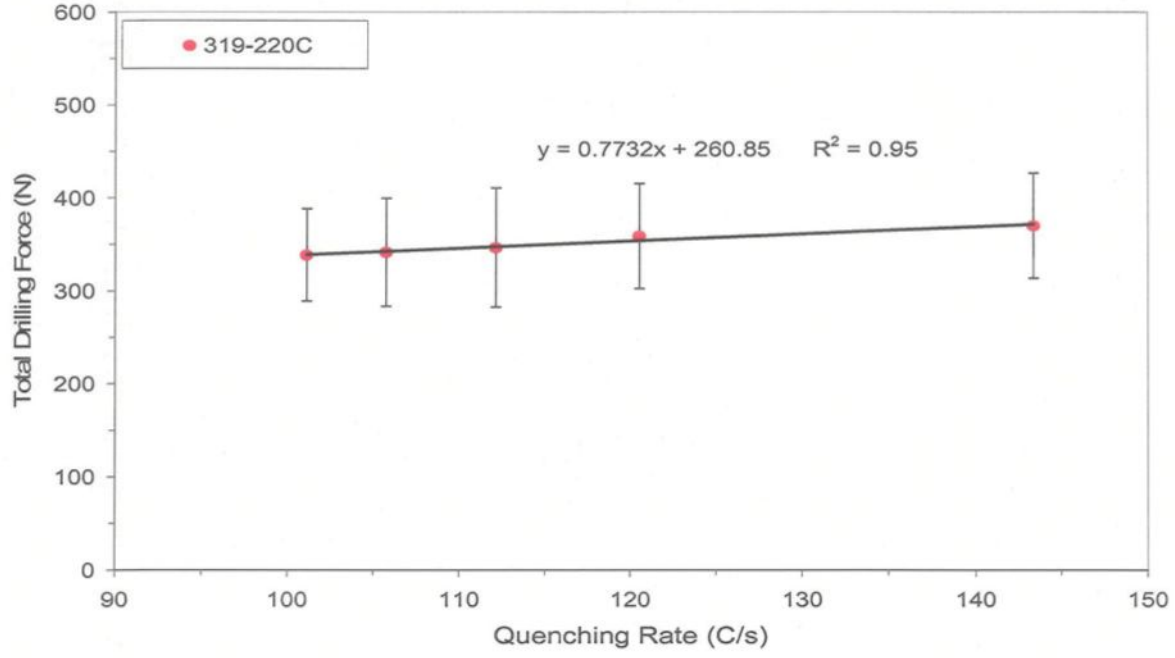

(a)

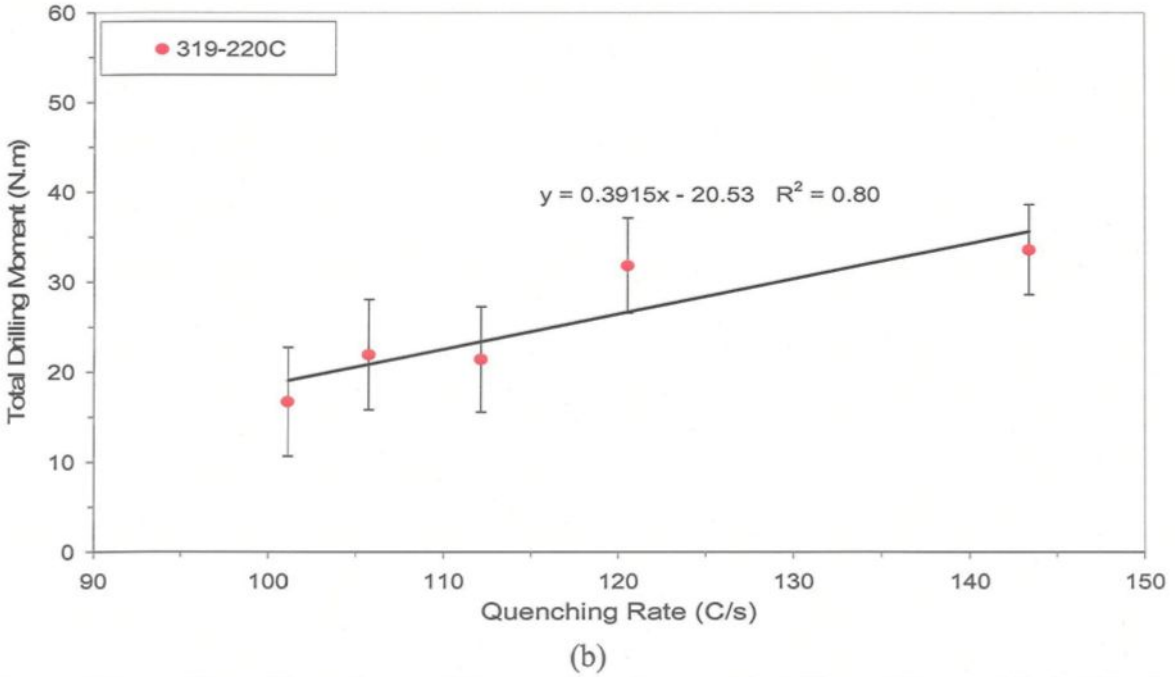

(b)

Figure 6.5 The effect of quenching rate on the machinability of Sr-modified 319 alloy corresponding to alloy code M4-T7 (100 HB-0.28%Mg): (a) average total drilling force of 46 holes (one rib), (b) average total drilling moment of 46 holes (one rib).

6.2.3. Effect of Hardness

Hardness is one of the most important metallurgical parameters that can control the alloy machinability, in fact, the aluminum alloys differ from many other metals in that machinability of aluminum generally improves as hardness increase. Most automotive machine shops agree that a minimum hardness of 80 Brinell is desirable. Heat treatment is one of the most important controlling factors used to enhance the mechanical properties and machinability of cast Al-Si alloys, through optimizing both solution and aging heat treatment given to those types of alloys. Heat treatments that increase the hardness will reduce the built-up-edge on the cutting tool and improve the surface finish of the machined part. Drilling forces are proportional to the hardness of wrought alloys and the feed rate.

In the aged M1-356 alloy (180°C/2h) the hardness are mainly a function of the microstructures containing coherent rods or needles of β' (Mg_2Si). Similar to 356 alloys, aging at 180°C/2h for Mg-containing 319 alloys (M2 to M5), yields a high hardness compared to aging at 220°C/2h. At 180°C aging, an increase in hardness is clearly due to the coherency of $CuAl_2$ (θ') plates and Mg_2Si (β') needles. However, at 220°C there is the incoherent equilibrium of β (Mg_2Si) and $CuAl_2$ (θ) phases, and thus the hardness is reduced.

The effect of three hardness levels i.e. 88, 110 and 100 (HB) related to the as cast, aging at 180° and at 220°C for two hour, respectively on the cutting force and moment of M4-319 alloy is displayed in Figure 6.6. Both aging treatment conditions show higher cutting force and moment than the as-cast ones.

The effect of hardness of heat treated 319 alloys (containing Mg and α-Fe intermetallic) on the cutting force, moment and heat-build-up are displayed in Figure 6.7. It was found that both cutting force and moment increase with the hardness while the heat build up depth on the cutting edge decreases. Best machinability in terms of optimum cutting force, moment and heat built-up were obtained at a hardness level of 100 HB. The hardness of heat-treated 319 alloys (containing Mg and α-Fe intermetallic) can be taken as a measurement for the cutting force, moment and heat build-up on the cutting edge through the following equations (Eq 6. 1 to Eq 6. 4)

Cutting Force= 6.3367*Hardness (HB)-314.24 $R^2 = 0.87$ Eq 6. 1

Cutting Moment= 0.4975*Hardness (HB)-27.638 $R^2 = 0.80$ Eq 6. 2

Heat Build-Up Depth (mm)= -0.0027*Hardness(HB)+ 0.3417 $R^2 = 0.80$ Eq 6. 3

Heat Build-Up Depth (mm)= -0.0003*Hardness(HB)+ 0.0477 $R^2 = 0.56$ Eq 6. 4

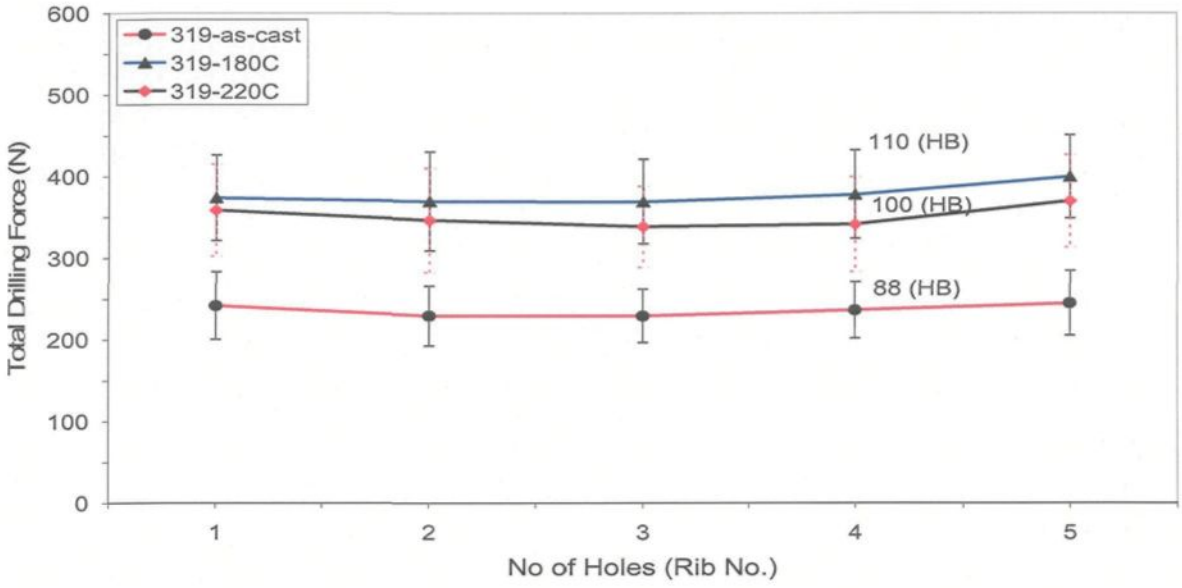

(a)

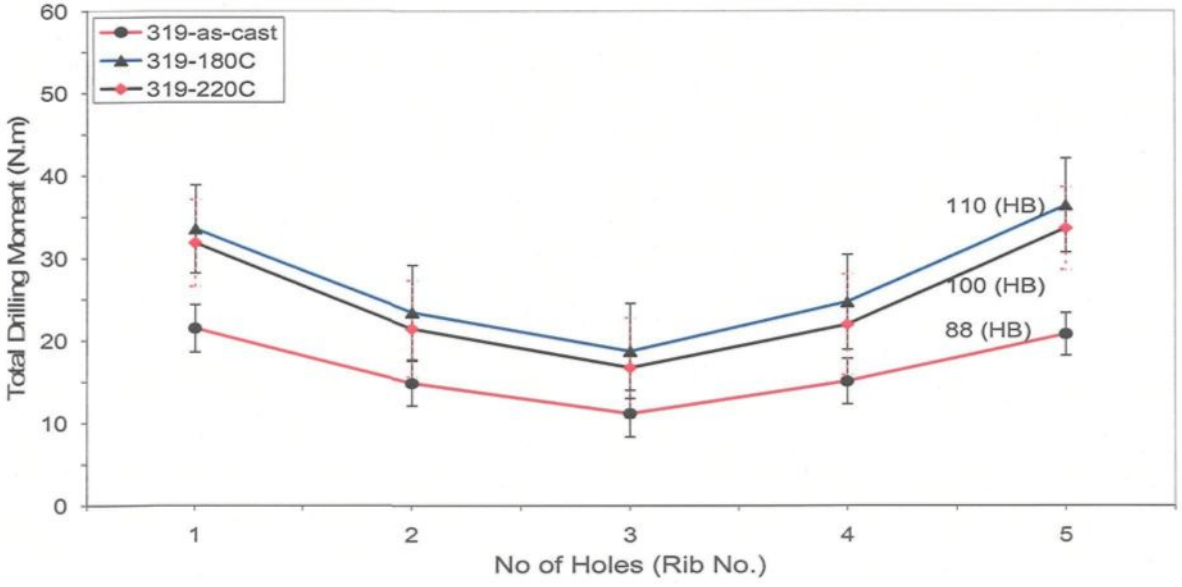

(b)

Figure 6.6 Effect of hardness (88, 110 and 100 HB) on the machinability of 319 alloy (M4) corresponding to as-cast, 2h aging at 180°C and at 220°C conditions, respectively): (a) average of total drilling force for 46 holes (one rib), (b) average of total drilling moment for 46 holes (one rib).

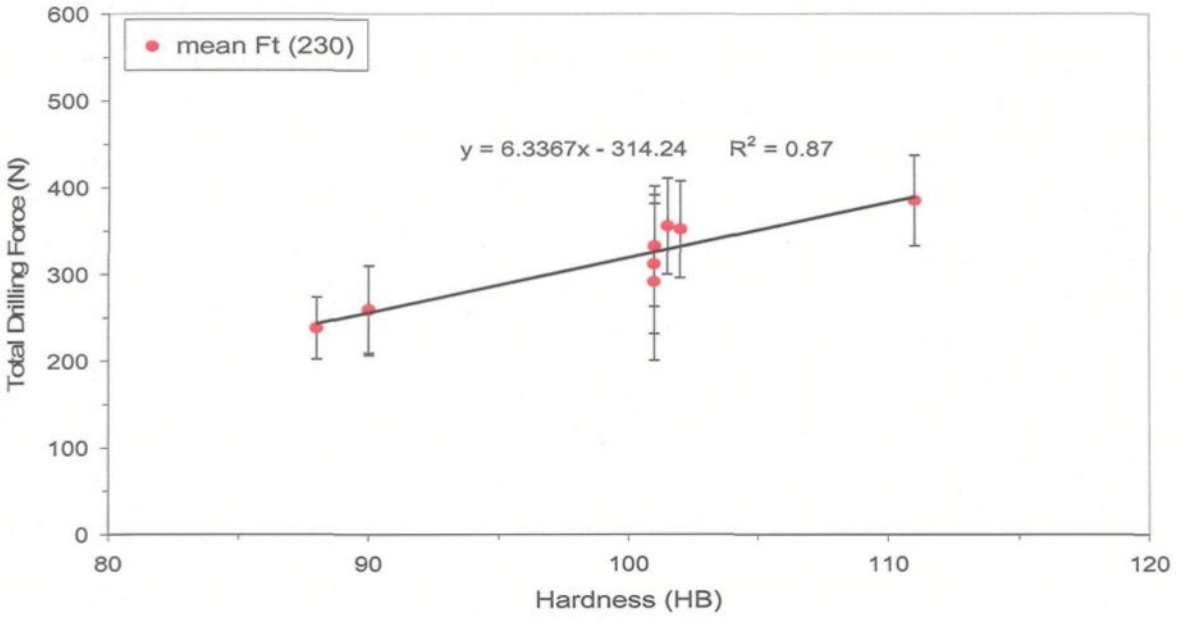

(a)

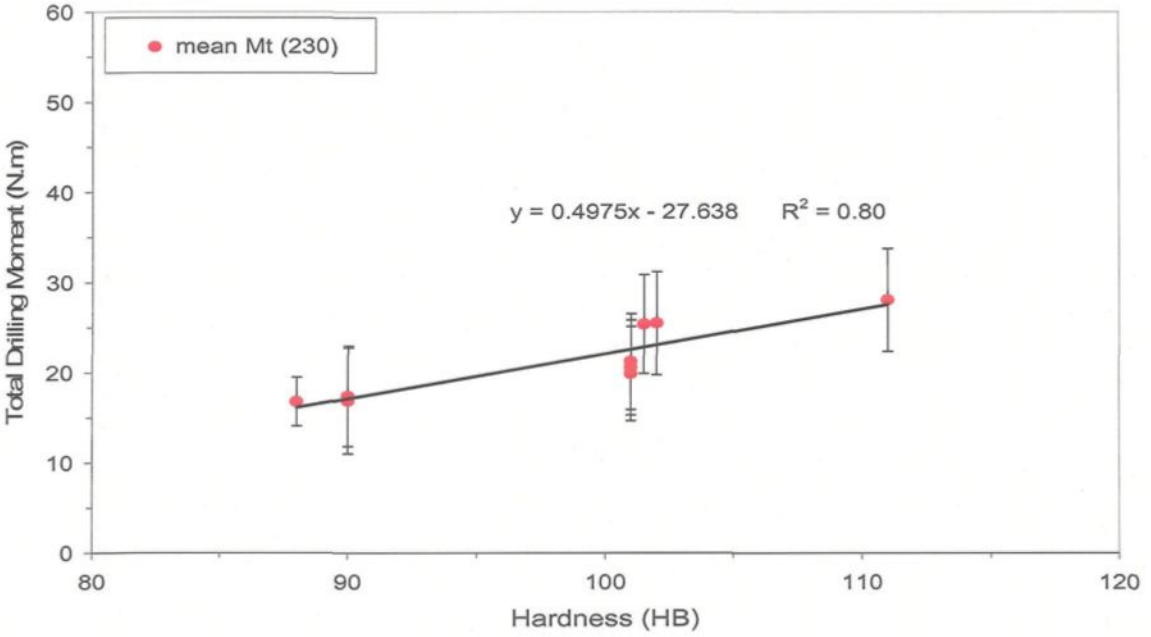

(b)

Figure 6.7 Effect of hardness on the machinability of 319 alloys; (a) average of total drilling force, (b) average of total drilling moment, (c) heat build-up depth and (d) heat build-up area.

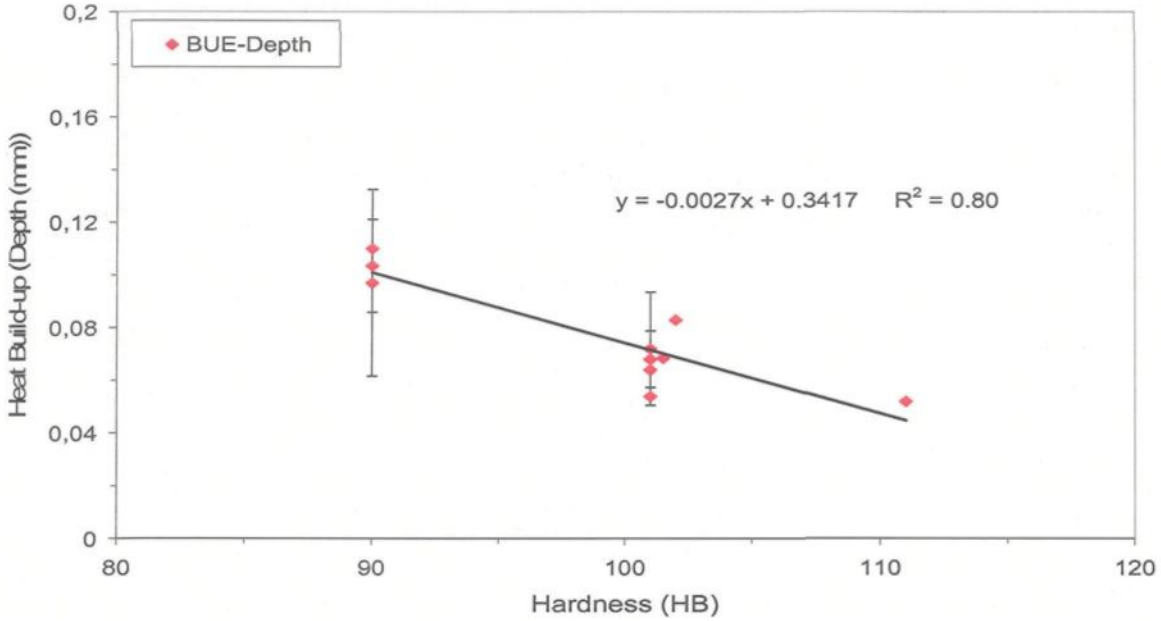

(C)

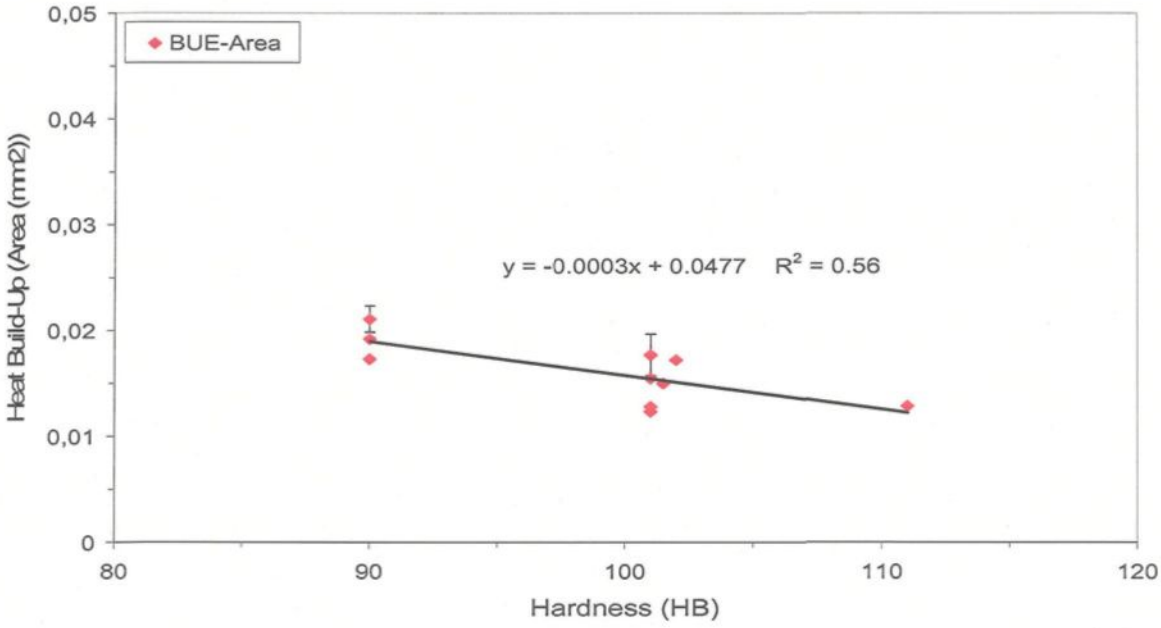

(d)

Figure 6.7 Effect of hardness on the machinability of 319 alloys; (a) average of total drilling force, (b) average of total drilling moment, (c) heat build-up depth and (d) heat build-up area.

6.2.4. Machinability Criteria

In a collective sense, the most important parameters that relate to the subject of machinability in drilling and tapping modes which were investigated in the present study are:

- Specific power consumed, cutting force, moment and tool life
- Heat built-up and hole accuracy and chip control (chip breakability)

6.2.4.1. Tool Life

For each of the alloy variations, tool life was measured in terms of the number of holes drilled and tapped, under constant machining conditions. The 319 alloys display lower cutting force and moment compared to 356 ones regardless of heat treatment. The low α-Fe-intermetallic volume fractions and Mg containing 319 alloy showed lower cutting force and moment and a higher number of holes (M2 condition-3680 holes) followed by the high α-Fe-intermetallic volume fractions and low Mg content 319 alloy (M3 condition-3565 holes) and by the high α-Fe-intermetallic volume fraction and high Mg content 319 alloy (M5 condition-2244 holes) and finally by the low α-Fe-intermetallic volume fractions 356 alloy (M1 condition-1840 holes).

Any increase in the Mg addition (more than 0.1%) to 319 alloys causes deterioration in tool life, higher cutting force and moment, and lower number of holes drilled and tapped. The addition of a small amount of magnesium to 319 alloys provided the desired drilling results in terms of number of holes drilled regardless of the aging treatment. However, the T6-conditions yielded better tapping results than the T7-one regardless of the alloy

chemistry, see the drilling and tapping results of M1 (356 alloy) and M2, M3 and M5 (319 alloys) in Table 6.2. Tool life results for different conditions of 356 and 319 alloys in terms of the number of holes drilled and tapped are listed in Table 6.2.

In tapping tests, it was observed that high speed steel tools react considerably more sensitively to the hardness and are less sensitive to abrasive wear than the carbide tools as in drilling. The tap (HSS-E) was broken when changed from tapping only 230 holes in the as-cast condition (88 HB) to tapping another 230 holes in the T6-condtion (110 HB) for alloy M4. The T6-aging treatment provided superior tapping results regardless of the alloy chemistry in terms of number of holes tapped (approximately 3220 holes).

The chipping failure mechanism for the 1st and 2nd tap teeth were observed when tapping high Mg-content 319 alloy (M5), see, Figure 6.8. On the other hand, drills were easily worn by friction, heat, etc. and sometimes broke when subjected to severe cutting forces at the lips, which are the main cutting regions and the weakest parts of the drill bit. With respect to the measurement of drill wear, it was frequently observed that this measurement was obscured by the high tendency of aluminum material to adhere to the portion of interest at the drill point, cutting lip and margin.

Table 6.2 Tool life results

Machining characteristics	M1-356 (0.3%Mg)	M2-319 (0.1%Mg)	M3-319 (0.1%Mg)	M5-319 (0.3%Mg)
Workpiece Hardness (HB)	100	90	100	100
Drill tool life (no of holes)	1840	>3680	>3565	2244
Cutting time (minutes)	80 min.	194 min.	188 min.	118 min.
Tap tool life (no of holes)	>3220	1955	>3220	1840
Cutting time (minutes)	243 min.	147 min.	243 min.	138.8 min.

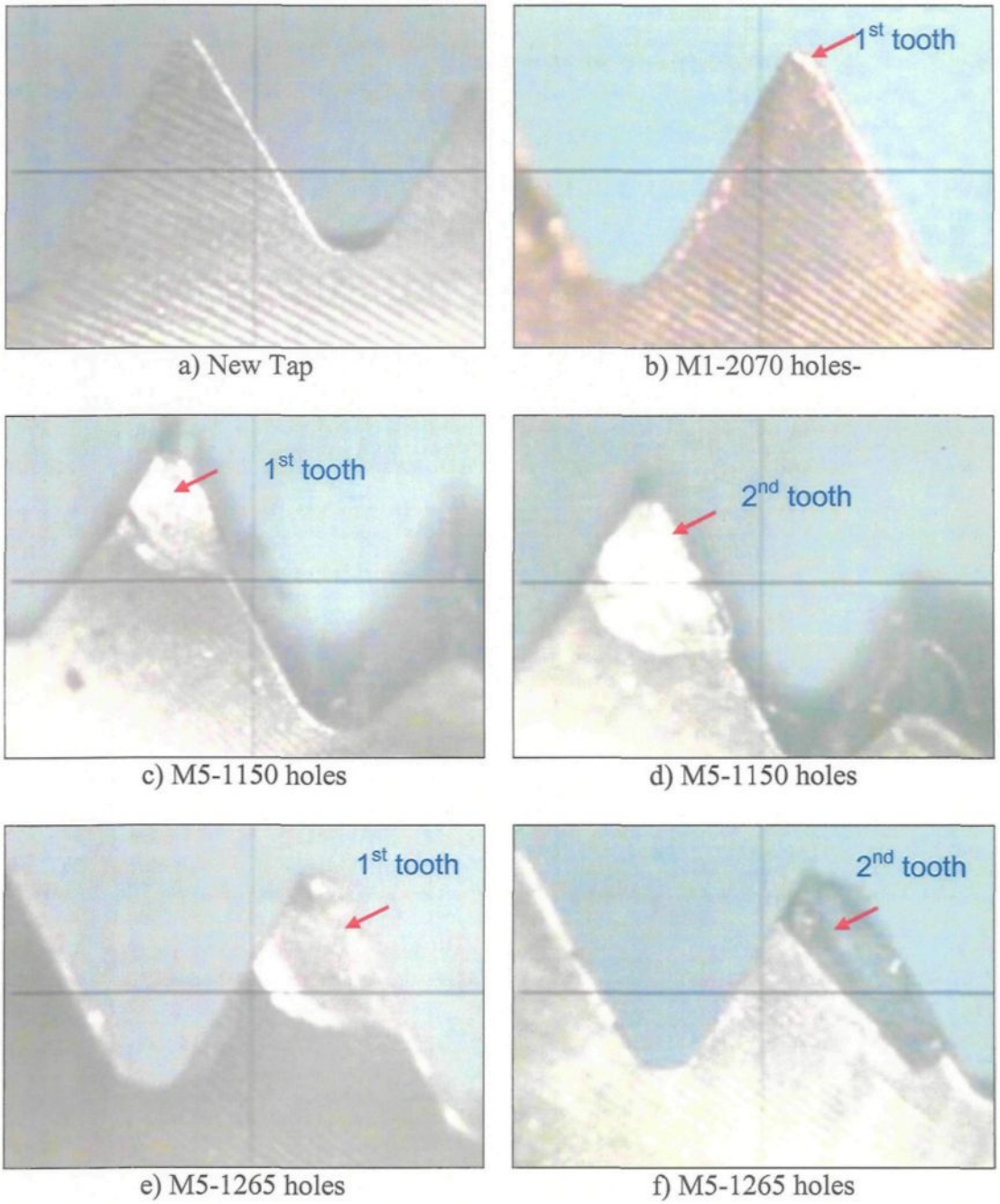

a) New Tap b) M1-2070 holes-

c) M5-1150 holes d) M5-1150 holes

e) M5-1265 holes f) M5-1265 holes

Figure 6.8 Optical micrographs taken from 1st and 2ed tap teeth after tapping different number of holes in M1-356 and M5-319 alloys showing new tap (a), rounded edge after 2070 holes in M1-356 alloy (b), chipping failure after 1150 holes in M5-319 alloy (c, d) and increasing failure after 1265 holes in M5-319 alloy (e, f).

6.2.4.2. Heat Built-Up Edge (BUE) Evolution and Hole Accuracy

As a result of high temperature, small particles of metal adhere to the edge of the cutting tool and build-up results. In practice the size and the shape of the built-up edge varies greatly with the work material and with the cutting conditions. For any material and cutting conditions the built-up edge seems to reach an equilibrium size and shape. It has to support the high compressive and shear stress imposed by the cutting process and therefore it cannot grow in height indefinitely. As it grows in height and changes in shape the stress system changes and parts of the built-up edge are broken away.

Smearing effect or built-up edge for different 356 and 319 alloy conditions where the aluminum welds itself to the cutting tool can seen in Figure 6.9. The adhesion phenomenon evolves during drilling and seems to be of a different nature at each stage. At the start of the drilling (i.e. a new drill), an aluminum layer does not tend to stick on the drill face, as shown in Figure 6.9 (a). After some drilled holes for 356 alloy (M1-T6 condition) i.e. 1265, 1610 and 2300, an aluminum deposit starts adhering to the tool face, mainly on the roughened area of the tool surface, Figure 6.9 (b, c and d) respectively. Similar behavior was observed in 319 alloys. Optical micrographs for heat built-up on the cutting drill (lip and margin) after a different number of holes were made i.e. (1495 and 3910) for M2-T7 condition, (2990 and 3680) for M3-T6 condition, 230 for M4-T7 condition and (1150 and 1840) for M5-T7 condition can be seen in Figure 6.9 (e and f), Figure 6.9 (g and h), Figure 6.9 (k, l) and Figure 6.9 (m, n), respectively.

The progress of the wear on the cutting edge results in high cutting forces and a rise in cutting temperatures at the chip formation area. The temperature rise can reach a point

where a so called deceptive chip formation occurs (welding). Behind the contact zone the material solidifies into a slowly growing, chip-like formation and firmly adheres to the flank of the tool. [136, 137] Also, the nest of chips impedes the flow of additional chips trying to escape from the flutes. This in turn can cause the flutes to pack and may result in drill breakage.

The pressure and the temperature in the contact zone are favorable to the diffusion of the aluminum towards the tool, and mico-weldings can be formed on the tool surface. Gradually, a strong aluminum layer is formed on the rake face and it extends into the flute area. After a significant number of holes, the accumulation of aluminum continues and clearly reaches the drill lip. Deceptive chip formation (welding) was observed on 356 (M1-T6 condition) and 319 alloys (M3-T6 condition), see Figure 6.10 (a, b and c) and Figure 6.10 (d, e and f), respectively.

An important assessment criterion during drilling and tapping is the quality of the hole; this is, in particular, understood to mean the precision of dimensions and shape of the hole and the surface quality at the side of the hole. The Go-No-Go test is taken as an assessment characteristic for hole accuracy. The reference diameter of Go-No-Go gauge test (6.5024-6.5278 mm and 7.02056-7.15518 mm) with acceptable tolerance of 0.39% and 1.9% is used for drilling and tapping respectively. For all alloy conditions the Go-No-Go gauge tests were carried out and the results are listed in Table 6.3.

Full, half turn and helical chips were observed when drilling 356 and 319 alloys while no chips were produced during tapping tests. A transition to the segmented chip is a consequence of competition between the two processes: the local strain hardening of the

metal at the place where the shearing begins and its local softening due to the essential heating within the shear plane. At the point of critical stress the hardening processes prevail over the softening processes and a main line crack develops which results in breaking some elements off the chip and thereby to the development of a completely broken chip as shown in Figure 6.11.

Table 6.3 Go-No-Go Test Results for the Hole Accuracy.

Alloy conditions	**Drilling Go-No-Go gage** (6.5024/6.5278 mm-0.39% acceptable tolerance)	**Tapping Go-No-Go gage** (7.02056/7.15518 mm-1.9% acceptable tolerance)	**No of drilled holes**	**No of tapped holes**
M1-T6	OK	OK	1840	3220
M2-T7	OK	OK	3680	1955
M2-T6	OK	OK	230	N/A
M3-T6	OK	OK	3565	3220
M3-T7	OK	OK	230	N/A
M4-as cast	OK	OK	230	230
M4-T6	OK	OK	230	230
M4-T7	OK	OK	230	N/A
M5-T7	OK	OK	2244	1840

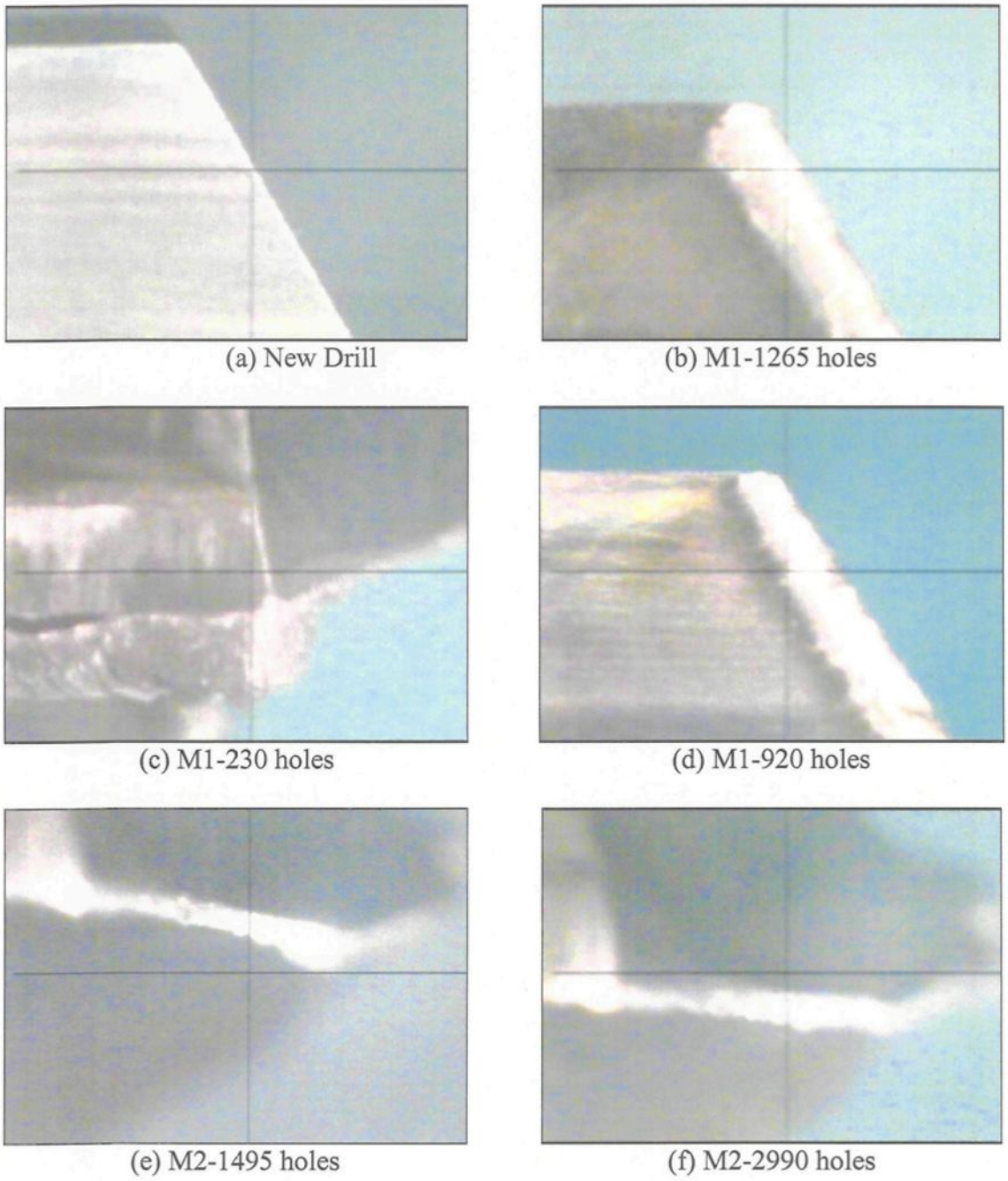

(a) New Drill (b) M1-1265 holes

(c) M1-230 holes (d) M1-920 holes

(e) M2-1495 holes (f) M2-2990 holes

Figure 6.9 Optical micrographs showing heat built-up on the cutting drill lip and margin point after drilling 356 (M1) and 319 (M2-M5) alloys for different numbers of holes: new drill (a), heat build-up for M1-100HB (b, c and d), for M2-90HB (e, f), for M3-100HB(g, h), for M4-100HB (k, l) and for M5-100-HB (m, n).

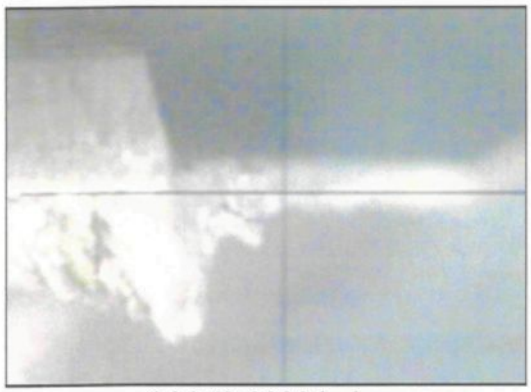

(g) M3-2990 holes

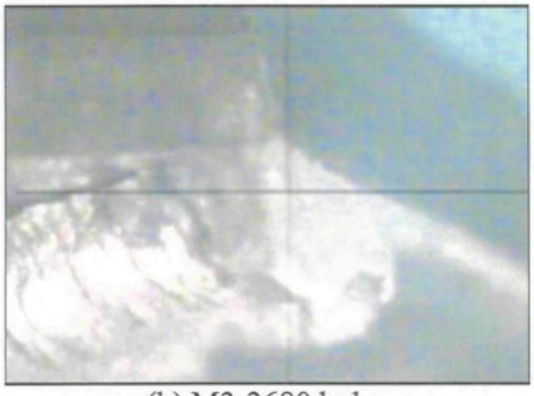

(h) M3-3680 holes

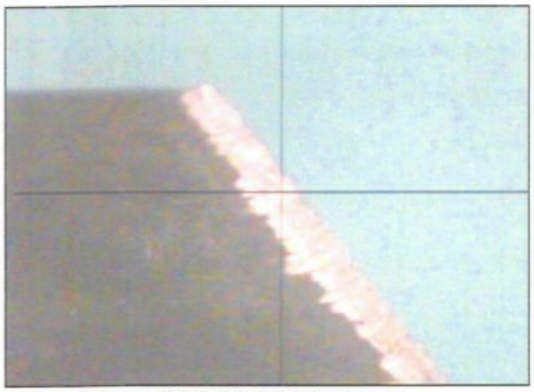

(k) M4-230 holes

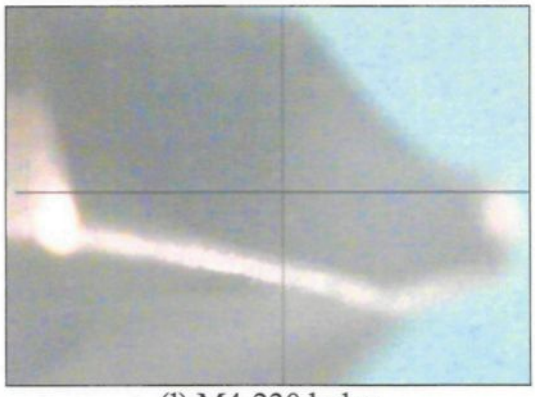

(l) M4-230 holes

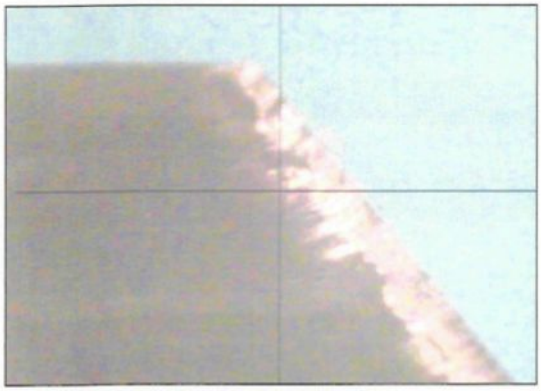

(m) M5-1150 holes

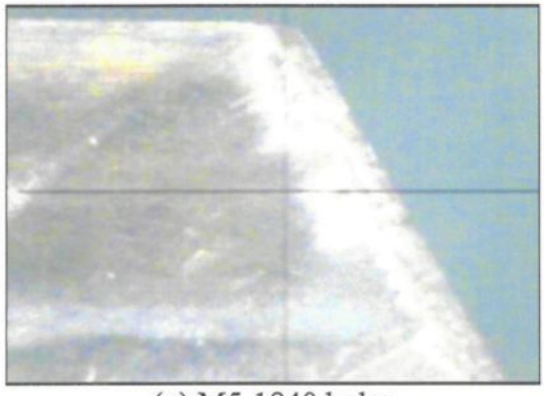

(n) M5-1840 holes

Figure 6.9 Optical micrographs showing heat built-up on the cutting drill lip and margin point after drilling 356 (M1) and 319 (M2-M5) alloys for different numbers of holes: new drill (a), heat build-up for M1-100HB (b, c and d), for M2-90HB (e, f), for M3-100HB(g, h), for M4-100HB (k, l) and for M5-100-HB (m, n).

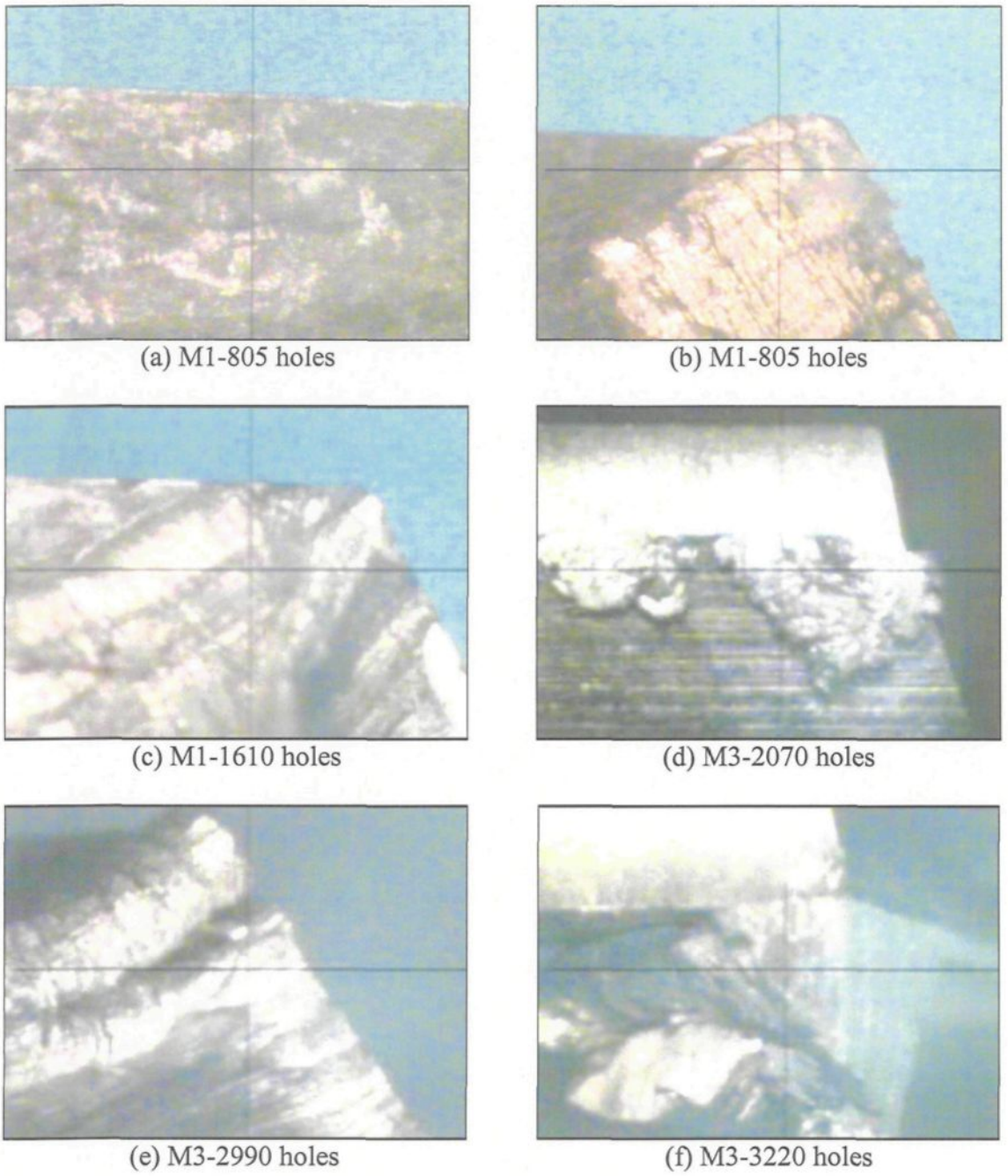

(a) M1-805 holes (b) M1-805 holes

(c) M1-1610 holes (d) M3-2070 holes

(e) M3-2990 holes (f) M3-3220 holes

Figure 6.10 Optical micrographs showing the chip welding or sticking on the flute surface of the cutting drill after drilling M1-356 and M3-319 alloys for different numbers of holes: M1-100HB(a, b and c), and M3-100HB (d, e and f).

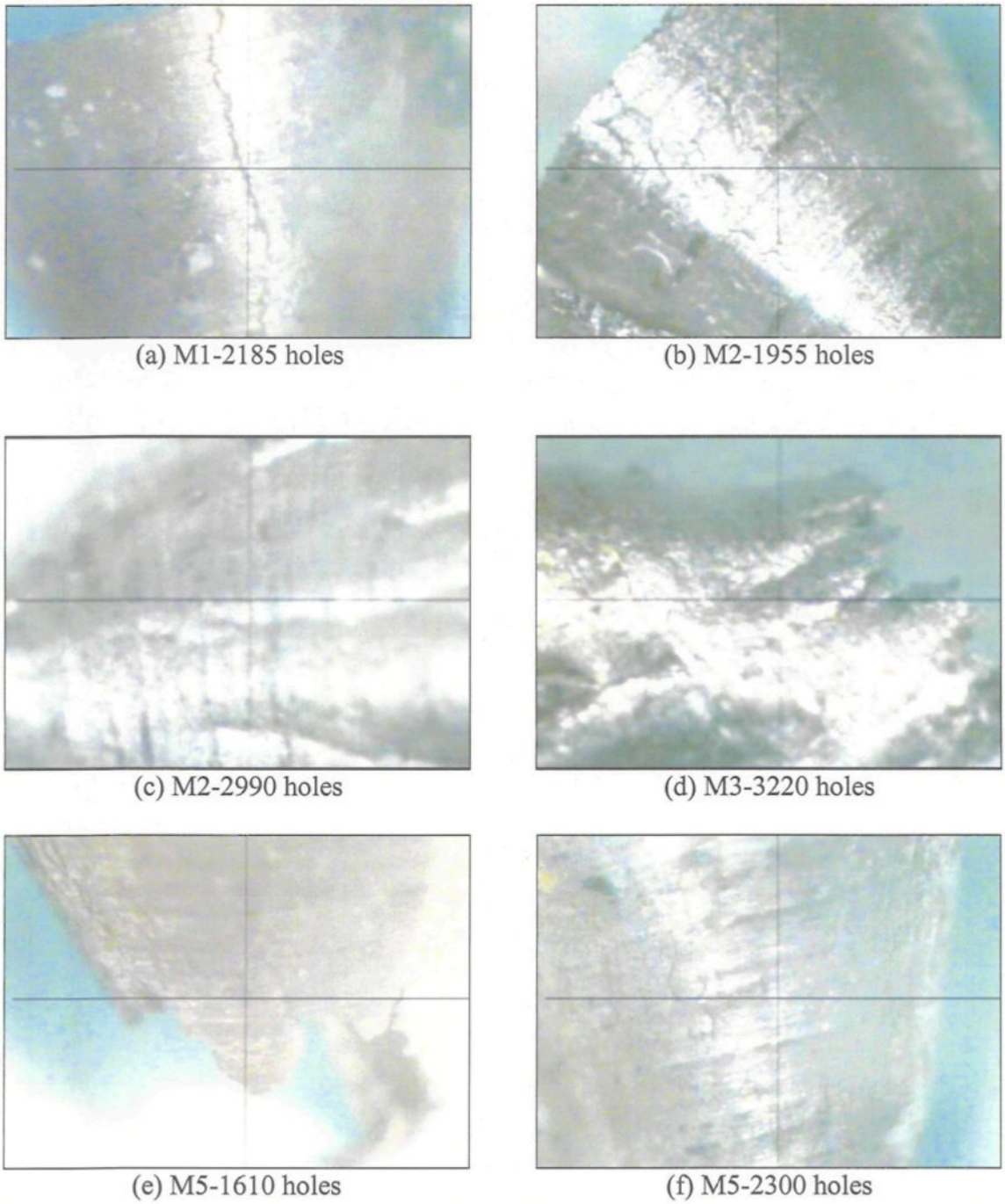

(a) M1-2185 holes (b) M2-1955 holes

(c) M2-2990 holes (d) M3-3220 holes

(e) M5-1610 holes (f) M5-2300 holes

Figure 6.11 Optical micrographs showing the surface of chips after drilling 356 (M1) and 319 (M2, M3 and M5) alloys for different number of holes: M1-100HB (a), M2-90HB (b, c) M3-100HB (d) and M5-100HB (e, f).

6.3. SUMMARY

The differences in machining behaviour between 356 and 319 alloys are mainly attributed to the difference in microstructural constituents and matrix hardness. The matrix hardness (beneficial) and alloy abrasiveness (detrimental) seem to be the real issues controlling the alloy machinability. Drilling and tapping study was carried out to investigate the machining performance of 356 and 319 alloys through the role of the following metallurgical factors;

- Chemistry and alloying additions (Cu, Mg and Fe intermetallic surface fractions)
- Solidification time and Quenching rate
- Hardness (HB)

Higher Mg content results in a higher cutting force at the same level of hardness. This can be explained by noting the high volume fraction of Mg-intermetallics or precipitates that can form within the alloy matrix in the high Mg content 319 alloy conditions (M4 and M5) compared to the low Mg content ones (M2 and M3). The low Mg-containing 319 alloys (0.1%) yield the longest tool life, more than two times that of 356 alloys (0.3% Mg) and one and half times that of high Mg-containing 319 alloys (0.28%). It is customary to rate the machinability of low Mg-containing 319 alloys higher than 356 alloys and also higher than 319 alloys of the high Mg-containing variety.

Lower copper content i.e. 356 alloy results in higher cutting force compared to 319 alloys at the same level of hardness. This may be explained by the improvement in the homogeneity of alloy matrix hardness in 319 alloys on the basis of the combined effect of

Cu-and Mg-intermetallics, whereas hardening occurs by cooperative precipitation of Al_2Cu and Mg_2Si phase particles compared to only Mg_2Si precipitation in the case of 356 alloys.

The iron intermetallic volume fraction and morphology can affect the cutting force results when aging was carried out for two hours at 180° and not at 220°C. It was observed that α-Fe intermetallic volume fractions can affect the cutting force and moment when aging was carried out at 180°C rather than at 220°C. Addition of Mg increase the α-Fe intermetallic volume fraction and hence, the cutting force and moment.

Heat treatments that increase the hardness will reduce the built-up-edge on the cutting tool. Hardness affects the machinability of 319 alloys in that machinability improves as the hardness increases. It is observed that both cutting force and moment increase with the hardness while the heat build up depth on the cutting edge decreases.

For solidification time in the range of 25 to 45 seconds, it seems that both cutting force and moment is slightly influenced by the cooling and quenching rate.

In tapping, it was observed that high speed steel tools react considerably more sensitively to the hardness. Heat built-up and chip welding was observed on 356 and 319 alloys (M1 and M3, respectively). Full, half turn and helical chips are generated at the start of a cutting operation when the drill is new (shearing process). As the drill begins to wear, the chips gradually become well deformed and then both shearing and deformation occur.

CHAPTER 7
QUANTITATIVE STUDY: APPLICATION OF STATISTICAL DESIGN

CHAPTER 7
QUANTITATIVE STUDY: APPLICATION OF STATISTICAL DESIGN

PART I: EFFECT OF METALLURGICAL PARAMETERS ON THE HARDNESS OF HEAT-TREATED 319 ALLOYS

7.1. INTRODUCTION

In contributing to what is already known, the present study was undertaken to investigate the effect of metallurgical parameters on the hardness of heat-treated 319 alloys. Experimental correlations of the results obtained from the hardness measurements (chapter 4) are analyzed and correlations that relate the alloying additions and heat-treatment to the hardness of such alloys are found. Statistical design was applied through factorial analysis methods of 2^n-design. The main parameters are: magnesium content (%Mg), volume fractions of the α-Fe-intermetallics (%V.F), Sr-modification (Sr-ppm), aging time (At) and aging temperature (AT). Regression equations were developed between the response variables (Hardness HB) and the factors varied, viz alloying elements and aging parameters for cast 319 alloys. This mathematical tool has been used profitably for various wrought aluminium alloys in the recent past by two of the authors.[138, 139] These correlations are valid for the aging time range (2-8 h) and aging temperature (180-220°C) where a linear or nearly linear relation in the hardness profile exists (peak-to-overaged regions).

Similarly, experimental results obtained from the drilling tests are analyzed and empirical models are established to estimate the relations between both the mean total drilling forces and moments as well as heat build up on the cutting tool edge and some of

the metallurgical parameters. Eight drilling tests were carried out at fixed machining conditions under two different levels of influencing metallurgical factors for the analysis of the cutting force and moment as well as heat build up on the cutting tool edge when the hardness was set within 100±10 HB.

In the Al-Si-Cu-Mg system (319 alloys), hardening may be caused by the precipitation of Al_2Cu, Mg_2Si, Al_2CuMg and $Al_4CuMg_5Si_4$ phases.[11] Addition of Mg to 319 alloys containing β- and/or α-Fe intermetallics produces a remarkable increase in hardness at all aging temperatures in both the unmodified and Sr-modified conditions. Aging of Mg-containing 319 alloys at 180°C for times up to eight hours yields a sharp rise in hardness during the first two hours of aging, followed by a broad peak or plateau spread across the 2-8 h time period. However, aging at 220°C revealed a hardness peak at 2 h

In the peak-aged condition, the higher hardness of 319 Mg-containing alloys is clearly due to the high concentration of $CuAl_2$ (θ') plates and Mg_2Si (β') needle-like metastable phases, where the thermal activation energy is enough to nucleate such intermediate phases coherent with the matrix, leading to a sharp rise in hardness at both 180°C and 220°C when aging is carried out for two hours. Increasing the ageing time or ageing temperature increases the size of these particles, with a gradual change in their chemical composition, resulting in the equilibrium θ (Al_2Cu) and β (Mg_2Si) phases in the form of incoherent particles, which are responsible for the observed drop in the alloy hardness.

7.2. RESULTS AND DISCUSSION

7.2.1. Metallurgical Parameters Effect on Hardness Generation Models

In this chapter, experimental correlations of the results obtained from the hardness measurements are analyzed through empirical models to establish the relations between the hardness and different metallurgical parameters of 319 alloys. Statistical design was applied through factorial analysis methods of 2^n-design. The main factors are magnesium content (%Mg), volume fractions of Fe-intermetallics (%V.F), Sr-modification (Sr-ppm) and aging parameters (Aging time (At) and Aging temperature (AT)). These correlations are valid for the aging time range (2-8 h) and aging temperature (180-220°C) where a linear or nearly linear relation in the hardness profile exists (peak-to-overaged regions).

7.2.2. Factorial Analysis

The 2^k factorial design (2^3-factorial experiment[140]) is the ideal choice for providing some information on the main effect and interaction of metallurgical factors on the hardness of the heat-treated 319 alloys containing mainly α-Fe intermetallics. The 2^5-factorial design is divided into a 2^3-factorial design (the effect of magnesium content (%Mg), volume fractions of α-Fe intermetallics (%V.F) and Sr-modification (Sr-ppm)) followed by a 2^2-factorial design (the effect of the aging parameters). The basic approach is to vary each factor within two level values one level is set as the minimum value and represented by -1 and the other level as the maximum and represented by +1.

Level values of these factors are listed in the 2^k design in Table 7.1. The response of these data is characterized by the mean values of the hardness. An empirical model can be

built through factorial analysis from the measured data and can be used for the hardness prediction as long as the metallurgical setting is within the limits represented by the upper and lower levels. This model consists of a mean value, three main effects and four interaction effects as can be seen in equation (Eq 7.1).

$$H_{predicted} = \mu + MF_{(\%Mg)} / 2 * \%Mg + MF_{(\%V.F)} / 2 * \%V.F) + MF_{(Sr)} / 2 * Sr(ppm) + IF_{(\%V.F*\%Mg)} / 2 * \%V.F * \%Mg + IF_{(\%V.F*Sr)} / 2 * \%V.F * Sr(ppm) + IF_{(\%Mg*Sr)} / 2 * \%Mg * Sr + IF_{(\%V.F*\%Mg*Sr)} / 2 * \%V.F * \%Mg * Sr(ppm)$$

Eq 7.1

Table 7.1 Design matrix and responses for 319 alloys containing mainly α-Fe intermetallics

α-Fe	Factors (j)			Response (Hardness-HB)				
Alloy Code	%Mg (1)	%V.F (2)	Sr (ppm) (3)	H1- 180°C-2h	H2- 180°C -8h	H3- 220°C -2h	H4- 220°C -8h	Yi
18	-1	-1	-1	117.0	119.0	108.0	103.0	y 1
20	1	-1	-1	131.5	132.5	119.0	116.0	y 2
19	-1	1	-1	117.5	123.0	106.0	101.0	y 3
21	1	1	-1	137.5	133.5	127.0	112.0	y 4
18s	-1	-1	1	108.5	109.0	94.0	96.5	y 5
20s	1	-1	1	120.5	119.0	114.0	99.0	y 6
19s	-1	1	1	117.5	115.0	96.0	95.5	y 7
21s	1	1	1	127.0	128.5	116.0	101.5	y 8

Let Y_i denote the response for the j combinations of levels. The generic design matrix is shown in Table 7.1. Using the design matrix one can easily calculate the main effects of varying each factor on the response variables. The mean value (μ) is calculated from averaging the eight measured values of hardness, see equation (Eq 7.2). Its physical interpretation is the predicted hardness when the three metallurgical variables (%Mg, %V.F

and Sr (ppm)) are set to the middle of their ranges (i.e. between their lower and upper limits).

$$Mean = (y1 + y2 + y3 + y4 + y5 + y6 + y7 + y8)/8 \quad \text{Eq 7.2}$$

Consider the first and the second hardness values in Table 7.1, and note that the corresponding values (117 and 131.5) differ by 14.5 because of the magnesium content (%Mg). The volume fraction of α-Fe-intermetallics (%V.F) and Sr-modification (Sr-ppm) settings are the same for both of these conditions. In addition to this pair, there are another three pairs of hardnesses ((117.5 and 137.5), (108.5 and 120.5) and (117.5 and 127)) that differ by 20, 12 and 9.5, respectively, and only because of the magnesium content (%Mg). The average of the four differences in the hardness measurements, (i.e. 14.0) represents the main effect of the magnesium content (%Mg) on the hardness. Similarly, the main effect of volume fraction of α-Fe-intermetallics (%V.F) and Sr-modification (Sr-ppm) can be estimated. All differences for the hardness as the average change in the response variable due to moving any factor (%Mg, %V.F and Sr-ppm) from its -1 level to its +1 level with all other factors held constant are listed in Table 7.2.

Table 7.2 Interaction check for 319 alloys containing mainly α-Fe intermetallics

α-Fe	Diff.	H1	H2	H3	H4
Mg	y 2-y 1	14.5	13.5	11.0	13.0
	y 4-y 3	20.0	10.5	21.0	11.0
	y 6-y 5	12.0	10.0	20.0	2.5
	y 8-y 7	9.5	13.5	20.0	6.0
V.F	y 3- y 1	0.5	4.0	-2.0	-2.0
	y 4- y 2	6.0	1.0	8.0	-4.0
	y 7-y 5	9.0	6.0	2.0	-1.0
	y 8- y 6	6.5	9.5	2.0	2.5
Sr	y 5- y 1	-8.5	-10.0	-14.0	-6.5
	y 6-y 2	-11.0	-13.5	-5.0	-17.0
	y 7-y3	0.0	-8.0	-10.0	-5.5
	y 8- y4	-10.5	-5.0	-11.0	-10.5

Thus, the main effect of varying factor j- MF_j is embodied in the average change in the response variable due to moving factor j from its -1 level to its +1 level with all other factors held constant. The main effects of the three metallurgical factors can be obtained by equation (Eq 7.3).

$$MF_{(\%Mg)} = ((y2 - y1) + (y4 - y3) + (y6 - y5) + (y8 - y7))/4$$
$$MF_{(\%V.F)} = ((y3 - y1) + (y4 - y2) + (y7 - y5) + (y8 - y6))/4$$
$$MF_{(Sr\text{-}ppm)} = ((y5 - y1) + (y6 - y2) + (y7 - y3) + (y8 - y4))/4$$

Eq 7.3

An advantage of the 2^k Factorial design method is that it provides some insight into the interactions of the factors on the response variable. In a similar way, the interaction effect between two factors can be thought of as the average change in the response when the two factors are at the same level and when they are at opposite levels. From Table 7.2,

one sees that the metallurgical variables do not behave additively and therefore "interact". A measure of the interaction between the magnesium (%Mg) and volume fraction of α-Fe intermetallics (%V.F) can be identified by the difference between the magnesium (%Mg) effects at low levels of volume fraction of α-Fe intermetallics (%V.F) and magnesium (%Mg) effect at high levels of volume fraction of α-Fe intermetallics (%V.F). Similarly, the interaction between the Magnesium (%Mg) and the Sr-modification (Sr-ppm) and between volume fraction of α-Fe intermetallics (%V.F) and Sr-modification (Sr-ppm) and between all of them can be obtained from Eq 7.4.

$$\begin{aligned}
IF_{(\%Mg*Sr\text{-}ppm)} &= ((y6 - y5) + (y8 - y7) - (y2 - y1) - (y4 - y3))/4 \\
IF_{(\%Mg*\%V.F)} &= ((y8 - y7) + (y4 - y3) - (y6 - y5) - (y2 - y1))/4 \\
IF_{(\%V.F*Sr\text{-}ppm)} &= ((y8 - y6) + (y7 - y5) - (y4 - y2) - (y3 - y1))/4 \\
IF_{(\%Mg*\%V.F*Sr\text{-}ppm)} &= ((y8 - y7) + (y2 - y1) - (y6 - y5) - (y4 - y3))/4
\end{aligned}$$

Eq 7.4

In general, one can determine the main effect of factor j and the interaction effect of factors i and j from the design matrix by using Eq 7.5 and Eq 7.6.[141]

$$MF_i = \frac{[Columnj]^T * Y_i}{2^{k-1}}$$

Eq 7.5

$$IF_{i*j} = \frac{[Columni * Columnj]^T * Y_i}{2^{k-1}}$$

Eq 7.6

The development of an empirical model for the hardness of 319 alloys containing mainly α-Fe has been obtained and is presented as Eq 7.7 which is coupled with the scaling

Eq 7.8. Effects estimated for 319 alloys containing mainly α-Fe intermetallics are listed in Table 7.3.

$$H1 = H_{(180°C-2h)} = 122.12 + 7.00\%Mg + 2.75\%V.F - 3.75Sr(ppm) - 1.62\%Mg * Sr(ppm) + 0.37\%Mg * \%V.F + 1.12\%V.F * Sr(ppm) - 1.00\%Mg * \%V.F * Sr(ppm)$$

$$H2 = H_{(180°C-8h)} = 122.44 + 5.94\%Mg + 2.56\%V.F - 4.56Sr(ppm) - 0.06\%Mg * Sr(ppm) + 0.06\%Mg * \%V.F + 1.31\%V.F * Sr(ppm) + 0.81\%Mg * \%V.F * Sr(ppm)$$

$$H3 = H_{(220°C-2h)} = 110.00 + 9.00\%Mg + 1.25\%V.F - 5.00Sr(ppm) + 1.00\%Mg * Sr(ppm) + 1.25\%Mg * \%V.F - 0.25\%V.F * Sr(ppm) - 1.25\%Mg * \%V.F * Sr(ppm)$$

$$H4 = H_{(220°C-8h)} = 103.06 + 4.06\%Mg - 0.56\%V.F - 4.94Sr(ppm) - 1.94\%Mg * Sr(ppm) + 0.19\%Mg * \%V.F + 0.94\%V.F * Sr(ppm) + 0.69\%Mg * \%V.F * Sr(ppm)$$

Eq 7.7

$$\%Mg = (\%Mg - 0.19)/0.1 \text{--------} Range(0.1 - 0.28\%)$$
$$\%V.F = (\%V.F - 3.75)/1.7 \text{--------} Range(2 - 5\%)$$
$$\%V.F_{\min} = (\%V.F - 2.4)/0.9$$
$$\%V.F_{\max} = (\%V.F - 5.0)/2.6$$
$$Sr_{ppm} = (Sr - 100)/100 \text{----------} Range(0 - 200ppm)$$

Eq 7.8

Table 7.3 Effects estimated for 319 alloys containing mainly α-Fe intermetallics

Alloy Code	Effect	H1	H2	H3	H4
18	Mean	122.12	122.44	110.00	103.06
20	MF1/2	7.00	5.94	9.00	4.06
19	MF2/2	2.75	2.56	1.25	-0.56
21	MF3/2	-3.75	-4.56	-5.00	-4.94
18s	IF1*3/2	-1.62	-0.06	1.00	-1.94
20s	IF1*2/2	0.37	0.06	1.25	0.19
19s	IF2*3/2	1.12	1.31	-0.25	0.94
21s	IF1*2*3/2	-1.00	0.81	-1.25	0.69

Similarly, an empirical model can be built through factorial analysis from the measured data and can be used for the hardness prediction of 319 alloys containing β-Fe intermetallics as long as the metallurgical setting is within the limits represented by the upper and lower levels. The generic design matrix is shown in Table 7.4. All differences for the hardness as the average change in the response variable due to moving any factor (%Mg, %V.F and Sr-ppm) from its -1 level to its +1 level with all other factors held constant are listed in Table 7.5. Again, effects estimated for 319 alloys containing mainly β-Fe intermetallics are listed in Table 7.6. The development of an empirical model for the hardness of 319 alloys containing β-Fe intermetallics has been obtained and is presented as Eq 7.9 which is coupled with the scaling equation (Eq 7.10).

Table 7.4 Design matrix and response for 319 alloys containing β-Fe intermetallics

β-Fe	Factors (j)			Response (Hardness-HB)				
Alloy Code	%Mg (1)	%V.F (2)	Sr (ppm) (3)	H1-180°C-2h	H2-180°C-8h	H3-220°C-2h	H4-220°C-8h	Yi
14	-1	-1	-1	116.5	121.0	104.5	96.5	y 1
16	1	-1	-1	130.0	132.0	120.5	110.0	y 2
15	-1	1	-1	112.5	120.0	104.0	101.0	y 3
17	1	1	-1	131.5	133.5	120.5	114.0	y 4
14s	-1	-1	1	104.0	114.5	97.5	89.0	y 5
16s	1	-1	1	121.0	119.5	108.5	107.0	y 6
15s	-1	1	1	112.5	109.5	99.5	95.5	y 7
17s	1	1	1	128.0	126.5	111.5	109.5	y 8

Table 7.5 Interaction check for 319 alloys containing β-Fe intermetallics

β-Fe	Diff.	H1	H2	H3	H4
Mg	y 2-y 1	13.5	11.0	16.0	13.5
	y 4-y 3	19.0	13.5	16.5	13.0
	y 6-y 5	17.0	5.0	11.0	18.0
	y 8-y 7	15.5	17.0	12.0	14.0
V.F	y 3- y 1	-4.0	-1.0	-0.5	4.5
	y 4- y 2	1.5	1.5	0.0	4.0
	y 7-y 5	8.5	-5.0	2.0	6.5
	y 8- y 6	7.0	7.0	3.0	2.5
Sr	y 5- y 1	-12.5	-6.5	-7.0	-7.5
	y 6-y 2	-9.0	-12.5	-12.0	-3.0
	y 7-y3	0.0	-10.5	-4.5	-5.5
	y 8- y4	-3.5	-7.0	-9.0	-4.5

Table 7.6 Effects estimated for 319 alloys containing β-Fe intermetallics

Alloy Code	Effect	H1	H2	H3	H4
14	Mean	119.50	122.06	108.31	102.81
16	MF1/2	8.12	5.81	6.94	7.31
15	MF2/2	1.62	0.31	0.56	2.19
17	MF3/2	-3.12	-4.56	-4.06	-2.56
14s	IF1*3/2	0.00	-0.31	-1.19	0.69
16s	IF1*2/2	0.50	1.81	0.19	-0.56
15s	IF2*3/2	2.25	0.19	0.69	0.06
17s	IF1*2*3/2	-0.87	1.19	0.06	-0.44

$$H1 = H_{(180°C-2h)} = 119.50 + 8.12\%Mg + 1.62\%V.F - 3.12Sr(ppm) + 0.00\%Mg * Sr(ppm) + 0.50\%Mg * \%V.F + 2.25\%V.F * Sr(ppm) - 0.87\%Mg * \%V.F * Sr(ppm)$$

$$H2 = H_{(180°C-8h)} = 122.06 + 5.81\%Mg + 0.31\%V.F - 4.56Sr(ppm) - 0.31\%Mg * Sr(ppm) + 1.81\%Mg * \%V.F + 0.19\%V.F * Sr(ppm) + 1.19\%Mg * \%V.F * Sr(ppm)$$

$$H3 = H_{(220°C-2h)} = 108.31 + 6.94\%Mg + 0.56\%V.F - 4.06Sr(ppm) - 1.19\%Mg * Sr(ppm) + 0.19\%Mg * \%V.F + 0.69\%V.F * Sr(ppm) + 0.06\%Mg * \%V.F * Sr(ppm)$$

$$H4 = H_{(220°C-8h)} = 102.81 + 7.31\%Mg + 2.19\%V.F - 2.56Sr(ppm) + 0.69\%Mg * Sr(ppm) - 0.56\%Mg * \%V.F + 0.06\%V.F * Sr(ppm) - 0.44\%Mg * \%V.F * Sr(ppm)$$

Eq 7.9

$$\%Mg = (\%Mg - 0.19)/0.09 \text{ ---------- } Range(0.1 - 0.28\%)$$
$$\%V.F = (\%V.F - 2.6)/0.9 \text{ ---------- } Range(1.5 - 3.5\%)$$
$$\%V.F_{\min} = (\%V.F - 1.9)/0.8$$
$$\%V.F_{\max} = (\%V.F - 3.2)/1.0$$
$$Sr_{ppm} = (Sr - 85)/85 \text{ ---------- } Range(0 - 170\,ppm)$$

Eq 7.10

In a similar manner, the main effect of aging time and aging temperature on the hardness can be estimated through 2^2-Factorial design for the above four hardness functions (H1-H4). The hardness for 319 alloys containing mainly α-Fe intermetallics at different aging conditions are given in equation (Eq 7.7) and for 319 alloys containing mainly β-Fe intermetallics are given in equation (Eq 7.9). Based on the four hardness values calculated at different aging conditions (temperature and time) for both cases i.e. design matrix and responses for 319 alloys containing mainly α-Fe intermetallics and for 319 alloys containing β-Fe intermetallics, Table 7.7 and Table 7.8, were constructed for the α-Fe and β-Fe intermetallics, respectively.

Table 7.7 Design matrix and response for 319 alloys containing mainly α-Fe intermetallics

Factor		Response								
At	AT		1	%Mg	%V.F	%Sr	%Mg* %Sr	%Mg* %V.F	%V.F* %Sr	%Mg* %V.F *%Sr
-1	-1	H1	122.10	7.00	2.75	-3.70	-1.62	0.37	1.12	-1.00
1	-1	H2	122.40	5.94	2.56	-4.60	-0.06	0.06	1.31	0.81
-1	1	H3	110.00	9.00	1.25	-5.00	1.00	1.25	-0.25	-1.25
1	1	H4	103.00	4.06	-0.56	-4.90	-1.94	0.19	0.94	0.69

Table 7.8 Design matrix and response for 319 alloys containing mainly β-Fe intermetallics

Factor		Response								
At (4)	AT (5)		1	%Mg	%V.F	%Sr	%Mg* %Sr	%Mg* %V.F	%V.F* %Sr	%Mg* %V.F *%Sr
-1	-1	H1	119.50	8.12	1.62	-3.10	0.00	0.50	2.25	-0.87
1	-1	H2	122.00	5.81	0.31	-4.50	-0.31	1.81	0.19	1.19
-1	1	H3	108.30	6.93	0.56	-4.00	-1.19	0.19	0.69	0.06
1	1	H4	102.80	7.31	2.18	-2.50	0.69	-0.56	0.06	-0.44

The empirical model used in this case (2^2-Factorial design) consists of a mean value, two main effects and an interaction effect, equations (Eq 7.11 and Eq 7.12).

$$H_{predicted} = Mean + MF_{At} / 2 * At + MF_{AT} / 2 * AT + IF_{At*AT} / 2 * At * AT$$

Eq 7.11

$$Mean = (H1 + H2 + H3 + H4)/4$$
$$MF_{(At)} = ((H2 - H1) + (H4 - H3))/2$$
$$MF_{(AT)} = ((H3 - H1) + (H4 - H2))/2$$
$$IF_{(At*AT)} = ((H4 - H2) - (H3 - H1))/2$$

Eq 7.12

Once the calculations outlined in Table 7.9 and Table 7.10 were performed, the final empirical models for the hardness of 319 alloys containing mainly α-Fe intermetallics or β-Fe intermetallics in terms of different metallurgical parameters could be obtained.

Table 7.9 Effect estimates for 319 alloys containing mainly α-Fe intermetallics

Effect	1	%Mg	%V.F	%Sr	%Mg *%Sr	%Mg* %V.F	%V.F* %Sr	%Mg* %V.F *%Sr
Mean = (H1+H2+H3+H4)/4	114.40	6.50	1.50	-4.60	-0.65	0.47	0.78	-0.19
$MF_{At}/2$ = ((H2-H1)+(H4-H3))/4	-1.60	-1.50	-0.50	-0.20	-0.34	-0.34	0.34	0.94
$MF_{AT}/2$ = ((H3-H1)+(H4-H2))/4	-7.80	0.03	-1.10	-0.40	0.19	0.25	-0.44	-0.09
$IF_{At*AT}/2$ = ((H4-H2)-(H3-H1))/4	-1.80	-1.00	-0.40	0.20	-1.10	-0.19	0.25	0.03

Table 7.10 Effect estimates for 319 alloys containing mainly β-Fe intermetallics

Effect	1	%Mg	%V.F	%Sr	%Mg *%Sr	%Mg* %V.F	%V.F* %Sr	%Mg* %V.F *%Sr
Mean = (H1+H2+H3+H4)/4	113.20	7.04	1.17	-3.60	-0.20	0.48	0.80	-0.016
$MF_{At}/2$ = ((H2-H1)+(H4-H3))/4	-0.73	-0.48	0.08	0.01	0.39	0.14	-0.67	0.39
$MF_{AT}/2$ = ((H3-H1)+(H4-H2))/4	-7.60	0.08	0.20	0.26	-0.05	-0.67	-0.42	-0.17
$IF_{At*AT}/2$ = ((H4-H2)-(H3-H1))/4	-2.01	0.67	0.73	0.73	0.54	-0.51	0.36	-0.64

7.2.3. Hardness Estimated Models Verifications

The regression equations obtained for 319 alloys (32-term) can predict the hardness of the heat-treated 319 alloys containing mainly α-Fe intermetallics or β-Fe intermetallics. The models are presented in Table 7.11 and Table 7.12 and are coupled with the scaling equations Eq 7.13 and Eq 7.14, respectively.

Table 7.11 Empirical model for 319 alloys containing mainly α-Fe intermetallics

HB=Σ x*y*f	1	%Mg	%V.F	Sr	%Mg*Sr	%Mg*%V.F	%V.F *Sr	%Mg*%V.F *Sr
1	114.40	6.50	1.50	-4.60	-0.66	0.47	0.78	-0.19
At	-1.60	-1.50	-0.50	-0.18	-0.34	-0.34	0.34	0.94
AT	-7.80	0.03	-1.16	-0.4	0.19	0.25	-0.44	-0.09
AT*At	-1.80	-0.97	-0.40	0.22	-1.10	-0.19	0.25	0.03

$$\%Mg = (\%Mg - 0.187375)/0.090125 \text{-----} Range(0.1-0.28\%)$$
$$\%V.F = (\%V.F - 3.734)/1.7325 \text{--------} Range(2-5\%)$$
$$Sr_{ppm} = (Sr - 100)/100 \text{----------} Range(0-200ppm)$$
$$At = (At - 5)/3 \text{----------} Range(2-8h)$$
$$AT = (AT - 200)/20 \text{----------} Range(180-220C)$$

Eq 7.13

Table 7.12 Empirical model for 319 alloys containing mainly β-Fe intermetallics

HB=Σ x*y*f	1	%Mg	%V.F	Sr	%Mg*Sr	%Mg*%V.F	%V.F *Sr	%Mg*%V.F *Sr
1	113.20	7.05	1.17	-3.60	-0.20	0.48	0.80	-0.01
At	-0.73	-0.48	0.08	0.01	0.40	0.14	-0.70	0.39
AT	-7.60	0.08	0.20	0.26	-0.05	-0.67	-0.42	-0.17
AT*At	-2.01	0.67	0.73	0.73	0.55	-0.51	0.36	-0.64

$$\%Mg = (\%Mg - 0.18825)/0.0875 \text{--------} Range(0.1-0.28\%)$$
$$\%V.F = (\%V.F - 2.57)/0.9 \text{----------} Range(1.5-3.5\%)$$
$$Sr_{ppm} = (Sr - 85)/85 \text{----------} Range(0-170ppm)$$
$$At = (At - 5)/3 \text{----------} Range(2-8h)$$
$$AT = (AT - 200)/20 \text{----------} Range(180-220C)$$

Eq 7.14

Note that x represents the horizontal terms (i.e. 1, %Mg, %V.F, Sr, %Mg*Sr, %Mg*%V.F, %V.F*Sr, and %Mg*V.F*Sr), and y represents the vertical terms (i.e. 1, At, AT and AT*At) and *f* is the 32-factor mentioned in Table 7.11 and Table 7.12. Hardness is

calculated directly in terms of the absolute values of metallurgical parameters (%Mg, %V.F, Sr-ppm, At (h) AT (°C)) through two programs developed by Matlab software. One program is for 319 alloys containing mainly α- Fe intermetallics and the other is for 319 alloys containing β-Fe intermetallics. In both programs, a mathematical method was developed for transforming the scaling equation from the standard code form ($\pm$1) to the absolute form of the variables, see Appendix (C). From the verification of the predicted model with the experimental results, it was found that there was a less than $\pm$ 8% error between the predicted and the experimental results in both cases of 319 containing mainly α–Fe intermetallics or β–Fe intermetallics, see Table 7.13, Table 7.14 and Figure 7.1.

Table 7.13 Verification of the predicted model for 319 alloys containing mainly α–Fe intermetallics

0.4%Fe-0.1%Mn 0.1Mg	**UM**	**UM***	**%Diff.**	**M**	**M***	**%Diff.**
200°C-4hr	116.0	112.0	-4.0	104.5	102.0	-2.5
180°C-2hr	117.0	117.0	0.0	108.5	108.0	-0.5
180°C-6hr	122.5	118.0	-4.5	116.5	108.5	-8.0
180°C-8hr	119.0	120.0	1.0	109.0	108.5	-0.5
220°C-2hr	108.0	107.5	-0.5	94.0	94.5	0.5
220°C-4hr	104.5	106.0	1.5	99.5	95.5	-4.0
220°C-6hr	106.5	104.0	-2.5	94.0	96.0	2.0
220°C-8hr	103.0	102.5	-0.5	96.5	97.0	0.5
1%Fe-0.36%Mn- 0.1%Mg	**UM**	**UM***	**%Diff.**	**M**	**M***	**%Diff.**
200°C-4hr	115.0	111.0	-4.0	103.5	106.5	3
180°C-2hr	117.5	117.0	-0.5	117.5	117.0	-0.5
180°C-4hr	117.5	119.0	1.5	108.0	116.0	8
180°C-6hr	120.0	120.5	0.5	119.0	115.5	-3.5
180°C-8hr	123.0	122.5	-0.5	115.0	115.0	0.0
220°C-2hr	106.0	104.5	-1.5	96.0	97.5	1.5
220°C-4hr	104.0	103.0	-1.0	93.0	97.0	4.0
220°C-6hr	99.0	101.5	2.5	91.5	96.5	5.0
220°C-8hr	101.0	100.0	-1.0	95.5	96.5	1.0
0.4%Fe-0.1%Mn-0.27%Mg	**UM**	**UM***	**%Diff.**	**M**	**M***	**%Diff.**
200°C-4hr	128.5	125.0	-3.5	113.0	114.0	1.0
180°C-2hr	131.5	132.0	0.5	120.5	119.5	-1.0
180°C-4hr	133.5	132.0	-1.5	118.0	119.0	1.0
180°C-6hr	135.0	132.5	-2.5	123.0	118.0	-5.0
180°C-8hr	132.5	132.5	0.0	119.0	118.0	-1.0
220°C-2hr	119.0	119.0	0.0	114.0	114.5	0.5
220°C-4hr	115.0	117.5	2.5	112.0	109.0	-3.0
220°C-6hr	112.5	116.0	3.5	100.0	104	4.0
220°C-8hr	116.0	114.5	-1.5	99.0	98.5	-0.5
1%Fe-0.37%Mn-0.29%Mg	**UM**	**UM***	**%Diff.**	**M**	**M***	**%Diff.**
200°C-4hr	130.0	131.0	1.0	122	118.0	-4.0
180°C-2hr	137.5	140.0	2.5	127	125.5	-1.5
180°C-4hr	134.0	138.0	4.0	123.5	126.0	2.5
180°C-6hr	137.5	136.0	-1.5	128	126.5	-1.5
180°C-8hr	133.5	134.5	1.0	128.5	127.0	-1.5
220°C-2hr	127.0	129.0	2.0	116	115.0	-1.0
220°C-6hr	116.5	117.5	1.0	102.5	106	3.5
220°C-8hr	112.0	111.5	-0.5	101.5	101.0	-0.5
* estimated value, UM= unmodified, M=Sr-modified, %Diff.= percent difference						

Table 7.14 Verification of the predicted model for 319 alloys containing β–Fe intermetallics

0.4%Fe-0.1Mg	**UM**	**UM***	**%Diff.**	**M**	**M***	**%Diff.**
200°C-4hr	113.5	109.0	-4.5	100	99.0	-1.0
180°C-2hr	116.5	115.5	-1.0	104	101.0	-3.0
180°C-4hr	115.0	117.0	2.0	109	105.5	-3.5
180°C-6hr	117.5	118.5	1.0	106.5	110.0	3.5
180°C-8hr	121.0	120.0	-1.0	114.5	114.5	0.0
220°C-2hr	104.5	103.0	-1.5	97.5	96.0	-1.5
220°C-4hr	101.5	101.0	-0.5	99	93.0	-6.0
220°C-6hr	100.0	98.0	-2.0	92	90.0	-2.0
220°C-8hr	96.5	95.5	-1.0	89	86.0	-3.0
1.1%Fe-0.1%Mg	**UM**	**UM***	**%Diff.**	**M**	**M***	**%Diff.**
200°C-4hr	117.0	111.0	-6.0	106.5	108.0	1.5
180°C-2hr	112.5	117.0	4.5	112.5	115.0	2.5
180°C-4hr	118.0	119.0	1.0	113.5	115.0	1.5
180°C-6hr	117.5	121.0	3.5	112.5	115.5	3.0
180°C-8hr	120.0	123.0	3.0	109.5	116	5.5
220°C-2hr	104.0	105.0	1.0	99.5	103.0	3.5
220°C-4hr	102.0	103.0	1.0	97.5	101.5	4.0
220°C-6hr	102.0	101.5	-0.5	103.5	100.0	-3.5
220°C-8hr	101.0	100.0	-1.0	95.5	98.5	3.0
0.4%Fe-0.275%Mg	**UM**	**UM***	**%Diff.**	**M**	**M***	**%Diff.**
200°C-4hr	125.0	125.0	0.0	113.5	114.5	1.0
180°C-2hr	130.0	132.0	2.0	121.0	121.5	0.5
180°C-4hr	130.0	132.0	2.0	119.0	120.5	1.5
180°C-6hr	128.5	132.5	4.0	121.0	120.0	-1.0
180°C-8hr	132.0	132.5	0.5	119.5	119.0	-0.5
220°C-2hr	120.5	119.0	-1.5	108.5	108.5	0.0
220°C-4hr	115.5	117.0	1.5	102.5	108.0	5.5
220°C-6hr	113.0	116.0	3.0	101.5	108.0	6.5
220°C-8hr	110.0	115.0	5.0	107.0	108.0	1.0
1%Fe-0.27%Mg	**UM**	**UM***	**%Diff.**	**M**	**M***	**%Diff.**
200°C-4hr	125.0	124.5	-0.5	119.0	119.5	0.5
180°C-2hr	131.5	130.5	-1.0	128.0	129.0	1.0
180°C-6hr	133.0	132.0	-1.0	131.5	128.0	-3.5
180°C-8hr	133.5	133.0	-0.5	126.5	127.0	0.5
220°C-2hr	120.5	120.0	-0.5	111.5	111.0	-0.5
220°C-4hr	116.5	118.0	1.5	106.0	110.5	4.5
220°C-6hr	111.5	115.5	4.5	104.5	110.0	6.5
220°C-8hr	114.0	113.0	-1.0	109.5	109.0	-0.5

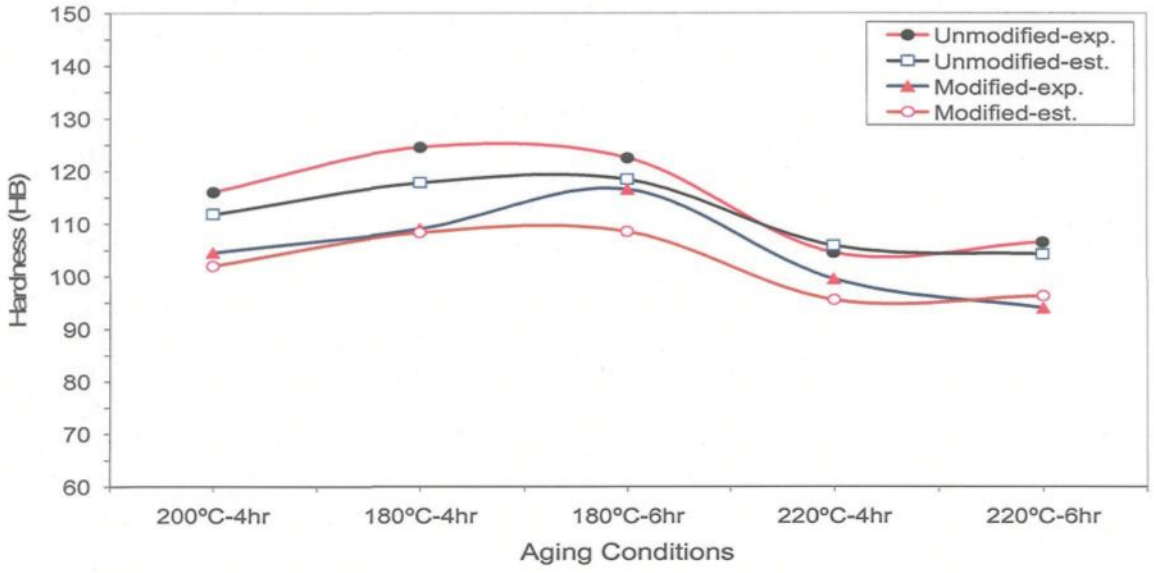

(a)

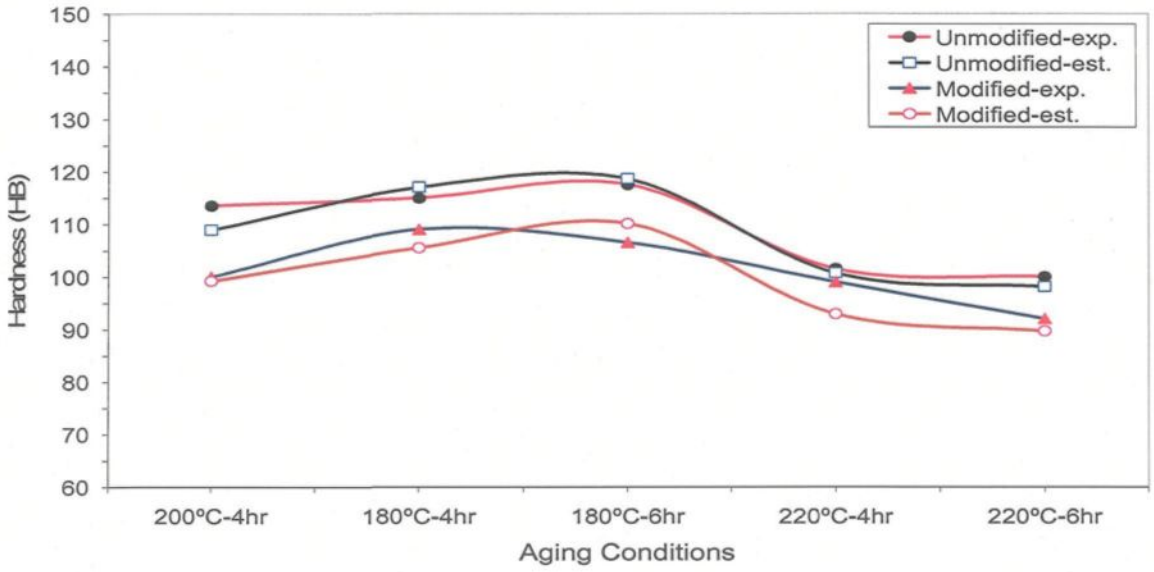

(b)

Figure 7.1 Experimental vs. predicted model results for 319 alloys (alloy codes 18 vs. 18S, 14 vs. 14S, 21 vs. 21S and 17 vs. 17S) containing: (a) low α-Fe intermetallic vol. fractions, (b) low β-Fe intermetallic vol. fractions, (c) high α-Fe intermetallic vol. fractions, and (d) high β-Fe intermetallic vol. fractions, respectively.

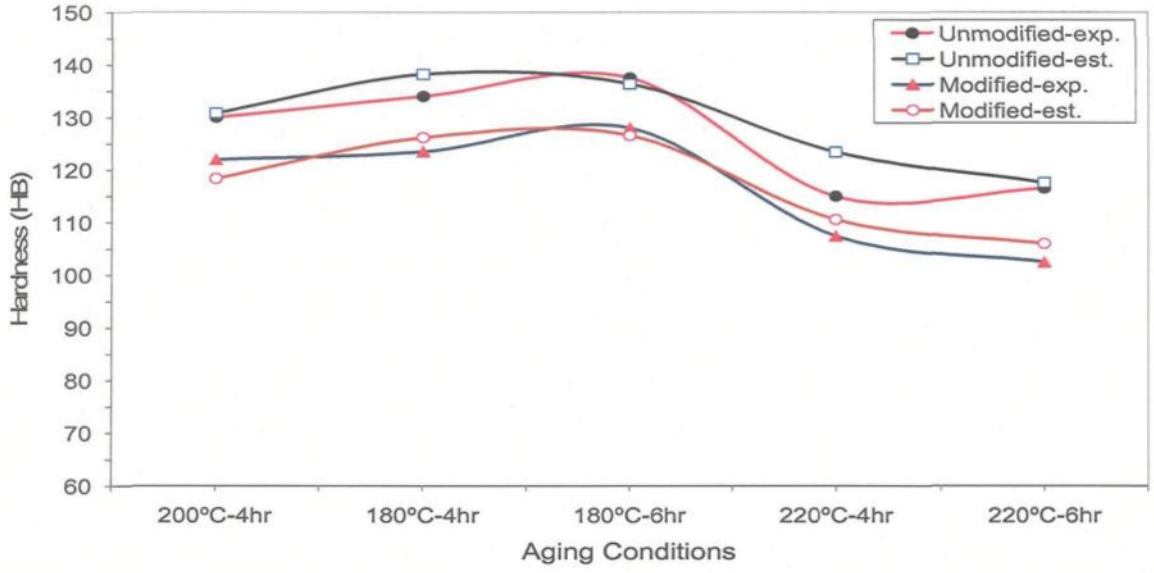

(c)

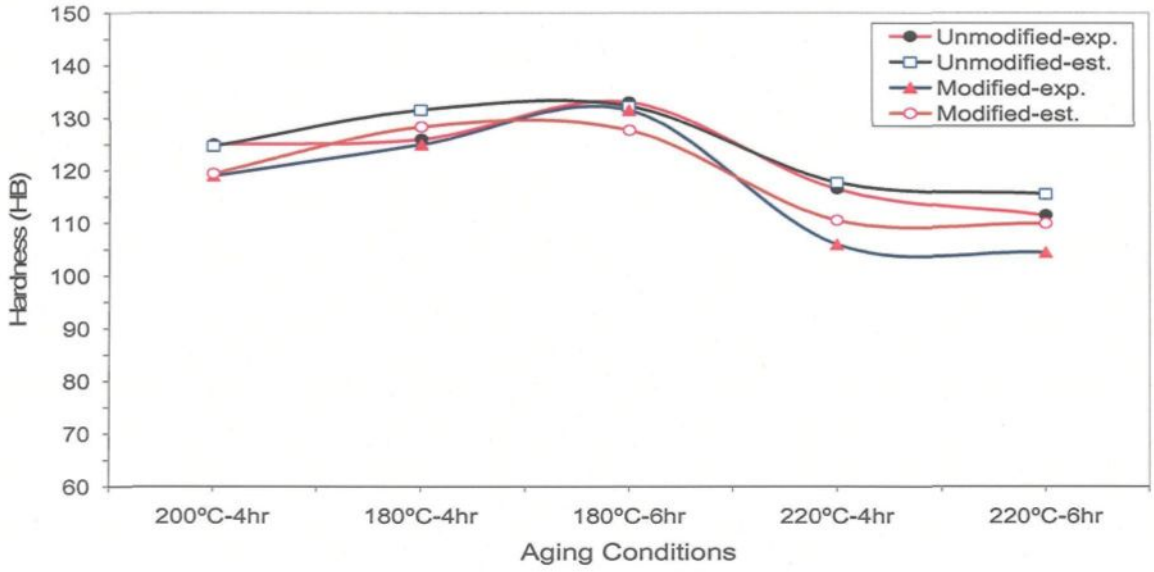

(d)

Figure 7.1 Experimental vs. predicted model results for 319 alloys (alloy codes 18 vs. 18S, 14 vs. 14S, 21 vs. 21S and 17 vs. 17S) containing: (a) low α-Fe intermetallic vol. fractions, (b) low β-Fe intermetallic vol. fractions, (c) high α-Fe intermetallic vol. fractions, and (d) high β-Fe intermetallic vol. fractions, respectively.

7.2.4. Interpretation of the Developed Empirical Model for Hardness

For the heat treated 319 alloys containing mainly α-Fe intermetallics, it was observed that the hardness increased with the magnesium content (%Mg) and only slightly increased with the volume fractions of the Fe intermetallics (%V.F) and decreased with the Sr-modification (Sr-ppm) and aging parameters. From the metallurgical parameters, Mg-content has the maximum effect in the range of compositions studied. Sr-modification has a negative effect on the hardness of 319 alloys regardless of the morphology of Fe-intermetallics at the two aging temperatures i.e. 180 and 220 °C for all aging times studied (2-8 h). In Mg-containing 319 alloys, Sr-modification has more negative effect on the hardness of the alloys containing α-Fe intermetallics compared to the alloys containing β-Fe intermetallics; see the coefficient of Mg-Sr in Table 7.11 and Table 7.12, respectively. These are in agreement with the experimental results for 319 alloys containing α-Fe intermetallics where the hardness of the modified alloys is lower than that of the unmodified ones at different aging times compared to the results of 319 alloys containing β-Fe intermetallics.

The regression coefficients attached to %Mg-%V.F, %Mg-Sr(ppm), %V.F-Sr(ppm), %Mg-%V.F-Sr(ppm) etc, in Table 7.11 and Table 7.12 suggests that the hardness equations are similar in nature. However, hardness values for the 319 alloys containing α-Fe intermetallics vs. β-Fe intermetallics (i.e. corresponding to the hardness values obtained from Table 7.11 and Table 7.12 by putting %Mg = %V.F = Sr (ppm) = At = AT = 0) are slightly different. In the former case it is 114.4 HB as against 113.2 for the latter. The contribution of Mg in increasing the hardness of 319 alloys containing β-Fe intermetallics

is slightly high if compared with their contribution for the 319 alloys containing α-Fe intermetallics i.e. comparison between coefficient of %Mg in Table 7.12 and Table 7.11, respectively. This may be attributed to lesser segregation of alloying elements in the alloy matrix of 319 alloys containing β-Fe intermetallics and thus causing more solid solution hardening due to Mg in such alloys. The interactions between metallurgical parameters for 319 alloys containing both α or β intermetallics are similar in nature.

Out of the aging parameters, aging temperature has the greatest influence and it has a negative effect on the hardness values. Aging time contributes negatively to the hardness but its effect is less severe as compared with the other variables. This can be attributed to the coarsening of the precipitates due to thermal softening and hence, loss of their coherency with the alloy matrix.

From the results of the above factorial analysis, the following important conclusions can be made. The hardness generated for 319 alloys increases with increasing magnesium content and α-Fe-intermetallic volume fraction. This is expected due to the precipitation of Mg_2Si and MgCuAl which increase the matrix microhardness and improve microstructure homogeneity. The hardness is decreased as the Sr-modification (Sr-ppm) and aging treatment parameters (aging temperature and aging time) are increased. Iron-intermetallic type/morphology slightly influences the hardness of the heat treated 319 alloys, while hardness also increases with increasing aging time (at 180°C and 220°C aging temperature). In both α- and β-Fe intermetallic-containing 319 alloys, the Sr modified alloys exhibit lower hardness levels compared to the unmodified case.

PART II: EFFECT OF METALLURGICAL PARAMETERS ON DRILLING FORCE, MOMENT AND HEAT BUILD-UP ON CUTTING TOOL EDGE OF HEAT TREATED 319 ALLOYS.

7.3. RESULTS AND DISCUSSIONS

7.3.1. The Effect of Metallurgical Parameters on Drilling Force, Moment and Heat Build-Up on Cutting Tool Edge

In the present work, experimental results obtained from the drilling tests are analyzed and empirical models are established to estimate the relations between both the drilling forces and moments as well as heat build up on the cutting tool edge and some of the metallurgical parameters. Heat build-up on the cutting tools is the biggest drawback to maintain both the characteristics of the material during machining and the productivity of the machining operations. Eight drilling tests were carried out at fixed machining conditions under two different levels of influencing metallurgical factors for the analysis of the cutting force and moment as well as heat build up on the cutting tool edge when the hardness was set within 100±10 HB. The main parameters include:

- Volume fractions of the α-Fe intermetallics (%V.F)
- Magnesium content (%Mg)
- Aging temperature (AT)

The low levels, coded -1, and the high levels, coded +1 comprise the eight tests that were used to perform a factorial analysis and to estimate the effects of such parameters on the cutting force and moment. Empirical models of force and moment and their standard deviations (S.D) as well as their peak-to-valley ranges (R_1 and R_2) were established to

represent the effects of the metallurgical parameters. Similarly, the effect of these parameters on the heat build-up (depth, width and area) on the cutting edge is estimated. The detail procedures and the results will be discussed as the following.

7.3.2. Factorial Analysis

The 2^k factorial design (2^3-factorial experiment[140]) is the ideal choice for providing some information on the main effect and interaction of metallurgical factors on the hardness of the heat-treated 319 alloys-containing mainly α-Fe intermetallics. The 2^5-factorial design is divided into 2^3-factorial design (the effect of magnesium content (%Mg), volume fractions of α-Fe intermetallics (%V.F) and Sr-modification (Sr-ppm)) followed by a 2^2-factorial design (the effect of the aging parameters). The basic approach is to vary each factor within a range (as defined by two values) whereby one level is set as minimum value and represented by -1 and the other level is the maximum and is represented by +1. Level values of these factors were listed in the 2^k design in Table 7.15. Examining the response of these data, they represent the mean values of the total force, standard deviation of the total cutting force, peak-to-valley of the total cutting force and the mean value of the total cutting moment, standard deviation of the total cutting moment and peak-to-valley of the total cutting moment during the drilling process of 230 holes.

An empirical model can be built through factorial analysis from the measured data and can be used for the different response predictions as long as the metallurgical setting is within the limits represented by the upper and lower levels. The model consists of a mean value, three main effects and four interaction effects as can be seen in equation (Eq 7.15).

$$F_{predicted} = Mean + MF_{(\%V.F)}/2*\%V.F + MF_{(\%Mg)}/2*\%Mg) + MF_{(AT)}/2*AT + IF_{(\%V.F*\%Mg)}/2*\%V.F*\%Mg + IF_{(\%V.F*AT)}/2*\%V.F*AT + IF_{(\%Mg*AT)}/2*\%Mg*AT + IF_{(\%V.F*\%Mg*AT)}/2*\%V.F*\%Mg*AT$$

Eq 7.15

Table 7.15 Design matrix and response for 319 alloys containing mainly α-Fe intermetallics

Level Combination	Factors (j)			Response						
HB = 100± 10	%V.F(A) (1)	%Mg(B) (2)	AT(C) (3)	Ft	S.D	R_1	Mt	S.D	R_2	Yi
M2-T6	-1	-1	-1	272.5	15.5	80.0	19.0	7.5	4.5	y 1
M3-T6	1	-1	-1	318.0	17.5	55.5	22.5	8.0	4.5	y 2
M4-T6	-1	1	-1	363.0	22.0	52.0	26.0	10.0	5.5	y 3
M5-T6*	1	1	-1	418.0	24.0	69.0	29.5	11.5	7.5	y 4
M2-T7	-1	-1	1	253.0	12.5	51.0	17.5	7.0	5.0	y 5
M3-T7	1	-1	1	269.5	18.5	56.0	17.5	7.0	6.0	y 6
M4-T7	-1	1	1	347.0	22.5	56.0	24.5	9.5	5.5	y 7
M5-T7	1	1	1	359.5	20.5	59.5	25.5	10.0	6.5	y 8

* = M5-T6 condition is estimated from M5-T7 ones by correction factor ~1.15

Let Y_i denote the response for the j combinations of levels. The generic design matrix is shown in Table 7.15. Using the design matrix one can easily calculate the main effects of varying each factor on the response variables. The mean value (μ) is calculated from averaging the eight measured values of the different responses (i.e. forces, moments and heat build-up depth, width and area), see equation (Eq 7.16). Its physical interpretation is the predicted response when the three metallurgical variables (%Mg, %V.F and Sr (ppm)) are set at the middle between their lower and the upper limits.

$$Mean = (y1 + y2 + y3 + y4 + y5 + y6 + y7 + y8)/8$$

Eq 7.16

Consider the first and the second cutting force in Table 7.15, with the corresponding values (272.6 N and 318.1 N) differing by 45.5 N because of the volume fraction of α-Fe-intermetallics (%V.F), the magnesium content (%Mg) and aging temperature (AT) setting are the same for both of these conditions. In addition to this pair, there are another three pairs of the cutting force ((363.3 N and 418.3 N), (252.72 N and 269.45 N) and (347.04 N and 359.54 N)) that differ by 55 N, 16.7 and 12.5, respectively only because of the volume fraction of α-Fe-intermetallics. The average of these four differential measurements (32.425 N) represents the main effect of the volume fraction of α-Fe-intermetallics on the cutting force. Similarly, the main effect of both magnesium and aging temperature can be estimated. All differences for the total cutting force (Ft), standard deviation (S.D) and peak-to-valley of the cutting force (R_1), total cutting moment (Mt), standard deviation (S.D) and peak-to-valley of the total cutting moment (R_2) are listed in Table 7.16.

Table 7.16 Interaction check for 319 alloys containing mainly α-Fe intermetallics

	Diff.	Ft	S.D	R_1	Mt	S.D	R_2
V.F	y 2-y 1	45.5	2.0	-24.5	3.5	0.5	0.0
	y 4-y 3	55.0	2.0	17.0	3.5	1.5	2.0
	y 6-y 5	16.5	6.0	5.0	0.0	0.0	1.0
	y 8-y 7	12.5	-2.0	3.5	1.0	0.5	1.0
Mg	y 3- y 1	90.5	6.5	-28.0	7.0	2.5	1.0
	y 4- y 2	100	6.5	13.5	7.0	3.5	3.0
	y 7-y 5	94	10.0	5.0	7.0	2.5	0.5
	y 8- y 6	90	2.0	3.5	8.0	3.0	0.5
AT	y 5- y 1	-19.5	-3.0	-29.0	-1.5	-0.5	0.5
	y 6-y 2	-48.5	1.0	0.5	-5.0	-1.0	1.5
	y 7-y3	-16	0.5	4.0	-1.5	-0.5	0.0
	y 8- y4	-58.5	-3.5	-9.5	-4.0	-1.5	-1.0

In other words, the main effect of varying factor j- MF_j is defined as the average change in the response variable due to moving factor j from its -1 level to its +1 level with all other factors held constant. The main effects of the three metallurgical factors can be obtained from equation (Eq 7.17).

$$MF_{(\%V.F)} = ((y2 - y1) + (y4 - y3) + (y6 - y5) + (y8 - y7))/4$$
$$MF_{(\%Mg)} = ((y3 - y1) + (y4 - y2) + (y7 - y5) + (y8 - y6))/4$$
$$MF_{(AT)} = ((y5 - y1) + (y6 - y2) + (y7 - y3) + (y8 - y4))/4$$

Eq 7.17

An advantage of the 2^k factorial design method is that it provides some insight into the interactions of the factors on the response variable. In a similar way, the interaction effect between two factors can be thought of as the average change in the response when the two factors are at the same level and when they are at opposite levels. One can see from Table 7.16 that the three metallurgical variables do not behave additively and therefore "interact". A measure of the interaction between the volume fraction of α-Fe intermetallics (%V.F) and magnesium (%Mg) can be identified by the difference between the magnesium (%Mg) effects at low levels of volume fraction of α-Fe intermetallics (%V.F) and magnesium (%Mg) effects at high levels of volume fraction of α-Fe intermetallics (%V.F). Similarly, the interaction between the volume fraction of α-Fe intermetallics (%V.F) and the aging temperature (AT) and between magnesium (%Mg) and aging temperature (AT) and between all of them can be obtained by equation (Eq 7.18).

$$IF_{(\%V.F*AT)} = ((y6 - y5) + (y8 - y7) - (y2 - y1) - (y4 - y3))/4$$
$$IF_{(\%V.F*\%Mg)} = ((y8 - y7) + (y4 - y3) - (y6 - y5) - (y2 - y1))/4$$
$$IF_{(\%Mg*AT)} = ((y8 - y6) + (y7 - y5) - (y4 - y2) - (y3 - y1))/4$$
$$IF_{(\%V.F*\%Mg*AT)} = ((y8 - y7) + (y2 - y1) - (y6 - y5) - (y4 - y3))/4$$

Eq 7.18

Again as with the hardness model, in general, one can determine the main effect of factor j and the interaction effect of factors i and j from the design matrix by applying (Eq 7.5) and (Eq 7.6)[141] which are reproduced below.

$$MF_i = \frac{[Columnj]^T * Y_i}{2^{k-1}}$$

Eq 7.5

$$IF_{i*j} = \frac{[Columni * Columnj]^T * Y_i}{2^{k-1}}$$

Eq 7.6

7.3.3. Drilling Cutting Force, Moment, and Peak-to-Valley Estimated Regression Equations for 319 Alloys-Containing α-Fe Intermetallics

Upon obtaining the eight estimates through the factorial analysis, the development of an empirical model for the cutting force prediction is complete, see Table 7.17. Based on the other values for the standard deviation of the total cutting force (S.D), peak-to-valley of the cutting force (R_1), total cutting moment (Mt), standard deviation of the total cutting moment (S.D) and peak-to-valley of the total cutting moment (R_2) and following the above calculations, the empirical models are listed in equation (Eq 7.19) and are coupled with the scaling equation (Eq 7.20).

$$Ft_{predicted} = 325.00 + 16.20\%V.F + 46.80\%Mg - 17.80AT - 8.95\%V.F * AT + 0.70\%V.F * \%Mg - 0.80\%Mg * AT - 1.70\%V.F * \%Mg * AT$$

$$Ft(S.D) = 19.10 + 1.00\%V.F + 3.10\%Mg - 0.60AT + 0.00\%V.F * AT - 1.00\%V.F * \%Mg - 0.10\%Mg * AT - 1.00\%V.F * \%Mg * AT$$

$$R_1(Peak - to - vally)_{predicted} = 59.85 + 0.10\%V.F - 0.75\%Mg - 4.25AT - 2.00\%V.F * AT + 5.00\%V.F * \%Mg + 2.85\%Mg * AT - 5.35\%V.F * \%Mg * AT$$

$$Mt_{predicted} = 22.75 + 1.00\%V.F + 3.60\%Mg - 1.50AT - 0.75\%V.F * AT - 0.10\%V.F * \%Mg + 0.10\%Mg * AT + 0.10\%V.F * \%Mg * AT$$

$$Mt(S.D) = 8.80 + 0.30\%V.F + 1.45\%Mg - 0.45AT - 0.20\%V.F * AT + 0.20\%V.F * \%Mg - 0.06\%Mg * AT - 0.06\%V.F * \%Mg * AT$$

$$R_2(Peak - to - vally)_{predicted} = 5.60 + 0.50\%V.F + 0.60\%Mg + 0.10AT - 0.00\%V.F * AT + 0.25\%V.F * \%Mg - 0.35\%Mg * AT - 0.25\%V.F * \%Mg * AT$$

Eq 7.19

%V.F = (%V.F - 3.5%)/1.5%;	Range (2 - 5%)
%Mg = (%Mg - 0.2%)/0.1%;	Range (0.1 - 0.3%)
AT = (AT - 200)/20;	Range (180 - 220 °C)

Eq 7.20

One should note that Ft is the mean total cutting force, Ft (S.D) is the standard deviation of the total cutting force, and R_1 (peak-to-valley) is the range or peak-to-valley range for the total cutting force. Similarly, Mt is the mean total cutting moment, Mt (S.D) is the standard deviation of the total cutting moment, and R_2 (peak-to-valley) is the range or peak-to-valley range for the total cutting moment.

Table 7.17 Effects estimated for 319 alloys containing mainly α-Fe intermetallics

HB =100± 10	Effect	Ft	S.D	R_1	Mt	S.D	R_2
M2-T6	Mean	325.00	19.10	59.85	22.75	8.80	5.60
M3-T6	MF1/2	16.20	1.00	0.10	1.00	0.30	0.50
M4-T6	MF2/2	46.80	3.10	-0.75	3.60	1.45	0.60
M5-T6	MF3/2	-17.80	-0.60	-4.25	-1.5	-0.45	0.10
M2-T7	IF1*3/2	-8.95	0.00	2.00	-0.75	-0.20	0.00
M3-T7	IF1*2/2	0.70	-1.00	5.00	0.10	0.20	0.25
M4-T7	IF2*3/2	-0.80	-0.10	2.85	0.10	-0.06	-0.35
M5-T7	IF1*2*3/2	-1.70	-1.00	-5.35	0.10	-0.06	-0.25

7.3.4. Heat build-Up Depth, Width and Area Estimated Regressions Equations for 319 Alloys-Containing α-Fe-Intermetallics

Similarly, an empirical model can be built through factorial analysis from the measured data and can be used for the heat build-up (BUE depth-mm, width-mm and area-mm^2) on the cutting tool edge prediction of 319 alloys containing mainly α-Fe intermetallics when the hardness is within 100±10 HB as long as the metallurgical setting is within the limits represented by the upper and lower levels. The generic design matrix for the heat build-up (BUE depth-mm, width-mm and area-mm^2) on the cutting tool edge is shown in Table 7.18. Differences that arise for the heat build-up (BUE depth-mm, width-mm and area-mm^2) on the cutting tool edge with an average change in the response variable due to moving any factor (%Mg, %V.F and Sr-ppm) from its -1 level to its +1 level with all other factors held constant are listed in Table 7.19.

Table 7.18 Design matrix and responses for 319 alloys containing α-Fe intermetallics

Level Combination	Factors (j)			Response			
HB = 100± 10	%V.F (1)	%Mg (2)	AT (3)	Yi	BUE-Depth (mm)	BUE-Width (mm)	BUE-Area (mm^2)
M2-T6	-1	-1	-1	y1	0.064	0.193	0.012
M3-T6	1	-1	-1	y2	0.072	0.235	0.017
M4-T6	-1	1	-1	y3	0.052	0,246	0,013
M5-T6*	1	1	-1	y4	0.025	0.442	0.011
M2-T7	-1	-1	1	y5	0.096	0.216	0.021
M3-T7	1	-1	1	y6	0.109	0.159	0.017
M4-T7	-1	1	1	y7	0.082	0.208	0.017
M5-T7	1	1	1	y8	0.054	0.224	0.012

* = M5-T6 condition is estimated from M5-T7 ones by correction factors 0.46 for BUE-Depth, 1.97 for BUE-Width and 0.9 for BUE-Area (product of width and depth).

Table 7.19 Interaction check for 319 alloys containing α-Fe intermetallics

	Diff.	BUE-Depth (mm)	BUE-Width (mm)	BUE-Area (mm2)
V.F	y 2-y 1	0.008	0.042	0.005
	y 4-y 3	-0.027	0.196	-0.002
	y 6-y 5	0.013	-0.057	-0.004
	y 8-y 7	-0.028	0.016	-0.005
Mg	y 3- y 1	-0.012	0.053	0.001
	y 4- y 2	-0.047	0.207	-0.006
	y 7-y 5	-0.014	-0.008	-0.004
	y 8- y 6	-0.055	0.065	-0.005
AT	y 5- y 1	0.032	0.023	0.009
	y 6-y 2	0.037	-0.076	0
	y 7-y3	0.030	-0.038	0.004
	y 8- y4	0.029	-0.218	0.001

Table 7.20 Effects estimated for 319 alloys containing α-Fe intermetallics

HB = 100± 10	Effect	BUE-Depth (mm)	BUE-Width (mm)	BUE-Area (mm2)
M2-T6	Mean	0.0692	0.2403	0.01500
M3-T6	MF1/2	-0.0042	0.0246	-0.00075
M4-T6	MF2/2	-0.0160	0.0396	-0.00175
M5-T6	MF3/2	0.0160	-0.0386	0.00175
M2-T7	IF1*3/2	0.0005	-0.0348	-0.00150
M3-T7	IF1*2/2	-0.0095	0.0284	-0.00100
M4-T7	IF2*3/2	-0.0012	-0.0254	-0.00050
M5-T7	IF1*2*3/2	-0.0007	-0.0101	0.00075

Upon obtaining the eight estimates through the factorial analysis, the development of an empirical model for the heat build-up prediction is completed. Again, effects estimated for 319 alloys containing mainly α-Fe intermetallics are listed in Table 7.20. The empirical models are listed in equation (Eq 7.21) with scaling equation (Eq 7.22).

$$Heat-build-up(Depth-mm)=0.0692-0.0042\%V.F-0.0160\%Mg+0.0160AT+$$
$$0.0005\%V.F*AT-0.0095\%V.F*\%Mg-0.0012\%Mg*AT-0.0007\%V.F*\%Mg*AT$$

$$Heat-build-up(Width-mm)=0.2403+0.0246\%V.F+0.0396\%Mg-0.0386AT-$$
$$0.0348\%V.F*AT+0.0284\%V.F*\%Mg-0.0254\%Mg*AT-0.0101\%V.F*\%Mg*AT$$

$$Heat-build-up(Area-mm^2)=0.01500+0.00075\%V.F-0.00175\%Mg+0.00175AT-$$
$$0.00150\%V.F*AT-0.00100\%V.F*\%Mg-0.00050\%Mg*AT+0.00075\%V.F*\%Mg*AT$$

Eq 7.21

%V.F = (%V.F - 3.5%)/1.5%; Range (2 - 5%)
%Mg = (%Mg - 0.2%)/0.1%; Range (0.1 - 0.3%)
AT = (AT - 200)/20; Range (180 - 220 °C)

Eq 7.22

7.3.5. Interpretation of the Cutting Force, Moment, and Heat build-Up Empirical Models

For the heat treated 319 alloys containing mainly α-Fe intermetallics, it was observed that the drilling force and moment increase with the magnesium content (%Mg) and only slightly increase with the volume fractions of the Fe intermetallics (%V.F) but they decrease with the aging temperature (AT). Aging temperature has a negative effect on the drilling force and moment of 319 alloys containing mainly α-Fe-intermetallics at the temperature range (180- 220°C) for an aging time of 2 hours.

From the results of the above factorial analysis, the following important conclusions were made. The drilling forces and moments generated for 319 alloys increase with increasing magnesium content. This is expected due to the precipitation of Mg_2Si and MgCuAl which increase the microhardness of the alloy matrix. Also the drilling forces and moments increase with increasing α-Fe-intermetallic volume fractions. This can be interpreted in terms of improving microstructure homogeneity and alloy microhardness by α-Fe-intermetallics. The drilling forces and moments decreased as the aging temperature increased.

From the results of heat build-up, the following important conclusions were made. The heat build-up generated during drilling decreases with the magnesium content and α-Fe-intermetallics volume fraction. This is expected due to the increase in microhardness of the alloy matrix. and improving microstructure homogeneity and alloy microhardness by α-Fe-intermetallics. Again, the aging temperature affects the heat build-up.

7.4. SUMMARY

In contributing to the original knowledge, experimental correlations relating the alloying additions and heat-treatment to the hardness were found from the experimental results. An attempt has been made to quantify the effects of alloying elements and aging parameters on the hardness of heat-treated 319 alloys containing α-Fe or β-Fe intermetallics. From these correlations, it was found that the hardness generated for 319 alloys increases with increasing magnesium content and α-Fe-intermetallics volume fractions and decreases as the Sr-modification (Sr-ppm) and aging treatment parameters (aging temperature and aging time) are increased. This is expected due to the precipitation of Mg_2Si and MgCuAl which increases the microhardness of the alloy matrix and there is an improvement in the microstructure homogeneity and alloy microhardness by α-Fe-intermetallics.

Out of the aging parameters, ageing temperature has the greatest influence; however, the ageing parameters have a negative effect on the hardness values. Ageing time contributes negatively to the hardness but its effect is less severe as compared with the other variables. The contribution of Mg-content in increasing the hardness of 319 alloys containing β-Fe intermetallics is more if compared with the 319 alloys containing mainly α-Fe intermetallics. The regression equations developed are fairly accurate in predicting the hardness of the alloys in the range of composition studied. The results obtained by these correlations closely agree with the findings from the experiments. It was found that there was less than $\pm$ 8% error between the predicted and the experimental results.

In another correlation an attempt has been made to quantify the effects of metallurgical parameters on the drilling forces and moments as well as heat build up on the cutting tool of heat-treated 319 alloys. It was observed that both cutting force and moment generated during drilling increase with increasing magnesium content and α-Fe-intermetallics volume fractions and decrease with the aging temperature (AT). This is expected due to the precipitation of Mg_2Si and MgCuAl which increases the microhardness of the alloy matrix and also because of the improvement in the microstructure homogeneity and alloy microhardness by α-Fe-intermetallics. Again, the heat build-up generated during drilling decreases with increasing magnesium content and α-Fe-intermetallics volume fractions and increases with aging temperature.

CHAPTER 8

CONCLUSIONS

CHAPTER 8

CONCLUSIONS

The present study was undertaken to investigate the effect of metallurgical parameters on the hardness and microstructural characterizations of as-cast and heat-treated 356 and 319 alloys, with the aim of adjusting these parameters to produce castings of suitable hardness and Fe-intermetallic volume fractions for subsequent use in studies relating to the machinability of these alloys. The range of the hardness and Fe-intermetallic volume fractions used in this study conform to the most common levels of the commercial applications of these alloys. Any metallurgical adjustment that can be made to the 356 and 319 alloys which results in an enhancement of the effectiveness of the coolant or reduces the amount of heat generated can be considered an improvement in the overall machinability of the product.

8.1. CHARACTERIZATION OF 356 AND 319 ALLOYS

Hardness measurements were carried out on specimens prepared from 356 and 319 alloys in the as-cast and heat-treated conditions, using different combinations of grain refining, Sr-modification, and alloying additions. Aging treatments were carried out at 155°C, 180°C, 200°C, and 220°C for 4 h, followed by air cooling, as well as at 180°C and 220°C for 2, 4, 6, and 8 h to determine conditions under which specific hardness levels *viz.*, 85 and 115 HBN could be obtained.

From an analysis of the results obtained, the following may be concluded:

1. For 356 containing both α-and β-Fe intermetallics, a peak hardness was observed at 180°C when aging was carried out at different temperatures for a time period of four hours. Aging at 180°C up to eight hours, yields a sharp rise in hardness during the first two hours of aging followed by a broad peak or plateau for 356 alloys containing mostly α-Fe intermetallics in the unmodified and modified conditions. Aging at 220°C had shown a hardness peak at two hours of aging for both 356 and 319 alloys.
2. For 356 and 319 alloys containing α and/or β- Fe intermetallics, the 319 alloys containing 0.29% Mg (~ the same as in 356 alloys) display higher hardness than 356 alloys at all aging times and temperatures under both unmodified and Sr-modified conditions.
3. Increasing Mg content from 0.1 to 0.28% in 319 containing α and/or β- Fe intermetallic alloys yields a remarkable increase in the hardness profile in the unmodified and Sr-modified conditions.
4. Conclusion 2 and 3 may be explained on the basis of the combined effect of Cu-and Mg-intermetallics in the 319 alloys, whereas hardening occurs by cooperative precipitation of Al_2Cu and Mg_2Si phase particles compared to only Mg_2Si precipitation in the case of 356 alloys. Unlike the Mg_2Si precipitates which are easily cut by dislocations, Cu-rich precipitates become more resistant to cutting by dislocations, leading to increased strain hardening rates.
5. The presence of Sr results in severe segregation of the α-Fe and Cu-intermetallics in areas away from the modified eutectic Si which improve the alloy strength. The

reduction in the volume fraction of β-Fe intermetallic phase platelets may be attributed to dissolution and fragmentation of β-intermetallics in the aluminium matrix, due to Sr-modification coupled with solution heat treatment.

8.2. DRILLING AND TAPPING STUDY

Drilling and tapping experiments were performed on a Makino A88E machine at fixed machining conditions to study the machining performance of the Sr-modified and α-Fe intermetallic-containing 356 and 319 alloys. Studies were carried out to investigate the machining behaviour of such alloys through the influence of the following parameters;

- Chemistry and additions (Cu, Mg and α-Fe-intermetallic volume fractions)
- Cooling rate and Quenching rate
- Hardness

From an analysis of the results obtained, the following may be concluded:

6. The differences in machining behaviour between 356 and 319 alloys are mainly attributed to the difference in matrix hardness, alloy chemistry, additions and heat treatment. The matrix hardness (beneficial) and alloy abrasiveness (detrimental) seem to be the real issues controlling the alloy machinability. Magnesium, Cu and α-Fe-intermetallic volume fractions strengthen the alloy matrix and hence improve the alloy machinability.
7. Higher Mg content results in a higher cutting force at the same level of hardness. This can be explained by noting the high volume fraction of Mg-intermetallics or precipitates that can form within the alloy matrix in the high Mg content 319 alloys (0.28%) compared to the low Mg content ones (0.1%). The low Mg-containing 319

alloys (0.1%) yield the longest tool life, more than two times that of 356 alloys (0.3% Mg) and one and half times that of high Mg-containing 319 alloys (0.28%). It is customary to rate the machinability of low Mg-containing 319 alloys higher than 356 alloys and also higher than 319 alloys of the high Mg-containing variety.

8. Lower copper content (i.e. 356 alloy) results in higher cutting force compared to 319 alloys at the same level of hardness. This may be explained by the improvement in the homogeneity of the alloy matrix hardness in 319 alloys on the basis of the combined effect of Cu-and Mg-intermetallics, where hardening occurs by cooperative precipitation of Al_2Cu and Mg_2Si phase particles compared to only Mg_2Si precipitation in the case of 356 alloys.
9. The morphology of iron intermetallics affected the cutting force results when the aging was carried out for two hours at 180° and not at 220°C.
10. Heat treatments that increase the hardness will reduce the built-up-edge on the cutting tool. Hardness affects the machinability of 319 alloys in that machinability improves as the hardness increases. It is observed that both cutting force and moment increase with the hardness while the heat build up depth on the cutting edge decreases. In tapping, it was observed that high speed steel tools react considerably more sensitively to the hardness.
11. For solidification time in the range of 25 to 45 seconds, it seems that both cutting force and moment is slightly influenced by the cooling and quenching rate.
12. Heat built-up and chip welding was observed on 356 and 319 alloys (M1 and M3). Full, half turn and helical chips are generated at the start of a cutting operation when

the drill is new (shearing process). As the drill begins to wear, the chips gradually become well deformed and then both shearing and deformation occur.

8.3. CORRELATION MODELS FOR HARDNESS, DRILLING FORCE, MOMENT AND HEAT BUILD-UP RESULTS

Experimental correlation of the results obtained from the hardness measurements is analyzed through empirical models to establish the relations between the hardness and different metallurgical parameters of 319 alloys. The main factors are magnesium content (%Mg), volume fractions of Fe-intermetallics (%V.F), Sr-modification (Sr-ppm) and aging parameters (Aging time (At) and Aging temperature (AT)). This correlations are valid for Mg-content (0.1-0.3%), Fe-intermetallic volume fractions (2-5%), Sr-modification (0-300ppm), aging time (2-8 h) and aging temperature (180-220°C) where a linear or nearly linear relation in the hardness profile is exits (in the peak-to-overaged regions).

Experimental results obtained from the drilling tests are analyzed and empirical models are established to estimate the relations between both the drilling forces and moments as well as heat build up on the cutting tool edge and different metallurgical parameters for the Sr-modified and α-Fe intermetallic-containing 319 alloys when the hardness set within 100±10 HB. Drilling tests are carried out at fixed machining conditions. The main parameters are volume fractions of Fe-intermetallics (%V.F), magnesium content (%Mg), and aging temperature (AT). The development of an empirical model for the prediction of cutting force and moments and their standard deviations (S.D) as well as their peak-to-valley ranges (R_1 and R_2) and for heat build-up (depth-mm, width-mm and area-

mm^2) on the cutting edge is obtained. From an analysis of the results obtained, the following may be concluded:

13. Statistical design of experiments is a satisfactory method for quantifying the effect of various metallurgical parameters on the hardness and drilling force, moment and heat build-up on the cutting tool when drilling heat treated 319 alloys.
14. Experimental correlations that relate the alloying additions and heat-treatment to the hardness were derived from the experimental results. From these correlations, it was found that the hardness generated for 319 alloys increases with increasing magnesium content and α-Fe-intermetallics volume fractions and decreases as the Sr-modification (Sr-ppm) and aging treatment parameters (aging temperature and aging time) increased.
15. The contribution of Mg in increasing the hardness of heat treated 319 alloys containing β-Fe intermetallics is more if compared with the 319 alloys containing mainly α-Fe intermetallics. There is a strong negative effect of Sr-modification on the hardness of Mg-content and heat treated 319 alloys containing mainly α-Fe intermetallics compared to 319 alloys containing β-Fe intermetallics.
16. Regression equations for the hardness of the heat treated 319 alloys containing different Fe-intermetallic morphologies in terms of metallurgical parameters are developed. The results obtained by these correlations closely agree with the findings from the experimental (other conditions), it was found that there was a less than $\pm$ 8% error between the predicted and the experimental results.

17. In another set of correlations that relate the alloying additions and heat-treatment to the drilling cutting force and moment as well as to the heat build-up, it was observed that both the cutting force and moment generated during drilling increases with increasing magnesium content and α-Fe-intermetallics volume fractions and decreases with the aging temperature (AT). Again, the heat build-up generated during drilling decreases with increasing magnesium content and α-Fe-intermetallics volume fractions and increases with aging temperature.
18. Regression equations for the drilling force and moment and their peak-to-vally values as well as heat build up on the cutting tool edge of the heat treated 319 alloys containing mainly α-Fe-intermetallics in terms of metallurgical parameters are developed.

REFERENCES

REFERENCES

1 M. Tash, F.H. Samuel, F. Mucciardi and H.W. Doty, "Effect of Metallurgical Parameters on the Hardness and Microstructural Characterization of As-Cast and Heat-Treated 356 and 319 Aluminum Alloys", Metallurgical and Materials Transactions A, submitted, Feb. 2004.

2 M. Tash, F.H. Samuel, F. Mucciardi and H.W. Doty, "Effect of Metallurgical Parameters on the Machinability of Heat-Treated 356 and 319 Aluminum Alloys", Prepared for submission to the Metallurgical and Materials Transactions A, 2005.

3 M. Tash, F.H. Samuel, F. Mucciardi and H.W. Doty, "Methodology for Data Processing: Calculation of Cutting Force, Moment and Peak-to Valley Range during Drilling Processes of Heat-Treated 356 and 319 Aluminum Alloys", Prepared for submission to Materials Science and Engineering, 2005.

4 M. Tash, F.H. Samuel, F. Mucciardi and H.W. Doty, "Experimental Correlation of the Effect of Metallurgical Parameters on the Hardness of Heat Treated 319 Alloys", Prepared for submission to Materials Science and Engineering, 2005.

5 M. Tash, F.H. Samuel, F. Mucciardi and H.W. Doty, "Experimental Correlation of the Effect of Metallurgical Parameters on the Drilling Force, Moment and Heat Build-Up in Heat Treated 319 Alloys", Prepared for submission to Materials Science and Engineering, 2005.

6 J. Jorstad, "Influence of Aluminum Casting Alloy Metallurgical Factors on Machinability", Society of Automotive Engineers, 400 Commonwealth Dr., Warrendale, PA, 1980 (Report, 15 pages).

7 J. Jorstad, "Machinability of 380 Alloy: Effect of Minor Elements and Impurities", Paper #G-T79-072, Transactions of the Society of Die Casting Engineers, 1979.

8 R.C. Lemon, "Metallurgical Factors Related to Machining Aluminum Castings", Paper# 607465 presented at SAE Congress and Exposition, January 1967.

9 *Registration Record of Aluminum Association Alloy Designation and Chemical Composition Limits for Aluminum Alloys in the Form of Casting and Ingot*, The Aluminum Association, Washington, DC, Aug. 1982.

10 J.E. Gruzleski and B.M. Closset, "The Treatment of Liquid Aluminum-Silicon Alloys", American Foundrymen's Society, Inc., Des Plaines, IL, USA, 1990.

11 L. Backerud, G. Chai and J. Tamminen, "Solidification Characteristics of Aluminum Alloys", Vol. 2: Foundry Alloys, AFS/SKANALUMINIUM, Des Plaines, IL, USA, 1990.

12 F.H. Samuel, A.M. Samuel and H.W. Doty, "Factors Controlling the Type and Morphology of Cu-Containing Phases in 319 Al Alloy", AFS Transactions, 1996, Vol. 104, pp. 893-901.

13 S. Shivkumar, L. Wang and C. Keller, "Impact Properties of Al-Si-Cu Alloys", Zeitschrift Fur Metallkunde, 1994,Vol. 85 (6), pp. 394-399.

14 P.N. Crepeau, "Effect of Iron in Al-Si Casting Alloys: A Critical Review", AFS Transactions, 1995, Vol.103, pp. 361-366.

15 S. Gowri and F.H. Samuel, "Effect of Alloying Elements on the Solidification Characteristics and Microstructure of Al-Si-Cu-Mg-Fe 380 Alloy", Metallurgical and Materials Transactions A, 1994, Vol. 25A, pp. 437-448.

16 A. Couture, "Iron in Aluminum Casting Alloys: A Literature Survey", AFS International Cast Metals Journal, 1984, Vol. 6 (4), pp. 9-17.

17 G.M. Vorob'ev, R.M. Golshtein and I.I. Maurits, "Effect of Impurities on the Main Properties of Silumin", Metallurgical Abstracts, 1964, Vol. 32, pp. 960-961.

18 L.F. Mondolfo, "Manganese in Aluminum Alloys", The Manganese Centre, France, 1990, pp. 1-35.

19 W. Bonsack, "Discussion on the Effect of Minor Alloying Elements on Aluminum Casting Alloys", ASTM Bulletin, Vol. 117, 1942, p. 45.

20 J.N. Pratt and G.V. Raynor, "The Intermetallic Compounds in the Alloys of Aluminum and Silicon with Cr, Mn, Fe, Co, Ni", Journal of the Institute of Metals, 1951, Vol. 79, pp. 211-232.

21 L.F. Mondolfo and J.G. Barlock, "Effect of Superheating on the Structure of Some Aluminum Alloys", Metallurgical Transactions B, 1975, Vol. 6B, pp. 565-572.

22 G.K. Sigworth, S. Shivkumar and D. Apelian, "The Influence of Molten Melt Processing on Mechanical Properties of Cast Al-Si-Mg Alloys", AFS Transactions, 1989, Vol. 97, pp. 811-824.

23 G. Gurtler and E. Schulz, Metallurgical Abstracts, 1940, Vol. 7, pp. 9.

24 A.M. Samuel, F.H. Samuel, C. Villeneuve, H.W. Doty and S. Valtierra, "Effect of Trace Elements on β-Al5FeSi Characteristics, Porosity and Tensile Properties of Al-Si-Cu (319) Cast Alloys", International Journal of Cast Metals Research, 2001, Vol. 14, pp. 97-120.

25 M.H. Mulazimoglu, A. Zaluska, J.E. Gruzleski and F. Paray, "Electron Microscope Study of Al-Fe-Si Intermetallics in 6201 Alloy", Metallurgical and Materials Transactions A, 1996, Vol. 27A, p. 929.

26 A.M. Samuel, H.W. Doty and F.H. Samuel, "Observations on the Formation of Beta-Al5FeSi Phase in 319 Type Al-Si Alloys", Journal of Materials Science, 1996, Vol. 31, pp. 5529-5539.

27 A.M. Samuel, H.W. Doty and F.H. Samuel, "Influence of Melt Treatment and Solidification Parameters on the Quality of 319.2 Endchill Aluminium Casting", Proc. 4th International Conference on Molten Aluminum Processing, Sheraton World Resort, Orlando, Florida, Nov. 12-14, 1995, pp. 261-294.

28 L.A. Narayanan, F.H. Samuel and J.E. Gruzleski, "Crystallization Behaviour of Iron-Containing Intermetallic Compounds in 319 Aluminum Alloy", Metallurgical and Materials Transactions A, 1994, Vol. 25A, pp. 1761-1773.

29 C.W. Meyers, K.H. Hinton and J.S. Chou, "Toward the Optimization of Heat Treatment in Aluminium Alloys", Materials Science Forum, 1992, Vols 102-104, pp. 75-84.

30 A. M. Samuel, F. H. Samuel, "Modification of Iron Intermetallics by Magnesium and Strontium in Al-Si Alloys", International Journal of Cast Metals Research, 1997, Vol. 10, pp. 147-157.

31 P.Y. Zhu and Q.Y. Liu, "Kinetics of Granulation of Discontinuous Phase in Eutectic Structures", Materials Science and Technology, 1986, Vol. 2, pp. 500-507.

32 P.Y. Zhu, Q.Y. Liu and T.X. Hou, "Spheroidization of Eutectic Silicon in Al-Si Alloys", AFS Transactions,1985, Vol. 93, pp. 609-614.

33 J.W. Martin and R.D. Doherty, "Stability of Microstructures in Metallic Systems", Cambridge University Press, Cambridge, U.K, 1980.

34 N. Crowell and S. Shivkumar, "Solution Treatment Effects in Cast Al-Si-Cu Alloys", AFS Transactions, 1995, Vol. 107, pp. 721-726.

35 G.W. Iorimer, "Precipitation Processes in Solids", K.C. Russel and H.I. Aoranson (Eds), Proc. TMS-AIME Symposium, Niagara Falls, New York, September 1976, p. 87.

36 J.B. Neukerk, "Precipitation from Solid Solution", American Society for Metals, Metals Park, OH, 1959.

37 D. Apelian; S. Shivkumar and G. Sigworth, "Fundamental Aspects of Heat Treatment of Cast Al-Si-Mg Alloys", AFS Transactions, 1989, Vol. 97, pp. 727-741.

38 J. Gauthier, P.R. Louchez and F.H. Samuel, "Heat Treatment of 319.2 Aluminium Automotive Alloy, Part 1: Solution Heat Treatment", Cast Metals, Vol. 8(2), pp. 91-106.

39 A.I. Garcia-Celis, R. Colas and S. Valtierra, "Aging in Heat Treatable Cast Aluminum Alloy", First International Automotive Heat Treating Conference, Puerto Vallarta, Mexico, 13-15 July, 1998, pp. 372-375.

40 P. Ouellet, F.H. Samuel, D. Gloria and S. Valtierra, "Effect of Mg content on the Dimensional Stability and Tensile Properties of Heat Treated Al-Si-Cu (319) Type Alloys", International Journal of Cast Metals Research, 1997, Vol. 10, pp. 67-78.

41 A.M. Samuel, J. Gauthier and F.H. Samuel, "Microstructural Aspects of the Dissolution and Melting of Al2Cu Phase in Al-Si Alloys During Solution Heat Treatment", Metallurgical and Materials Transactions A, 1996, Vol. 27A, pp. 1785-1798.

42 D. Gloria, F. Hernandez and S. Valtierra, "Dimensional Changes During Heat Treating of an Automotive 319 Alloy", 20th ASM Heat Treating Society Conference Proceedings, 9-12 October 2000, St. Louis, MO, ASM International Materials Park, OH, 2000, pp. 674-679.

43 M. Murayama and K. Hono, "Pre-precipitate Clusters and Precipitation Process in Al-Mg-Si Alloys" Acta Metallurgica, 1999, Vol. 47 (5), pp. 1537-1548.

44 S. Shivkumar, C. Keller and D. Apelian, "Aging Behaviour in Cast Al-Si-Mg Alloys", AFS Transactions, 1990, Vol. 98, pp. 905-911.

45 M. Drouzy, S. Jacob and M. Richard, "Interpretation of Tensile Results by Means of Quality Index and Probable Yield Strength: Application to Al-Si7-Mg Foundry Alloys", International Casting Metals Research Journal, 1980, pp. 390-393.

46 M. Tsukuda, S. Koike and M. Harada; Journal of Japan Institute of Light Metals, 1978, Vol. 28 (1), pp. 8-14.

47 M. Tsukuda, S. Koike and K. Asano, "Heat Treatment of Al-7%Si-0.3%Mg Alloy", Journal of Japan Institute of Light Metals,1978, Vol. 28 (11), pp. 531-540.

48 J.E. Davis (Ed.), "Aluminum and Aluminum Alloys", ASM Specialty Handbook, ASM International, Materials Park, Ohio, USA, 1993.

49 J.E. Hatch (Ed), "Aluminum Properties and Physical Metallurgy", First edition, American Society for Metals, Metals Park, Ohio, 1988.

50 C. Brichet, Thèse Ingénieur-Docteur, Université de Paris-Sud, 1971.

51 L. Zhen, W.D. Wfel, S.B. Kang and H.W. Kim, "Precipitation Behavior of Al-Mg-Si Alloys with High Silicon Content", Journal of Materials Science, 1997, Vol. 32, pp. 1895-1902.

52 K.T. Kashyap, S. Murali, K.S. Raman and K.S.S. Murthy, "Casting and HeatTreatment Variables of Al-7Si-Mg Alloy", Materials Science and Technology,1993, Vol. 9, pp. 189-203.

53 H. Chandrasekaran, "Material Development and its Role in Advanced Machining Situations" Swedish Institute for Metals Research, Drottning Kristinas, Feb 2003, Vol. 48, 114- 28, Stockholm, Sweden.

54 R. Sharan and N.P. Saksena, "Influence of Rare Earth Additions on the Forgeability and Machinability of Forgeable Aluminium Alloy", Proceedings of International Forgeability Conference, Paris, April 1975.

55 H. Yamada and T. Tanaka, "Combined Effect of Copper and Manganese on the Machinability of Aluminum Casting Alloys", Journal of Japan Institute of Light Metals, April 1977, Vol. 27 (11), pp. 542-547.

56 S. Zaima, Y. Takatsuji, M. Lio and S. Yamada, "Adding Effects of Strontium and Antimony on High Speed Steel Tool Wear in AC3A Dry Cutting", Journal of Japan Institute of Light Metals, 1982, Vol. 32 (10), pp. 523-529.

57 S. Sato, T. Saga and S. Nagai, "Effects of Additional Elements on the Machinability of Al-Si Casting Alloys", Journal of Japan Institute of Light Metals, 1983, Vol. 33, pp. 649-654.

58 R. Sharan, N. Prasad and B. Kumar, "Influence of Rare Earth Additions on Machinability of Aluminum Alloys and Aluminum Bronzes", Proc. of 12th AIMTDR Conference, New Delhi, 1986, Tata-McGraw Hill Place, 1986, pp. 292-294.

59 K.A. Saha, K.A. Chakraborthy and B.A. Chattaopadhyay, 25th Annual Conf. of Metallurgists, 1986, Toronto, pp. 59-70.

60 H. Zoller, G. Enzler and C.J. Fornevord, "The Machinability of Aluminium Alloys", Aluminium, 1969, Vol. 45, pp. 49-54.

61 W. Kônig and D. Erinski,"Machining Properties of Alumium Casting Alloys with Various Silicon Contents", Aluminium, 1981, Vol. 57, pp. 719-721.

62 H. Yamada and T. Tanaka, "Effect of Cast Structure on the Machinability of Aluminium Alloys", Journal of Japan Institute of Light Metals, 1976, Vol. 26(11).

63 J.l. Jorstad, "Influence of Metallurgical Factors on Machinability of Aluminium Casting Alloys", Die Casting Engineer, 1980, pp. 26-32.

64 C.H. Caceres, I.L. Svensson and J.A. Taylor, "Strength-Ductility Behavior of Al-Si-Cu-Mg Casting Alloys in T6 Temper", International Journal of Cast Metals Research, 2003, Vol. 15, pp. 531-543.

65 C.A. Queener, "Effect of Iron Content and Sodium Modification on the Machinability of Aluminum Alloy", AFS Transactions, 1966, Vol. 73, pp. 14-19.

66 Q.T. Fang and D.A. Granger, "Porosity Formation in Modified and Unmodified A356 Alloy Casting", AFS Transactions, 1989, Vol. 97, pp. 989-1000.

67 W.J. Sylly, "The Machinability of Cast Aluminum Alloys", ISI-Special Report 94, The Iron and Steel Institute, London, 1967, pp. 127-133

68 B. Chamberlain "Machinability of aluminum Alloys", Metals handbook, Vol. 2, Properties and Selection: Nonferrous Alloys and Pure Metals, 9 th Edition, ASM International Materials Park, OH, 1989.

69 J.M. Fox, "Aluminum Alloy Casting Inclusions", AFS Transactions, 1961, Vol. 69, pp. 737-742.

70 D. Apelian, G.K. Sigworth and K.R. Whaler, "Assessment of Grain Refinement and Modification of Al-Si Foundry Alloys by Thermal Analysis", AFS Transactions, 1984, Vol. 92, pp. 297-307.

71 R. DasGupta, C.G. Brown and S. Marek, "Analysis of Overmodified 356 Aluminum Alloy", AFS Transactions, 1988, Vol. 96, pp. 297-310.

72 R. Sharan and N.P. Saksena "Rare Earth Additions as a Modifier of Aluminum Silicon Alloys", AFS International Cast Metals Journal, 1978, Vol. 3 (1), pp. 29-33.

73 M. Ravi, U.T.S. Pillai, B.C. Pai, A.D. Damodaran and E.S. Dwarakadasa, "The Effect of Mischmetal Addition on the Structure and Mechanical Properties of a Cast Al-7Si-0.3Mg Alloy Containing Excess Iron (up to 0.6 Pct)", Metallurgical and Materials Transactions A, 2002, Vol. 33A, pp. 391-400.

74 G. Lorenz, "Notes on the Effect of Heat Treatment on the Machinability of Al-Cu-Type Free-Cutting Alloy", Annals of CIRP, 1970, Vol. 18, pp. 25 l-256.

75 K. Asano and A. Fujiwara, Journal of Japan Institute of Light Metals, 1973, Vol. 23 (7), pp. 340-344.

76 T. Saga and S. Nagai, "Simple Method For Determining Machinability of Aluminium Alloy 2011", Journal of Japan Institute of Light Metals, 1972, Vol. 22 (5), pp. 297-302.

77 ASM Metals Handbook Ninth Edition Volume 16, "Machining", ASM International, Materials Park, OH, 1989, p. 643.

78 K.G. Budinski, "Engineering Materials Properties and Selection", Prentice-Hall, Englewood Cliffs, NJ, 1992, p. 588.

79 M. Kronenberg, "Machining Science and Application", Pregamon, London, 1966, pp 265-268.

80 www.toolingandproduction.com, G. Schneider, "Cutting Tool Applications", 2002.

81 http://www.me.metu.edu.tr/me535/Lecture%20Notes/Chapter%204/index.html, Department of Mechanical Engineering, Metal Cutting, Machinability, 2005"

82 R. Komanduri, D.G. Flom and M. Lee, "Highlights of the DARPA Advanced Machining Research Program", Journal of Engineering for Industry, Vol. 107, 1985, pp. 325-335.

83 H. Schultz, "High-Speed Milling of Aluminum Alloys: High Speed Machining", Winter Annual Meeting of the ASME, 1984, pp. 241-244.

84 H. Schultz, "High-Speed Machining", Annals of the CIRP, 1992, Vol. 41, pp. 637-643.

85 M. Nouari, G. List, F. Girot and D. Coupard, "Experimental Analysis and Optimisation of Tool Wear in Dry Machining of Aluminium Alloys", Wear xxx (2003) xxx-xxx, pp. 1-10., available online at www.sciencedirect.com.

86 B. Rao and Y.C. Shin, "Analysis on High-Speed Face Milling of 7075-T6 Aluminum Using Carbide and Diamond Cutters", International Journal of Machine Tools and Manufacture, 2001, Vol. 41, pp. 1763-1781.

87 P. Mathew and P.L.B. Oxley, "Predicting the Effects of Very High Cutting Speeds on Cutting Forces, etc.", Annals of the CIRP,1982, Vol. 31 (1), pp. 49-52.

88 G. Byrne and E. Scholta, "Environmentally clean Machining Processes: A Strategic Approach", Annals of the CIRP, 1993, Vol. 42, p. 471.

89 P.S. Sreejith and B.K.A. Ngoi, "Dry Machining: Machining of the Future", Journal of Materials. Processing Technology, 2000, Vol. 101, p. 287.

90 A. Moufki, A. Molinari, D. Dudzinski, "Modeling of Orthogonal Cutting with a Temperature Dependent Friction Law", Journal of Mechanical Physics of Solids, 1998, Vol. 46, pp. 2103-2138.

91 H. K. Tonshoff, W. Spintig and W. Konig, "Machining of Holes Developments in Drilling Technology", Annals of the CIRP, 1994, Vol. 43, p. 551.

92 S. Kalidas, R.E. DeVor and S.G. Kapoor, "Experimental Investigation of the Effect of Drill Coatings on Hole Quality Under Dry and Wet Drilling Conditions", Surface and Coatings Technology, 2001, Vol. 148, p. 117.

93 Toru Sekiguchi, Journal of JSME, 2001, Vol. 104, p. 60.

94 K. Tonshoff, A. Mohlfeld, T. Leyendecker, H.G. Fuss, G. Erkens, R. Wenke and T. Cselle, " Wear Mechanisms of (Ti1-xAlx)N Coatings in Dry Drilling", Surface and Coating Technology, 1997, Vols. 94-95, p. 603.

95 F. Klocke and G. Eisenblatter, " Dry Cutting" Annals of the CIRP, 1997, Vol. 46, p. 1.

96 E.M. Trent and P.K. Wright, "Metal Cutting", 4th Edition, Butterworths-Heinemann, London, 2000, pp. 149-166.

97 M.Z. Zhang, Y.B. Liu and H. Zhou, "Wear Mechanism Maps of Uncoated HSS Tools Drilling Die-Cast Aluminum Alloy", Tribology International, 2001, Vol. 34, pp. 727-731.

98 K.M. Vernaza-Pena, J.J. Mason and M. Li, "Experimental Study of the Temperature Field Generated During Orthogonal Machining of an Aluminum Alloy", Experimental Mechanics, 2002, Vol. 42, pp. 221-229.

99 D.U Braga, A.E. Diniz, G.W.A. Miranda and N.L. Coppini, "Using a Minimum Quantity of Lubricant (MQL) and a Diamond Coated Tool in the Drilling of Aluminium-Silicon Alloys", Journal of Materials Processing Technology, 2002, Vol. 122, pp. 127-138.

100 S.A. Batzer, D.M. Haan, P.D. Rao, W.W. Olson and J.W. Sutherland, "Chip Morphology and Hole Surface Texture in the Drilling of Cast Aluminium Alloys", Journal of Materials Processing Technology, 1998, Vol. 79, pp. 72-78.

101 http://www.me.metu.edu.tr/me535/Lecture%20Notes/Chapter%203/index.html, Department of Mechanical Engineering, "Metal Cutting: Temperature in Metal Cutting", 2005.

102 L. Wang, K. Saito and I.S. Jawahir, "Infrared Temperature Measurement of Curled Chip Formation in Metal Machining", Transactions of NAMRI/SME,1996, Vol. XXIV, pp. 87-92.

103 E.M. Trent, "Metal Cutting and the Tribology of seizure: II Movement of Work Material over the Tool in Metal Cutting", Wear, 1988, Vol. 128, pp. 47-64.

104 K. Nakayama and M. Ogawa "Basic Rules on the Form of Chip in Metal Cutting", Annals of the CIRP, Vol. 27 (1), 1978, pp. 17-21.

105 B. Worthington and M.H. Rahman, "Predicting Breaking with Grooved-Type Breakers", International Journal of Machine Tool Design Researches, 1979, Vol. 19, pp. 121-132.

106 V. Kruzhanov and V. Zeitz, "Investigation of Chip Formation During High Speed Drilling", Scientific Fundamentals of HSC, Herbert Schulz (Ed.), HanserGardner Publication, Inc., OH, USA 2001.

107 M. Ortiz and D.T. Marusich, "Modelling and Simulation of High-Speed Machining", International Journal for Numerical Methods in Engineering, 1995, Vol. 38, pp. 3675-3694.

108 G. Poulachon and A. Moisan, "A study of Chip Formation Mechanisms in High Speed Cutting of Hardened Steel", Scientific Fundamentals of HSC, Herbert Schulz (Ed.), HanserGardner Publication, Inc., OH, USA, 2001.

109 D.M. Haan, W.W. Olson and J.W. Suttherland, "The Mechanisms of Metal Cutting Fluids in Machining Aluminium Alloys", AAMA Metalworking Fluids Symposium, Dearborn, Michigan; The Industrial Metalworking Environment: Assessment and Control, November 13-16, 1995.

110 C.M. Shaw, "Metal Cutting Principles", Clarendon Press, Oxford, 1984, pp. 461-481.

111 C. Cassin and G. Boothroyed "Lubricating Action of Cutting Fluids", Journal of Mechanical Engineering Science, 1965, Vol. 7(1), pp. 67-81.

112 O. R. Burant and T. J. Skingle, "Machining the Silicon Containing Aluminium Alloys", SAE Technical Paper Series 800489, Inc.Congress and Exposition Cobo Hall, Detroitt, February 25-29, 1980 pp. 1-13.

113 C. Schmidt E.Y.C. Yen, "Tool Wear Prediction and Verification in Orthogonal Cutting", May, 2003, http://nsmwww.eng.ohiostate.edu/6thCIRP_toolwear_Toronto.pdf.

114 http://www.manufacturingcenter.com/online_book/chap_2.pdf, G. Schneider, "Cutting Tool Applications", 2002

115 http://www.manufacturingcenter.com/online_book/chap_8.pdf, G. Schneider, "Cutting Tool Applications", 2002.

116 C.T.L. Rolt, "A short Story of Machine Tools", The M.I.T. Press, Massachusetts Institute of Technology, Cambridge, Massachusetts 1965.

117 W.W. Bird and P.H. Fairfield, "A Twist Drill Dynamometer", Transactions of ASME, 1904/1905, Vol. 26, pp. 355-366.

118 M.S. Wu and M.J. Shen, "Mathematical Model of Multifaceted Drills", Transactions of ASME, Journal of Engineering for Industry, 1983, Vol. 105, pp. 173-182.

119 E.M. Merchant, "Basic Mechanics of the Metal Cutting Process", Journal of Applied Mechanics, September 1944, pp. A-168 to A-175.

120 http://www.manufacturingcenter.com/online_book/TP%20Chapter%2011.pdf, G. Schneider, "Cutting Tool Applications", 2002.

121 Special Report on "The Mechanical Properties of Permanent Mold Aluminium Alloy Test Casting", The Aluminium Association, 1990.

122 A. Kelly and R.B. Nicholson, "Precipitation Hardening", Progress in Materials Science, 1963, Vol. 10, p. 149.

123 M.H. Jacoby, Philosophical Magazine, 1972, Vol. 26, 1972, p. 1.

124 I. Dutta and S.M. Allen, "A Calorimetric Study of Precipitation in Commercial Aluminum Alloy-6061 Alloy", Journal of Materials Science Letters, 1991, Vol. 10, p. 323.

125 A. Guinier, Acta Crystallographica, 1953, Vol. 90, p. 57.

126 J. Krol, "The Precipitation Strengthening of Directionally Solidified Al-Si-Cu Alloys", Materials Science and Engineering, 1997, Vols A234 -A236, pp. 169-172.

127 J.W. Martin, "Micromechanisms in Particle Hardened Alloys", Cambridge University Press, Cambridge, 1980, p. 122.

128 J.M. Dowling and J.W. Martin, "The Influence of Mn Additions on the Deformation Behavior of an Al-Mg-Si Alloy", Acta Metallurgica, 1976, Vol. 24, pp. 1147-1153.

129 P.N. Crepeau, S.D. Antolovich and J.A. Worden, "Structure-Property Relationships in Aluminium Alloy 339-T5: Tensile Behavior at Room and Elevated Temperature", AFS Transactions, 1990, Vol. 98, pp. 813-822.

130 S. Shivkumar, S. Ricci, Jr. and D. Apelian, "Production and Electrolysis of Light Metals, B. Clossest (Ed), Pergamon Press, New York, NY, 1989, pp. 173-182.

131 J. Sakwa, "Application of the Thermal Analysis and the Derivative Differential Thermal Analysis for Estimation of Influences of Mg, P and Cu as well as of Na and Ti on the Process of Crystallization of Aluminum-Silicon Alloys", Giesserei-Forschung, Vol. 38, 1986, pp. 112-118.

132 S. Bercovici, "Control of Solidification Structure and Properties of Al-Si Alloys", Presentation at 45th International Foundry Congress, Dales, 1978.

133 www.kistler.com

134 J.R. Taylor, "An Introduction to Error Analysis: The Study of Uncertainties in Physical Measurements", University Science Books, Mill Valley, California, 1982.

135 R.W. Bruner, "Heat Treatment of Al-Alloy Castings", Aluminum Conference Detroit, MI, Sept 25-26, 1979, pp. 209-216.

136 G.H. Bech, Untersuchung der Zerspanbarkeit von LeichtmetallGuBlegierungen Dissertation, RWTH Aachen, 1963.

137 W. Konig and D. Erinski "Machinability of Al-Si Pressure Die Cast Alloys", Proc. of the 20th MTDR-Conference, Dep. of Mach. Eng., University of Birmingham, Birmingham, 10-14 Sept. 1979, pp. 337-344

138 R.L Ganguly. B.K. Dhindaw and P.R. Dhar, "Application of Statistical Design of Experiments to the Quantitative Study of the Strengthening Characteristics of Al-Zn-Mg-Cu Alloys", Metals Technology 1977, Vol. 4, Part 2, p. 57.

139 R.L Ganguly. B.K. Dhindaw.and P.R. Dhar, "Study and Control of Properties and Behavior of Al-Mg-Si Alloys by Application of Statistical Design of Experiments", Transactions of the Japan Institute of Metals.1977, Vol. 17, p. 511.

140 C.R. Hicks, "Fundamental Concepts in The Design of Experiments", (4th Edition), Oxford University Press, Inc. New York, 1993, pp. 217-230.

141 http://www.sis.pitt.edu/~dtipper/2120/2120_notes4.pdf.

APPENDIX

APPENDIX A
IRON AND COPPER INTERMETALLICS SURFACE FRACTIONS RESULTS FOR 356 AND 319 ALLOYS

APPENDIX A: IRON AND COPPER INTERMETALLICS SURFACE FRACTIONS RESULTS FOR 356 AND 319 ALLOYS

Table A.1: Fe- and Cu-intermetallics surface fractions obtained for 356 and 319 alloys in the as-cast and solution heat treated conditions used in this work

Sample Code	Fe-Intermetallics				Fe-Intermetallic Morphology	Cu-Intermetallics			
	Un-modified (As Cast)		Sr-Modified (As Cast)			Un-modified (As Cast)		Sr-Modified (As Cast)	
	S. F. (%)	S.D	S. F. (%)	S.D		S. F. (%)	S.D	S. F. (%)	S.D
1	0.6	0.1	0.65	0.19	β	0.00	0.00	0.00	0.00
2	0.49	0.11	1.08	0.33	β	0.00	0.00	0.00	0.00
3	1.56	0.44	1.24	0.27	β	0.00	0.00	0.00	0.00
4	2.40	0.47	2.20	0.25	β	0.00	0.00	0.00	0.00
5	0.89	0.21	0.91	0.12	β	0.00	0.00	0.00	0.00
6	2.25	0.55	1.73	0.18	β	0.00	0.00	0.00	0.00
7	4.56	1.10	3.23	1.58	α	0.00	0.00	0.00	0.00
8	1.55	0.23	1.68	0.34	β	1.65	0.39	1.92	0.52
9	3.08	0.39	2.25	0.30	β	1.62	0.26	1.81	0.36
10	4.04	0.46	3.65	0.36	β	1.49	0.25	1.79	0.42
11	3.15	0.35	1.96	0.25	β	1.83	0.23	2.27	0.54
12	2.90	0.47	2.69	0.31	β	1.19	0.25	2.11	0.44
13	4.78	0.98	4.00	1.29	α	1.19	0.25	1.87	0.60
14	1.95	0.46	1.86	0.27	β	2.17	0.32	2.11	0.57
15	5.02	0.91	3.61	0.46	β	1.82	0.43	1.95	0.37
16	1.62	0.33	1.98	0.38	β	2.00	0.30	2.00	0.98
17	3.90	0.69	3.62	0.34	β	2.10	0.43	2.11	0.56
18	1.79	0.40	1.82	0.27	β	1.82	0.23	1.94	0.50
19	4.15	0.70	5.18	1.27	α	1.16	0.24	1.60	0.58
20	2.49	0.40	2.16	0.35	β	2.47	0.39	2.09	0.62
21	5.68	1.23	4.82	0.95	α	1.32	0.41	1.67	0.70
22	0.6	0.1	0.64	0.19	β	2	0.5	2.30	0.77
Sample Code	Fe-Intermetallics				Fe-Intermetallic Morphology	Cu-Intermetallics			
	Un-modified (SHT)		Modified (SHT)			Un-modified (SHT)		Modified (SHT)	
	S. F. (%)	S.D	S. F. (%)	S.D		S. F. (%)	S.D	S. F. (%)	S.D
1	0.80	0.20	0.79	0.35	B	0.00	0.00	0.00	0.00
2	0.48	0.11	1.16	0.34	B	0.00	0.00	0.00	0.00

3	1.56	0.44	1.78	0.41	B	0.00	0.00	0.00	0.00
4	2.40	0.47	2.97	0.30	B	0.00	0.00	0.00	0.00
5	0.89	0.21	1.12	0.35	B	0.00	0.00	0.00	0.00
6	2.25	0.55	1.81	0.44	B	0.00	0.00	0.00	0.00
7	4.56	1.11	4.39	1.55	A	0.00	0.00	0.00	0.00
8	1.19	0.40	1.68	0.44	β	0.09	0.06	1.21	0.79
9	1.86	0.36	2.25	0.40	β	0.40	0.20	1.17	0.97
10	3.41	0.70	3.52	0.77	β	0.40	0.28	0.72	0.58
11	1.53	0.45	1.76	0.36	β	0.36	0.18	1.17	0.58
12	2.77	0.69	2.55	0.36	β	0.28	0.17	0.89	0.60
13	4.74	1.43	4.24	0.95	α	0.39	0.26	0.51	0.65
14	1.68	0.73	1.42	0.29	β	1.01	0.50	1.10	0.69
15	3.67	0.95	3.05	0.69	β	0.40	0.50	0.65	0.44
16	1.9	0.55	1.68	0.52	β	1.52	0.58	1.52	1.25
17	3.37	0.81	3.85	0.62	β	0.70	0.58	1.18	0.51
18	1.88	0.47	1.85	0.42	β	0.80	0.49	1.08	0.83
19	5.42	2.13	5.16	1.74	α	0.08	0.09	0.39	0.33
20	2.40	0.63	1.88	0.33	β	0.84	0.38	0.85	0.43
21	6.00	2.65	5.30	2.30	α	0.15	0.27	0.47	0.58
22	1.21	0.41	0.79	0.20	β	0.77	0.37	0.85	0.51

APPENDIX B
MATLAB DRILLING AND TAPPING PROGRAMS

APPENDIX B: MATLAB DRILLING AND TAPPING PROGRAMS

Part A-Drilling Program

```
close all;clear all,clc
[fi,ch]=uigetfile('C:\machinabilityCTA\M1-drilling\*.*','Ouvrir...');
if ch==0
return
end;
Threshold=170;
nom=[ch fi];
k=load(nom);
k1=k(3,:);
figure(14);plot(k1);grid on
title('original plot (Fz=k)')
xlabel('time (msec)')
ylabel('Fz (N)')
b=[1 1];b=b/sum(b);
k2=k1;
nlevel=9;
for i=1:nlevel
k1=filter(b,1,k1);
k1=k1(1:2:end);
end
t1=1:length(k);
t2=t1(1:2^nlevel:end);
figure(15);plot(t1,k2,'b',t2-0*2^nlevel,k1,'r');grid on
title('method of detection step (1); filtering')
xlabel('time (msec)')
ylabel('Fz and mFz (N)')
diffk=diff(k1);
figure(16),plot(1:length(k1),k1,1:length(k1)-1,diffk),grid on
title('step (2), difference(diff mFz) and comparison')
xlabel('time (msec)/ No of filtering')
ylabel('mFz and diff mFz (N) ')
diffk(diffk<Threshold)=0;
diffk(diffk>0)=350;
difffk=diff(diffk);
figure(17);plot(1:length(k1),k1,1:length(diffk),diffk,1:length(difffk),difffk),grid on
title('step (3) diffecnce (diff(diff mFz), comparison and detection')
xlabel('time (msec)/ No of filtering')
```

```
ylabel('mFz, diff mFz, and diff (diff mFz) (N) ')
ind=find(difffk==350);
ind=ind(1:end-1);
%number of elements of diff(ind)=number of elements of (ind) - 1
min(diff(ind))
max(diff(ind))
nmin=5;
indd=zeros(1,length(ind)*nmin);
for i=1:nmin
indd(i:nmin:end)=ind+i-1;
end
tt=k1(indd);
tt1=buffer(tt,nmin);
[mfzup jj1]=max(tt1);
[mfzdown jj2]=min(tt1);
timeup=(ind+jj1+3)*2^9;
timedown=(ind+jj2-2.375)*2^9;
NN=1200;
MM=10;
ZZ=200;
n=((0:NN)-NN/2)';
m=((0:MM)-MM/2)';
z=((0:ZZ)-ZZ/2)';
N=length(timeup);
M=length(timedown);
time1=ones(NN+1,1)*timeup+n*ones(1,N);
time2=ones(MM+1,1)*timedown+m*ones(1,M);
time3=ones(ZZ+1,1)*timeup+z*ones(1,N);
mfxup=mean(buffer(k(1,time1),1201));
smfx=std(buffer(k(1,time3),201));
mfyup=mean(buffer(k(2,time1),1201));
smfy=std(buffer(k(2,time3),201));
smfz=std(buffer(k(3,time3),201));
mMxup=mean(buffer(k(4,time1),1201));
smMx=std(buffer(k(4,time3),201));
mMyup=mean(buffer(k(5,time1),1201));
smMy=std(buffer(k(5,time3),201));
mMzup=mean(buffer(k(6,time1),1201));
smMz=std(buffer(k(6,time3),201));
mfxdown=mean(buffer(k(1,time2),11));
mfydown=mean(buffer(k(2,time2),11));
mMxdown=mean(buffer(k(4,time2),11));
```

```
mMydown=mean(buffer(k(5,time2),11));
mMzdown=mean(buffer(k(6,time2),11));
mfx=(mfxup-mfxdown);
mfy=(mfyup-mfydown);
mfz=(mfzup-mfzdown);
mMx=(mMxup-mMxdown);
mMy=(mMyup-mMydown);
mMz=(mMzup-mMzdown);

results=[timeup;mfx;smfx;mfy;smfy;mfz;smfz;mMx;smMx;mMy;smMy;mMz;smMz];
txt1=['%4.4f' char(9) '%4.4f' char(9) '%4.4f',...
char(9) '%4.4f' char(9) '%4.4f' char(9),...
'%4.4f' char(9) '%4.4f' char(9) '%4.4f' char(9),...
'%4.4f' char(9) '%4.4f' char(9) '%4.4f' char(9),...
'%4.4f' char(9) '%4.4f' char(13) char(10)];
fid=fopen([fi '.xls'],'w');
txt2=['timeup' char(9) 'mfx' char(9) 'smfx',...
char(9) 'mfy' char(9) 'smfy' char(9),...
'mfz' char(9) 'smfz' char(9) 'mMx' char(9),...
'smMx' char(9) 'mMy' char(9) 'smMy' char(9),...
'mMz' char(9) 'smMz' char(13) char(10)];

fwrite(fid,txt2,'char');
fprintf(fid,txt1,results(:));fclose all;
figure;plot(t1,k(1,:),'b',timeup,mfx,'.-m',timeup,mfxup,'.-r',timedown,mfxdown,'.-y'),grid on
xlabel('Time (msec)')
ylabel('Drilling Force (N)')
figure;plot(t1,k(2,:),'b',timeup,mfy,'.-m',timeup,mfyup,'.-r',timedown,mfydown,'.-y'),grid on
xlabel('Time (msec)')
ylabel('Drilling Force (N)')
figure;plot(t1,k(3,:),'b',timeup,mfz,'.-m',timeup,mfzup,'.-r',timedown,mfzdown,'.-y'),grid on
xlabel('Time (msec)')
ylabel('Drilling Force (N)')
figure;plot(t1,k(3,:),'b',timeup,mfzup,'.-r',timedown,mfzdown,'.-y',timeup,mfz,'.-m'),grid on
xlabel('Time (msec)')
ylabel('Drilling Force (N)')
figure;plot(t1,k(4,:),'b',timeup,mMx,'.-m',timeup,mMxup,'.-r',timedown,mMxdown,'.-
y'),grid on
xlabel('Time (msec)')
ylabel('Drilling Moment (N.m)')
figure;plot(t1,k(5,:),'b',timeup,mMy,'.-m',timeup,mMyup,'.-r',timedown,mMydown,'.-
y'),grid on
```

```
xlabel('Time (msec)')
ylabel('Drilling Moment (N.m)')
figure;plot(t1,k(6,:),'b',timeup,mMz,'.-m',timeup,mMzup,'.-r',timedown,mMzdown,'.-
y'),grid on
xlabel('Time (msec)')
ylabel('Drilling Moment (N.m)')
figure;plot(mfx);
xlabel('No of holes')
ylabel('Drilling Force (N)')
figure;plot(mfy)
xlabel('No of holes')
ylabel('Drilling Force (N)')
figure;plot(mfz)
xlabel('No of holes')
ylabel('Drilling Force (N)')
figure;plot(mMx);
xlabel('No of holes')
ylabel('Drilling Moment (N.m)')
figure;plot(mMy);
xlabel('No of holes')
ylabel('Drilling Moment (N.m)')
figure;plot(mMz);
xlabel('No of holes')
ylabel('Drilling Moment (N.m)')
```

Part B-Tapping Program

```
close all;clear all,clc
[fi,ch]=uigetfile('C:\machinabilityCTA\M1-Tapping\*.*','Ouvrir...');
if ch==0
return
end;
Threshold=-50;
nom=[ch fi];
k=load(nom);
k1=k(3,:);
figure(2);plot(k1);grid on
title('original plot (Fz)')
xlabel('time (msec)')
ylabel('Fz (N)')
b=[1 1];b=b/sum(b);
k2=k1;
%k1=buffer(k2,5160);
nlevel=9;
for i=1:nlevel
k1=filter(b,1,k1);
k1=k1(1:2:end);
end
%break
t1=1:length(k);
t2=t1(1:2^nlevel:end);
figure(1);plot(t1,k2,'b',t2-0*2^nlevel,k1,'r');grid on
title('method of detection step (1); filtering')
xlabel('time (msec)')
ylabel('Fz and mFz (N)')
diffk=diff(k1);
figure(3),plot(1:length(k1),k1,1:length(k1)-1,diffk),grid on
title('step (2), difference(diff mFz) and comparison')
xlabel('time (msec)/ No of filtering')
ylabel('mFz and diff mFz (N) ')
diffk(diffk>Threshold)=0;
diffk(diffk<0)=-250;
difffk=diff(diffk);
figure(2);plot(1:length(k1),k1,1:length(diffk),diffk,1:length(difffk),difffk),grid on
title('step (3) diffecnce (diff(diff mFz), comparison and detection')
xlabel('time (msec)/ No of filtering')
ylabel('mFz, diff mFz, and diff (diff mFz) (N) ')
```

```
ind=find(difffk==-250);
ind=ind(1:end-1);
%number of elemebts of diff(ind)=number of elements of (ind) - 1
min(diff(ind))
max(diff(ind))
nmin=7;
indd=zeros(1,length(ind)*nmin);
for iii=1:nmin
indd(iii:nmin:end)=ind+iii-4;
end
tt=k1(indd);
tt1=buffer(tt,nmin);
[mfz,iii]=max(tt1);
ind1=ind+iii-4;
mfzup1=mean([k1(ind1);k1(ind1-1)]);
mfzdown1=mean([k1(ind1+2);k1(ind1+3)]);
timeup1=(ind1-1.5)*2^9;
timedown1=(ind1+1.5)*2^9;
timedown2=(ind1-5.5)*2^9;
NN=1000;
MM=1000;
ZZ=10;
n=((0:NN)-NN/2)';
m=((0:MM)-MM/2)';
z=((0:ZZ)-ZZ/2)';
N=length(timeup1);
M=length(timedown1);
Z=length(timedown2);
time1=ones(NN+1,1)*timeup1+n*ones(1,N);
time2=ones(MM+1,1)*timedown1+m*ones(1,M);
time3=ones(ZZ+1,1)*timedown2+z*ones(1,Z);
mfxup1=mean(buffer(k(1,time1),1001));
smfxup=std(buffer(k(1,time1),1001));
mfyup1=mean(buffer(k(2,time1),1001));
smfyup=std(buffer(k(2,time1),1001));
smfzup=std(buffer(k(3,time1),1001));
mMxup1=mean(buffer(k(4,time1),1001));
smMxup=std(buffer(k(4,time1),1001));
mMyup1=mean(buffer(k(5,time1),1001));
smMyup=std(buffer(k(5,time1),1001));
mMzup1=mean(buffer(k(6,time1),1001));
smMzup=std(buffer(k(6,time1),1001));
```

```
mfxdown1=mean(buffer(k(1,time2),1001));
smfxdown=std(buffer(k(1,time2),1001));
mfydown1=mean(buffer(k(2,time2),1001));
smfydown=std(buffer(k(2,time2),1001));
smfzdown=std(buffer(k(3,time2),1001));
mMxdown1=mean(buffer(k(4,time2),1001));
smMxdown=std(buffer(k(4,time2),1001));
mMydown1=mean(buffer(k(5,time2),1001));
smMydown=std(buffer(k(5,time2),1001));
mMzdown1=mean(buffer(k(6,time2),1001));
smMzdown=std(buffer(k(6,time2),1001));
mfxdown2=mean(buffer(k(1,time3),11));
mfydown2=mean(buffer(k(2,time3),11));
mfzdown2=mean(buffer(k(3,time3),11));
mMxdown2=mean(buffer(k(4,time3),11));
mMydown2=mean(buffer(k(5,time3),11));
mMzdown2=mean(buffer(k(6,time3),11));
mfxup=(mfxup1-mfxdown2);
mfyup=(mfyup1-mfydown2);
mfzup=(mfzup1- mfzdown2);
mMxup=(mMxup1-mMxdown2);
mMyup=(mMyup1-mMydown2);
mMzup=(mMzup1-mMzdown2);
mfxdown=(mfxdown1-mfxdown2);
mfydown=(mfydown1-mfydown2);
mfzdown=(mfzdown1- mfzdown2);
mMxdown=(mMxdown1-mMxdown2);
mMydown=(mMydown1-mMydown2);
mMzdown=(mMzdown1-mMzdown2);

results=[timeup1;mfxup;smfxup;mfyup;smfyup;mfzup;smfzup;mMxup;smMxup;mMyup;s
mMyup;mMzup;smMzup;timedown1;mfxdown;smfxdown;mfydown;smfydown;mfzdown;
smfzdown;mMxdown;smMxdown;mMydown;smMydown;mMzdown;smMzdown];
txt1=['%4.4f' char(9) '%4.4f' char(9) '%4.4f',...
char(9) '%4.4f' char(9) '%4.4f' char(9),...
'%4.4f' char(9) '%4.4f' char(9) '%4.4f' char(9),...
'%4.4f' char(9) '%4.4f' char(9) '%4.4f' char(9),...
'%4.4f' char(9) '%4.4f' char(9) '%4.4f' char(9) '%4.4f',...
char(9) '%4.4f' char(9) '%4.4f' char(9),...
'%4.4f' char(9) '%4.4f' char(9) '%4.4f' char(9),...
'%4.4f' char(9) '%4.4f' char(9) '%4.4f' char(9),...
'%4.4f' char(9) '%4.4f' char(9) '%4.4f' char(13) char(10)];
```

```
fid=fopen([fi '.xls'],'w');
txt2=['timeup1' char(9) 'mfxup' char(9) 'smfxup',...
char(9) 'mfyup' char(9) 'smfyup' char(9),...
'mfzup' char(9) 'smfzup' char(9) 'mMxup' char(9),...
'smMxup' char(9) 'mMyup' char(9) 'smMyup' char(9),...
'mMzup' char(9) 'smMzup' char(9) 'timedown1' char(9) 'mfxdown' char(9) 'smfxdown',...
char(9) 'mfydown' char(9) 'smfydown' char(9),...
'mfzdown' char(9) 'smfzdown' char(9) 'mMxdown' char(9),...
'smMxdown' char(9) 'mMydown' char(9) 'smMydown' char(9),...
'mMzdown' char(9) 'smMzdown' char(13) char(10)];

fwrite(fid,txt2,'char');
fprintf(fid,txt1,results(:));fclose all;
figure(1);plot(t1,k2,'b',(ind1-1.5)*2^9,mfzup1,'.r',(ind1+1.5)*2^9,mfzdown1,'.g',(ind1-
5.5)*2^9,mfzdown2,'.y');grid on
xlabel('Time (msec)/ No of filtering')
ylabel('mFz,  mFzup1, mFzdown1 and mFzdown2) (N) ')
figure;plot(t1,k(1,:),'b',timeup1,mfxup,'.-r',timeup1,mfxup1,'.-y',timedown2,mfxdown2,'.-
g'),grid on
xlabel('Time (msec)')
ylabel('Tapping Force (N)')
figure;plot(t1,k(2,:),'b',timeup1,mfyup,'.-r',timeup1,mfyup1,'.-y',timedown2,mfydown2,'.-
g'),grid on
xlabel('Time (msec)')
ylabel('Tapping Force(N)')
figure;plot(t1,k(3,:),'b',timeup1,mfzup,'.-r',timeup1,mfzup1,'.-y',timedown2,mfzdown2,'.-
g'),grid on
xlabel('Time (msec)')
ylabel('Tapping Force(N)')
figure;plot(t1,k(4,:),'b',timeup1,mMxup,'.-r',timeup1,mMxup1,'.-
y',timedown2,mMxdown2,'.-g'),grid on
xlabel('Time (msec)')
ylabel('Tapping Moment(N.m)')
figure;plot(t1,k(5,:),'b',timeup1,mMyup,'.-r',timeup1,mMyup1,'.-
y',timedown2,mMydown2,'.-g'),grid on
xlabel('Time (msec)')
ylabel('Tapping Moment(N.m)')
figure;plot(t1,k(6,:),'b',timeup1,mMzup,'.-r',timeup1,mMzup1,'.-
y',timedown2,mMzdown2,'.-g'),grid on
xlabel('Time (msec)')
ylabel('Tapping Moment(N.m)')
figure;plot(mfxup);
```

```
xlabel('No of holes')
ylabel('Tapping Force(mFxup (N))')
figure;plot(mfyup);
xlabel('No of holes')
ylabel('Tapping Force(mFyup (N))')
figure;plot(mfzup);
xlabel('No of holes')
ylabel('Tapping Force(mFzup (N))')
figure;plot(mMxup);
xlabel('No of holes')
ylabel('Tapping Moment(mMxup (N.m))')
figure;plot(mMyup);
xlabel('No of holes')
ylabel('Tapping Moment(mMyup (N.m))')
figure;plot(mMzup);
xlabel('No of holes')
ylabel('Tapping Moment (mMzup (N.m))')
figure;plot(t1,k(1,:),'b',timedown1,mfxdown,'.-r',timedown1,mfxdown1,'.-
y',timedown2,mfxdown2,'.-g'),grid on
xlabel('Time (msec)')
ylabel('Tapping Force(N)')
figure;plot(t1,k(2,:),'b',timedown1,mfydown,'.-r',timedown1,mfydown1,'.-
y',timedown2,mfydown2,'.-g'),grid on
xlabel('Time (msec)')
ylabel('Tapping Force(N)')
figure;plot(t1,k(3,:),'b',timedown1,mfzdown,'.-r',timedown1,mfzdown1,'.-
y',timedown2,mfzdown2,'.-g'),grid on
xlabel('Time (msec)')
ylabel('Tapping Force(N)')
figure;plot(t1,k(4,:),'b',timedown1,mMxdown,'.-r',timedown1,mMxdown1,'.-
y',timedown2,mMxdown2,'.-g'),grid on
xlabel('Time (msec)')
ylabel('Tapping Moment(N.m)')
figure;plot(t1,k(5,:),'b',timedown1,mMydown,'.-r',timedown1,mMydown1,'.-
y',timedown2,mMydown2,'.-g'),grid on
xlabel('Time (msec)')
ylabel('Tapping Moment(N.m)')
figure;plot(t1,k(6,:),'b',timedown1,mMzdown,'.-r',timedown1,mMzdown1,'.-
y',timedown2,mMzdown2,'.-g'),grid on
xlabel('Time (msec)')
ylabel('Tapping Moment(N.m)')
figure;plot(mfxdown);
```

```
xlabel('No of holes')
ylabel('Tapping Force(mFxdown (N))')
figure;plot(mfydown);
xlabel('No of holes')
ylabel('Tapping Force (mFydown (N))')
figure;plot(mfzdown);
xlabel('No of holes')
ylabel('Tapping Force (mFzdown (N))')
figure;plot(mMxdown);
xlabel('No of holes')
ylabel('Tapping Moment(mMxdown (N.m))')
figure;plot(mMydown);
xlabel('No of holes')
ylabel('Tapping Moment(mMydown (N.m))')
figure;plot(mMzdown);
xlabel('No of holes')
ylabel('Tapping Moment(mMzdown (N.m))')
```

APPENDIX C
TRANSFORMATION FROM STANDARDIZED TO ABSOLUTE SCALING EQUATIONS IN HARDNESS EMPERICAL MODELS

APPENDIX C: TRANSFORMATION FROM STANDARDIZED TO ABSOLUTE SCALING EQUATIONS IN HARDNESS EMPERICAL MODELS

Program 1-319 alloys containing α-Fe

```
% Program (1) is necessary  for execution of Program (2)
x=zeros(5,1);
for i=1:5
x(i)=str2num(get(edite(i),'string')); end
rang2=[11.095;0.5772;0.01;0.3333;0.05];
mean2=[-2.079;-2.15526;-1;-1.666;-10];
facteurs=[114.40625 6.5 1.5 -4.5625 -0.65625 0.46875 0.78125 -0.1875
-1.65625 -1.5 -0.5 -0.1875 -0.34375 -0.34375 0.34375 0.9375
-7.875 0.03125 -1.15625 -0.040625 0.1875 0.25 -0.4375 -0.09375
-1.8125 -0.96875 -0.40625 0.21875 -1.125 -0.1875 0.25 0.03125];
x=x.*rang2+mean2;
X=[1;x(1:3);x(1)*x(3);x(1)*x(2);x(2)*x(3);x(1)*x(2)*x(3)];
Y=[1;x(4:5);x(4)*x(5)];
H=sum((facteurs*X).*Y)
set(texte(6),'string',num2str(H))
```

Program 2-319 alloys containing α-Fe

```
%Program (2) is the one should be executed and require program (1) for execution
close all
clear all
clc
fig1=figure(1);
edite(1)=uicontrol(fig1,'style','edit','position',[100 200 50 20],'string','0.093');
texte(1)=uicontrol(fig1,'style','text','position',[40 200 50 20],'string','Mg%');
edite(2)=uicontrol(fig1,'style','edit','position',[100 175 50 20],'string','1.85');
texte(2)=uicontrol(fig1,'style','text','position',[40 175 50 20],'string','Vf%');
edite(3)=uicontrol(fig1,'style','edit','position',[100 150 50 20],'string','0');
texte(3)=uicontrol(fig1,'style','text','position',[40 150 50 20],'string','Sr(ppm)');
edite(4)=uicontrol(fig1,'style','edit','position',[100 125 50 20],'string','4');
texte(4)=uicontrol(fig1,'style','text','position',[40 125 50 20],'string','At(hr)');
edite(5)=uicontrol(fig1,'style','edit','position',[100 100 50 20],'string','200');
texte(5)=uicontrol(fig1,'style','text','position',[40 100 50 20],'string','AT(°C)');
edite(6)=uicontrol(fig1,'style','push','position',[300 100 50 25],'string','Calcul
H','callback','Calcul_H');
texte(6)=uicontrol(fig1,'style','text','position',[250 200 200 50],'string','00','FontSize',20);
```

Program 3-319 alloys containing β-Fe

```
% Program (3) is necesary  for ecxecution of Program (4)
x=zeros(5,1);
for i=1:5
x(i)=str2num(get(edite(i),'string')); end
rang2=[11.4286;1.0995;0.011765;0.3333;0.05];
mean2=[-2.15143;-2.83425;-1;-1.666;-10];
facteurs=[113.172 7.0468 1.17187 -3.57812 -0.20312 0.48437 0.79687 -0.01562
-0.734375 -0.484375 0.078125 0.015625 0.390625 0.140625 -0.671875 0.390625
-7.609375 0.078125 0.203125 0.265625 -0.046875 -0.671875 -0.421875 -0.171875
-2.015625 0.671875 0.734375 0.734375 0.546875 -0.515625 0.359375 -0.640625];
x=x.*rang2+mean2;
X=[1;x(1:3);x(1)*x(3);x(1)*x(2);x(2)*x(3);x(1)*x(2)*x(3)];
Y=[1;x(4:5);x(4)*x(5)];
H=sum((facteurs*X).*Y)
set(texte(6),'string',num2str(H))
```

Program 4- 319 alloys containing β-Fe

```
%Program (4) is the one should be executed and require program (3) for execution
close all
clear all
clc
fig1=figure(1);
edite(1)=uicontrol(fig1,'style','edit','position',[100 200 50 20],'string','0.1');
texte(1)=uicontrol(fig1,'style','text','position',[40 200 50 20],'string','Mg%');
edite(2)=uicontrol(fig1,'style','edit','position',[100 175 50 20],'string','2');
texte(2)=uicontrol(fig1,'style','text','position',[40 175 50 20],'string','Vf%');
edite(3)=uicontrol(fig1,'style','edit','position',[100 150 50 20],'string','0');
texte(3)=uicontrol(fig1,'style','text','position',[40 150 50 20],'string','Sr(ppm)');
edite(4)=uicontrol(fig1,'style','edit','position',[100 125 50 20],'string','4');
texte(4)=uicontrol(fig1,'style','text','position',[40 125 50 20],'string','At(hr)');
edite(5)=uicontrol(fig1,'style','edit','position',[100 100 50 20],'string','200');
texte(5)=uicontrol(fig1,'style','text','position',[40 100 50 20],'string','AT(°C)');
edite(6)=uicontrol(fig1,'style','push','position',[300 100 50 25],'string','Calcul
H','Callback','Calcul_H');
texte(6)=uicontrol(fig1,'style','text','position',[250 200 200 50],'string','00','FontSize',20);
```